The Role of Wetting Effects on The Development of Latent Fingermarks

Thesis submitted for the degree of

Doctor of Philosophy

by

Tshaiya Devi Thandauthapani

School of Physics & Astronomy

University of Nottingham

2019

ABSTRACT

Fingermarks are believed to be unique to each individual and hence play a pivotal role as a form of evidence. However, despite significant ongoing research into fingermark recovery techniques, there are still many areas that need to be explored. Due to the immense potential of fingermarks as an effective method of identifications an attempt has been made in the present work to analyse one particular area that has been overlooked - the impact of wetting properties of different surfaces.

The aim of the study is to investigate the physical and chemical changes in fingermark constituents deposited on polymer substrates of different water contact angles when recovered using the cyanoacrylate fuming technique with the use of camera and FTIR spectroscopy. The effect of aging and the environmental conditions on latent fingermarks was also studied. Meanwhile, visualisation of latent fingermark on metal substrates developed using the conventional technique (cyanoacrylate fuming and staining) was compared with the chemical images obtained from ToF-SIMS.

Images from optical microscope showed the influence of substrate wetting properties in the distribution of both types of sweat material (sebaceous and eccrine) which in turn affected the cyanoacrylate polymerisation. On hydrophilic substrates, the fingermark was deposited as a continuous film that allowed higher cyanoacrylate polymerisation whereas on hydrophobic surfaces an irregularly shaped fingermark deposit led to lower amount of cyanoacrylate polymerisation.

Aging of fingermarks was shown to be influenced by the underlying substrate wetting properties as fingermark constituents decreased more rapidly on hydrophobic surfaces. The eccrine fingermark aged significantly faster than sebaceous fingermark due to the more volatile nature of the fingermark constituents. Experimental evidence showed that both types of marks developed well by producing a clear fingermark pattern with cyanoacrylate fuming after aged for a week when the marks were not exposed to environmental conditions in comparison to the marks that were aged for the same period of time but exposed to airflow and light.

The chemical images from ToF-SIMS demonstrated an exceptional quality of fingermarks (clear ridge definitions and sweat pore position) on the metal surfaces for

periods of up to 26 days after deposition when the samples were stored at ambient conditions whereas conventional techniques showed little to no evidence of fingermarks being present on the metal surfaces after a few days.

List of Publications

Chapter 6 of this thesis have been published in Science & Justice and was presented orally in

- Fingerprint Industry Academia Conference that was held at University of Leicester on the 5th July 2018.
- Annual Student Conference - Advancing Forensics: Current and Future Directions that was held at the University of Derby on the 1st December 2018.

Published Papers

- Thandauthapani, T. D., Reeve, A. J., Long, A. S., Turner, I. J., & Sharp, J. S. (2018). Exposing latent fingermarks on problematic metal surfaces using time of flight secondary ion mass spectroscopy. *Science & Justice*.

Chapter 4 of this thesis have been presented as a poster in Surfaces & Interfaces Summer School that was held in San Sebastian, Spain on the 19th – 24th June 2017.

ACKNOWLEDGEMENTS

First and foremost, I convey my interminable gratitude, sincere and honest thanks to my Supervisor, Associate Professor. Dr. James Sharp to acquaint me to this research topic and his valuable time for guiding me throughout my PhD work. His encouragement for deep understanding with a view to gain knowledge has made this work successful. With immense pleasure, I convey my sincere thanks and deep gratitude to Dr. Mike Smith for his continuous support and teaching me the laboratory skills (FTIR).

I would also like to extend my thanks to Long Jiang and James Kerfoot for teaching how to use ToF-SIMS and AFM instrument used in this thesis. I am thankful to the School of Physics and Astronomy for allowing me the generous use of facilities in the department. Thanks also to the School of Physics and Astronomy technical staff, especially Ian Taylor and Dave Taylor for their advice and help.

Special thanks must be given to my colleague Nathan for his continuous help, especially in the early days for helping me with the Matlab coding when I am lost with all the errors popping up and to Sathish for being a great motivator and an amazing friend that I could count on throughout my PhD work.

I gratefully acknowledge the encouragement and support from my friends Srikanth, Arun, Gaurav, Santhini, Manal, Mano, Mastika, Roshini, Mathulah, and Helen during my PhD work.

I did also like to thank my parents for their blessings and to my sister, who has always been there for me; without them I wouldn't have been able to reach this doctorate, and for that I will be eternally grateful.

Table of Contents

CHAPTER 1

Introduction

1.1 Motivation

When a finger touches a surface, sweat and other substances present on the skin are transferred reproducing a complex pattern of ridges on the surface. Very often the resulting marks are not visible to the naked eye (i.e. they are latent) and must therefore be developed using one or more of a variety of techniques before they can be analysed and compared to an existing database of fingermarks [1]. There has been significant research into improving the existing detection techniques and development of new approaches to successively detect a fingermark.

The success (or lack thereof) of the techniques chosen to develop the marks depend on the surface / substrate on which the marks are deposited and the nature or composition of the fingermarks. The properties of the substrate influence the transfer of substances present on the skin and the way in which, the latent fingermark alters with the time after deposition [2,3]. Obtaining more thorough knowledge of the interaction between the fingermark and the substrate is an important step towards understanding the chemical and physical mechanisms of fingermark deposition and changes that occur within the fingermark with respect to the time [3].

Due to the sparsity of truly quantitative experimental studies, this work provides a timely investigation on the effect of surface wettability in fingermark deposition and fingermark development using cyanoacrylate fuming. An understanding of the

mechanisms of surface wettability in fingermark deposition and subsequent effect on fingermark development with cyanoacrylate fuming technique will therefore be of substantial value in crime scene investigations. The influence of surface wettability in fingermark alteration since the time of deposition and its impact on cyanoacrylate polymerisation was studied.

In addition to the main body of work, an additional study was performed on fingermark recovery from metal surfaces using conventional techniques and surface sensitive technique. This line of research arose from an interest in looking at different types of surfaces, is also an area of operational interest due to the increasing incidence in metal theft and the association of metals as weapons used in violent crime.

The aim of this study is to gain a better understanding of the substrate wetting properties and their impact in the fingermark deposition and enhancement process, which would enable researchers and practitioners to develop fingermarks successfully on any type of surfaces.

1.2 Thesis Outline

Chapter 2: This chapter briefly discusses the history of fingermarks and surveys the current scientific understanding of the fingermark constituents and fingermark enhancement techniques. The effect of different substrates in the fingermark deposition and the development process in forensic research is reviewed.

Chapter 3: The chapter elaborates the different substrates used for fingermark deposition, fingermark development techniques – cyanoacrylate fuming process and staining dyes along with basic principles of different characterisation techniques used in the present study.

Chapter 4: The role of wetting properties of the surface and their influence on the deposited latent fingermark during the application of a common latent fingermark development technique (cyanoacrylate fuming) was studied. The physical and chemical changes occurred within the fingermark on the different surfaces during the development of fingermark was observed and analysed using camera observation and

Fourier Transform Infrared (FTIR) spectroscopy with Attenuated Total Reflection (ATR) technique.

Chapter 5: An investigation was carried out to study the effect of aging on latent fingermarks deposited on different surfaces of varying wetting properties. The physical and chemical changes of the deposited fingermarks as a function of time was observed using optical microscopy and analysed using ATR-FTIR spectroscopy. The influence of the environmental conditions on the deposited latent fingermarks during aging and the impact on cyanoacrylate polymerisation was also studied.

Chapter 6: An experimental study of visualising fingermarks on metal substrates was carried out. This study compares the use of conventional techniques - cyanoacrylate fuming and staining with surface sensitive technique, time-of-flight secondary ion mass spectrometry (ToF-SIMS) for fingermarks deposited and aged on a stainless steel metal surface.

Chapter 7: In this chapter the key conclusions from the work are drawn together and extended work for the future are suggested.

References

1. Moret, S., Spindler, X., Lennard, C., & Roux, C. (2015). Microscopic examination of fingermark residues: Opportunities for fundamental studies. *Forensic science international*, *255*, 28-37.

2. Girod, A., Ramotowski, R., & Weyermann, C. (2012). Composition of fingermark residue: a qualitative and quantitative review. *Forensic science international*, *223*(1-3), 10-24.

3. Bobev, K. (1995). Fingerprints and factors affecting their condition. *Journal of Forensic Identification*, *45*(2), 176-183.

CHAPTER 2

Latent Fingermarks and their Development

2.1 Introduction

2.1.1 Fingermarks

Fingermarks are attributed to the revived traces of material that was left on a surface at the time of the skin ridges of the fingertips touch the surface [1]. Fingerprints are referred to the friction ridges found on the skin obtained in a controlled way from known individuals to another surface using either ink or digital imaging [2]. Fingermarks played a pivotal role for over 100 years and are still one of the most important types of identification evidence because fingermarks are easily recognisable by forensic investigators and their uniqueness to individuals [3].

The value of fingermarks lies in the fact that the chances of finding two identical marks are one in 64 billion as they are "one-of-a-kind" as even identical twins do not have the same fingermark pattern [4]. Besides that, another reason for fingermarks to be classified as vital and to be used in criminal investigations is the ridge patterns found on the fingertips are persistent throughout a person's lifetime.

2.1.2 History of Fingermarks and their Applications to Solving Crimes

The use of friction ridge detail was first used by the Chinese for personal identification that dates back to the time period of 221 B.C. to 220 A.D. [5]. However, it was not until the late 17th century, the first recorded study of friction ridge skin was carried out by Nehemiah Grew in 1684, who is considered as the fingerprint pioneer. He published various precise drawings of the different fingerprint patterns portrayed by the ridges and furrows [6].

About a century and a half later in 1823, Joaness Evanelista Purkinje (1787 – 1869) published the first thesis that contributed a significant academic investigation of fingerprints. He is well-known for his discovery of sweat glands, fingerprint pattern and the function of ridges, furrows and pores that are present on the tip of fingers. He classified different patterns of fingerprints into nine main groups which include one arch, one tent, two types of loop and five types of whorl as shown in Figure 2.1 [5].

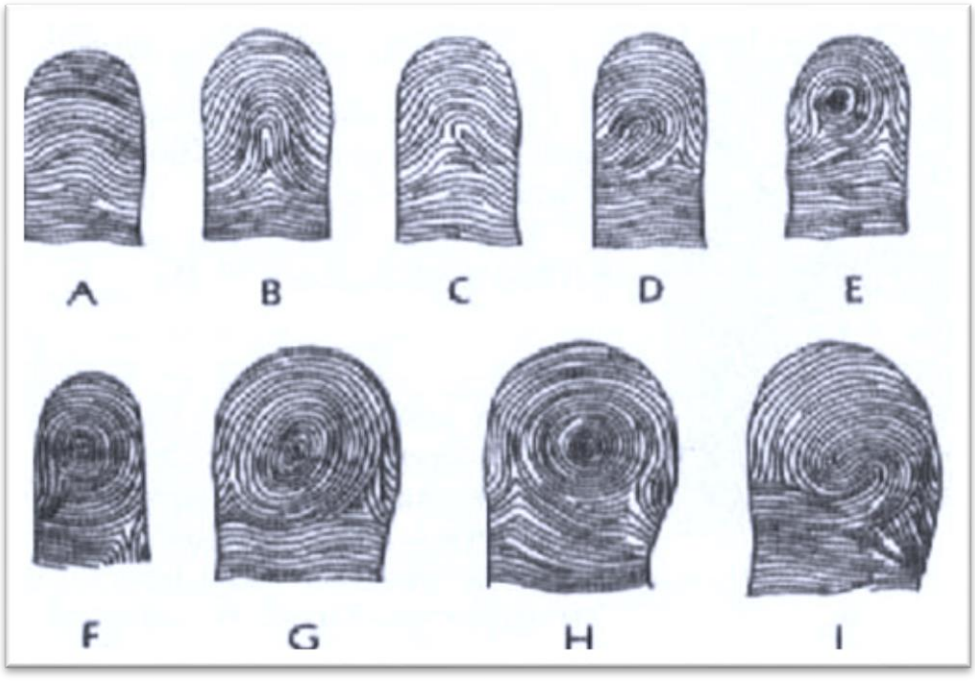

Figure 2. 1: Figure depicts the nine types of fingerprint patterns discovered by Purkinje are described as: A- transverse curves, B- central longitudinal stria, C- oblique stria, D- oblique sinus, E- almond, F- spiral, G- elliptical whorl, H- circular whorl and I- double whorl. Image is reproduced from The Fingerprint Sourcebook [5].

Less than 40 years later, Sir William Herschel (1833 – 1917) carried out a study looking into the changes in friction ridge skin over time by taking his own palm prints in 1860 and again in 1888 to demonstrate that the fingerprint pattern and ridge detail remained unchanged throughout a person's lifetime, with the exemption of some additional wrinkle lines due to aging [5].

About the same time, Dr Henry Faulds (1843 – 1930) studied the permanence of fingerprint along with his medical students by removing the printed skin after the fingerprinting process. When the skin had re-grown, he fingerprinted them again, making an observation of the friction ridge pattern to grow back exactly as the initial prints. He is known for being the first one to perceive the importance of fingerprints in criminal investigations [5].

In the late 19th century, Sir Francis Galton (1822 – 1911) administered a broad investigation into fingerprints that originated from his primary interest in thumb impressions. His research had further advanced the knowledge in fingerprints that initiated the application of fingerprints as a more effective form of individual identification. This was mainly due to the disclosure of fingerprint's uniqueness that simultaneously contributed to the decrease in common anthropometric methods for crime scene investigations [5,7].

At the beginning of the 20th century, influenced by Sir Galton's publication *Finger Prints*, Sir Edward Henry (1850 – 1931) developed a method of classification for fingerprints known as the 'Henry System'. His approach to record the fingerprint was based on logical characterization whereby he assigned a value to each of the 10 fingers based on the fingerprint pattern type (see Figure 2.1). The values were assigned to each whorl pattern based on which finger it was found, starting with the right thumb and ending with the left little finger [8]. In the case of a finger did not have a whorl pattern, it was assigned to zero. This classification system allowed for 1024 primary grouping had significantly reduced the effort necessary to look up for a large number of fingerprint records. Henry's system was so successful whereby all criminal identification records were recommended to be classified based on it.

2.1.3 Current Fingerprint Searching

Fingerprint databases were established in the early 20th century when forensic science began to adapt fingerprints as a form of personal identification as a standard procedure.

Fingerprints were taken from every person who has been taken into custody for accusation, or for being reported, or summoned for a crime. These prints were then stored on a progression of card records that was documented, searched and recovered manually prior to 1970. This lengthy and inconvenient process of fingerprint comparison and identification was put to an end by the innovation of Automatic Fingerprint Recognition (AFR) technology that was used to develop the computer-based database known as National Automated Fingerprint Intelligence System (NAFIS). Each police force in the UK had the innovation accessible to them by the year 2001. The technology operates using a special algorithm that chooses a few characteristics to determine the nearest matches between a suspect's fingerprints retained in the database with the mark recovered from a crime scene [9]. This invention allows for a much quicker and straightforward checking between different fingerprint bureaus across the nation or world.

One such example bureau used by Northumbria Police is known as Tenprints. The name Tenprints originates from the process of acquiring a person's ten distinctive fingerprints using an ink pad and paper. Northumbria bureau holds roughly 700,000 sets of fingerprint receives nearly hundreds of fingerprint forms each day to be fed into the IDENT1 database [10]. In April 2005, IDENT1 replaced NAFIS and is presently the central national database for all 43 forces in England and Wales and the Scottish forces to search and compare the fingerprint details of offenders within the UK [11]. The IDENT1 database consists of 8.9 million sets of ten prints of known individuals, 12 million palm print pairs along with 1.9 million unidentified marks recovered from crime scenes.

Once a fingerprint examiner marks up the individual characteristics from a fingermark scanned into the bureau (after being recovered from scenes of crime), the computer determines the likely matches from the database. To analyse and compare, a fingerprint examiner will use three criteria as follows: type of fingerprint pattern, type of finger (right or left hand, thumb, etc.) and ridge characteristics. As of not long ago, at least 16 matching characteristics were required in the UK for a positive identification to be made. However, this is can be overruled as the general decision on identification lies solely with the fingerprint examiners with no minimum quantitative matching characteristics required [12].

2.1.4 Fingermark Deposits

The unique pattern of the friction ridge skin found on the fingertips of humans is formed during foetal stage, roughly four months after conception. As the term suggests, the existence of the friction ridges is to improve the friction of skin primarily to aid grip with increased sensory abilities as there are no hair follicles present on the fingertips [13]. The scenario of a mark that is left behind upon the contact of friction ridge skin on any surface is best described by Locard's exchange principle, which implies that each contact leaves a piece of evidence [14]. The indentation of the ridge pattern or fingermark is transferred on as a result of secretion of perspiration from the sweat pores which are located along the friction skin ridges, present on the fingertip onto the substrate/surface upon touching [15].

2.1.5 Fingermark Composition

The composition of fingermarks relies on the nature of sweat. The human body is comprised of three primary types of sweat glands - namely, eccrine, sebaceous and apocrine [3]. Eccrine sweat glands are all over the body with the highest density on the palms of hand [16]. Eccrine sweat is composed of as much as 99% of water with less than 1% of the composition made up of both organic and inorganic components [17]. Sebaceous glands are generally identified in the areas that are enclosed by hair follicles and they secrete an oily secretion called 'sebum' comprised of mainly organic constituents, with most being triglycerides and fatty acids [16]. Apocrine glands can be found in areas like armpits, genitals, and breast [16]. As a result of the region in which the apocrine glands are present, it is unlikely to encounter this type of sweat as one of the predominant components of a mark, but the existence of this sweat is important in a crime involving sexual nature [18].

It might be expected that the fingermark composition is made up of predominantly eccrine sweat due to the location of the sweat glands as mentioned earlier, but in practice fingertips can have contact with different parts of the body and through this way there is a tendency for the fingertip to pick up the sebaceous and apocrine sweat [3]. The primary components secreted from the three main types of sweat glands are tabulated in Table 2.1, yet fingermark composition remains to be complex. The fingermark composition can be further varied between person to person as the fingertip is also prone to pick up extrinsic contaminants when it touches or encounters other

surfaces such as food residues, cosmetics and perfumes [19]. Additionally, intrinsic contaminant including metabolites, medicines and drugs can also affect the fingermark composition [19].

Type of sweat gland	Inorganic components	Organic components
Eccrine	Chlorides Ammonia Phosphate Sulphate Metal ions (Sodium, Potassium, Magnesium, Calcium, Iron, Copper, Manganese) Halide ions (Iodide, Bromide, Fluoride)	Amino acids Urea Lactic acids Sugars Creatinine Choline Uric acid
Sebaceous	-	Fatty acids Glycerides Sterol Wax esters Hydrocarbons Squalene Alcohols
Apocrine	Iron	Proteins Cholesterol Carbohydrates

Table 2. 1: The main inorganic and organic constituents of secretions of the three primary types of sweat glands (excluding water) [17-20].

The fingermark composition of an individual varies throughout the day as the amount of sweat produced differs in accordance with the changes in weather, physical activities, emotional response, and diet [3]. The quality of enhanced fingermark is influenced by the age of the donor and the mark since enhanced marks of children in general, are of poorer quality in comparison to adults mainly because of the chemical variations in fingermark deposits [21-23]. The chemical composition of fingermark can undergo various physical and chemical changes over time after fingermark deposition. The aging process of fingermark can pursue numerous different pathways such as drying, degradation, migration, oxidation and evaporation, which can occur at considerably different rates [24]. These processes will rely upon a few variables that include the initial composition of fingermark, the underlying substrate on which the fingermark residue is deposited and exposure to different environmental conditions. A summary of the main factors that could affect the fingermark composition are listed in Table 2.2.

Variable	**Examples of variable influencing the fingermark**
Sweat glands	Eccrine (fingers and palm only have eccrine glands), Sebaceous, Apocrine
Contaminants	Anything that is touched since touching is a two-way process, Pollution
Ambient conditions	Temperature, Humidity, Air-flow, Light
Donor factors	Time of day/year, Diet, Medication and recreational drugs, Gender, Age, Mental and physical states, Racial origin, Cleaning regime, Smoker/non-smoker
Deposition	Pressure, Angle, Movement at the moment of touch
Surface	Porosity (porous to non-porous ratio), Condition (Wetted / non-wetted), Surface chemistry/physics, Contamination, Temperature
Biological	Bacteria; viruses

Table 2. 2: Lists of variables that influence the composition of a fingermark with examples is adapted from Reference 3.

All areas of the skin, including the fingertips, can accommodate bacteria and viruses, in which case these microbes can be transferred along with the other chemicals present on the fingertips to the surface by contact where the growth of these microorganisms may be elevated under suitable conditions [25]. The study made by Harper *et al.* found a variety of microorganisms existing on the skin which were not only able to grow but also to form colonies on sebaceous material [26]. This analysis showed that microbes (biological variables) can influence the fingermark composition when transferred from the fingertip to the surface upon contact, which could cultivate to produce an identifiable fingermark depending on the substrate (e.g. nutrient agar) it was touched upon.

2.1.6 Types of Mark

Materials are left in the form of a mark when an object or surface is handled or comes into contact with fingertips. A patent mark is visible to the unaided eye which is usually left by paint, dirt, grease, blood or foodstuffs from the hand to a surface (Figure 2.2a) could be photographed without any further treatment. Impressions also known as plastic marks (Figure 2.2b) refer to the three-dimensional indentation of the fingertip left in the soft material such as butter, putty and tar. This type of mark also does not need processing as it can normally be photographed under special lighting conditions.

However, the majority of fingermarks deposited are of latent mark type that literally means hidden or not visible to the naked eye (Figure 2.2c). The composition of a latent mark is dependent on the eccrine sweat that is comprised of 99% water being secreted from the sweat pores located on the fingertips [5]. Nevertheless, as mentioned previously there is a tendency for the eccrine sweat to be contaminated with sebaceous sweat [27]. The sebaceous sweat contains main constituents such as triglycerides and fatty acids attribute to an oily, tacky characteristic of fingermark deposits. Latent marks require physical and / or chemical enhancement in order to visualise them unlike patent or plastic fingermarks, can be easily photographed in most cases without any further treatment.

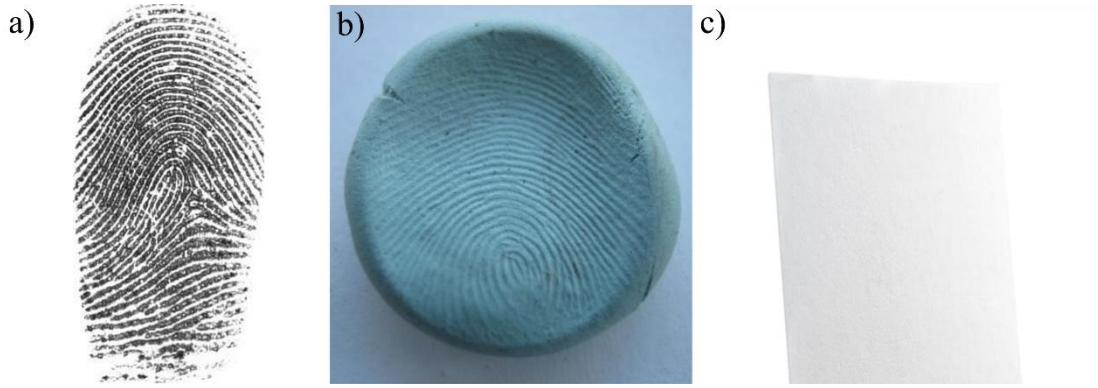

Figure 2. 2: Examples of mark types a) patent fingermark that is visible to the naked eye upon deposition that does not require any development, b) plastic fingermark on a blu tack (similar characteristic to putty) modelling three-dimensional indentation of the fingertip and c) latent fingermark on a paper that is not visible to the naked eyes and requires physical and/or chemical enhancement in order to visualise it.

2.2 Latent Fingermark Development

Several methods have been explored to 'visualise' and 'acquire' the latent marks since fingermarks were recognised to be used as a form of identification. Acquiring fingermarks is very important as it permits one to go back to view the image for evaluation and to identify likely matches located in the database (see previous Sections 2.1.2 – 2.1.3). Crime scene investigators focus on looking for fingermark evidence and collecting fingermark including by means of developing fingermark at the crime scene. For the cases where fingermark development could not be carried out at the crime scene, the items that are smaller in size or evidence with more essential values will be taken away from the crime scene to the research facility. This decision is also commonly taken when it is felt that improved contrast can be obtained between the fingermark and the substrate. However, in the case of huge and heavy items or bulky surfaces that could have fingermark evidence are encountered, they will be left as they were found in the initial state at the crime scene. The following section outlines the approach where a latent fingermark is made visible by employing various development techniques that include the use of optical, physical, and/or chemical [28].

2.2.1 Latent Fingermark Development Techniques

Optical methods are utilised to visualise latent fingermarks using visible light, infrared (IR) and ultraviolet (UV) regions of the electromagnetic spectrum. Development of latent fingermarks by physical methods involve physical interaction (i.e. physical adsorption, electrostatic attraction and adherence) with deposits of fingermark. Chemical methods target a particular constituent of sweat (see previous Section 2.1.5) and convert it into a coloured derivative enabling the latent fingermark to be visualised. These techniques can be either used by itself or in combination to improve the clarity of developed marks.

The composition and quality of a developed fingermark depend on phases of the fingermark deposition including pre, mid and post [29]. The factors that influence the pre-deposition entirely rely upon the donor conditions (see Table 2.2) and foreign substances on the fingertips which could have come into contact prior to deposition. These are extremely hard to account when development choice must be made. Mid-deposition factors correspond to the contact dynamics of fingertips with a substrate and the surface properties of the substrate on which the fingermark was deposited onto. The effect on mark quality due to contact conditions (see Table 2.2) will only be disclosed after the development process. Nevertheless, surface conditions are generally important in choosing the right development techniques. Post-deposition factors, for example, exposure to water, surface chemistry, ambient temperature, surface porosity, and environmental contamination can influence the optimisation of development effectiveness.

A systematic approach and a thorough consideration before choosing a technique are required to attain the best quality of the developed mark since recovery of fingermarks is a very important process in order to identify the criminal. The process selection of techniques will change relying upon the type of mark as well as the substrate the fingermark is deposited on to (see Figures 2.3 and 2.4). The type of substrate plays a vital role when it comes to choose the right technique as few methods will surely not work on certain types of surfaces.

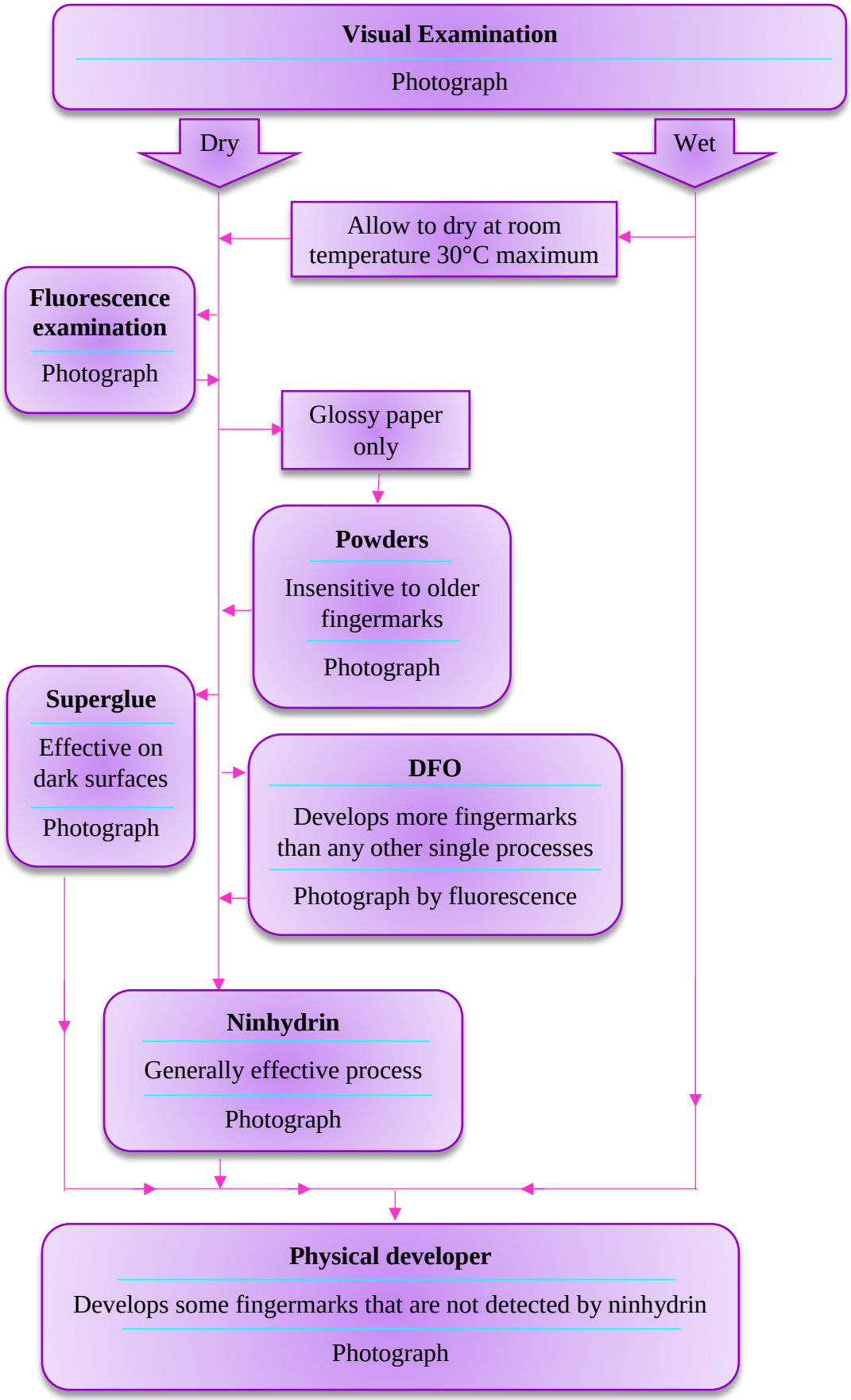

Figure 2.3: The systematic process selection for fingermark development on a porous surface. Flow chart is adapted from Kent, T., 2016. [30]

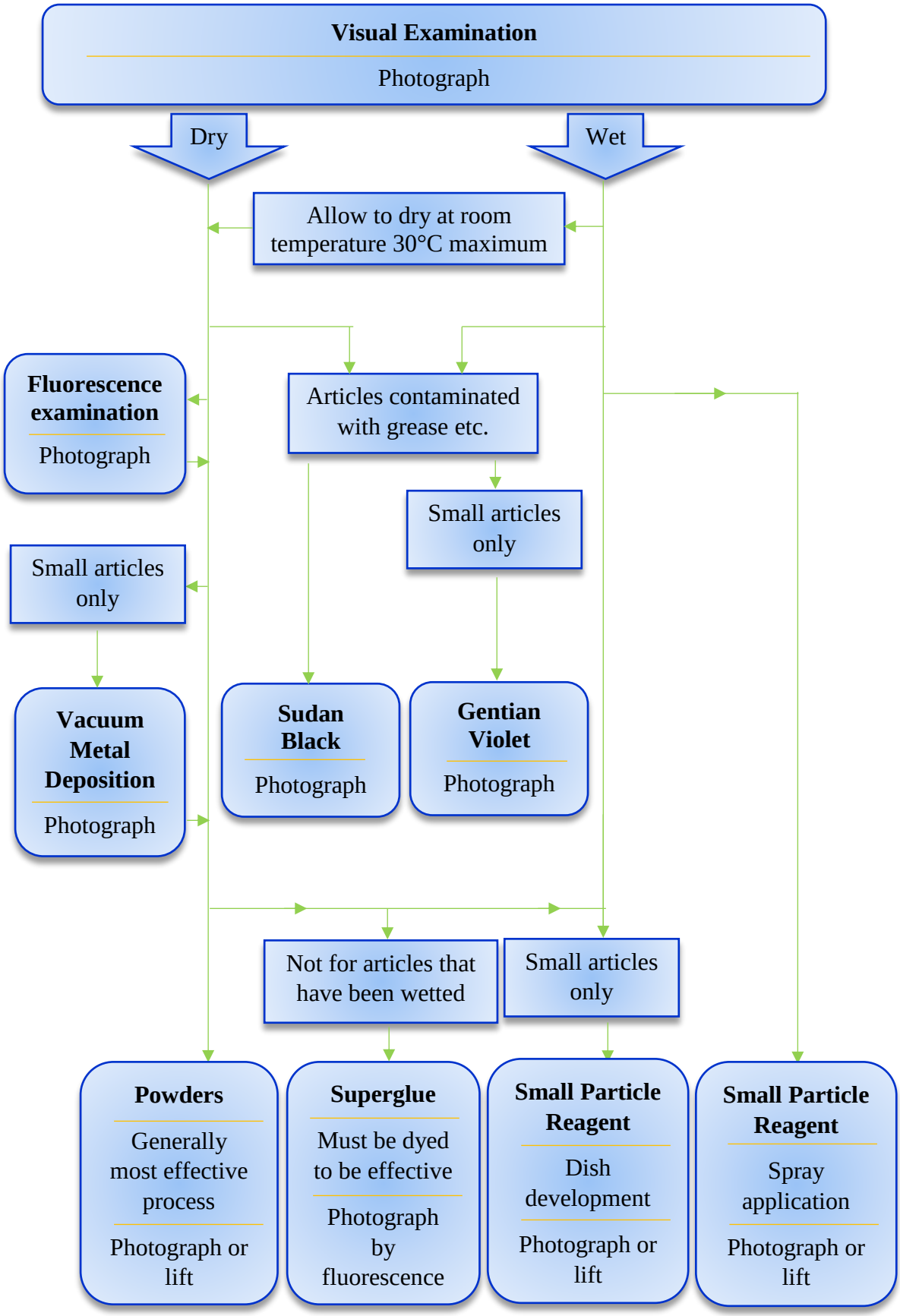

Figure 2.4: The systematic process selection for fingermark development on a non-porous surface. Flow chart is adapted from Kent, T., 2016. [30]

Choosing the right technique for retrieval is of a great consequence because in most of the situations there will be just a single try to obtain a proper image of the fingermark where it is not possible for further enhancement once the mark is developed. A photograph of the recovered mark is taken to be uploaded in the database to search for a match and for future references.

2.2.2 Optical Methods

Optical methods are the first procedures that ought to be considered for detecting and enhancing fingermark, especially in the case where sequential treatments are being used. Optical methods can be utilised to visualise marks prior to any processing sequence due to their non-destructive nature as this method does not have any contact with the fingermark deposit. Moreover, marks that were developed with either physical or chemical methods can be further enhanced using a suitable optical method, which relies upon the characteristics of the treated mark (e.g. colour or luminescence) [31,32].

2.2.2.1 Visual examination with white light

Examining visually under white light is the most basic, simplest optical technique and non-destructive to the fingermark residue and any other forensic evidence. Visible fingermarks which can be seen sometimes on surfaces that are smooth and non-porous can be photographed because of the reflection or scattering of the white light. However, it is more likely that only contaminated fingermarks tend to appear visible when deposited onto porous surfaces. Examining at different angles of illumination and observation is essential in order to obtain a clear and detailed photograph of the fingermark particularly for fingermarks found on surfaces that are reflective or textured. This is mainly because these type of surfaces would need the light source to be manipulated in order to achieve both the high and low point of illumination that can significantly influence the contrast and visibility of the fingermarks.

2.2.2.2 Epitaxial white light visual examination

Epitaxial simply refers to the arrangement of the apparatus in such a manner is aligned the same as that of the surface under examination. The design incorporates a white light source together with either a semi-silvered mirror or prism beam splitter that is being held at 45° to the axis of the imaging system (see Figure 2.5). The illuminating

beam is reflected by the beam splitter downwards to the surface with the observer viewing the light reflected from the surface after passing through the beam splitter. Although this technique can be effective in detecting untreated fingermarks on smooth, shiny and flat surfaces, it is not used extensively.

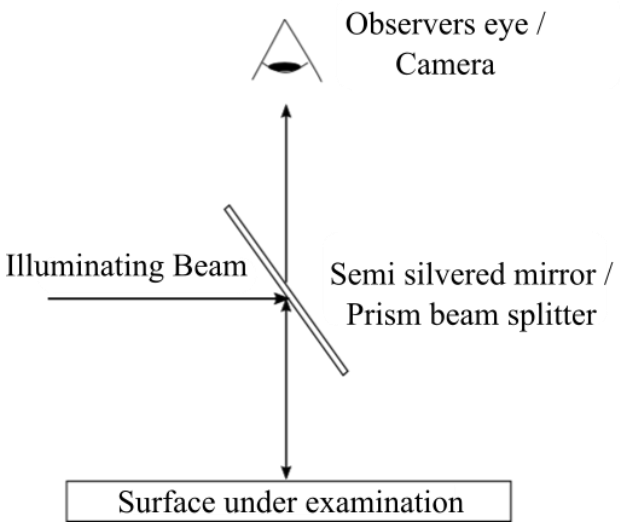

Figure 2.5: Schematic displaying the optical path for epitaxial viewing.

2.2.2.3 Fluorescence examination

Fluorescence is a process that implies a material can emit light because of an external stimulus. Fluorescent compounds absorb light of a specific colour of visible light, which then immediately emits the absorbed energy as light that is usually of a different colour and longer wavelength. If a light source of an appropriate wavelength is used to illuminate a fluorescent molecule, it gets excited. The photon absorption from the shorter wavelength light radiation leads to excitation of electrons that results in the excited electrons to fall back to the 'ground state' over a long time period (but still within nanosecond) by emitting a photon with lower energy, and consequently of longer wavelength [33,34].

Most commonly used light spectrum to excite fluorescence are UV light, blue, green or yellow components of the visible light, resulting in the emission of light in the red, orange, infra-red (IR) or yellow regions. It is vital to take note that when a light is illuminated on the surface that is being examined, most of it is not absorbed but instead

is scattered or reflected. Therefore, filters are required to be placed in front of the eye and/or camera as they can transmit the fluorescence and block the light used for illumination to view the fluorescence and to be imaged.

In order to transmit the highest emission of the fluorescent species it is important to make sure that the illuminating wavelength of light sources correspond as close as possible to the excitation of the fluorescent species present (if it is known) and be used with viewing filter that blocks all the illuminating wavelength (see Figure 2.6). Fluorescence examination for fingermarks can be grouped into two main categories as follows:

1. Initial examination of untreated or latent fingermarks
2. Imaging of enhanced fingermark that has been developed with reagents that produce fluorescence

2.2.2.3.1 Fluorescence – initial examination

Providing fluorescent treatment is basically a non-destructive process, it is usually used in the initial stage of a sequential processing regime (see Figures 2.3 and 2.4). There are three factors for fingermarks to be revealed at the time of initial examination although fluorescence of untreated fingermarks is usually weak. The foremost reason for the fingermarks could be detected is due to the possible presence of the intrinsic fluorescence components in the sweat. Even though most of the latent fingermarks constituents cannot fluoresce, three types of amino acids namely - tyrosine, phenylalanine and tryptophan do fluoresce in the visible light region [34].

Secondly, when untreated fingermarks exhibit enhanced fluorescence it may be more likely that they are contaminated with extrinsic substances such as greases, cosmetics, industrial chemicals, creams, or even environmental dust that are fluorescent [33,34]. Final reason corresponds to the underlying surfaces like cardboard or paper, which display background fluorescence that could enhance the contrast of fingermarks stained with substances like blood or dirt by absorbing the light and tend to appear darker in colour against the light fluorescing background.

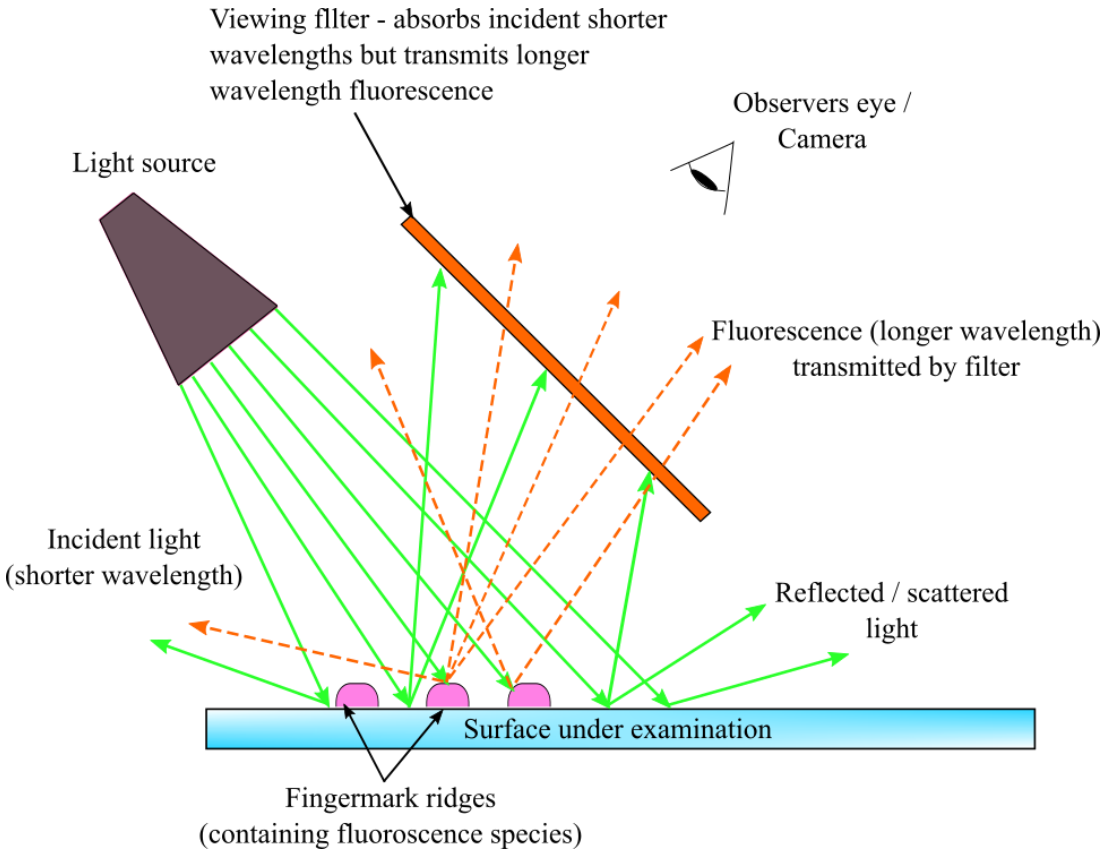

Figure 2.6: Schematic diagram representing the observance of fluorescence species in fingermark ridges.

2.2.2.3.2 Fluorescence – enhancement of developed fingermarks

Fluorescence treatment may likewise be used as a technique for enhancing the contrast of fingermarks developed with either physical or chemical methods. There are four main ways to enhance fingermark post-development by the application of fluorescence examination. The first type refers to the treated fingermark that fluoresces because of the chemicals present in the dyes to stain the fingermarks itself is fluorescent, for example, basic violet 3 and acid yellow 7. This approach will reveal the weak or invisible fingermarks under normal light. The next type is when the background surface can fluoresce with the fingermark appearing black by either absorbing or scattering the incident light. For instance, fingermarks developed on coloured paper with ninhydrin are sometimes enhanced in this way [34].

Another type involves the enhancement of developed fingermark by treating it with either a secondary reagent or stain before fluorescence examination. In both the cases, the fingermark is converted from being a non-fluorescent into a mark that fluoresces, thus enhancing the fingermark in detail. Examples for this type include the use of zinc salt toning to fluoresce marks developed with ninhydrin [33] and enhancing the marks treated with superglue by staining using fluorescent dyes such as Basic Yellow 40 and Basic Red 14 [33]. The final type corresponds to the application of a reagent, for example, Crystal Violet (CV), Sudan Black (SB), 1,8-diazafluoren-9-one (DFO), and 1,2 indandione that can react directly with fingermark constituents to produce a product that fluoresces [33]. The fluorescent fingermark powders also fall into this type.

2.2.2.4 Ultraviolet imaging

Detecting latent fingermarks using shortwave ultraviolet (UV) reflection also referred to as reflected ultraviolet imaging system (RUVIS), was first proposed by Okhi in 1970 [35]. Nearly 20 years later, usage of reflection techniques comprising of both the long- and shortwave UV region on various types of surfaces was reported by London Metropolitan Police. A UV-sensitive digital camera that is equipped with both quartz lens and a source of UV light is the only required apparatus for UV imaging that enables to detect traces of fingermarks, impressions left by footwear, and even bite marks left on the skin. Ultraviolet fluorescence generates contrast between the surface and the fingermark deposit by either absorbing or reflecting the UV light. For this reason, relying upon both the nature of the surface and the constituents in the fingermark residue, this technique will result in either by producing light ridges on a dark background or vice versa. Given that UV imaging is a non-destructive technique, the fingermarks that are revealed by UV fluorescence can be further improved with either physical/chemical methods (see Figure 2.7).

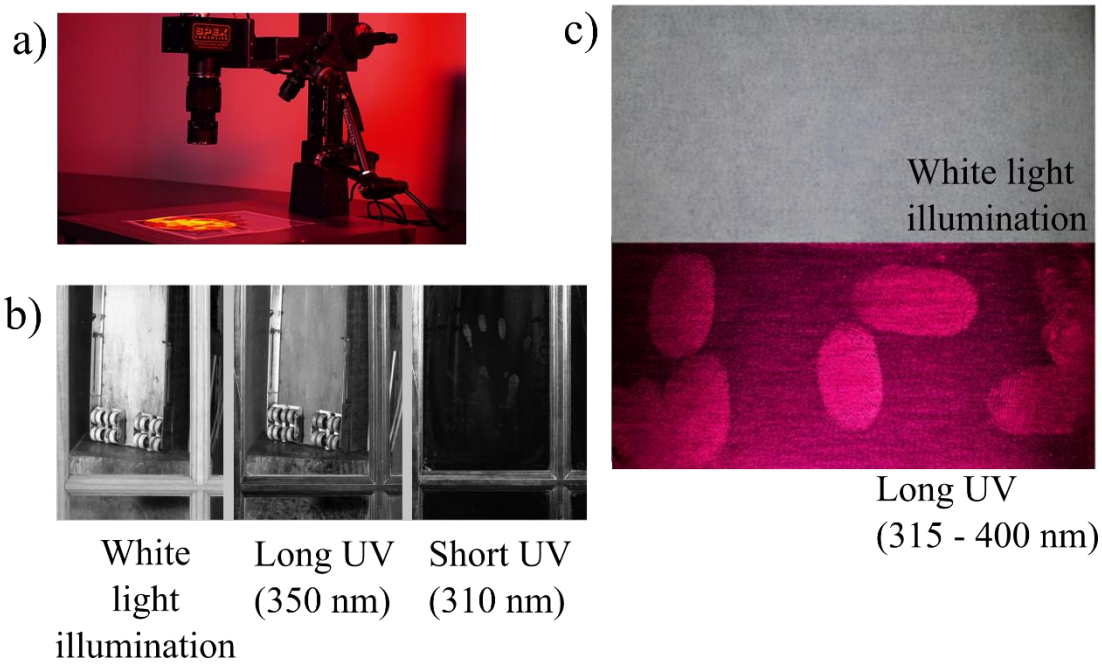

Figure 2.7: a) Example of a reflected ultraviolet imaging system to examine fingermark [36]. b) Latent handmark on the glass window was imaged using visible monochrome light (left), longwave ultraviolet radiation of 350 nm (middle), and shortwave ultraviolet radiation of 310nm (right) [37]. c) Adhesive side of paper-based packaging tape (masking tape) treated with cyanoacrylate (superglue) fuming and viewed under white light illumination (top) and longwave ultraviolet radiation (bottom) [38].

2.2.2.5 Infrared imaging

The potential use of infrared (IR) imaging to visualise fingermarks was first considered in the 1970s, mostly utilising the near IR (NIR) region from 700 – 1100 nm. Generally, latent fingermarks are not revealed by NIR, but it can aid to visualise fingermarks after being developed by different techniques. There are two observation modes available to acquire a fingermark image, namely NIR reflection and NIR luminescence emission (excitation occurs under visible light).

In order to image fingermarks with NIR reflection mode, a light source that emits within NIR wavelength range, for example, conventional tungsten lamps or NIR light emitting diodes (NIR LEDs) is required. A filter with a cut off wavelength of 700 nm should be placed in front of the camera to only transmit the NIR radiation while blocking all the reflected visible light. To image fingermark in the NIR luminescence

emission mode, a NIR-sensitive camera fitted with a filter similarly as for the NIR reflection mode is required. This is to be able to view the transmitted NIR radiation due to the excitation that occurs when a suitable monochromatic (e.g. laser) visible band is shone onto the surface containing fingermark.

Later in the year of 2000, Bramble and co-workers proved that imaging in the luminescence mode to be effective for enhancing the developed fingermarks with gentian violet where luminescence emission was observed in the NIR region (>620 nm) when excited at shorter wavelengths of about 400 – 600 nm. This study demonstrated to be efficient for faint marks on both dark and light surfaces [39]. Then in 2005, a study was conducted in the NIR reflection mode, using IR filters with a NIR-sensitive digital camera to eliminate the background with coloured patterns from fingermark images was successful. They displayed to remove the multi-coloured backgrounds from marks that were developed using physical developer (PD), vacuum metal deposition (VMD), aluminium powder, small particle reagent (SPR) and black powder suspension (BPS) sufficiently [40].

2.2.3 Physical Methods

2.2.3.1 Powders

Powder dusting is one of the oldest and most frequently used technique to develop latent fingermarks. This physical method depends on adherence of the powder to the fingermark residue that gives an instant development, defining the ridge pattern. Though the technique is more reliable and widely used, use of a brush to dust the powder over the substrate can leave destructive effects on the ridge details.

In general, the powders are grouped into four categories that include:

1. **Regular** – consists of a resinous polymer -made up of starch, silica gel and rosin to provide adhesion with the moisture and oily constituents of the sweat residue [41]. The regular powder also consists of colourant to provide contrast between the fingermark and the surface [42] it is deposited onto is either made up of organic derivative or inorganic salt. Colourant based on organic formulations, in general, comprises of organic dye and in order to obtain better results, fluorescent and laser active dyes are used [43]. A few examples of the regularly used organic

based fingermark powders include formulations that contain fluorescein and rhodamine B [44]. The use of inorganic salt based fingermark powders containing a combination of ferric oxide and rosin, lampblack and fuller's earth, and titanium dioxide and kaolin [45] reduced over time mainly because of their potential health hazards and toxicity to the user.

2. **Luminescent** – consists of either natural or synthetic organic mixtures which can fluoresce or phosphoresce when illuminated with laser light, ultraviolet (UV) light and any other light sources [46-48]. This type of powder is most effective to visualise latent marks deposited on a multi-coloured surface.
3. **Metallic** – consists of coarse, spherically shaped iron particles incorporated with regular powders. Magnetic powders are also referred to as Magna-powders due to the use of magnetic applicator during its application [49]. The iron in the magnetic powder serves as a carrier for the particles that are non-magnetic by creating a 'brush' like effect when picked up using the magnetic applicator [50,51]. The fine particles of the formulation will adhere to the mark and outline the ridge detail when the magnetic applicator is passed over the surface. The standard Magna-powders were replaced by flake metal powders that are attracted to the magnetic powder for a better performance of magnetic applicators. This enabled all the magnetic flakes to be lifted with the applicator allowing for more powder to be available for the fingermark development, unlike standard magna-powder that contained only 1% of the fine particles that can adhere to the fingermark residue [50,52-53]. Metallic powders have proved successful for fingermark development on plastic or leather substrates and specifically useful for recovering latent fingermarks on surfaces that are rough or porous, for example, polyethene, paper and painted walls [43,54-55].
4. **Thermoplastic** – consists of photocopier toners or dry inks that can develop latent fingermarks by fusing to the substrate when exposed to heat [56].

2.2.3.2 Small Particle Reagent

Small particle reagent (SPR) is another effective physical method that depends on fine particles adhering to the oily components of the sweat, on a wet non-porous surface [57-59]. Originally, molybdenum disulphide was used, but with time progress fine titanium dioxide [60-62], iron oxide [63] or zinc carbonate [64] particles were used by suspending them in a solution that contains a surfactant such as 10% dioctyl sulfosuccinate, sodium salt in water [65]. SPR can be applied either by spraying the solution on the surface or by submerging the surface entirely in the solution. The developed fingermark tend to appear as dark or light grey depending on the suspension particle used. This technique has proven to be effective in developing latent fingermarks on various types of surfaces like glass, metal, plastics and adhesive sides of tape [66].

2.2.3.3 Lifting Tape

Lifting tape is commonly used to lift off the developed fingermark after a powder application process in the crime scene for further examination [50]. There is an extensive range of various types of tape that are accessible to lift the powdered fingermarks from a variety of substrates which also includes human skin [67]. The procedure of lifting tape is the same, irrespective of the tape type used. The process involves pressing down the tape onto the developed mark, ensuring no air bubbles are present by using a short length of the tape. The tape is then lifted gradually from the substrate which is then transferred to a support sheet [68]. Lifting tape is also known as the adhesive tape is used collectively with various spectroscopic techniques mainly to analyse if any contaminants, for example, explosives [69] and drug metabolites [68, 70-71] are present within the collected fingermark residue.

2.2.4 Chemical Methods

Chemical methods can be classified into two categories, namely – vapour phase technique and chemical reagents. Both techniques, particularly target one of the constituents within the fingermark for development, commonly targeting amino acids or lipids. Generally, vapour phase techniques have a low effect on the surface that is

treated with, so for this reason they are usually used at the beginning of a processing sequence. Meanwhile, surfaces treated with lipid reagents are in the potential of getting damaged in most of the cases due to the high staining features of the dyes, hence these dyes are in general used towards the end of a processing sequence.

2.2.4.1 Vapour Phase Techniques

2.2.4.1.1 Cyanoacrylate Fuming

Among the two techniques that utilise fuming of a substance, the employment of cyanoacrylate (superglue) is the oldest and most common fuming technique [72]. Cyanoacrylate (CNA) fuming is proven to be one of the most efficient processes to develop fingermarks on most of the non-porous surfaces that have not been wetted. Latent marks are developed by being exposed to ethyl-2-cyanoacrylate vapour in a confined chamber. White deposits on fingermark ridges are formed when the cyanoacrylate monomer comes in contact with the fingermark residue and polymerises [73]. The polymerised deposits are known as polycyanoacrylate. The polymerisation of cyanoacrylate monomer undergoes three definite steps that are initiation, propagation and termination. The molecular structure of ethyl-2-cyanoacrylate is displayed in Figure 2.8, is the most routinely used monomer for enhancing fingermark.

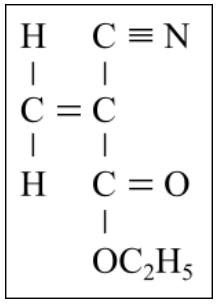

Figure 2.8: The molecular structure of ethyl-2-cyanoacrylate.

Cyanoacrylate is referred to as an extremely strong electrophile that is attracted by electrons. According to the terms of the organic synthetic chemistry, the polymerisation reaction of cyanoacrylate needs to be initiated by a transfer of electrons from a nucleophile [74] or anionic initiators such as chloride, carboxylic acids and

amines as shown in Figure 2.9. This implies any constituents in a fingermark that carries a free electron pair will be able to initiate the polymerisation of cyanoacrylate. The electron transferred from the nucleophile denoted as Nu^- to the CH_2 side group of the ethyl cyanoacrylate is represented by an arrow. The more reactive double carbon-carbon bond will be broken by leaving a single carbon-carbon bond which is attached to the nucleophile [75].

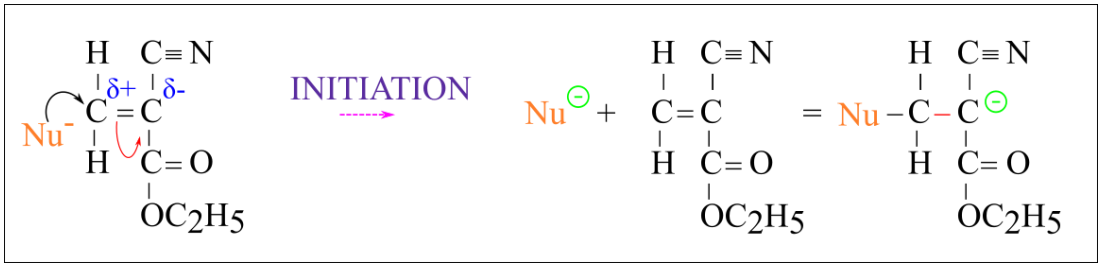

Figure 2.9: Mechanism for the initiation process of ethyl-2-cyanoacrylate polymerisation by a nucleophile, Nu^-.

That specific step will trigger for the propagation reaction, the next step that enables for further nucleophilic attack on another monomer of ethyl-2-cyanoacrylate. The propagation reaction then continues by the resulting expansion of ethyl-2-cyanoacrylate monomer units to the carbanion end of the developing chain. It is necessary to take note that the propagation reaction undergoes a negatively charged intermediate is displayed in Figure 2.10.

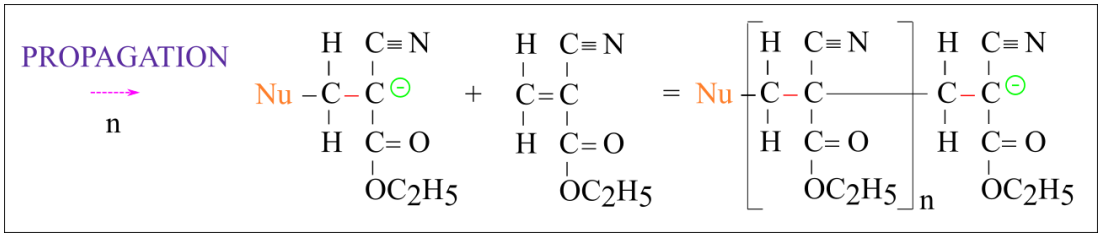

Figure 2.10: Chain propagation step in the polymerisation process of ethyl-2-cyanoacrylate after monomers are activated [76].

The propagation step of the ethyl-2-cyanoacrylate polymerisation will proceed until the point when every single available monomer is expended or until the point, the termination step intervenes [77]. The duration of the propagation process very much relies upon the definite length of the polymer. Eventually, at one point, the growth of the polymer will cease, and the polymerisation will be terminated when a proton is accepted as displayed in Figure 2.11.

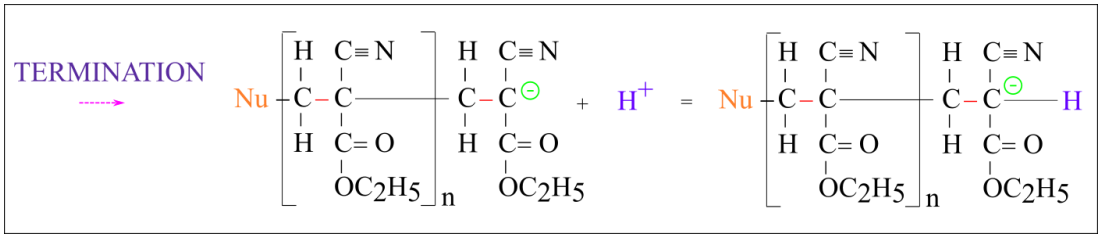

Figure 2.11: Termination step of ethyl-2-cyanoacrylate polymerisation reaction occurs by accepting a proton, H^+.

Knowing that cyanoacrylate polymerisation is initiated by a nucleophile, weak bases, for example, water was thought to be the prominent constituent in fingermark that was responsible to initiate the polymerisation process. Lewis and co-workers confirmed the significance of moisture being present in the fingermark residue prior to fuming. They observed the development of eccrine and sebaceous marks. Eccrine marks exhibited poor quality development due to the loss of moisture whereas sebaceous marks displayed better quality as they tend to retain the moisture better, even though sebaceous constituents do not contribute by themselves in initiating the cyanoacrylate polymerisation [78].

However, further investigations exploring individual fingermark components that could contribute to initiating the cyanoacrylate polymerisation were carried out. Lewis *et al*. suggested in addition to water, fingermark residue contained multiple bases which can initiate cyanoacrylate polymerisation. Wargacki *et al.* reported lactate and alanine components found in eccrine sweat are capable of initiating cyanoacrylate polymerisation by their carboxylate functionality [79]. Presence of sodium chloride (NaCl, salt) in fingermark residue was thought to be essential due to their capability to absorb water when the relative humidity is elevated above 75% which, in turn,

initiates the polymerisation reaction [80]. It is a very well-known fact that the fingermark residue is of complex nature, where combinations of the components present in the fingermark residue contribute for an optimum polymerisation rather than just one constituent in isolation.

Post processing of cyanoacrylate fumed marks

At times marks developed by cyanoacrylate fuming can be hard to visualise or will be lacking in contrast, where further enhancement is required. Hence, applying dusting powders as a post-treatment enables better visualisation of the developed marks [81]. Especially on multi-coloured or shiny backgrounds (e.g. metal substrates, cardboard packaging, and plastic carrier bags), luminescent or fluorescent dyes such as Basic Yellow 40 (BY40) have been most useful for additional contrast enhancement to present a clearer image of the fingermark [82-84]. In the United Kingdom, the number of marks identified after developed by cyanoacrylate fuming is very often enhanced with the staining of fluorescent dye, for example, Basic Yellow 40 and Basic Red 14 that is followed with fluorescence examination. The items needed to be dyed are immersed in the fluorescent dye solution (where fluorescent dye is dissolved in either solvent (usually ethanol) or water) for approximately 1 minute for solvent dissolved dye and approximately 2 minutes for water-based dye. The item is then rinsed with water to discard any excess dye. The item is then allowed to dry with a stream of air at room temperature. For imaging items dyed with BY40, a blue light source emitting a wavelength in the range of 420 – 470 nm with a yellow filter bandpass of excitation wavelength, 510 – 530 nm was used because of its fluorescence in the blue-green region of the spectrum. Sometimes these excitation wavelengths can create high fluorescence in the background for certain types of the materials, where Basic Red 14 is used as the substitute. In order to image the item dyed with Basic Red 14, a green light source is required for excitation along with a red filter as its fluorescence in the orange-red region, with generally much lower background fluorescence [85]. Vapour-phase staining has been suggested to provide contrast and enhance fingermark developed using superglue on surfaces that are made up of materials which are sensitive to solvent, for example, oil marker writings and rough surface materials, for example, unglazed earthenware [86]. The only disadvantage of this method is a mark

can be overdeveloped, where the polymerisation of cyanoacrylate occurs on both the ridges and in between the ridges that reduce the contrast of the developed mark. However, this can be avoided by monitoring closely during the fuming process to remove the item when the fingermark has developed appropriately.

2.2.4.1.2 Iodine Fuming

The second and less commonly used fuming technique is iodine. Iodine crystals are heated up gently to create iodine vapour that is generally purple in colour gets absorbed by the sebaceous material present in the fingermark residue by revealing a pale brown developed mark [87]. Iodine fuming can be used on an extensive variety of both porous and non-porous surfaces, for example, plastic, paper, glass, and wood. Despite this technique being simple and rapid, it has a few disadvantages including the iodine vapour being toxic as well as corrosive, the developed marks rapidly fade upon standing in the air due to iodine sublimation at the room temperature and aged marks are difficult to develop [88]. In order to prolong the developed colour of iodine fumed marks, a few attempts were carried out by chemical fixing using starch, steam or water [89], benzoflavone reagent [90] and very recently with a brucine-based reagent [87].

2.2.4.2 Chemical Reagents

The most preferred chemical reagents to develop fingermarks found on porous surfaces, for example, paper and cardboard are ninhydrin, 1,8-diazofluoren-9-one (DFO) and physical developer [91]. These reagents are applied by either spraying the respective reagent solution, swabbing the solution onto the substrate or submerging the substrate in the solution. Applications of these reagents cause changes in colour where the mark detail is present because of the reaction between the reagents and the amino acids present in the fingermark residue (see Figure 2.12) [35]. It has been demonstrated that optimal results can be attained at higher temperature and humidity [35], whereby in later years analogues of ninhydrin were introduced with the objective of improving the capabilities in fingermark detection [92-94]. Ninhydrin analogues are reagents with a similar structure to ninhydrin itself, however with different

functional groups that react with amino acid [35]. 1,2-Indandione replaced ninhydrin and DFO as the favoured amino acid reagent as it provides the best response in enhancing fingermark left on most porous surfaces, particularly on brown paper and cardboard. Unlike ninhydrin, 1,2-indandione produces a reaction product which can fluoresce rather than developing an intense colour of developed fingermark. The developed marks fluoresce strongly when illuminated with a green light (500 – 550 nm), allowing for best visualisation [93,95].

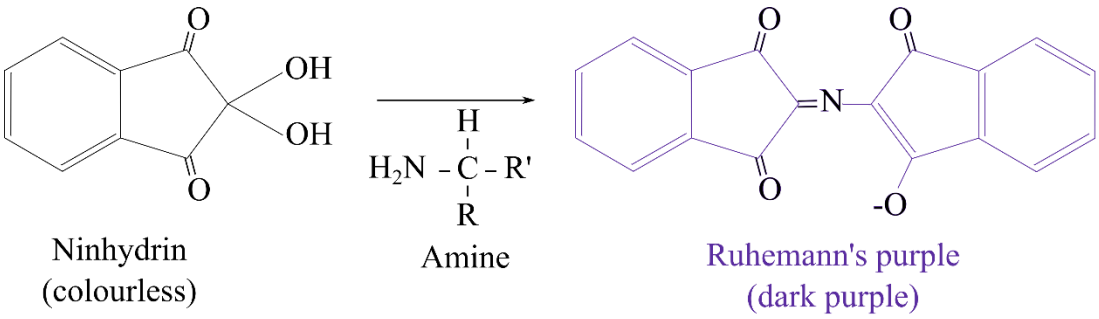

Figure 2.12: Schematic diagram displaying chemical reaction between a primary or secondary amine and ninhydrin which produces the end product of a dark purple colour referred as Ruhemann's purple.

There are several chemical dyes available for enhancing fingermark which depends upon the interactions between the reagent and the sebaceous components within fingermark residue. Crystal Violet (CV), also identified by other names such as Gentian Violet and Basic Violet 3, is of purple shade that stains saturated and unsaturated fat constituents in the sweat by either dissolving into or potentially binding with the lipid components present in fingermark. Crystal Violet also is capable of staining skin cells (epithelial cells) shed from the fingertips if at all present in fingermark residue. Crystal Violet has a net positive charge and so, are attracted towards the epithelial cells that are negatively charged, resulting them to be strongly stained [96]. Crystal Violet proves particularly useful in improving the quality of fingermarks developed by cyanoacrylate fuming technique on adhesive surfaces like Sellotape® [97] and known to be effective on non-porous surfaces like plastics and metals [98,99]. Sudan Black (SB), alternatively known as Solvent Black 3 was demonstrated to work well for developing marks from surfaces that have been

contaminated with oils or grease [96,100-101]. The dye works well on non-porous surfaces like glass, metal or plastic surfaces and used to enhance fingermark developed by cyanoacrylate fuming process [102]. Enhancing fingermark with SB results in a blue-black colouration due to the transfer of the dye molecules into the fatty components of the fingermark residue.

2.2.5 Analytical Techniques

The common circumstance with all techniques depicted earlier demonstrates that when a mark was found on surfaces with backgrounds of either dark or multi-coloured it will be very difficult to visualise the mark due to the lack in contrast between them or cannot be made visible. In recent years, there have been some fascinating approaches to deal with this circumstance by implementing analytical techniques. These techniques are used to visualise fingermarks by operating in the imaging mode that can map the chemical information collected from both the fingermark residue and the surface. These techniques can also be utilised to get additional contextual information from fingermarks developed using other enhancement techniques. Therefore, these techniques could contribute towards beneficial contextual information to an investigation, through the distribution of chemicals present within the fingermark residue and surface of deposition, such as, if at all a person has handled drugs [103] or explosives [104] as well as the order of fingermark deposition and printed text [105].

2.2.5.1 Attenuated total reflection Fourier transform infrared spectroscopy (ATR-FTIR Spectroscopy)

ATR-FTIR spectroscopy is a vibrational spectroscopy technique which relies upon absorption of the infrared (IR) radiation that is totally internally reflected in the ATR mode. This enables the IR to interact with the molecular species present in the compound being studied hence providing the information about the molecular structure characteristics. When the technique is combined with microscopy (usually referred to as microscopic IR spectroscopy) it provides both chemical information and

physical visualisation, allowing to generate an image of the fingermark ridge detail without requiring any reagents to enhance it [106].

The fingermark can be identified using FTIR spectroscopy regardless of the background colour and visual contrast with substrate is because the technique images fingermarks by utilising the different functional groups of the molecular constituents present in the fingermark residue [107]. Thus, this non-invasive technique easily overcomes the trouble in finding fingermarks deposited on surfaces with their backgrounds made up of either writing or images, for example, drink cans and banknotes [108]. This technique requires no additional sample treatment after collection as fingermarks can either be analysed directly with the substrate [109] or after lifting the fingermark from a surface [110].

The technique also allows chemical changes that occur within the fingermark residue to be studied over time by monitoring changes in the intensity spectral band [106,111]. Fingermarks that are developed, for example, with cyanoacrylate fuming technique can also be used to image using this technique [112]. The drawback of this technique is that it cannot identify individual constituents within fingermark residue, as the spectrum provides the information of functional groups within a compound [25].

2.2.5.2 Time of flight secondary ion mass spectrometry (ToF-SIMS)

ToF-SIMS is a mass spectrometry technique capable of generating chemical images of the fingermarks by mapping the presence of both the endogenous and exogenous constituents. The chemical image of a fingermark is produced by scanning an energetic (usually in keV-MeV) ion beam across the sample surface while measuring the molecular species that are ejected from the surface at each point. This is particularly valuable in constructing the distribution maps of a variety of both the inorganic and organic constituents present in the fingermark which includes sodium, potassium, squalene and fatty acids [113].

ToF-SIMS is capable of further enhancing the fingermarks developed with the conventional enhancement technique, for example, cyanoacrylate fuming and wet powders [99]. It can also determine the order of fingermark deposition and ink by

concentrating the ion beam at a single point while gathering molecular information of the point over time as the ion beam etching further into the surface [105,114]. This technique is non-destructive to the fingermarks as it can be repeatedly used to image fingermarks without compromising their quality under the high vacuum imaging conditions [115]. ToF-SIMS is very surface sensitive as it could go down up to 1-2 monolayers with a high lateral resolution of a few tens of nanometres depending on the ion dose and a finely focused ion beam [116]. This technique also has the best resolution in an order of submicron [113]. However, it requires the area that is of interest to be cut small enough from a large item in order to fit inside the imaging chamber of the ToF-SIMS instrument, that will be destructive to the evidence item obtained from a crime scene. Another drawback is that this equipment is still very much specialised and is not generally accessible [117].

2.2.5.3 Matrix-assisted laser desorption ionisation-mass spectrometry (MALDI-MS)

The additional chemical imaging technique includes MALDI-MS. This technique employs a matrix to aid in desorption and ionization procedure of laser desorption ionisation that improves the output of the analyte ions. With the increase in analyte ion output, tandem MS can be carried out to give structural information of the molecule of interest [116]. Fingermarks are imaged in MALDI-MS by creating 2D molecular images and choosing known to be abundant fingermark components such as fatty acids, cholesterol and diacylglycerols to provide a physical image of the fingermark ridge detail [118]. Moreover, chemical information of what an individual has ingested such as, caffeine or dealt with, for instance, drugs, condom lubricants and toiletries can also be obtained [118-120]. MALDI-MS is a non-destructive technique and particularly suitable for detecting large molecules, including triacylglycerol (a major component of human skin oils) species commonly found in fingermarks [121].

2.3 Substrate Effects

The ‘surface’ or also known as ‘substrate’ a fingermark is deposited onto plays a huge effect on formation/generation of the reproduction of fingermark ridge pattern that had

contact with the substrate [122]. There are two vital results that can emerge from the interaction between the fingertip and substrate at the point of deposition, namely positive marks and negative marks, in addition to the most common types of marks encountered in crime investigation described in sub-section 2.2.6. The most commonly found fingermarks in a crime scene are positive marks, where the residue is transferred onto the substrate from the fingertips. However, there are also possibilities for the less common negative marks to be found in the cases when the fingertip picks up dust, the presence of additives or contaminant on the surface, in this manner will end up leaving a negative impression of fingermark ridge detail in the material that remains on the substrate [123,124].

The initial interaction between the fingertips and surface influences the type of mark that is formed, while the interaction that occurs between the fingermark components and the substrate after deposition determines if the mark continues to remain and is possible for enhancement. Thus, the properties of the substrate are important as they influence the fingermark deposition and affect the fingermark once it has been transferred onto the substrate. The composition of fingermark, the environment the substrate and the mark are exposed to after deposition, and nature of the substrate the mark has been deposited onto plays an important role in choosing the right technique that will probably be the most effective in enhancing the fingermark. The interaction of fingermark, environment and substrate can be described by the concept known as 'Triangle of Interaction' [3,125].

The surface properties that play a significant role by interacting with both the fingermark composition and environment are porosity of the surface and surface chemistry. Porosity of a surface is divided into three main categories including porous, semi-porous and non-porous. Table 2.3 lists the substrate's porosity and describes their respective interactions between fingermark constituents with example substrates encountered in daily life as well as techniques used to develop the marks deposited onto each type of substrates.

Other important substrate properties that influence the interaction which occurs when a fingertip touches a surface are the substrate's physical properties and surface chemistry. Wettability of a substrate is one of the physical properties that influence the fingermark deposition onto a substrate. The affinity of a substrate species for water

(hydrophobic or hydrophilic) for most non-porous substrates, determines how a fingermark spreads across the surface (e.g. either it forms droplets or not), but does not penetrate it [126].

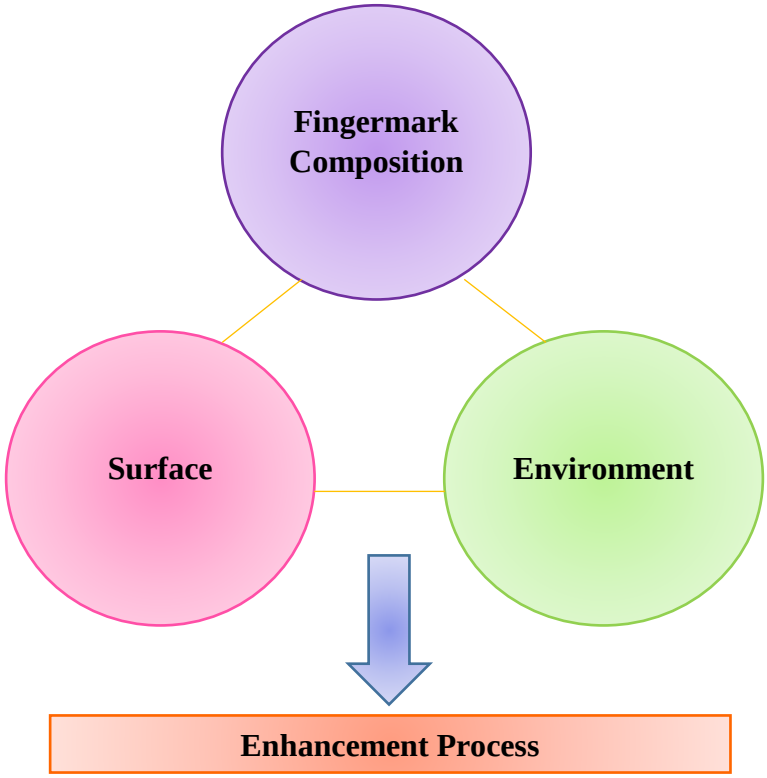

Figure 2.13: Schematic representation of the 'triangle of interaction' concept, adapted from Reference [3].

After fingermark deposition, the reactivity of substrate determines if any chemical reaction is expected to happen either at the surface or fingermark interface. The situation described is for a specific kind of metal substrates that can chemically react with the constituents that are present in the fingermark residue that leads to either etching or corrosion of the metal substrates [127].

The degree of differences in chemical properties of the fingermark residue and the substrate affects the assessment of a technique adequacy since fingermark enhancement relies upon the interaction/reaction with chemical targets in the mark as well as the substrate it is deposited onto. As described in earlier subsections, the type of the surface the fingermark is deposited onto plays a pivotal role in selecting the most effective enhancement process.

Substrate Porosity	The interaction between fingermarks and the surface	Examples	Techniques used to develop the marks
Porous	• Rapid absorption of water soluble fingermark residue components (amino acids, urea and chlorides) following deposition • Penetration depth relies upon: level of porosity and the overall size of every components e.g. amino acids that are generally bigger in size than urea molecules will penetrate lesser into the surface	Paper, cardboard, wood	Ninhydrin / Amino acid treatment
Semi-porous	• Surfaces that falls in the middle of porous and non-porous • Absorbs water soluble constituents at a much more slower rate than porous substrates • Lipid-soluble residue will remain on the surface at a longer period of time than on a porous surface	Varnished wood, waxed surfaces, glossy papers	Developed with procedures recommended for both porous and non-porous substrates
Non-porous	• Does not absorb any of the component present in the fingermark residue • Fingermark will remain as a complete emulsion (both water and lipid soluble components) on the substrate surface	Glass, metal, plastics	Cyanoacrylate (CNA) fuming, staining with dyes, powder dusting and vacuum metal deposition (VMD)

Table 2.3: Summary of the interaction between fingermarks and different types of substrate's porosity with the techniques used to develop the latent marks on the respective substrate. [16,29]

2.3.1 Interaction between substrate, environment and fingermark

After fingermark deposition, time plays a very important role in what manner the environment would influence the fingermark and the substrate. This is because fingermarks encountered in a crime scene are seldom freshly deposited fingermarks, instead, they could be expected to be left in a span of few days up to several years before investigated by crime scene investigators [128]. Knowing an estimated time and environmental exposure conditions of both fingermark and the substrate, is therefore, beneficial to the investigation in choosing the most suitable sequence of fingermark enhancement techniques.

In general, the indoor environment is regarded as more protected from the harsh environmental conditions and controlled, however, there are possibilities for the substrates and fingermarks getting exposed to other types of settings including air flow, heat, humidity, airborne substances and light. Indoor environments can affect substrates with fingermarks as they are exposed to the movement of air flow across them (by a fan and air conditioning), consequently the fingermark constituents get dried off. In addition to that, moving air can contain dust particles including fragments of fibers from textiles, paper products, skin cells that were shed off could end up attaching to the fingermark. In certain circumstances, these particles will be favoured by fingermark enhancement techniques and shield the reagents from interacting with the fingermark constituents [129]. The effect of exposure to airflow and indirect light during the aging process on the enhancement of sebaceous fingermarks was explored by Wargacki *et al.* They found that quality of the sebaceous marks left to age dropped drastically as a function of time for marks that were placed under light and air flow when developed by the cyanoacrylate fuming method [130].

In the UK, outdoor temperatures are well within the limits of 1-22°C according to statistics [131] while indoor temperatures are more controlled with the use of heating and cooling systems. These low temperatures will not cause any changes in fingermark residue as only when the temperatures are elevated, changes occurring in both the fingermark constituents and substrate can be observed. Some of the effects that may be observed on fingermark constituents at high temperatures include evaporation of volatile constituents, acceleration in the drying of fingermark residue and oxidation of

some constituents, while substrates can be deformed, burned and oxidised. This is supported by Johnston *et al.*'s observation that certainly at temperatures 25°C and 35°C there are no changes observed within the fingermark constituents up to 5 hours, however, if the fingermarks were to be left longer at these temperatures temporal degradation was observed using FTIR microspectroscopy [132]. In a similar way, changes in the substrate's physical state or composition can only happen at elevated temperatures.

The relative humidity of air corresponds to the ratio of water vapour present in the air to the amount of water vapour could be present at a specific temperature. This can influence the rate of evaporation of water if any was present in the fingermark or the surface. In the indoor environment, changes in relative humidity can occur by reducing the temperature of air by air conditioning or increasing the temperature of air with central heating. Fingermarks absorbing water from the ambient air when relative humidity is high were studied by Merkel *et al.* who concluded that the speed of the aging process is much slower at higher relative humidity [133]. Moisture absorption from the air by non-porous surfaces, such as nylon polymers are possible due to their hygroscopic nature can significantly affect the fingermark composition when exposed to high humidity.

Light exposure has been identified to affect fingermark composition and more rapidly when exposed to ultraviolet radiation, from sunlight [19]. Considering most of the ultraviolet radiation from sunlight is blocked by the standard window glass blocks, surfaces indoors are less prone to be affected by the ultraviolet radiation. However, specific components in the fingermark residue tend to degrade faster when exposed to indoor-light. This observation is supported by investigation made by Archer *et al.* where the sebaceous component, particularly fatty acids in fingermark residue displayed a rapid loss when stored under light [134]. The impact of being exposed to light on the enhancement of both sebaceous and eccrine latent fingermarks over time via powder development was studied by De Alcaraz-Fossoul *et al.* [135]. In their study, they observed a range of visual degradation on both types of sweat after a week of fingermark deposition.

2.4 Importance of Substrate Wettability in Fingermark Deposition and Development

It should be apparent from the discussion in section 2.3 that deposition of latent fingermarks and success in detecting the fingermarks are greatly influenced by the nature of the underlying substrate the marks were deposited onto. Therefore, we might expect that a substrate's properties will influence the effectiveness or performance of conventional fingermark development techniques. Whilst experimental work in this field is relatively sparse, some studies have been performed to suggest that substrates do indeed influence deposition and influence the efficiency of fingermark development. The efficiency of fingermark development is also attributed to the substantial variability in latent fingermarks [136] as the quality and number of developed fingermarks by the same donor on the same substrate differs significantly [137] leading to the complexity of sampling fingermarks.

Scruton *et al.* showed that the distribution of material within a fingermark deposit depends on the composition of fingermark residue and nature of the substrate it is transferred onto by taking either the form of continuous pools of material or by large irregularly shaped islands of material [17]. They observed a continuous film of sebaceous deposit on substrates of contact angle less than 70° while eccrine sweat formed droplets on substrates of either low or high surface energy.

Jones *et al.* showed that understanding the nature of the substrate is important in determining the optimum fingermark development by vacuum metal deposition (VMD) [138]. VMD comprises two-stage vacuum process where gold metal is evaporated and deposited followed by a similar process with the zinc metal. The gold particles situated between the fingermark ridges act as nucleation sites for the metal, zinc. They observed that the structure and thickness of the gold film is a critical factor in determining whether additional gold deposition continues to act as the nucleation sites or not. The results indicated that difference in polymer structure of low-density polyethylene (LDPE) with high-density polyethylene (HDPE) affected formation of the gold film structure whereby gold clusters on LDPE are larger and more spread out leading to no gold clusters to serve as binding sites for zinc, and therefore, resulted in no zinc deposition on this surface.

While the effects of surface chemistry have been briefly investigated, no studies have yet been published indicating how the surface wettability might affect the development of latent fingermark. Recent reports have expressed concern at the very limited state of knowledge concerning the degree of surface interaction, associated with surface wettability (i.e. hydrophilicity or hydrophobicity) that is defined by water contact angle measurement of the surface [121].

Interactions between fingermark and surface wettability currently represent a relatively unknown result in the development of fingermarks. In chapter 4, we focus systematically on elucidating the role played by surface wettability in developing latent fingermark via cyanoacrylate fuming method.

References

1. Wolstenholme, R., Bradshaw, R., Clench, M. R., & Francese, S. (2009). Study of latent fingermarks by matrix-assisted laser desorption/ionisation mass spectrometry imaging of endogenous lipids. *Rapid Communications in Mass Spectrometry: An International Journal Devoted to the Rapid Dissemination of Up-to-the-Minute Research in Mass Spectrometry*, *23*(19), 3031-3039.

2. Emerson, B., Gidden, J., Lay Jr, J. O., & Durham, B. (2011). Laser desorption/ionization time-of-flight mass spectrometry of triacylglycerols and other components in fingermark samples. *Journal of forensic sciences*, *56*(2), 381-389.

3. Sears, V. G., Bleay, S. M., Bandey, H. L., & Bowman, V. J. (2012). A methodology for finger mark research. *Science & Justice*, *52*(3), 145-160.

4. Neumann, C. (2012). Fingerprints at the crime-scene: Statistically certain, or probable?. Significance, 9(1), 21-25.

5. Barnes, J.G. (2011). Chapter 1: History. *The Fingerprint Sourcebook, US Dept. of Justice, Office of Justice Programs, National Institute of Justice, Washington, DC*, pp. 1-7 – 1-22.

6. Gaensslen, R. E., Ramotowski, R., & Lee, H. C. (2001). Chapter 1: History and Development of Fingerprinting. *Advances in fingerprint technology*. CRC press, pp. 14.

7. Stigler, S. M. (1995). Galton and identification by fingerprints. *Genetics*, *140*(3), 857.

8. Henry Classification System, *International Biometric Group*, 2003, New York.

9. White, P. (Ed.). (2010). *Crime Scene to Court: The Essentials of Forensic Science*. Royal Society of Chemistry, pp. 156.

10. Northumbria Police, Crime Scene Investigation, https://www.northumbria.police.uk/about_us/crime_scene_investigation/fingerprint_bureau/ten_prints/ (Accessed on 6th August 2018).

11. Homeland Security, https://www.homelandsecurity-technology.com/projects/ident1-automated-fingerprint-system-northrop-grumman-uk/ (Accessed on 6th August 2018).

12. Jackson, A. R., & Jackson, J. M. (2004). *Forensic Science*. Pearson Education, pp. 86.

13. Hicklin, R. A. (2015). Anatomy of Friction Ridge Skin. *Encyclopedia of Biometrics*, 14-19.

14. Horswell, J. (Ed.). (2004). *The practice of crime scene investigation*. CRC Press, pp. 46.

15. Olsen, R. D. (1972). The chemical composition of palmar sweat. *Fingerprint and Identification Magazine*, *53*(10), 3-23.

16. Girod, A., Ramotowski, R., & Weyermann, C. (2012). Composition of fingermark residue: a qualitative and quantitative review. *Forensic science international*, *223*(1-3), 10-24.

17. Scruton, B., Robins, B. W., & Blott, B. H. (1975). The deposition of fingerprint films. *Journal of Physics D: Applied Physics*, *8*(6), 714.

18. Ramotowski, R. S. (2001). Composition of latent print residue. *Advances in fingerprint technology*, *2*, pp. 63-104.

19. Cadd, S., Islam, M., Manson, P., & Bleay, S. (2015). Fingerprint composition and aging: a literature review. *Science & Justice*, *55*(4), 219-238.

20. Knowles, A. M. (1978). Aspects of physicochemical methods for the detection of latent fingerprints. *Journal of Physics E: Scientific Instruments*, *11*(8), 713.

21. Buchanan, M. V., Asano, K., & Bohanon, A. (1997, February). Chemical characterization of fingerprints from adults and children. In *Forensic Evidence Analysis and Crime Scene Investigation* (Vol. 2941, pp. 89-96). International Society for Optics and Photonics.

22. Antoine, K. M., Mortazavi, S., Miller, A. D., & Miller, L. M. (2010). Chemical differences are observed in children's versus adults' latent fingerprints as a function of time. *Journal of Forensic Sciences*, *55*(2), 513-518.

23. Bohanan, A. M. (1998). Latents from pre-pubescent children versus latents from adults. *Journal of Forensic Identification*, *48*(5), 570.

24. Weyermann, C., & Ribaux, O. (2012). Situating forensic traces in time. *Science & Justice*, *52*(2), 68-75.

25. Bleay, S. M., Croxton, R. S., & De Puit, M. (2018). 3. Chemical composition of fingermarks. Fingerprint Development Techniques: Theory and Application. John Wiley & Sons, pp. 49-55.

26. Harper, D. R., Clare, C. M., Heaps, C. D., Brennan, J., & Hussain, J. (1987). A bacteriological technique for the development of latent fingerprints. *Forensic Science International*, *33*(3), 209-214.

27. Croxton, R. S., Baron, M. G., Butler, D., Kent, T., & Sears, V. G. (2010). Variation in amino acid and lipid composition of latent fingerprints. *Forensic Science International*, *199*(1-3), 93-102.

28. Bumbrah, G. S., Sharma, R. M., & Jasuja, O. P. (2016). Emerging latent fingerprint technologies: a review. *Research and Reports in Forensic Medical Science*, *6*, 39-50.

29. Yamashita, B., & French, M. (2011). Chapter 7: Latent print development. *The Fingerprint Sourcebook, US Dept. of Justice, Office of Justice Programs, National Institute of Justice, Washington, DC*, pp. 7.1-7.67.

30. Kent, T. (2016). Section 2: Chemistry and Visualization (Sequential Treatment and Enhancement). *Forensic Fingerprints*. Academic Press, pp. 40-41.

31. Bleay, S. M., Croxton, R. S., & De Puit, M. (2018). 6. Optical detection and enhancement techniques. *Fingerprint Development Techniques: Theory and Application*. John Wiley & Sons, pp. 111-144.

32. Lennard, C. (2001, October). The detection and enhancement of latent fingerprints. In *13th INTERPOL Forensic Science Symposium, Lyon, France* (pp. 16-19). US Department of Justice.

33. Bleay, S. M., Sears, V. G., Bandey, H. L., Gibson, A. P., Bowman, V. J., Downham, R., Fitzgerald, L., Ciuksza, T., Ramadani, J. & Selway, C. (2012). Finger mark examination techniques within scope of ISO 17025 (2.2 Fluorescence examination). *Fingerprint Source Book, Home Office Centre for Applied Science and Technology (CAST)*, pp.18-25.

34. Kent, T. (2016). Section 2: Chemistry and Visualization (Visualization or development of Crime Scene Fingerprints). *Forensic Fingerprints*. Academic Press, pp. 43-57.

35. Lennard, C. J., Champod, C., Margot, P., & Stoilovic, M. (2004). Chapter 4: Fingermark detection and Enhancement. *Fingerprints and other ridge skin impressions*. CRC press, pp. 112-132.

36. Horiba Products, SceneScope RUVIS UHD System, https://www.horiba.com/en_en/products/detail/action/show/Product/scenescope-ruvis-uhd-system-1839/ (Accessed on 16th August 2018).

37. Richards, A., & Partner, O. P. (2010). Reflected ultraviolet imaging for forensics applications. *Online] http://www. uvcorder. com/pdf/Reflected_UV_Imaging_for_Forensics_V2. pdf*.

38. King, R. S., Davis, L. W., & Skros, D. A. (2018). The Use of Longwave Reflected UV Imaging for the Enhancement of Cyanoacrylate Developed

Fingermarks; a Simple, Safe and Effective Imaging Tool. *Forensic Science International*.

39. Bramble, S. K., Cantu, A. A., Ramotowski, R. S., & Brennan, J. S. (2000). Deep red to near infrared (NIR) fluorescence on gentian violet-treated latent prints. *Journal of Forensic Identification*, *50*(1), 33-49.

40. Bleay, S. M., & Kent, T. (2005). The use of infra-red filters to remove background patterns in fingerprint imaging. *Fingerprint Whorld*, *31*(122), 225-238.

41. Sodhi, G. S., & Kaur, J. (2001). Powder method for detecting latent fingerprints: a review. *Forensic science international*, *120*(3), 172-176.

42. Olsen, R. D. (1978). *Scott's fingerprint mechanics*. C.C. Thomas.

43. Menzel, E. R. (1980). *Fingerprint detection with lasers*. New York: M. Dekker, (pp. 45-78).

44. Kerr, F. M., Haque, F., & Westland, A. D. (1983). "Organic Based Powders for Fingerprint Detection on Smooth Surfaces": Part I. *Canadian Society of Forensic Science Journal*, *16*(3), 140-142.

45. Goode, G. C., & Morris, J. R. (1983). *Latent fingerprints: A review of their origin, composition and methods for detection*. Atomic Weapons Research Establishment, Aldermaston.

46. Choi, M. J., Smoother, T., Martin, A. A., McDonagh, A. M., Maynard, P. J., Lennard, C., & Roux, C. (2007). Fluorescent TiO2 powders prepared using a new perylene diimide dye: Applications in latent fingermark detection. *Forensic Science International*, *173*(2-3), 154-160.

47. Sodhi, G. S., & Kaur, J. (2000). Organic Fingerprint Powders Based on Fluorescent Phloxine B Dye. *Defence Science Journal*, *50*(2), 213.

48. Choi, M. J., McBean, K. E., Ng, P. H. R., McDonagh, A. M., Maynard, P. J., Lennard, C., & Roux, C. (2008). An evaluation of nanostructured zinc oxide as a fluorescent powder for fingerprint detection. *Journal of Materials Science*, *43*(2), 732-737.

49. Choi, M. J., Smoother, T., Martin, A. A., McDonagh, A. M., Maynard, P. J., Lennard, C., & Roux, C. (2007). Fluorescent TiO2 powders prepared using a new perylene diimide dye: Applications in latent fingermark detection. *Forensic Science International*, *173*(2-3), 154-160.

50. Wilshire, B. (1996). Advances in fingerprint detection. *Endeavour*, *20*(1), 12-15.

51. MacDonell, H. L. (1961). Bristleless brush development of latent fingerprints. *Ident. News*, *11*(3), 7-15.

52. James, J. D., Pounds, C. A., & Wilshire, B. (1991). Flake metal powders for revealing latent fingerprints. *Journal of Forensic Science*, *36*(5), 1368-1375.

53. James, J. D., Pounds, C. A., & Wilshire, B. (1991). Production and characterisation of flake metal powders for fingerprint detection. *Powder Metallurgy*, *34*(1), 39-44.

54. James, J. D., Pounds, C. A., & Wilshire, B. (1993). Magnetic flake powders for fingerprint development. *Journal of Forensic Science*, *38*(2), 391-401.

55. Seah, L. K., Dinish, U. S., Phang, W. F., Chao, Z. X., & Murukeshan, V. M. (2005). Fluorescence optimisation and lifetime studies of fingerprints treated with magnetic powders. *Forensic science international*, *152*(2-3), 249-257.

56. Gaensslen, R. E., Ramotowski, R., & Lee, H. C. (2001). Chapter 4: Methods of Latent Fingerprint Development. *Advances in fingerprint technology*. CRC press, pp. 113.

57. Pounds, C. A., & Jones, R. J. (1981). The use of powder suspensions for developing latent fingerprints. *Home Office Central Research Establishment (HOCRE), Aldermaston, England*.

58. Jasuja, O. P., Singh, G. D., & Sodhi, G. S. (2008). Small particle reagents: development of fluorescent variants. *Science & Justice*, *48*(3), 141-145.

59. Sodhi, G. S., & Kaur, J. (2012). A novel fluorescent small particle reagent for detecting latent fingerprints on wet non-porous items. *Egyptian Journal of Forensic Sciences*, *2*(2), 45-47.

60. Polimeni, G., Foti, B. F., Saravo, L., & De Fulvio, G. (2004). A novel approach to identify the presence of fingerprints on wet surfaces. *Forensic science international*, *146*, S45-S46.

61. Cuce, P., Polimeni, G., Lazzaro, A. P., & De Fulvio, G. (2004). Small particle reagents technique can help to point out wet latent fingerprints. *Forensic science international*, *146*, S7-S8.

62. Reynolds, A. J., Jones, B. J., Sears, V., & Bowman, V. (2008). Nano-scale analysis of titanium dioxide fingerprint-development powders. In *Journal of Physics: Conference Series* (Vol. 126, No. 1, p. 012069). IOP Publishing.

63. Haque, F., Westland, A. D., Milligan, J., & Kerr, F. M. (1989). A small particle (iron oxide) suspension for detection of latent fingerprints on smooth surfaces. *Forensic Science International*, *41*(1-2), 73-82.

64. Rohatgi, R., & Kapoor, A. K. (2016). Development of latent fingerprints on wet non-porous surfaces with SPR based on basic fuchsin dye. *Egyptian Journal of Forensic Sciences*, *6*(2), 179-184.

65. Bleay, S. M., Croxton, R. S., & De Puit, M. (2018). 12. Liquid phase selective deposition techniques. *Fingerprint Development Techniques: Theory and Application*. John Wiley & Sons, pp. 326-330.

66. Bumbrah, G. S. (2016). Small particle reagent (SPR) method for detection of latent fingermarks: A review. *Egyptian Journal of Forensic Sciences*, *6*(4), 328-332.

67. Trapecar, M. (2009). Lifting techniques for finger marks on human skin previous enhancement by Swedish Black powder—A preliminary study. *Science & Justice*, *49*(4), 292-295.

68. West, M. J., & Went, M. J. (2008). The spectroscopic detection of exogenous material in fingerprints after development with powders and recovery with adhesive lifters. *Forensic Science International*, *174*(1), 1-5.

69. Rowell, F., Seviour, J., Lim, A. Y., Elumbaring-Salazar, C. G., Loke, J., & Ma, J. (2012). Detection of nitro-organic and peroxide explosives in latent

fingermarks by DART-and SALDI-TOF-mass spectrometry. *Forensic Science International*, *221*(1-3), 84-91.

70. West, M. J., & Went, M. J. (2009). The spectroscopic detection of drugs of abuse in fingerprints after development with powders and recovery with adhesive lifters. *Spectrochimica Acta Part A: Molecular and Biomolecular Spectroscopy*, *71*(5), 1984-1988.

71. Rowell, F., Hudson, K., & Seviour, J. (2009). Detection of drugs and their metabolites in dusted latent fingermarks by mass spectrometry. *Analyst*, *134*(4), 701-707.

72. Chesher, B. K., Stone, J. M., & Rowe, W. F. (1992). Use of the Omniprint™ 1000 alternate light source to produce fluorescence in cyanoacrylate-developed latent fingerprints stained with biological stains and commercial fabric dyes. *Forensic science international*, *57*(2), 163-168.

73. Czekanski, P., Fasola, M., & Allison, J. (2006). A mechanistic model for the superglue fuming of latent fingerprints. *Journal of forensic sciences*, *51*(6), 1323-1328.

74. Mankidy, P. J., Rajagopalan, R., & Foley, H. C. (2008). Influence of initiators on the growth of poly (ethyl 2-cyanoacrylate) nanofibers. *Polymer*, *49*(9), 2235-2242.

75. Coover, H. W., Dreifus, D. W., & O'connor, J. T. (1990). Cyanoacrylate adhesives. In *Handbook of adhesives* (pp. 463-477). Springer, Boston, MA, pp. 466.

76. Day, J. S., Edwards, H. G., Dobrowski, S. A., & Voice, A. M. (2004). The detection of drugs of abuse in fingerprints using Raman spectroscopy II: cyanoacrylate-fumed fingerprints. *Spectrochimica Acta Part A: Molecular and Biomolecular Spectroscopy*, *60*(8-9), 1725-1730.

77. Duffy, C., Zetterlund, P. B., & Aldabbagh, F. (2018). Radical polymerization of alkyl 2-cyanoacrylates. *Molecules*, *23*(2), 465.

78. Lewis, L. A., Smithwick, R. W., Devault, G. L., Bolinger, B., & Lewis, S. A. (2001). Processes involved in the development of latent fingerprints using the cyanoacrylate fuming method. *Journal of Forensic Science*, *46*(2), 241-246.

79. Wargacki, S. P., Lewis, L. A., & Dadmun, M. D. (2007). Understanding the chemistry of the development of latent fingerprints by superglue fuming. *Journal of forensic sciences*, *52*(5), 1057-1062.

80. Farrugia, K. J., Fraser, J., Friel, L., Adams, D., Attard-Montalto, N., & Deacon, P. (2015). A comparison between atmospheric/humidity and vacuum cyanoacrylate fuming of latent fingermarks. *Forensic science international*, *257*, 54-70.

81. Liu, L., Zhang, Z., Zhang, L., & Zhai, Y. (2009). The effectiveness of strong afterglow phosphor powder in the detection of fingermarks. *Forensic Science International*, *183*(1-3), 45-49.

82. Farrugia, K. J., Fraser, J., Calder, N., & Deacon, P. (2014). Pseudo-Operational Trials of Lumicyano Solution and Lumicyano Powder for the Detection of Latent Fingermarks on Various Substrates. *Journal of Forensic Identification*, *64*(6).

83. Farrugia, K. J., Deacon, P., & Fraser, J. (2014). Evaluation of Lumicyano™ cyanoacrylate fuming process for the development of latent fingermarks on plastic carrier bags by means of a pseudo operational comparative trial. *Science & Justice*, *54*(2), 126-132.

84. Dominick, A. J., & Laing, K. (2011). A comparison of six fingerprint enhancement techniques for the recovery of latent fingerprints from unfired cartridge cases. *Journal of Forensic Identification*, *61*(2), 155-165.

85. Bleay, S. M., Croxton, R. S., & De Puit, M. (2018). 7. Vapour phase techniques. Fingerprint Development Techniques: Theory and Application. John Wiley & Sons, pp. 159-171.

86. Takatsu, M., Shimoda, O., & Teranishi, H. (2012). Vapor-phase Staining of Cyanoacrylate-Fumed Latent Fingerprints Using p-Dimethylaminobenzaldehyde. *Journal of forensic sciences*, *57*(2), 515-520.

87. Jasuja, O. P., Kaur, A., & Kumar, P. (2012). Fixing latent fingermarks developed by iodine fuming: A new method. *Forensic science international*, *223*(1-3), e47-e52.

88. Jasuja, O. P., & Singh, G. (2009). Development of latent fingermarks on thermal paper: Preliminary investigation into use of iodine fuming. *Forensic Science International*, *192*(1-3), e11-e16.

89. Almog, J., Sasson, Y., & Anati, A. (1979). Chemical reagents for the development of latent fingerprints. II: controlled addition of water vapor to iodine fumes—a solution to the aging problem. *Journal of Forensic Science*, *24*(2), 431-436.

90. Haque, F., Westland, A., & Kerr, F. M. (1983). An improved non-destructive method for detection of latent fingerprints on documents with iodine-7, 8-benzoflavone. *Forensic Science International*, *21*(1), 79-83.

91. Bowman, V. (2004). Manual of fingerprint development techniques, 2nd edition. *Sandridge: Home Office Police Scientific Development Branch*.

92. Conn, C., Ramsay, G., Roux, C., & Lennard, C. (2001). The effect of metal salt treatment on the photoluminescence of DFO-treated fingerprints. *Forensic science international*, *116*(2-3), 117-123.

93. Berdejo, S., Rowe, M., & Bond, J. W. (2012). Latent Fingermark Development on a Range of Porous Substrates Using Ninhydrin Analogs—A Comparison with Ninhydrin and 1, 8-Diazofluoren. *Journal of forensic sciences*, *57*(2), 509-514.

94. Hansen, D. B., & Joullié, M. M. (2005). The development of novel ninhydrin analogues. *Chemical Society Reviews*, *34*(5), 408-417.

95. Bicknell, D. E., & Ramotowski, R. S. (2008). Use of an optimized 1, 2-indanedione process for the development of latent prints. *Journal of Forensic Sciences*, *53*(5), 1108-1116.

96. Bleay, S. M., Croxton, R. S., & De Puit, M. (2018). 11. Lipid reagents. Fingerprint Development Techniques: Theory and Application. John Wiley & Sons, pp. 283-295.

97. Wilson, H. D. (2010). RAY dye stain versus gentian violet and alternate powder for development of latent prints on the adhesive side of tape. *Journal of Forensic Identification*, *60*(5), 510.

98. Kobus, H. J., Warrener, R. N., & Stoilovic, M. (1983). Two simple staining procedures which improve the contrast and ridge detail of fingerprints developed with "Super Glue"(cyanoacrylate ester). *Forensic Science International*, *23*(2-3), 233-240.

99. Bailey, M. J., Ismail, M., Bleay, S., Bright, N., Elad, M. L., Cohen, Y., Geller, B., Everson, D., Costa, C., Webb, R.P. & Watts, J. F. (2013). Enhanced imaging of developed fingerprints using mass spectrometry imaging. *Analyst*, *138*(21), 6246-6250.

100. Cadd, S. J., Bleay, S. M., & Sears, V. G. (2013). Evaluation of the solvent black 3 fingermark enhancement reagent: part 2—investigation of the optimum formulation and application parameters. *Science & Justice*, *53*(2), 131-143.

101. Gaskell, C., Bleay, S. M., Willson, H., & Park, S. (2013). The Enhancement of Fingermarks on Grease-Contaminated, Nonporous Surfaces: A Comparative Assessment of Processes for Light and Dark Surfaces. *Journal of Forensic Identification*, *63*(3), 286.

102. Tilstone, W. J., Savage, K. A., & Clark, L. A. (2006). *Forensic science: An encyclopedia of history, methods, and techniques*. ABC-CLIO, pp. 151.

103. Groeneveld, G., De Puit, M., Bleay, S., Bradshaw, R., & Francese, S. (2015). Detection and mapping of illicit drugs and their metabolites in fingermarks by MALDI MS and compatibility with forensic techniques. *Scientific reports*, *5*, 11716.

104. Mou, Y., & Rabalais, J. W. (2009). Detection and identification of explosive particles in fingerprints using attenuated total reflection-Fourier transform infrared spectromicroscopy. *Journal of forensic sciences*, *54*(4), 846-850.

105. Attard-Montalto, N., Ojeda, J. J., Reynolds, A., Ismail, M., Bailey, M., Doodkorte, L., de Puit, M. & Jones, B. J. (2014). Determining the chronology

of deposition of natural fingermarks and inks on paper using secondary ion mass spectrometry. *Analyst*, *139*(18), 4641-4653.

106. Ricci, C., Phiriyavityopas, P., Curum, N., Chan, K. A., Jickells, S., & Kazarian, S. G. (2007). Chemical imaging of latent fingerprint residues. *Applied spectroscopy*, *61*(5), 514-522.

107. Worley, C. G., Wiltshire, S. S., Miller, T. C., Havrilla, G. J., & Majidi, V. (2006). Detection of visible and latent fingerprints using micro-x-ray fluorescence elemental imaging. *Journal of forensic sciences*, *51*(1), 57-63.

108. Tahtouh, M., Despland, P., Shimmon, R., Kalman, J. R., & Reedy, B. J. (2007). The application of infrared chemical imaging to the detection and enhancement of latent fingerprints: method optimization and further findings. *Journal of forensic sciences*, *52*(5), 1089-1096.

109. Crane, N. J., Bartick, E. G., Perlman, R. S., & Huffman, S. (2007). Infrared spectroscopic imaging for noninvasive detection of latent fingerprints. *Journal of forensic sciences*, *52*(1), 48-53.

110. Ricci, C., & Kazarian, S. G. (2010). Collection and detection of latent fingermarks contaminated with cosmetics on nonporous and porous surfaces. *Surface and Interface Analysis: An International Journal devoted to the development and application of techniques for the analysis of surfaces, interfaces and thin films*, *42*(5), 386-392.

111. Girod, A., Xiao, L., Reedy, B., Roux, C., & Weyermann, C. (2015). Fingermark initial composition and aging using Fourier transform infrared microscopy (μ-FTIR). *Forensic science international*, *254*, 185-196.

112. Tahtouh, M., Kalman, J. R., Roux, C., Lennard, C., & Reedy, B. J. (2005). The detection and enhancement of latent fingermarks using infrared chemical imaging. *Journal of Forensic Science*, *50*(1), JFS2004213-9.

113. Bailey, M. J., Bright, N. J., Croxton, R. S., Francese, S., Ferguson, L. S., Hinder, S., Jickells, S., Jones, B.J., Jones, B.N., Kazarian, S.G. & Ojeda, J. J. (2012). Chemical characterization of latent fingerprints by matrix-assisted laser desorption ionization, time-of-flight secondary ion mass spectrometry,

mega electron volt secondary mass spectrometry, gas chromatography/mass spectrometry, X-ray photoelectron spectroscopy, and attenuated total reflection Fourier transform infrared spectroscopic imaging: an intercomparison. *Analytical chemistry*, *84*(20), 8514-8523.

114. Bright, N. J., Webb, R. P., Bleay, S., Hinder, S., Ward, N. I., Watts, J. F., Kirkby, K.J. & Bailey, M. J. (2012). Determination of the deposition order of overlapping latent fingerprints and inks using secondary ion mass spectrometry. *Analytical chemistry*, *84*(9), 4083-4087.

115. Thandauthapani, T. D., Reeve, A. J., Long, A. S., Turner, I. J., & Sharp, J. S. (2018). Exposing latent fingermarks on problematic metal surfaces using time of flight secondary ion mass spectroscopy. *Science & Justice*, *58*(6), 405-414.

116. Wei, Q., Zhang, M., Ogorevc, B., & Zhang, X. (2016). Recent advances in the chemical imaging of human fingermarks (a review). *Analyst*, *141*(22), 6172-6189.

117. Bleay, S. M., Croxton, R. S., & De Puit, M. (2018). 15. Miscellaneous processes: lifting and specialist imaging. Fingerprint Development Techniques: Theory and Application. John Wiley & Sons, pp. 401-416.

118. Wolstenholme, R., Bradshaw, R., Clench, M. R., & Francese, S. (2009). Study of latent fingermarks by matrix-assisted laser desorption/ionisation mass spectrometry imaging of endogenous lipids. *Rapid Communications in Mass Spectrometry: An International Journal Devoted to the Rapid Dissemination of Up-to-the-Minute Research in Mass Spectrometry*, *23*(19), 3031-3039.

119. Bradshaw, R., Wolstenholme, R., Blackledge, R. D., Clench, M. R., Ferguson, L. S., & Francese, S. (2011). A novel matrix-assisted laser desorption/ionisation mass spectrometry imaging based methodology for the identification of sexual assault suspects. *Rapid Communications in Mass Spectrometry*, *25*(3), 415-422.

120. Ferguson, L., Bradshaw, R., Wolstenholme, R., Clench, M., & Francese, S. (2011). Two-step matrix application for the enhancement and imaging of latent fingermarks. *Analytical chemistry*, *83*(14), 5585-5591.

121. O'neill, K. C., & Lee, Y. J. (2018). Effect of Aging and Surface Interactions on the Diffusion of Endogenous Compounds in Latent Fingerprints Studied by Mass Spectrometry Imaging. *Journal of forensic sciences*, *63*(3), 708-713.

122. Bleay, S. M., Croxton, R. S., & De Puit, M. (2018). 2. Formation of fingermarks. Fingerprint Development Techniques: Theory and Application. John Wiley & Sons, pp. 11-33.

123. Lennard, C. J., Champod, C., Margot, P., & Stoilovic, M. (2004). Chapter 4: Fingermark detection and Enhancement. Fingerprints and other ridge skin impressions. CRC press, pp. 108-111.

124. Jones, N., Mansour, D., Stoilovic, M., Lennard, C., & Roux, C. (2001). The influence of polymer type, print donor and age on the quality of fingerprints developed on plastic substrates using vacuum metal deposition. *Forensic science international*, *124*(2-3), 167-177.

125. Rosa, R., Giovanardi, R., Bozza, A., Veronesi, P., & Leonelli, C. (2017). Electrochemical impedance spectroscopy: A deeper and quantitative insight into the fingermarks physical modifications over time. *Forensic science international*, *273*, 144-152.

126. Scruton, B., Robins, B. W., & Blott, B. H. (1975). The deposition of fingerprint films. *Journal of Physics D: Applied Physics*, *8*(6), 714.

127. Bond, J. W. (2008). The thermodynamics of latent fingerprint corrosion of metal elements and alloys. *Journal of forensic sciences*, *53*(6), 1344-1352.

128. Johnston, A. (2018). The Temporal Degradation of Illicit Contaminants in Latent Fingermarks Using Fourier Transform Infrared Spectroscopic Imaging. *Journal of Forensic Research, 9*(2), 1-6.

129. Bleay, S. M., Croxton, R. S., & De Puit, M. (2018). 4. Ageing of fingermarks. Fingerprint Development Techniques: Theory and Application. John Wiley & Sons, pp. 69-97.

130. Wargacki, S. P., Lewis, L. A., & Dadmun, M. D. (2008). Enhancing the quality of aged latent fingerprints developed by superglue fuming: loss and replenishment of initiator. *Journal of Forensic Sciences*, *53*(5), 1138-1144.

131. Statistica, Monthly average daily temperatures in the United Kingdom (UK) from 2013 to 2018 (in degree Celsius) https://www.statista.com/statistics/322658/monthly-average-daily-temperatures-in-the-united-kingdom-uk/ (Assessed on 28th October 2018).

132. Johnston, A., & Rogers, K. (2017). The effect of moderate temperatures on latent fingerprint chemistry. *Applied spectroscopy*, *71*(9), 2102-2110.

133. Merkel, R., Gruhn, S., Dittmann, J., Vielhauer, C., & Bräutigam, A. (2012). On non-invasive 2D and 3D Chromatic White Light image sensors for age determination of latent fingerprints. *Forensic Science International*, *222*(1-3), 52-70.

134. Archer, N. E., Charles, Y., Elliott, J. A., & Jickells, S. (2005). Changes in the lipid composition of latent fingerprint residue with time after deposition on a surface. *Forensic Science International*, *154*(2-3), 224-239.

135. De Alcaraz-Fossoul, J., Mestres Patris, C., Barrot Feixat, C., McGarr, L., Brandelli, D., Stow, K., & Gené Badia, M. (2016). Latent fingermark aging patterns (part I): minutiae count as one indicator of degradation. *Journal of forensic sciences*, *61*(2), 322-333.

136. Ulery, B. T., Hicklin, R. A., Buscaglia, J., & Roberts, M. A. (2011). Accuracy and reliability of forensic latent fingerprint decisions. *Proceedings of the National Academy of Sciences*, *108*(19), 7733-7738.

137. Chadwick, S., Moret, S., Jayashanka, N., Lennard, C., Spindler, X., & Roux, C. (2018). Investigation of some of the factors influencing fingermark detection. *Forensic science international*, *289*, 381-389.

138. Jones, N., Stoilovic, M., Lennard, C., & Roux, C. (2001). Vacuum metal deposition: factors affecting normal and reverse development of latent fingerprints on polyethylene substrates. *Forensic science international*, *115*(1-2), 73-88.

CHAPTER 3

Experimental Techniques

In this chapter, sample preparation including sample cleaning and fingermark deposition are discussed. The basic principles behind the methods used during this study are then discussed followed by the experiments that were carried out using these techniques.

3.1 Fingermark Donors

Fingermark samples were taken from one female donor for the experiment investigating the effect of wetting properties on fingermark development while the experiment conducted to investigate the enhancement of fingermark residue deposited on the metal substrate were taken from six different donors. The donors varied in age (20 – 49 years old), gender and ethnicity. Fingermarks were taken as closely as possible within the time frame, 10:00 am – 5:00 pm.

3.2 Types of Fingermark Deposits

Two kinds of fingermark deposits were used in the study is stated of the specific type in the results when necessary. The two fingermark types were eccrine and sebaceous; deposited following the protocol based on UK Home Office internal guidelines [1-2]. Prior to fingermark deposition, the donors washed their hands thoroughly with soap,

rinsed with water and dried with a paper towel to remove excess sebaceous material and any contaminants that may present on the skin. To obtain a sebaceous mark the fingertips were rubbed around the chin and nose region. An even spread of perspiration was achieved by rubbing the fingertips together before fingermark were deposited on the substrate. To obtain an eccrine print, powder free nitrile gloves (VWR) were worn immediately after washing the hands for 30 minutes. However, the gloves were worn for longer times (~ 1 hour) to generate sufficient eccrine sweat at colder times of the year [1].

Fingermarks were deposited on the substrates by application of a maximum force of 2N for a contact duration of 2 seconds before the finger was removed. To ensure the force was maintained at a constant 2N throughout the deposition process in all experiments, it was measured by placing the substrates on a weighing scale (Model CS 5000E, Ohaus Corporation) during the deposition process. Their subsequent development was carried out over a wide time period following their deposition, between 15 minutes – 14 days.

3.3 Substrates

Several types of substrate were used in this study. Initial work was carried out on polymer substrates of varying water contact angle that were spin coated onto glass microscope slides and zinc selenide (ZnSe) crystal for analysis using both the camera and FTIR measurements respectively. Work was then extended on to study some metal substrates of viable forensic value.

Glass microscope slides of 76 x 24 mm and 1 mm thickness (Thermo Scientific), Figure 3.1a, were cleaned prior to fingermark deposition by placing them in a beaker of methanol and sonicating for 15 minutes. A further 15 minutes of sonication was then performed in a beaker of distilled, deionised water to remove impurities from the surface of glass microscope slides. The glass microscope slides were dried using nitrogen air before being spin coated with polymer solution.

Zinc selenide crystal of 72 x 10 mm and 6 mm thickness (GS11145, Specac), Figure 3.1b, was cleaned with a piece of lens tissue using acetone, toluene and finally with

methanol before it was spin coated with the polymer solution. List of polymers used in this study along with their measured water contact angle are tabulated in Table 3.1.

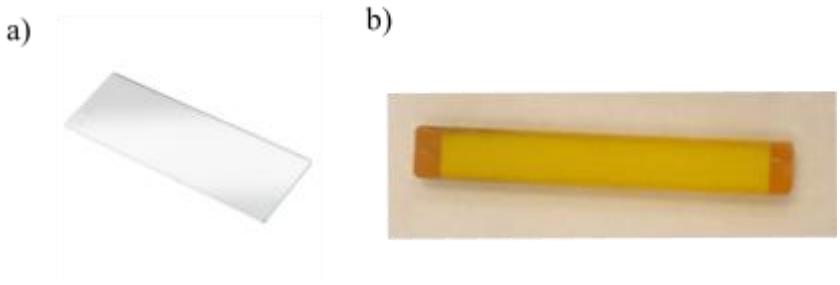

Figure 3. 1: Photographs of a) glass microscope slide and b) zinc selenide crystal that were used to spin coat polymer solution of varying water contact angle.

Polymer	**Measured Water Contact Angle (Degrees)**
Polystyrene treated with oxygen plasma (PS Plasma)	15.0° ± 6.6°
Polyvinyl Acetate (PVA)	60.2° ± 1.3°
Polyethylene / Cling Film (PE)	65.9° ± 4.8°
Poly (methyl methacrylate) (PMMA)	74.2° ± 2.3°
Polystyrene (PS)	86.0° ± 2.4°
Polydimethylsiloxane (PDMS)	101.3° ± 3.5°
Poly (t-butyl methacrylate) (PtBMA)	102.8° ± 1.6°

Table 3. 1: Table above lists the types of polymers that were used to study in this research with their measured water contact angle. Uncertainty was calculated using the standard error of the mean values obtained for the measured water contact angle (n = 10) on the same polymer surface.

Metal substrates of stainless steel, brass and aluminium of approximately 30 mm in diameter and 1 mm thick, Figure 3.2, were cleaned by placing them in a beaker of methanol and sonicating for 15 minutes. A further 15 minutes of sonication was then performed in a beaker of distilled, deionised water to remove water soluble or polar

contaminants from the metal surfaces. The metal disks were then ready to be deposited with fingermarks.

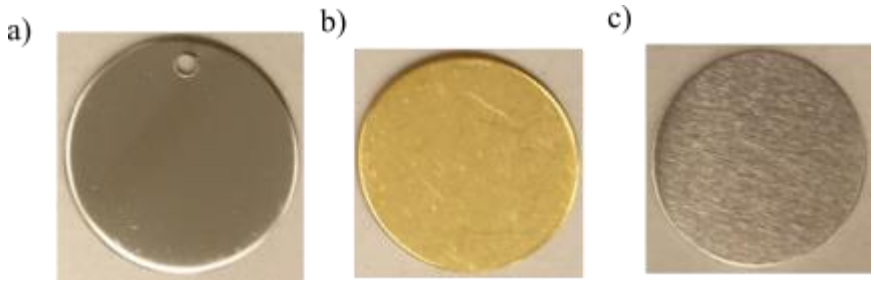

Figure 3. 2: Photographs of a) stainless steel b) brass and c) aluminium metal disks that were used to deposit fingermark.

3.4 Storage Conditions of Fingermark Deposits

If not otherwise stated, polymer substrates were stored under ambient conditions (kept in open box) on the bench in the laboratory at a temperature of 20.4 – 26.5 ± 0.5°C and relative humidity of 38.8 – 44.9 ± 1% after the fingermark deposit was made till the subsequent development was carried out over a time period of 1 - 7 days.

The metal disks were attached to the glass microscope slides post fingermark deposition using double sided adhesive tabs (Leit Adhesive Carbon Tabs 12mm, Agar Scientific) and placed in a closed microscope slide box at room temperature, 22°C and relative humidity of 40+/-1 %, ready for further treatment and analysis.

3.5 Spin Coater

A spin coater, Figure 3.3, was used to produce thin uniform films of polymer (listed in Table 3.1) on which the fingermarks were deposited. Polymer solution was pipetted covering the entire substrate, which was then rotated. During spinning, the solution spreads and the solvent present in the solution evaporates rapidly producing a uniform thin layer film of polymer on the substrate. All the polymers were spin coated at a speed of ~ 2500 rpm for about 1 minute. The thickness of the polymer film depends on viscosity of solution (dependent upon the molecular weight and concentration of

the polymer) as well as the speed used for spinning. The films spin coated on both the glass microscope slides and zinc selenide crystal were then annealed in the oven at ambient pressure at ~ 120° C for ~ 45 minutes to remove any residual stresses and trapped solvent.

Figure 3. 3: Photo shows the spin coater used in this experiment. The substrate that is to be coated is positioned in the central turntable and it is held on place by suction of vacuum pump.

3.6 Plasma Cleaner

In this study, a wide range of polymer substrates of varying water contact angle were required in order to study the effect of polymer wetting properties in fingermark development. However, it must be noted that polymers have quite high water contact angle (not less than 50°), where polyvinyl alcohol polymer with the lowest water contact angle is of 51° [3]. Therefore, plasma treatment was used in this study to acquire a polymer substrate with a low water contact angle by altering the surface energy of the polystyrene polymer.

A plasma cleaner (Model 1020, Fischione) that generates a high frequency plasma with a gas mixture of 25% oxygen and 75% argon was used in this study. Plasma is an ionised gas consisting of electrons and ions. When a gas under sufficiently low pressure is subjected to a high frequency oscillating electromagnetic field of 13.56

MHz, the accelerated free electrons gain kinetic energy in excess of the first ionisation threshold in the neutral gas species. Collisions of these electrons with the neutral gas molecules lead to further ionisation and forming plasma [4]. A simple schematic of plasma process is shown in Figure 3.4.

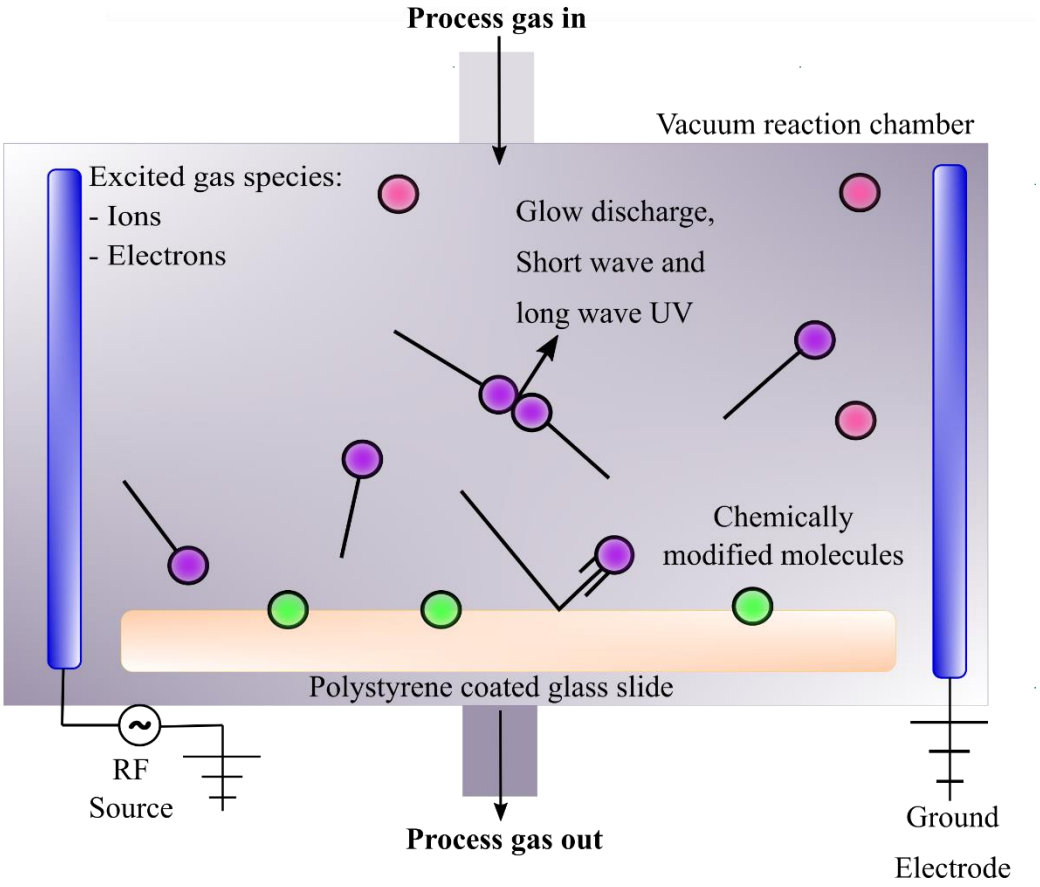

Figure 3. 4: Figure demonstrates the reaction between oxygen plasma and the surface of polystyrene polymer resulting in formation of high energy surface of the polystyrene.

Plasma cleaning involves the mechanical removal of surface contaminants by energetic electron and ion bombardment with sufficient energy to break down the weak covalent bonds in polymeric contaminants. Surface contaminants undergo repetitive chain scission until their molecular weight is sufficiently low for them to boil away in the vacuum. This affects only the contaminant layers and the outermost molecular layers of the substrate material. Inert gas is often used for this purpose as it is chemically inert and get ionised easily. Argon was selected as it has a smaller

ionisation energy and greater ionisation efficiency, enhancing plasma creation compared to other inert carriers [5].

Plasma cleaning also involves the creation of surface chemical functional groups using plasma gases such as oxygen, hydrogen, nitrogen and ammonia which dissociate and react with the surface. An oxygen plasma is highly effective in removing organic (hydrocarbon) in the polymer and replaces those surface polymer groups with highly reactive chemical groups such as carbonyl, carboxyl, and hydroxyl from the plasma gas [5]. This alters the chemical activity and characteristics of the surface, such as wetting and adhesion of the substrate.

Polystyrene was chosen since this surface displayed low hydrophobic recovery as even after 7 days the water contact angle was still well below 20° and also because this substrate demonstrated a water contact angle as low as 15° after plasma treatment. The polymer surface when exposed to oxygen plasma became more hydrophilic due to the high energy surface groups formed on it. This is a result of, energy transfer from the reactive oxygen plasma species to the surface groups of the polymer creating high wettability polymer surface [6].

3.7 Simple Contact Angle Measurements

The water contact angle of all the polymer films was measured using a simple equipment setup as displayed in Figure 3.5.

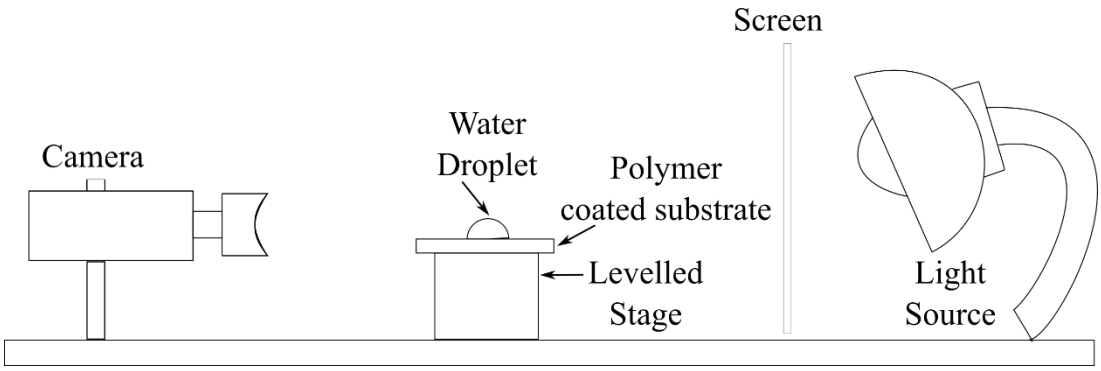

Figure 3. 5: Equipment setup from the side view for contact angle measurements of different polymer surfaces spin coated on a microscopic glass slide.

The measurement was made to obtain the exact water contact angle of the polymers that were used in this study. This is important as the aim of the research is to study the effect of the polymer wetting properties in fingermark development using cyanoacrylate fuming technique.

The polymer coated substrate was kept on a levelled stage in front of the camera. Then, a 270µL water droplet was dropped using a micropipette (Gilson™ PIPETMAN Classic™ Pipets, Gilson F123601) on all the polymer surfaces (see Table 3.1) used in this study. A uniform, diffuse light source (LLOYTRON Flexi Desk Lamp Black, Model L958BK) was placed behind the drop through a piece of white paper to get a clear droplet image. An example of a water droplet image on a polymer substrate obtained from the setup is shown in Figure 3.6.

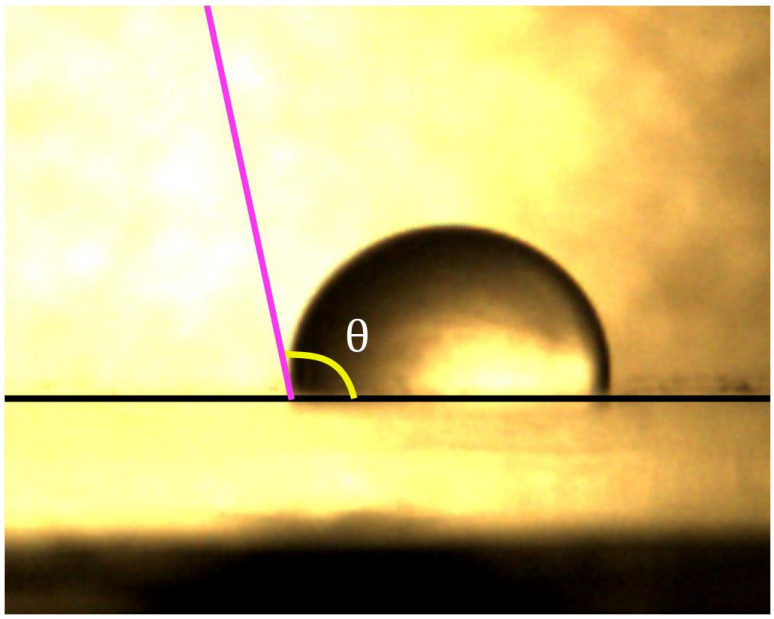

Figure 3. 6: Image of a water droplet on polydimethylsiloxane (PDMS) polymer surface taken using the above setup. It was then analysed manually using a protractor. The water contact angle on the PDMS surface, referred as θ in diagram is 101.3°.

3.8 Atomic Force Microscope

The atomic force microscope (AFM) was invented by Gerd Binnig, Calvin Quate and Christoph Gerber in 1985 [7]. Along with other scanning probe techniques, AFM

provides a relatively simple way of imaging the surfaces with features that are well below the diffraction limit, which are not visible using optical microscopy. The AFM consists of a sharp tip attached at the end of a cantilever, a laser, a position sensitive photodiode and a piezo scanner. The AFM cantilever can be scanned horizontally and vertically by piezo-motors, usually made from silicon or silicon nitride, sometimes with a coating of aluminium, although other specialised coatings are sometimes used.

Interactions between a tip and the surface result in a deflection of the cantilever. This deflection is caused by the force between the tip and the surface. Measuring the deflection of a cantilever of known stiffness allows the force between the tip and sample to be extracted using Hooke's law, given by equation 3.1 [8].

$$k = \frac{\mathrm{F}}{\Delta \mathrm{x}} \tag{3.1}$$

Where the deflection, Δx, due to an applied force, F, is determined by the spring constant, k, of the cantilever. An image is formed by mapping the interaction between the tip and the sample laterally across the surface.

When the tip approaches the sample surface, interactions with the substrate lead to attractive or repulsive forces depending upon the tip-sample separation. The interaction between two atoms can be modelled by the Lennard-Jones potential, given by equation 3.2.

$$V(r) = 4\varepsilon \left(\left(\frac{\sigma}{r}\right)^{12} - \left(\frac{\sigma}{r}\right)^{6} \right) \tag{3.2}$$

Where r is the separation, σ is the separation at which the potential is zero and ε is the maximum attractive potential. At tip-surface separations larger than σ, weaker attractive Van der Waals interactions predominate, which arise from the coulombic attraction of induced dipoles. This leads to an attractive force, modelled by the second term in equation 3.2. At small separations, the force arises predominantly from short range Van der Waals repulsive interactions. When two atoms are brought increasingly close together there is a large energetic cost as the orbitals start to overlap. This arises from the Pauli exclusion principle, which states that no two electrons can share the same state. As the two atomic nuclei approach the same point, half of the electrons of the system would have to go into orbitals with an energy higher than the ground state. This energetic penalty is modelled by a repulsive r^{-12} term in equation 3.2. The

deflection of a cantilever due to the interactions with a substrate is shown in Figure 3.7.

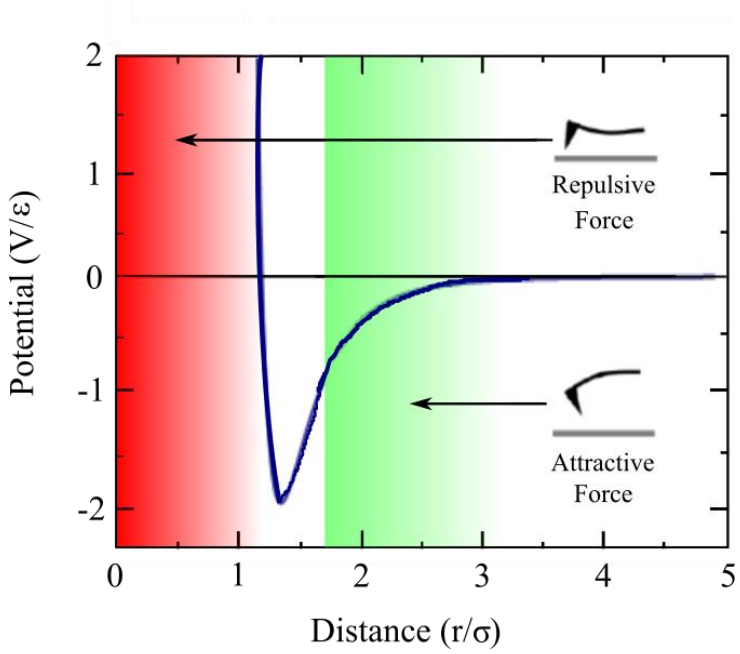

Figure 3. 7: The Lennard-Jones potential is used to model the potential between two atoms. For separations, r that are smaller than σ, the tip experiences a repulsive force and is deflected away from the surface. For separations greater than σ, the tip experiences an attractive force and deflects towards the surface.

In AFM, the position of the tip is controlled very precisely with nanometre resolution using a *z*-piezo motor. A piezo-motor is a stack of piezoelectric crystals (usually ceramic) which undergo a deformation related to the voltage applied across the crystals. The electric field induces polarisation which distorts the unit cell of the crystal by causing small change in the dimensions of the unit cell and a small contraction or extension of the whole crystal [9]. By incrementing the voltage applied, the piezo motor can be used to carefully and accurately move the tip to the desired position.

In order to measure the topography of a sample, the tip is scanned along the surface in a raster pattern. The tip sample interaction can be monitored by measuring the deflection of the cantilever arising from the forces between the tip and sample. The AFM technique measures the deflection of the cantilever by focusing a laser beam onto the back of the cantilever. The reflected light from the laser beam is collected by

a position sensitive photodiode which has 4-quadrants [10]. The bending of the cantilever can be measured precisely with the help of position sensitive photodiode. The cantilever deflects according to the atomic force variations between the tip and the sample and thereby the photodetector measures the deflection. The created image is a topographical illustration of the sample is shown in Figure 3.8.

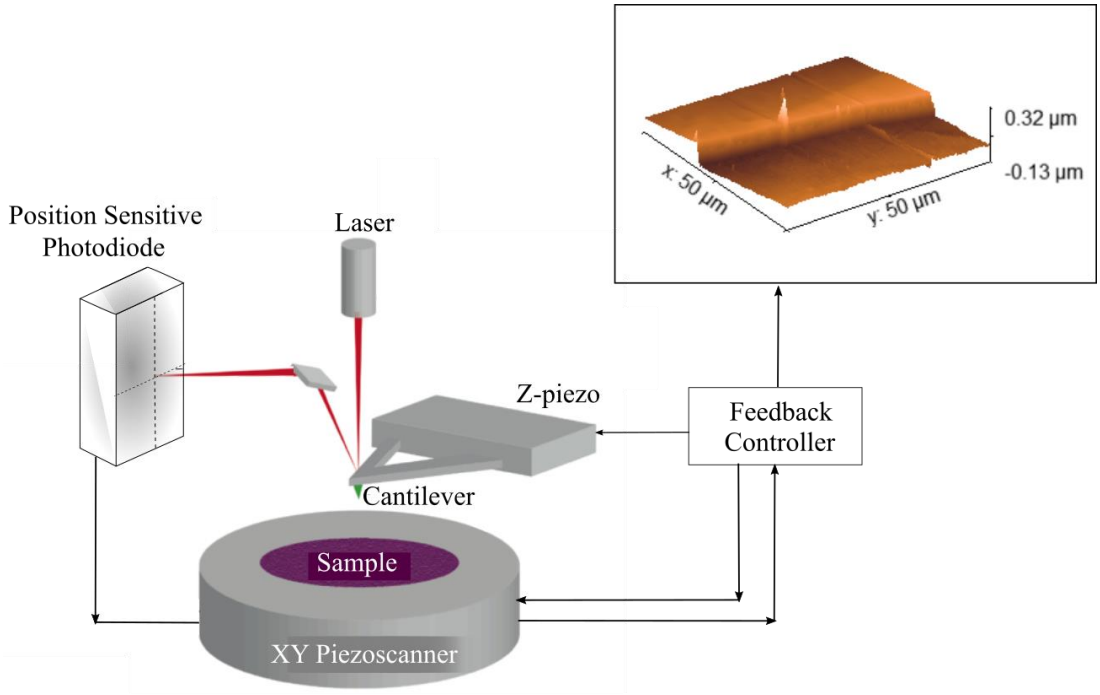

Figure 3. 8: Schematic of an atomic force microscope (AFM). A laser beam is reflected off the back of a cantilever onto a position sensitive photodiode. Changes in the deflection of the cantilever by the surface-tip interaction results in a change in the different voltages measured in each quadrant of the photodiode. Feedback controller takes this input and applies an appropriate voltage to the *z*-piezo motor to keep the cantilever at a constant distance from the surface. The tip is raster scanned across the surface by moving the sample relative to the tip using the *xy* piezo scanner. The measurement of the voltages applied to the piezos can be used to construct an image of the sample.

3.8.1 AFM Imaging Modes

Contact Mode

In contact mode AFM, the tip and surface maintain constant contact. The tip can move above the surface with a specific height or under a constant force. When the spring constant of the cantilever is less than that of the surface, the cantilever bends away from the surface due to the repulsive force on the tip and when the height of the sample increases, the cantilever deflect upwards due to the increased repulsive force. Analysis of the resultant deviation of the laser beam from the centre of the photodiode enables the deflection of the cantilever to be measured. A feedback voltage is then applied to the *z*-piezo motor (see Figure 3.8) to increase the height of the cantilever and restore the original amount of deflection. In this way the tip is kept at a constant distance from the surface. By measuring changes in the voltage applied to the *z*-piezo motor using this method, it is possible to produce the image of the sample surface.

Contact mode enables the surface topography of the samples to be measured more quickly and often with greater resolution than in other imaging modes but has some disadvantages which make it unsuitable for certain types of samples. In contact mode the sample and tip are always in contact, the tip-sample interaction may lead to blunt tip and damage weakly bound molecular layers of sample's that are fragile. Thus, contact mode is only used for small scans of molecular monolayers when high resolution scans of substrate surfaces are needed, where damage is limited to a very small area of the sample or very hard surfaces.

Tapping Mode

Considering the limitations outlined above, contact mode is not particularly useful for scanning fingermark residue or the film thickness on ZnSe crystal because soft matter such as this is susceptible to damage. A far more suitable mode of operation for the AFM is known as tapping mode also known as AC mode or non-contact mode. The laser is aligned on the back of the cantilever just as it is for the contact mode. In tapping mode, the tip is driven on-resonance using a piezo crystal located in the cantilever holder. When the cantilever is far from the surface, the piezo oscillates the cantilever over a range of frequencies at the free air amplitude. As the tip of the cantilever is

lowered into contact with the surface, the surface interacts with the tip. The repulsive forces between the sample and tip results in a reduction in the measured amplitude of oscillation of the cantilever. When a sufficient reduction in amplitude is detected, indicating contact with the surface, feedback electronics stop the tip from being lowered any further as the amplitude of the cantilever is used as the feedback parameter.

An image is collected using the same principle as in contact mode but keeping the amplitude of oscillation, rather than the deflection of the cantilever constant. Feedback electronics adjust the voltage applied to the *z*-piezo to compensate for the changes in height of the surface. Point by point, line by line an image is built up of the sample surface.

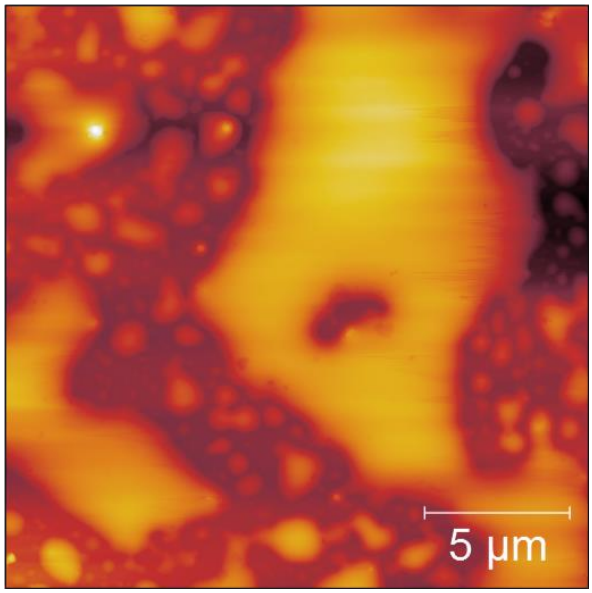

Figure 3.9: Example AFM image of an eccrine fingermark residue on glass microscope slide that was spin coated with polyvinyl acetate (PVA) polymer solution (20 × 20 µm). The image is collected in tapping mode by raster scanning the tip across the surface.

In this study, tapping mode was used to acquire all the AFM images as it is far less destructive to the samples as the tip is only in contact with the surface for a small percentage of each oscillation. The reduced interaction between the tip and sample does not affect the molecular layers sturdily during scanning and the degradation in

the tip will not occur as quickly. In this work, images were acquired under ambient conditions using the Asylum Research MFP-3D (Asylum Research, Atomic Force Microscopes, Santa Barbara, CA), operated via version 13.16.99 software (Asylum Research). The tips used were made of antimony (n-) doped silicon from Bruker (Bruker model RTESPA part MPP-11120-10; operating frequency 303 – 380 kHz and spring constant 20 – 80 Nm^{-1}).

3.9 Cyanoacrylate Fuming

Fingermark residue on polymer and metal substrates were developed with cyanoacrylate (CNA) fuming. CNA fuming was carried out slightly different between the polymer and metal substrates to suit the objective of each study.

Chapter 4 and 5 study the chemical and physical changes that occurs in fingermark residue due to CNA fuming. Chapter 4 involves fresh fingermarks and chapter 5 focuses on aging of fingermarks (1 – 7 days) deposited on polymer surfaces of different wettability.

The polymer surfaces deposited with either sebaceous or eccrine fingermark residue were enhanced with CNA fuming in a fuming cell. The fuming cell is fitted in with a beaker of saturated sodium chloride (NaCl) solution with a heating element. The salt solution was used to increase the humidity in the cell to approximately ~ 60% – 70%, in order to achieve the best condition for the fuming process. The humidity was measured using a humidity sensor (DLP-TH1, DLP Design) prior to the fuming process. The heating element was used to heat up the superglue to 60°C, evaporating the superglue by creating a concentration of gaseous cyanoacrylate, see Figure 3.10. The exposure of cyanoacrylate evaporation by heating coupled with optimum humidity from saturated salt solution were enough to trigger the reaction, producing a perfect setting for fingermark development [11].

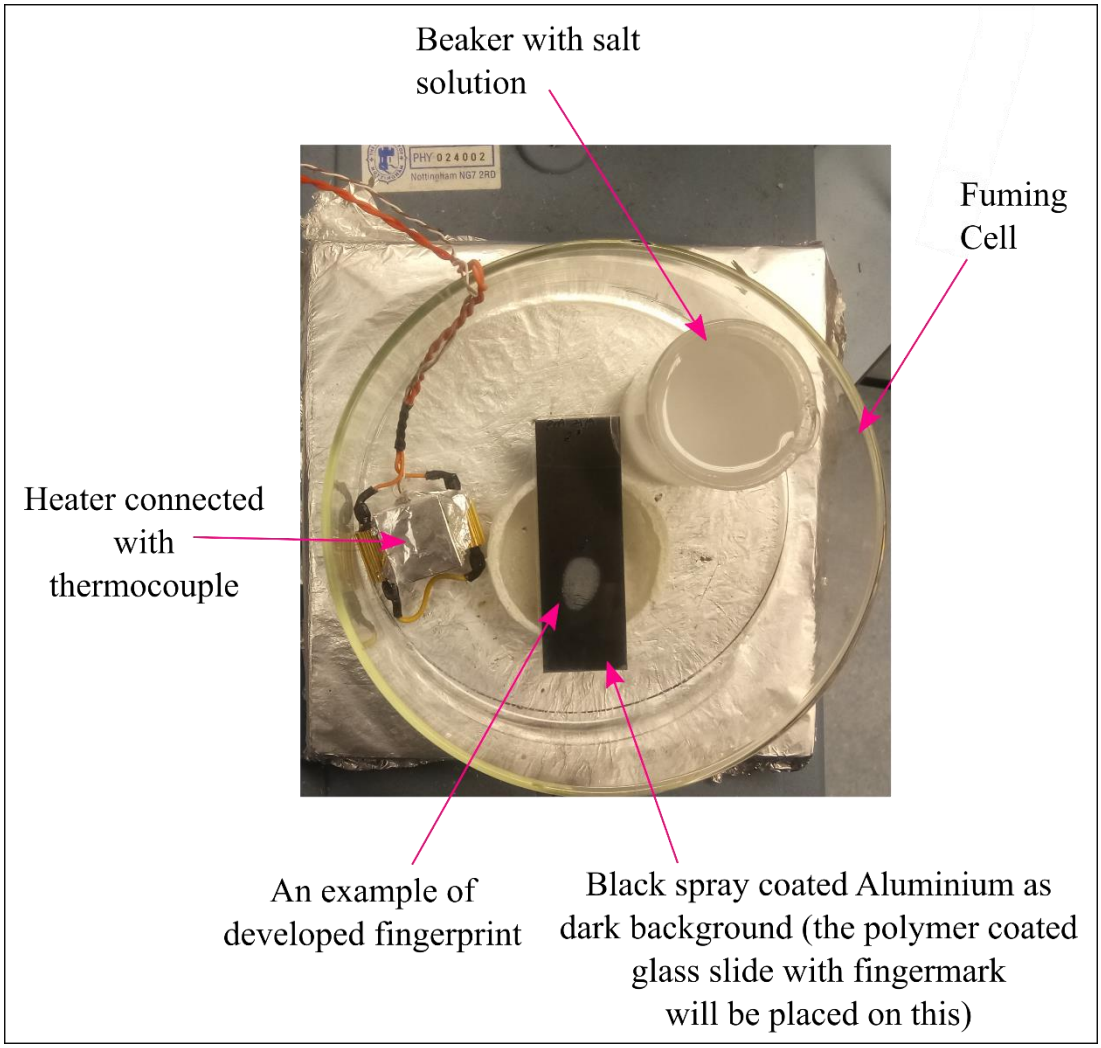

Figure 3.10: The fuming cell contained a beaker of concentrated sodium chloride (NaCl) solution and a heating element. The NaCl solution was to increase humidity level to about 60% while the heating element was used to heat up the superglue to 60°C. This was to ensure that the fingermark developed well. The black spray coated aluminium was used as a background below the polymer coated microscopic glass slides with fingermark deposit, to provide a good contrast as the white polymerisation of the superglue occurs on the fingermark residue.

Chapter 6 involves the aging (1 – 28 days) of fingermarks on metal substrates. The fingermarks were developed using techniques that are employed by East Midlands Special Operations Unit – Forensic Sciences (EMSOU-FS) and other police forensics laboratories across the UK when trying to develop fingermarks on non-porous metal substrates. The cyanoacrylate fuming was then carried out at the EMSOU-FS forensics

lab using a superglue fuming cabinet (MVC5000 Mason Vactron, Foster and Freeman) to obtain the same result as for any other metal objects found in crime scenes that would be treated similarly. The relative humidity in the fuming chamber was set and maintained at 75-80 % throughout the fuming cycle. 3.5g cyanoacrylate (superglue) was heated to 120°C and allowed to form a vapour inside the fuming cabinet chamber once the desired humidity is established. Samples were exposed to the cyanoacrylate vapour for a total of 15 minutes, the cabinet was then purged to remove all traces of the vapour and halt the fuming process. All the samples were fumed simultaneously in the same chamber to ensure that all were exposed to identical fuming conditions.

3.10 Other Enhancement Techniques

Even though cyanoacrylate fuming is an excellent method, the eccrine marks developed on the metal substrates do lack in contrast therefore difficult to visualise [12]. In order to visualise the fingermark, the mark developed using cyanoacrylate was enhanced by sequential staining of dyes, basic yellow 40 (BY40), crystal violet (CV) and sudan black (SB) is described below.

This sequence was chosen because these are the most popular visualisation techniques used by UK police forensic labs when developing fingermarks on metal surfaces obtained from a crime scene. The staining procedure and the photographs of the samples acquired between each staining procedure were carried out at the University of Derby.

Basic Yellow 40 (BY40)

BY40 of 2% w/v in ethanol was applied to the fumed metal disks by laying them flat and soaking in the dye for five seconds before rinsing in water and drying in a stream of air at room temperature. The disks were then photographed using a Nikon D7200 digital camera with yellow filter (75mm x 75mm No.12, Kodak Wratten gelatin filter, excitation wavelength: 510 – 530 nm) under blue light illumination with CrimeLite 2 (Foster and Freeman) light source emitting wavelengths in the range 420 – 470 nm (Crimelite 2, Foster and Freeman).

Crystal Violet (CV)

Once all the samples were photographed, the samples were immersed in CV (0.03% w/v in 1:50 ethanol/water mixture) for five minutes. The metal substrates were rinsed, dried and then photographed using the same camera but under white light illumination (Crimelite 2, Foster and Freeman, wavelength range 400 – 700 nm) without any filters.

Sudan Black (SB)

The metal substrates were then finally immersed in SB (1% w/v in 2:1 ethanol/water mixture) dye for five minutes. The metal substrates were rinsed with water and photographed using the same camera under the similar illumination, as used for photographing the metal substrates after CV dye application without any filters.

3.11 Camera Measurements

Camera measurements were used in this study to observe the physical changes that occurs in fingermark residue during the cyanoacrylate fuming process. Figure 3.11 depicts the apparatus set up in such, the fuming process would be captured by a camera (Manta G-125B, Allied Vision Technologies). The photographs that appear in this thesis are the original raw images, unless otherwise stated in their respective figure legends that image has been altered for the purpose of extracting fingermark brightness.

Figure 3.12 displays examples of photographs that were obtained during the development of latent fingermark with cyanoacrylate fuming technique at the fuming time t = 0 minutes, 20 minutes and 35 minutes. The development of the mark in the fuming cell were captured by the camera is as shown in the apparatus set up in Figure 3.11.

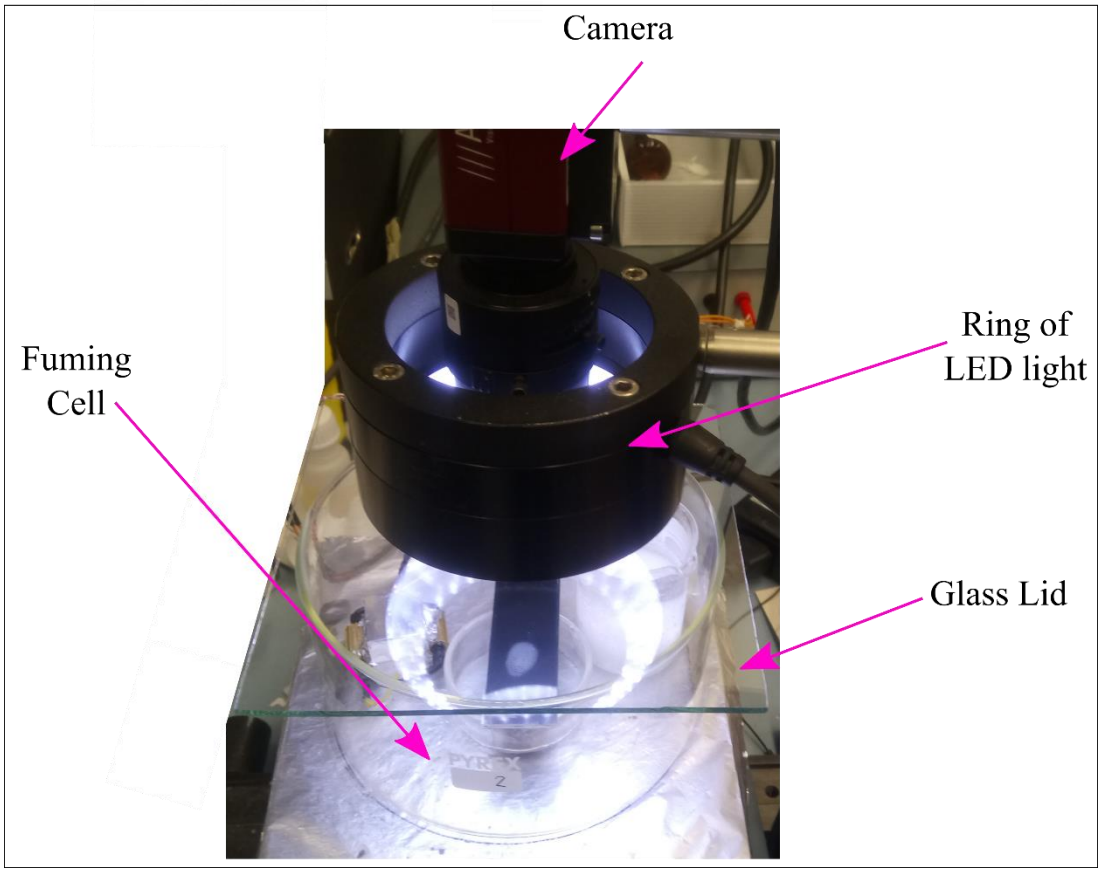

Figure 3.11: Cyanoacrylate fuming set up for camera measurements. A ring of LED light was used to provide an even illumination while the camera took images throughout the fuming process.

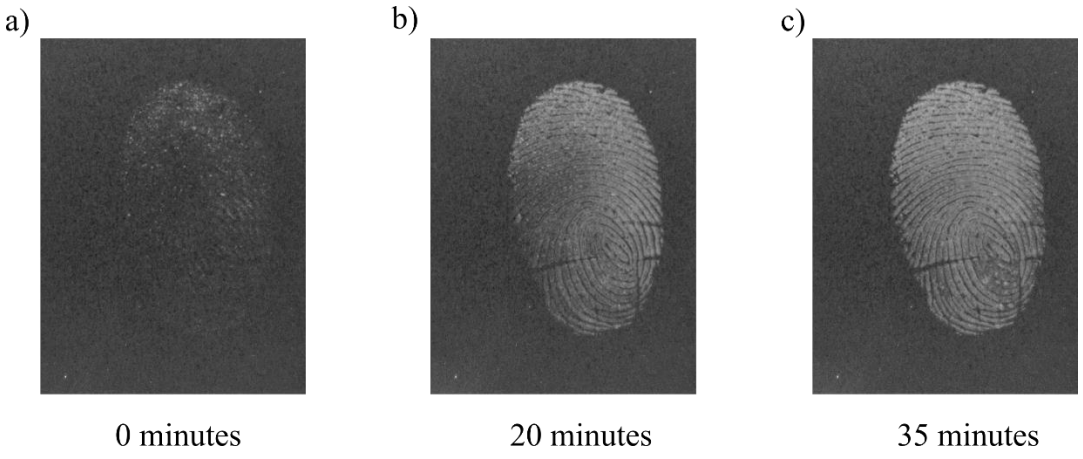

Figure 3.12: Examples of photographs of latent fingermark deposited on polymer coated glass microscope slides that were developed with cyanoacrylate fuming technique. The photographs were taken at different times of fuming process starting with the time t at a) 0 minutes, b) 20 minutes and c) 35 minutes.

3.12 Fourier Transform Infrared Spectroscopy

3.12.1 Introduction

Fourier Transform Infrared spectroscopy (FTIR) is a method of probing chemical structure of material by studying molecular vibrations. Every molecule has a specific number and arrangement of bonds and each having their own characteristic vibrational frequencies [13]. When broadband infrared radiation is passed through the sample, it is partially absorbed and excites the various vibrations within the bonds.

The infrared spectrum of a sample is recorded with a spectrometer which examines the transmitted light of an infrared beam, used to illuminate the sample. Each molecule in the sample absorbs photons of certain energies, characteristic for that molecule are then revealed in the IR spectrum as a well-defined and reproducible absorption bands. For a given frequency of IR radiation striking the sample, the absorbance (A) of incident radiation is defined through equation 3.3.

$$A = -log_{10}\left(\frac{I}{I_0}\right) \qquad (3.3)$$

Where I_0 is the initial beam intensity and I is the beam intensity once it has passed through the sample.

3.12.2 The Michelson Interferometer

To understand the operation of an FTIR it is necessary to start with the basic Michelson Interferometer.

The Michelson Interferometer consists of a light beam (Infrared source), beam splitter (BS), stationary mirror (M_1) and moving mirror (M_2). The Infrared (IR) radiation emitted from the point source passes through a beam splitter. As the name implies, the beam splitter splits half of the beam to the fixed mirror and the remaining half to the moving mirror (see Figure 3.13). Half of the wave that is reflected from M_1 is then transmitted through the BS, where it recombines with the reflected half of the wave returning from M_2 [14]. Hence, the combined electric field ($\mathbf{E_T}$) associated with the reflected infrared beams can be expressed in the form of:

$$\boldsymbol{E}_T = \boldsymbol{E}_0\, e^{i\omega t} + \boldsymbol{E}_0\, e^{i(\omega t+\phi)} \tag{3.4}$$

where

E_0 = amplitude of the incident infrared beam

ω = angular frequency of the infrared beam ($2\pi f$)

ϕ = phase difference between the two beams after being reflected from the stationary mirror and the moving mirror

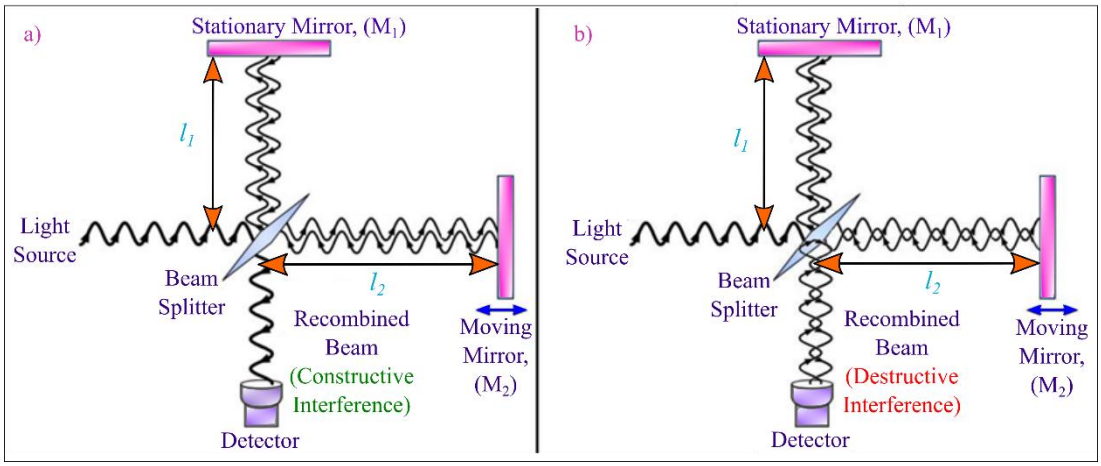

Figure 3.13: The schematic diagram of Michelson Interferometer showing the changes in the interference pattern of the light source that passes through the detector. The a) constructive and b) destructive interference pattern depends on the position of the moving mirror.

When these beams recombine at the beam splitter they can interfere constructively or destructively depending on the change in relative path length of the two beams. Distance from beam splitter to M_1 and M_2 differs by optical path length difference, δ of x in the two paths, and θ is the angle of interfering beams to the beam splitter. Resulting phase difference can be deduced as in equation (3.5).

$$\phi = \frac{2\pi}{\lambda}\delta = k\delta = \frac{2\pi}{\lambda}\,[2x\cos\theta] \tag{3.5}$$

Whereby the value for δ was derived as:

x = denotes the path difference from a point on BS to M_1 and M_2 along the optical axes respectively with a factor of 2 appearing as the result of the waves traveling to the mirrors and back again to the BS

θ = light incident on interferometer mirrors at an angle of θ = 0° to the normal

k = wavenumber $\left(\frac{2\pi}{\lambda}\right)$

The superimposed recombined infrared beam intensity, *I* that reaches the detector can then be written as [15]:

$$I = |\boldsymbol{E_T}\,\boldsymbol{E_T^*}| = \boldsymbol{E_0}^2 + \boldsymbol{E_0}^2\left(e^{i\phi} + e^{-i\phi}\right) + \boldsymbol{E_0}^2 \tag{3.6}$$

$$= 2\,\boldsymbol{E_0}^2 + 2\,\boldsymbol{E_0}^2 cos\ \phi \tag{3.7}$$

It must be noted that the intensity and electric field of the electromagnetic wave are related by equation (3.8).

$$I = \frac{1}{2}\,c\epsilon_0 E_0{}^2 \tag{3.8}$$

Where I is the intensity of the infrared beam, E_0 is the electric field of the infrared beam. The two physical constants in this equation are the permittivity of free space, ϵ_0 and the speed of light, c. Given that both c and ϵ_0 are physical constants, equation (3.8) can then be written as in equation (3.9).

$$I = \frac{1}{2}\,E_0{}^2 \tag{3.9}$$

Hence, equation (3.7) can then be rewritten in terms of intensity as in equation (3.10).

$$I = I_0(1 + cos\phi) \tag{3.10}$$

$$= I_0(1 + cos(k\delta)) \tag{3.11}$$

Where $\boldsymbol{E}_T$ is the combined electric field associated with the reflected infrared beams, $\boldsymbol{E_T^*}$ is a complex conjugate of $\boldsymbol{E}_T$ and I_0 is intensity of the infrared beam.

As one mirror is moved, a repeatedly cosine pattern variation in intensity can be observed. In FTIR the emission from infrared source is not monochromatic, but it has a broadband spectral distribution over a wide wavenumber range. The intensity of the infrared source is denoted by I(k), to indicate that is a function of different wavenumbers, k. The total intensity that reaches the detector I(δ) can be deduced by adding all the intensities for different values of k:

$$I(\delta) = \int_0^\infty I(k)(1 + \cos(k\delta))\, dk \tag{3.12}$$

$$I(\delta) = \int_0^\infty I(k)\, dk + \int_0^\infty I(k)\cos(k\delta))\, dk \tag{3.13}$$

The first term in equation (3.10) is the constant level in the absence of modulation, and the second term is the power spectrum of the source called the interferogram which depends on the δ, and contains all the information on the spectrum. Hence, only the modulated part of the interferogram, F(δ) could then be expressed in the form of equation (3.14). Now I(k) = 0 for k < 0, so second term may be written as:

$$F(\delta) = \int_{-\infty}^\infty I(k)\cos(k\delta))\, dk \tag{3.14}$$

Interferogram, F(δ) is the Fourier cosine transform of I(k). So, the inverse Fourier cosine transform of F(δ) can be deduced as I(k) according to the theory of Fourier transforms.

$$I(k) = \int_{-\infty}^\infty F(\delta)\cos(k\delta))\, d\delta \tag{3.15}$$

I(k) and F(δ) are a Fourier transform pair indicating the relationship between the intensity as a function of path difference and the intensity as a function of wavenumber. This is important to the interpretation of FTIR data because it enables one to convert between the path difference and wavenumber dependence. Hence, the absorption spectrum of the infrared radiation (intensity as a function of wavenumber) is computable from the inverse Fourier transform of the observed interferogram (intensity as a function of path difference) in the Michelson interferometer. An interferogram has information about every infrared frequency that comes from the

source because this signal is made up of every data point as a function of the moving mirror position. This means that as the interferogram is measured, all frequencies are being measured simultaneously with a single detector. This interferogram is the one that undergoes Fourier transformation in the computer to produce the final spectrum [16].

3.12.3 Resolution

Resolution is the smallest difference in frequency or wavelength between two absorbance peaks that can be separated by the FTIR spectrometer. Experimentally, a complete interferogram that is infinite as indicated by equation (3.14) can never be recorded. The movable mirror only has a finite range of motion, and this puts a limit on the resolution obtainable with the spectrometer. To account for the finite distance moved by the mirror, equation (3.12) must be multiplied by a rectangular function D(δ) defined as:

$$D(\delta) = 1 \quad \text{for} \quad -L \leq \delta \leq L \tag{3.16}$$

$$D(\delta) = 0 \quad \text{for} \quad |\delta| > L \tag{3.17}$$

where: – L is the minimum path difference the moving mirror could move while L is the maximum path difference the moving mirror could move. Then, equation (3.15) now reads as:

$$\mathrm{I(k)} = \int_{-\infty}^{\infty} \mathrm{D(\delta)F(\delta)\cos(k\delta))\,d\delta} \tag{3.18}$$

The Fourier transform (F.T) of the product of the two functions could be obtained using the convolution theorem stated below:

$$F.T\left(\mathrm{D(\delta)} * \mathrm{F(\delta)}\right) = F.T\left(\mathrm{D(\delta)}\right) * F.T\ (\mathrm{F(\delta)})$$

$$= \mathrm{D}(k) * \mathrm{I}(k)$$

where D(k) is the Fourier Transform of D(δ) and I(k) is the Fourier transform of F(δ). The convolution theorem indicates that the effect of a limited path length upon the computed intensity as a function of wavenumber is simply equal to the Fourier transform of the finite path length interferometer multiplied by the Fourier transform of the rectangular function [17].

The Fourier transform of the rectangular function, D(δ) is given by equation (3.19):

$$\mathrm{D(k)} = \int_{-\infty}^{\infty} \mathrm{D(\delta)}\cos(\mathrm{k\delta}))\,\mathrm{d\delta} \tag{3.19}$$

$$= \int_{-\mathrm{L}}^{\mathrm{L}} \cos(\mathrm{k\delta}))\,\mathrm{d\delta} \tag{3.20}$$

$$= 2L\frac{(\sin kL)}{kL} \tag{3.21}$$

$$= 2L\,\mathrm{sinc}(kL) \tag{3.22}$$

Combining this result with equation (3.15) and the convolution theorem gives an expression for the intensity as a function of wavenumber, G(k):

$$\mathrm{G}(k) = \mathrm{D}(k) * \mathrm{I}(k) = 2L\,\mathrm{sinc}(kL) * \int_{-\infty}^{\infty} \mathrm{F}(\delta)\cos(\mathrm{k\delta}))\,\mathrm{d\delta} \tag{3.23}$$

The wavenumber resolution dk is defined by the relation dk = 1/L, then the wavenumber resolution of 1,2, and 4 cm^{-1} could be obtained by setting the value of L with 1,0.5 and 0.25 cm respectively. Increased resolution means a better ability to detect peaks that are close together. However, it could not be done much only by resolution. In order to obtain best spectrum possible, the signal to noise ratio should be minimised. This can be done by increasing the number of scans being averaged because the signal to noise ratio increases as the square root of the number of scans being signal averaged [18].

3.12.4 The FTIR system

The FTIR used in this study (FTS40 Pro) has the same Michelson Interferometer principles with a slightly different set up. It uses two beams which are Helium-Neon (He-Ne) laser of wavelength 633nm and a mid-IR radiation (Silicon Carbide also known as Globar) source, that are passed through a Michelson Interferometer (see Figure 3.14). The interferometer contains one mirror that is moved by an air piston. This changes the relative path length between the different arms of the interferometer. The He-Ne laser is used to measure the position of the mirror and hence calculate the path difference as a function of time. This is done by recording the sinusoidally varying intensity pattern at photodiode with the time. Since the laser is a monochromatic light source (single wavelength/frequency) with wavelength, λ, the path difference can be related with the varying intensity pattern by counting the maxima with time. If δT is the time between maxima and t is the total time elapsed then the path difference, x can be calculated by equation (3.24). This method, for determining the path difference between two arms of the interferometer, enables a very precise measurement of the mirror position.

$$x = \frac{dx}{dt}t = \frac{\lambda}{\delta T}t \qquad (3.24)$$

The second beam which uses a broad spectral range IR source (heated ceramic of Silicon Carbide, SiC) is passed through the sample and it is this beam from which the interferogram is recorded.

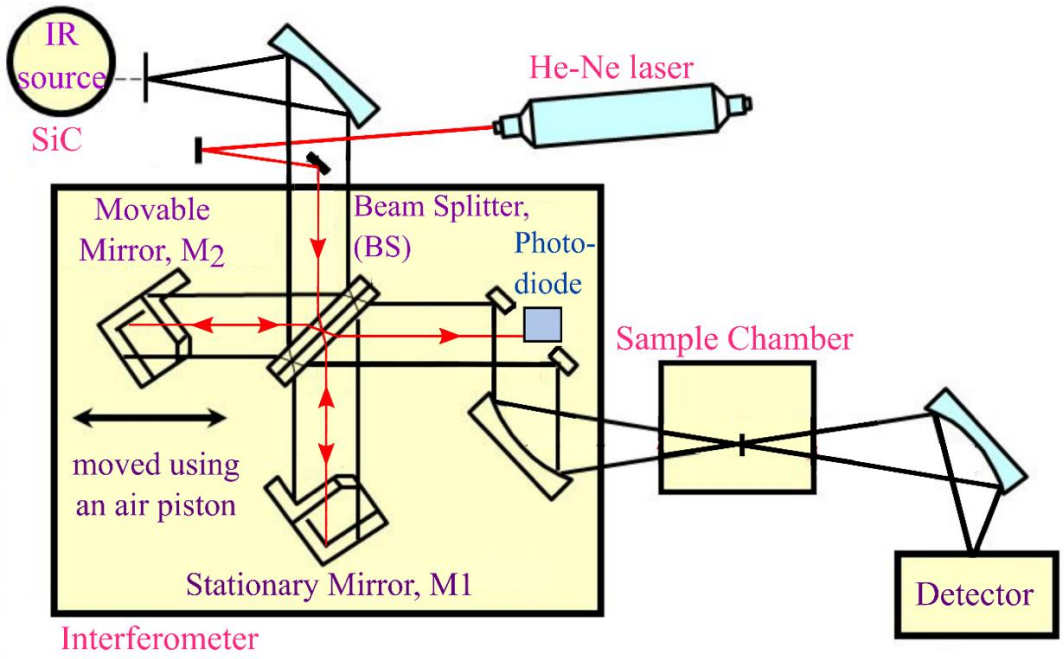

Figure 3.14: A schematic diagram of the FTIR used in this study consists of two beams within the spectrometer. The laser beam (red line) is passed through the Michelson interferometer, hence measuring the resulting intensity of the interference pattern at the photodiode. The IR light source (black line) producing a continuous spectrum in the mid IR region is passed through the same interferometer and then the sample before being recorded at the detector.

3.12.5 Collecting Spectra

The atoms and molecules in the fingermark residue are bonded chemically can be modelled as two atoms attached to each other by a massless spring. Considering the diatomic molecule as a simple harmonic oscillator, the vibrational frequency, f can be written as in equation (3.25).

$$f = \frac{1}{2\pi}\sqrt{\frac{k}{\mu}} \tag{3.25}$$

where k is the force constant determined by the strength of the bond (spring constant) while μ is the effective mass of the two atoms in the bond $\left(\mu = \frac{m_1 m_2}{m_1 + m_2}\right)$ with m_1 and m_2 as the atomic masses. When the IR beam is directed through the sample, the molecules in sample absorb the IR radiation of the frequency that is equal to the

frequency of vibration of the molecules, which then modifies the IR radiation giving rise to an absorption spectrum (see Figure 3.15). In IR spectroscopy the frequency is expressed in terms of wavenumbers, ν ($f = c\,\nu$) where $\nu = \frac{1}{\lambda}$. Hence, equation (3.25) can then be written as:

$$\nu = \frac{1}{2\pi c}\sqrt{\frac{k}{\mu}} \tag{3.26}$$

The intensity of any peak is related to the concentration of the molecules that absorb the IR radiation [19,20].

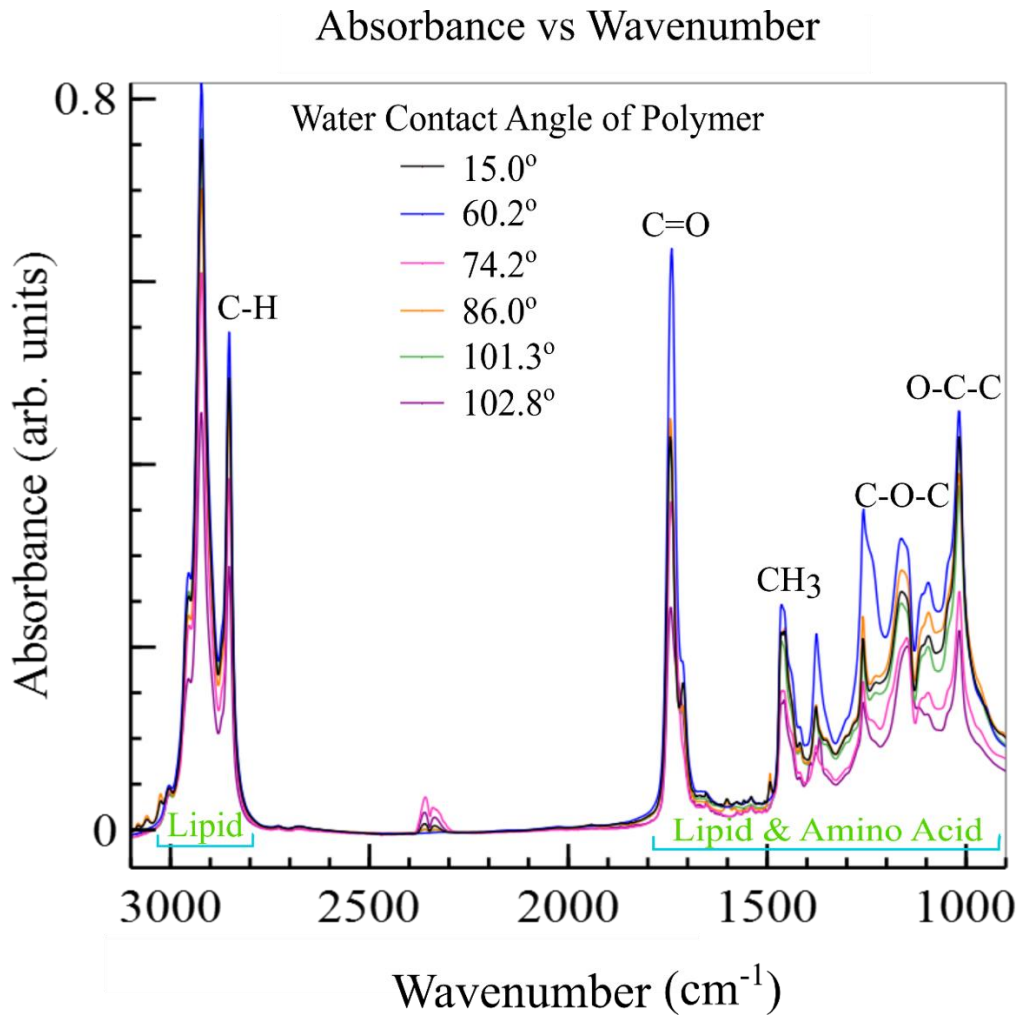

Figure 3.15: Figure displays six infrared absorption spectra of sebaceous fingermark residue that were deposited on six different polymers with water contact angle varying from 15° to 102.8°. The list of polymers along with their water contact angle can be found in Table 3.1, Section 3.3.

An example of a FTIR spectrum of sebaceous fingermark residue on the six different wetting substrates is represented in Figure 3.15, including the contribution from any ambient water (two irregular groups of lines at about 3600 cm^{-1} and about 1600 cm^{-1}) present in the FTIR cell [21] and carbon dioxide (doublet at 2360 cm^{-1}) [22]. A complete functional groups corresponding to eccrine and sebaceous compounds found in fresh latent fingermark residue is tabulated in Table 4.2 (Chapter 4, sub-section 4.3.1).

3.12.6 Sample Accessory: Attenuated Total Reflectance (ATR) cell

The sampling technique used in the experiments was Attenuated Total Reflectance (ATR). The IR beam entering an optical medium which is transparent in the infrared region and has a high refractive index will undergo total internal reflection when the angle of incidence at the interface between the sample and crystal is greater than the critical angle. The optical medium used in this study was Zinc Selenide (ZnSe) crystal with a refractive index of 2.40 for ZnSe/air medium that enables the total internal reflectance to occur when the incident light is greater than the critical angle of ZnSe. When the IR beam irradiates the polymers used in this study plus the fingermark residue with refractive index of about 1.40 – 1.59 after passing through the ZnSe crystal, the critical angle θ_c for ZnSe is about 40° [23]. A series of pictures demonstrating the process when the total internal reflection happens is illustrated in Figure 3.16.

The incident light refracts through and reflects from the interface depending on the incidence angle with respect to the critical angle, θ_c at an interface of two different mediums with refractive indices of n_1 and n_2. Hence, there are incident, refracted and reflected waves whereby the incident and reflected waves are in the first medium while the refracted (transmitted) wave is in the second medium.

For angles of incidence below the critical angle, θ_c there are incident, refracted and reflected waves as illustrated in Figure 3.16. However, when the angle of incidence exceeds the critical angle, only the incident and reflected waves remain. The refracted wave is transformed into evanescent wave [24].

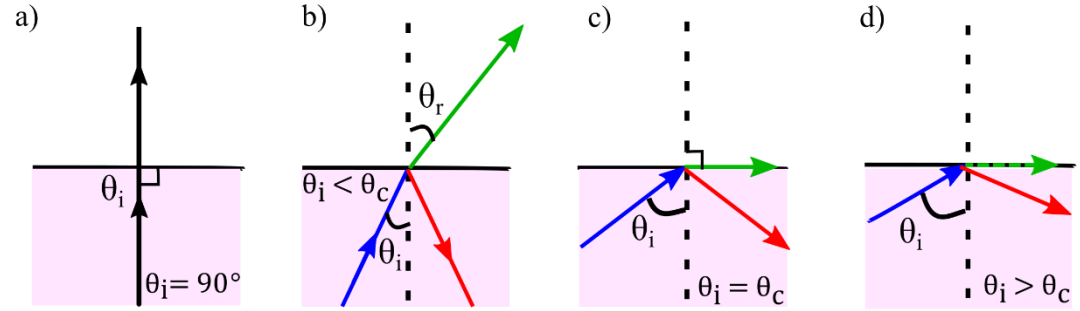

Figure 3.16: Figure above shows how the light travels from a dense to less dense medium depending on the angle of incidence of the light. a) Shows that nothing happens to the light when the angle of incidence is 90°. b) As the angle of incidence is reduced from 90°, refraction occurs till the angle of incidence is less than the critical angle, θ_c with a weak reflection. c) The light is refracted along the boundary between the two mediums when the angle of incidence is equal to the critical angle with a strong reflection. d) Exhibits the total internal reflection back into the medium when the angle of incidence is greater than the critical angle with an evanescent wave formed at the second medium.

To understand the formation of evanescence wave better, the propagation of the electric field in the refracted wave in medium 2 can be written as:

$$\widetilde{\overrightarrow{E_{2z}}} = \overrightarrow{E_{02z}} e^{i(k_{2z}z - \omega t)} \qquad (3.27)$$

Where,

$\vec{E}_{2z}$ = amplitude of the refracted wave is in medium 2 in z-direction

$\vec{E}_{02z}$ = amplitude of the electric field vector at position z in medium 2

k_{2z} = wavenumber component in medium 2 along z-axis

z = position along the wave's direction of travel

ω = angular frequency

t = time at which the wave is described

The wavenumber, k_2 points in the direction of wave propagation in medium 2 and has a magnitude that is given by:

$$\left|\vec{k}_2\right| = \frac{2\pi}{\lambda_2} = \frac{2\pi}{\lambda_0} n_2 \tag{3.28}$$

λ_0 = wavelength of infrared beam in air, n_2 = refractive index of second medium, λ_2 = wavelength of infrared beam in medium 2

Therefore, the wave vector component along z-axis can be calculated as:

$$k_{2z} = \left|\vec{k}_2\right| \cos\ \theta_2 = \frac{2\pi}{\lambda_0} n_2 \sqrt{1 - \ sin^2\theta_2} \tag{3.29}$$

θ_2 = angle of refraction

but $\sin\theta_2 = \frac{n_1}{n_2}\sin\ \theta_1 = \frac{\sin\ \theta_1}{\sin\ \theta_c}$ using Snell's law and definition of critical angle. So the wavevector then can be rewritten as:

$$k_{2z} = \frac{2\pi}{\lambda_0} n_2 \sqrt{1 - \left(\frac{\sin\ \theta_1}{\sin\ \theta_c}\right)^2} \tag{3.30}$$

where θ_1 = angle of incidence and θ_c = critical angle.

When total internal reflection occurs $\theta_1 > \theta_c$, k_{2z} is a complex quantity:

$$k_{2z} = i\frac{2\pi}{\lambda_0} n_2 \sqrt{\left(\frac{\sin\ \theta_1}{\sin\ \theta_c}\right)^2 - 1} \tag{3.31}$$

Therefore, when equation (3.31) is substituted in equation (3.27) the propagation of the refracted wave along the z-axis will then be:

$$\widetilde{\overrightarrow{E_{2z}}} = \overrightarrow{E_{02z}} \exp\left(-z\frac{2\pi}{\lambda_0} n_2 \sqrt{\left(\frac{\sin\ \theta_1}{\sin\ \theta_c}\right)^2 - 1}\right) \exp(-i\omega t) \qquad (3.32)$$

This expression shows that the evanescent wave (exponential decay) penetrates to the second medium but the amplitude decreases rapidly with depth.

While the propagation wave along x-axis is:

$$\widetilde{\overrightarrow{E_{2x}}} = \overrightarrow{E_{02x}} e^{i(k_{2x}x - \omega t)} \qquad (3.33)$$

$$k_{2x} = \left|\vec{k}_2\right| \sin\ \theta_2 = \frac{2\pi}{\lambda_0}\frac{n_1}{n_2} \sin\ \theta_1 \qquad (3.34)$$

The electric field of the evanescent wave penetrates a certain distance into the sample, known as penetration depth is illustrated in Figure 3.17.

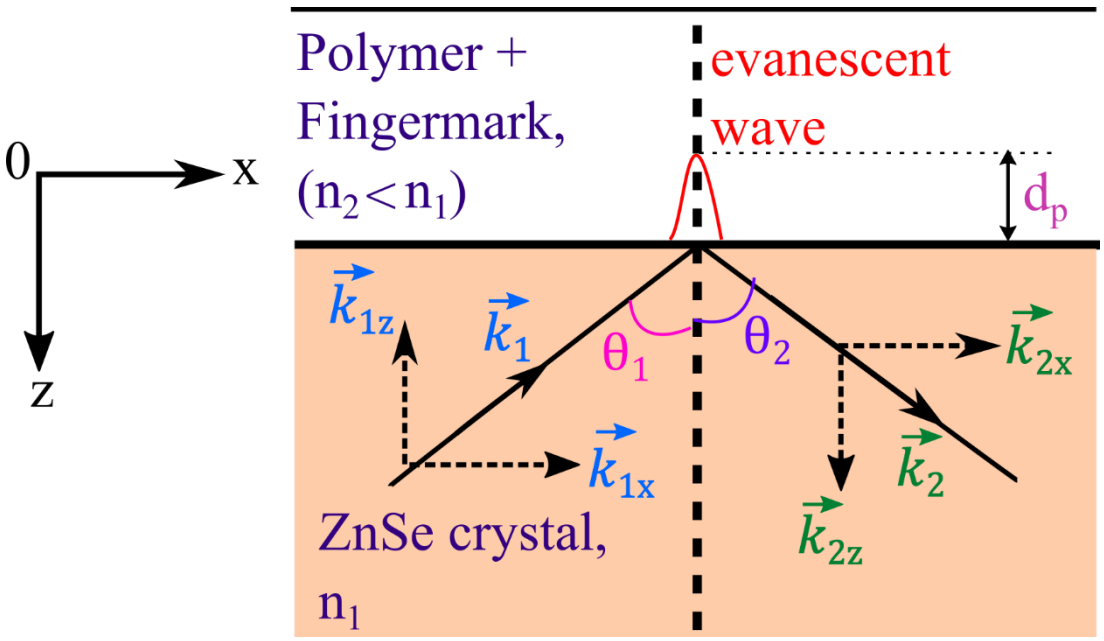

Figure 3.17: Schematic picture of attenuated total reflection (ATR) occurring in ZnSe crystal, producing an evanescent wave within the polymer and fingermark residue deposited region. d_p, is the depth of penetration of the evanescent wave.

This is defined as the depth at which the amplitude of the evanescent wave attenuates by a factor of e in the z direction (see equation 3.32). The evanescent wave travelling in the x direction (see equation 3.34) can interact with and be absorbed by the molecules in the second medium which are in the vicinity of the interface. In the

experiments described here, this evanescent wave was used to obtain information about the fingermark residue deposited on surfaces of different types of polymers (see Figure 3.18). The penetration depth, d_p defined as the distance required for the electric field amplitude to fall to 1/e of its value at the surface is given as:

$$d_p = \frac{\lambda}{2\pi n_1 \sqrt{(sin^2\theta - \left(\frac{n_2}{n_1}\right)^2)}} \tag{3.35}$$

where

λ = wavelength of infrared source

θ = angle of incidence of the infrared beam into the ZnSe crystal

n_1 = refractive index of the ZnSe

n_2 = refractive index of the sample

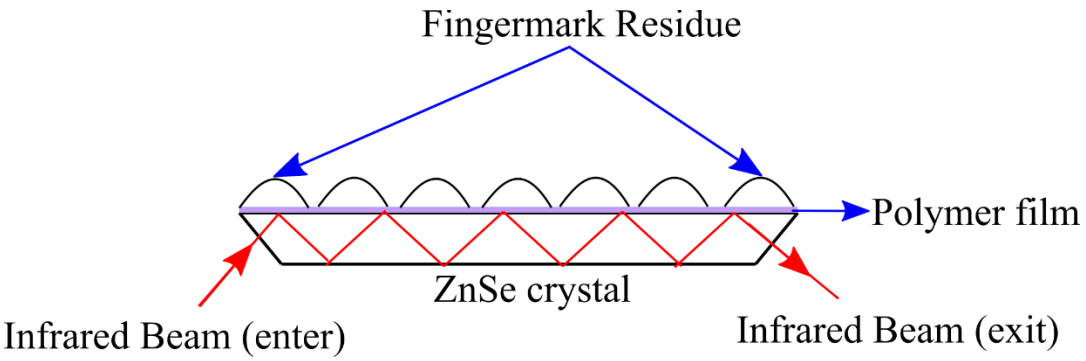

Figure 3.18: Schematic representation of infrared beam undergoes multiple internal reflection effect in attenuated total reflectance before reaching the detector. It also demonstrates the experimental setup in this study with fingermark residue being deposited on a thin layer of polymer film that is fully in contact with ZnSe crystal.

3.12.7 FTIR Measurements

This section relates on the use of FTIR as a part of this study in taking measurements. FTIR technique was coupled with the cyanoacrylate fuming method to quantify the

changes in the chemical composition of fingermark residue during the cyanoacrylate fuming process. It is important to note that the fuming process was modified so that it could be carried out in a similar way for both the camera and FTIR measurements, in order to draw a direct correlation between these two methods. The setup modification implemented for the CNA fuming to take place in the FTIR is illustrated in Figure 3.19.

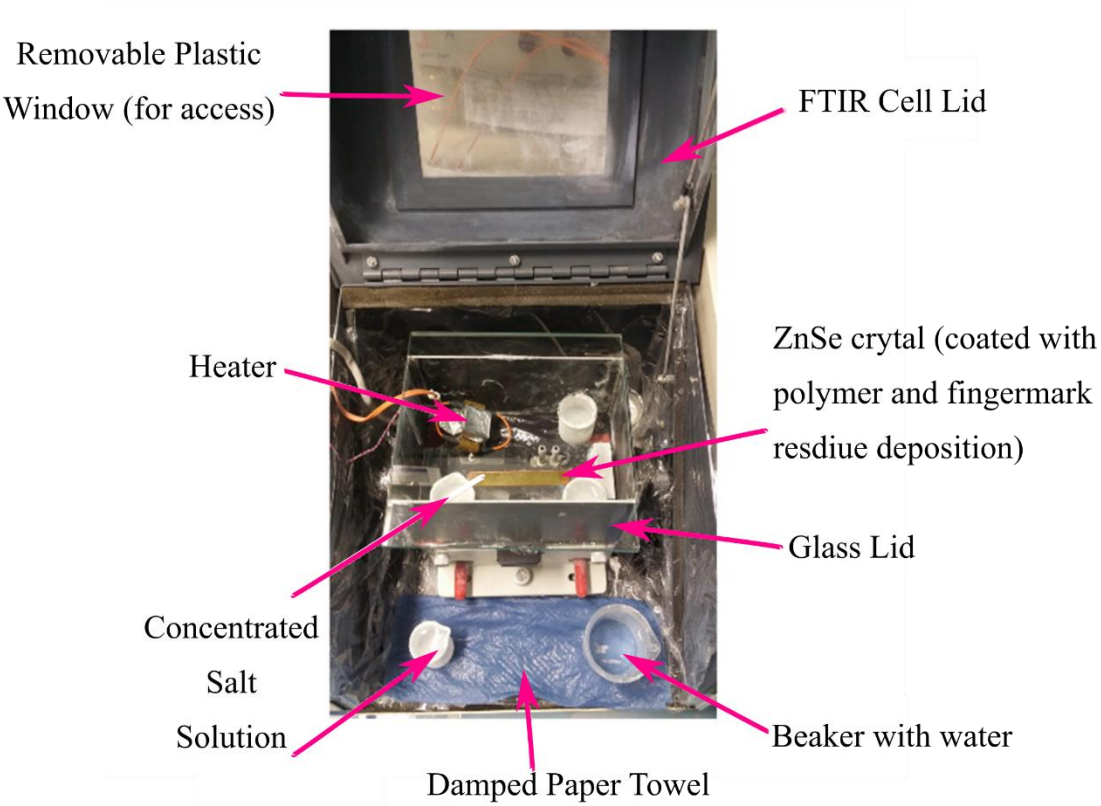

Figure 3.19: Cyanoacrylate fuming set up in FTIR cell. Damped paper towel was included besides the concentrated salt solution in order to maintain humidity in the FTIR cell at 60% throughout the fuming process and a heater to heat up the superglue at 60°C. This is due to the dry air purge connected to the FTIR cell that ensures to keep water vapour at a constant low level in the cell.

Once set up was ready as shown in Figure 3.19, the background scan of ZnSe crystal with the polymer coating was collected before fingermark residue was smeared on the polymer. Later, a five drops of superglue were dropped on the heater and the environmental chamber was closed with a glass lid. At last, the FTIR cell lid was

closed and the kinetics scan was initiated. The absorbance spectra were collected at every 300 seconds (i.e. 5 minutes) by averaging 265 scans. By following the height of a peak in the absorbance spectra as a function of time using the FTIR technique, it is possible to measure the amount of superglue deposited on the fingermark residue is discussed in greater detail in Chapter 4.

3.13 Time-of-Flight Secondary Ion Mass Spectrometry (ToF-SIMS)

Time-of-flight secondary ion mass spectrometry (ToF-SIMS) is a robust and extensively used technique for surface chemical analysis [25]. ToF-SIMS is useful for the identification of different chemical species on surfaces and has an elemental detection limit ranging from 1 part per million sensitivity for some molecules to parts per billion sensitivity for some chemical elements [26]. ToF-SIMS is extremely surface sensitive, as it can acquire molecular composition information of the sample surface to a depth of 1 to 2 nm in static SIMS mode.

3.13.1 Fundamental Principles of ToF-SIMS

ToF-SIMS is a technique based on bombardment of an energetic (keV) primary ion beam on the sample surface in an ultra-high vacuum (UHV) environment. When the energetic ions impinge upon the surface, molecules in the surface layer are subjected to collision. These collisions produce a number of charged atoms, neutral species, molecules and molecular fragments that are ejected from the surface. The ejected species are known as secondary ions and the ejection process is referred as sputtering. The emitted secondary ions which can be either positively or negatively charged, are extracted to the mass analyser using a static electric field in the extractor and identified based on their *m/z* ratio in mass spectrometer, as shown in Figure 3.20.

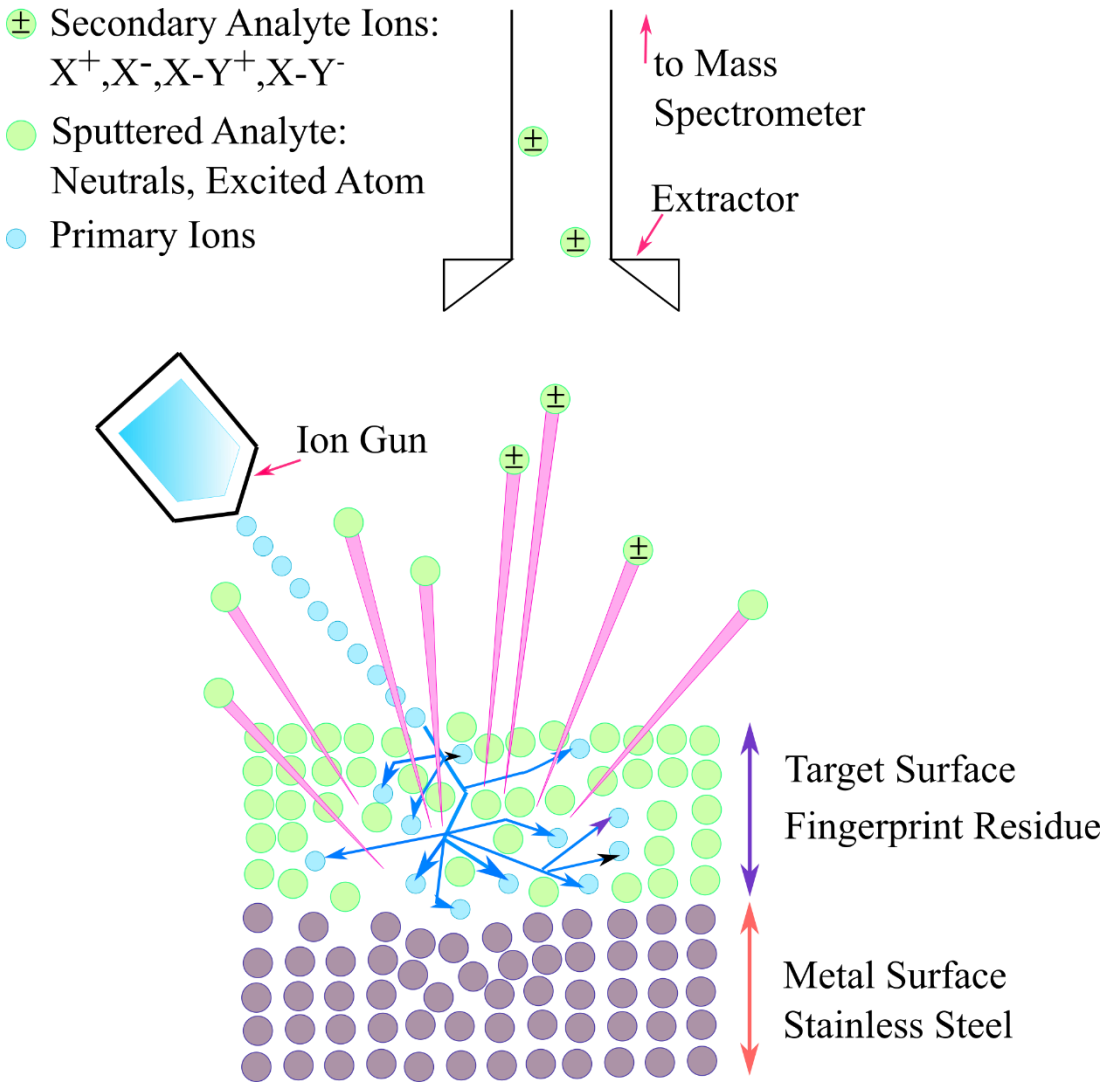

Figure 3.20: Figure represents the interaction of impact ion with the surface. High energy primary ions hit the target surface and causes series of collision between the atoms (collision cascade) of the target leading to ejection of one or more atoms from the target surface. This desorption of atoms or ions from the target surface, is a consequence of primary ion bombarding, is known as ion sputtering. The secondary analyte ions are then extracted by the immersion lens (extractor) and sent to the mass spectrometer.

Traditionally, SIMS employs atomic primary ions such as Ga^+, Ar^+, Cs^+, and Au^+ with the impact energy lie within the range of about 0.5 – 30 keV [25]. However, these atomic primary ions, implant deep into the target surface causing massive sub-surface damage (i.e. displaced atoms), while only a small amount of material is sputtered.

Thus, over the last decade, there has been a significant research focused on the implementation of cluster ion sources such as fullerene C_{60}^+, large gaseous argon clusters, Ar_n^+, Bi_n^+ and SF_5^+ as primary ions in SIMS [27]. Cluster primary ions, on the other hand deposit their energy closer to the surface (i.e. lower penetration into the sample) and form a large impact crater resulting in a higher amount of material sputtered with minimal sample degradation. This allows the sputter removal of the material layer-by-layer without comprehensive build-up of damage or mixing [28].

Furthermore, higher deposition of energy near the surface results in the desorption of larger molecules species that contain higher mass chemical information. This theory is supported by an example of molecular dynamics simulation, of both the cluster ion (C_{60}^+) impact and atomic primary ion (Ga^+) impact on an Ag (111) surface which is represented in Figure 3.21 that was reproduced from Postawa *et al*. [29].

Figure 3.21 show that upon impact at 15keV the cluster ion, C_{60}^+ dissociates into 60 constituents carbon atoms and each carbon atom carrying energy of 250 eV that creates their own cascade of moving particles. So, these atoms will deposit energy very close to the target surface, resulting in the amount of material sputtered by a single ion impact increases while reducing the damage caused.

Meanwhile, when the same 15keV Ga^+ atomic beam strikes the surface, it penetrates deep into the target sample (i.e. implantation of primary ions), depositing the energy many monolayers below the target sample. This causes sub-surface atoms relocation (i.e. mixing) and less amount of material is sputtered per impact.

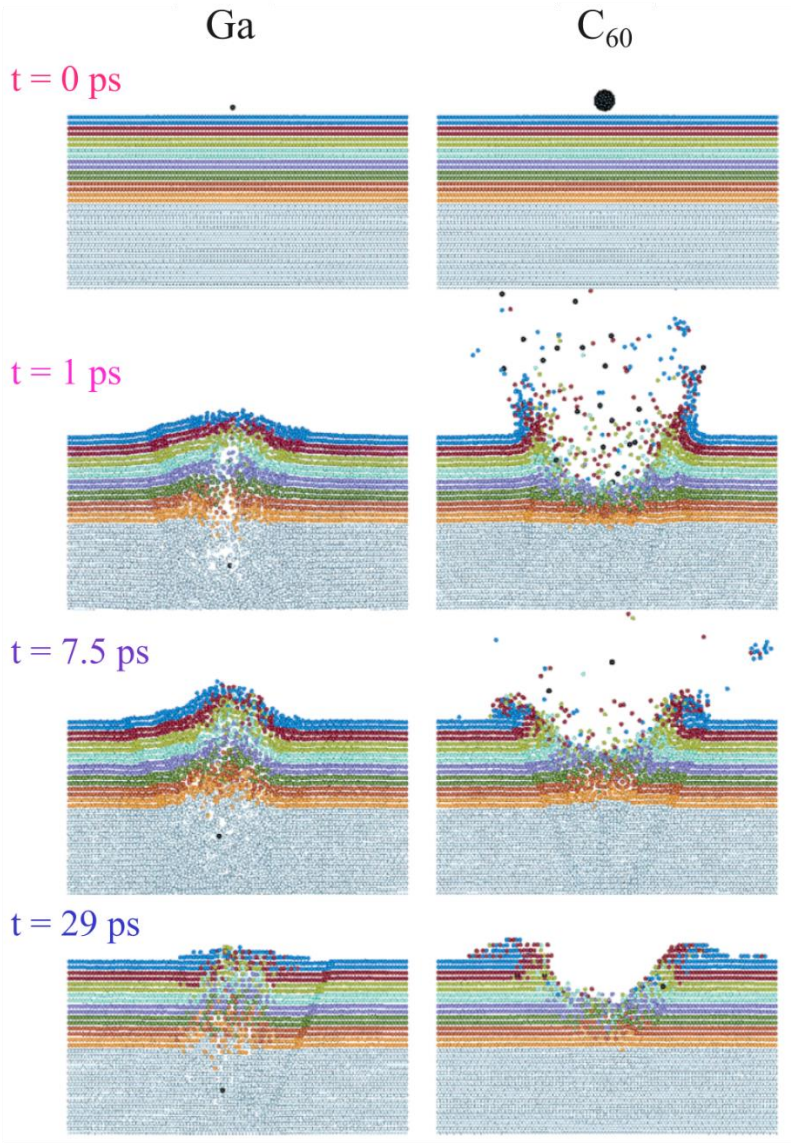

Figure 3.21: Figure represents molecular dynamics simulation of an atomic primary ion beam (Ga^+) and cluster ions primary beam (C_{60}^+) both of 15 keV energy hit on an AG (1 1 1) surface at normal incidence. At the time of 29 ps the atomic beam, Ga^+ has penetrated many monolayers of the sample while the cluster ions, C_{60}^+ managed to sputter more material from the target sample at that time. Figure is reproduced from Reference 29.

3.13.2 Instrumentation

A secondary ion mass spectrometer comprises (1) a primary ion gun – to generate the primary ion beam, (2) a primary ion column – to accelerate and focus the beam onto the sample, (3) high vacuum sample chamber - to hold the sample and the secondary ion extractor with analyser lens, (4) a mass analyser – to separate the ions based on their mass-to-charge ratio, and (5) a detector. The schematic diagram of ToF-SIMS instrument used in this study with pulsed primary ion beam and single stage reflectron analyser design is presented in Figure 3.22.

Primary Ion Gun

In ToF-SIMS, a liquid metal ion gun (LMIG), which has a focused ion beam (<50 nm), is commonly used as the primary ion source which can achieve pulses of a few hundred picoseconds. The ion sources are chosen from the following 3 types, Ga, Au, and Bi, where Ga ion beams are all monomers, while Au and Bi are cluster ion sources. The metal is heated under a nozzle in a high extraction field, causing a needle shaped tip to be formed and field ionisation produces the primary ions.

In general, the pulsed primary ion beam is accelerated by around 20 – 30 kV, with a typical pulse width of 25 ns. It is then combined with electromagnetic bunching techniques, to further compress the primary ion pulse length so that it arrives at the sample within ~ 1 ns [30].

The primary ion pulse comprised of several hundred primary ions has the capacity to sputter secondary ions from the sample. The primary ion pulse provides the start signal as the time t = 0 for the time-of-flight measurement of the secondary ions. The secondary ions generated at the target surface are extracted into the time-of-flight mass analyser via the extractor.

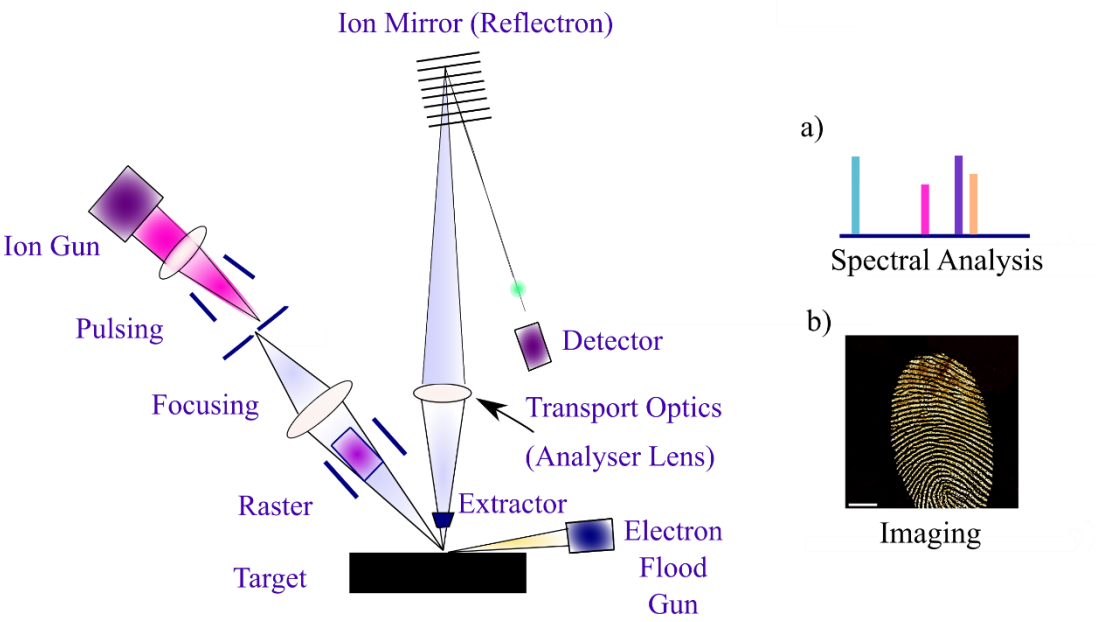

Figure 3.22: A schematic view of a ToF-SIMS IV instrument used in this study. The ion gun generates energetic pulsed primary ion beam that bombards the target surface, sputtering secondary ions up to two uppermost monolayers of the target surface [31]. The secondary ions are extracted by the extractor which then all are accelerated to the same nominal kinetic energy towards ion mirror. The ion mirror compensates the small differences in the initial energy of the secondary ions and reflect the ions into field free region before reaching the detector. The schematic represents the options for surface and bulk analysis of solid samples by (a) obtaining mass spectrometric analysis of surface by measuring the time of the secondary ions arrive at the detector for each primary ion pulse, and (b) imaging of the lateral distribution of secondary ions. Electron flood gun neutralises any charging created to the target surface during the bombardment of the primary ion beam.

Secondary ions are then accelerated in a static field via an electric potential difference, V and all ions acquire the same kinetic energy. If the ions travel a field-free distance, D to the detector, their flight time is given by:

$$t = \frac{D}{v} = D\sqrt{\frac{m}{2zeV}} \tag{3.36}$$

where m is the mass of the ion, v is the ion's velocity, z is the number of charges of the ion and e is the fundamental charge. The distance between the potentials is typically about 0.5 cm and the length of flight path, D can range between 15 cm and 8 m [32]. Acceleration voltages range between 3 kV and 30 kV and the flight time amounts 100 μs during standard analysis. Then time can be converted to *m/z* by:

$$\frac{m}{z} = 2eV\left(\frac{t}{D}\right)^2 \tag{3.37}$$

However, in reality the secondary ions are not all emitted with the same energy but with a more or less broad energy distribution. Hence, secondary ions with a small spread of initial kinetic energy of several eV for the ions of the same mass will lead to a broadening of the peaks. To reduce the effects of a spread in initial kinetic energy, a high extraction voltage of typically -2000 V for positive secondary ions and +2000 V for secondary ions is applied and a reflectron that consists of a single stage ion mirror is used, see Figure 3.23 [33]. A reflectron is a post-source compensation method for energy inhomogeneity and consists of a retarding electric field that reverses the direction of the ions. Ions with a higher kinetic energy will have a larger penetration depth so their travel distance also increases, and different ions of the same mass arrive at the detector with improved time-focus. A full mass spectrum is obtained for each primary ion pulse by measuring the arrival times of the secondary ions at the detector and summed over many pulses (typically $10^5 – 10^7$).

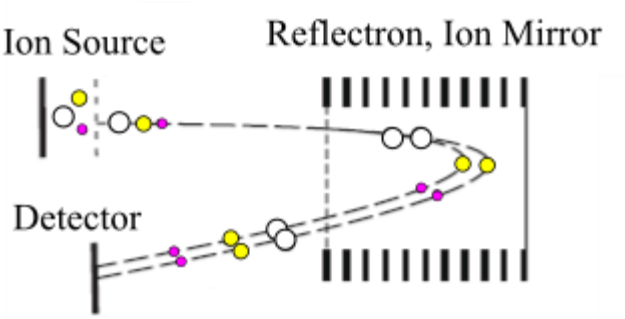

Figure 3.23: Schematic of the ion optics of a ToF-SIMS with one-stage ion mirror. The potentials are visualised along the ion optical axis. Figure is reproduced from Reference 34.

Electron Gun

When the primary ion beam bombards the surface, along with the emission of secondary ions, an excess of electron emission occurs as well which causes positive charging of dielectric samples (change in surface potential). Consequently, the local extraction voltage is altered, and the measurements is interrupted. Thus, electron flood gun is necessary as a charge compensation for insulating samples during analysis. This is to neutralise the positive charging by delivering a beam of low energy (~20 eV) electrons during the mass separation to the sample surface [35].

Analysis Mode

For this study purpose, ToF-SIMS technique was used to attain surface spectroscopy and surface imaging. ToF-SIMS images are obtained by rastering a fine focused primary ion beam across the sample and collecting mass resolved secondary ion images (chemical maps, i.e. full mass spectrum recorded) at each pixel. The resulting image resolution relies upon the primary ion beam focus and the availability of signal. Afterward, ion images are reconstructed by showing the intensity of specific ions per pixel. The ion images visualise the distribution of components at the surface. Low secondary ion yields limit the ion intensity and therefore the contrast of the ion images. Cluster ions are generated by the liquid metal ion gun (LMIG), can readily achieve a typical focus of about 3 – 5 μm with a bunched pulse width of 1 ns in high mass

resolution mode. However, the beam focus can be improved to approximately 100 nm by employing longer primary ion pulses and compromising on the mass resolution of the spectrum [36].

Time-of-flight secondary ion mass spectrometry (ToF-SIMS) was used in Chapter 6 to visualise latent fingermarks on stainless steel.

References

1. Sears, V. G., Bleay, S. M., Bandey, H. L., & Bowman, V. J. (2012). A methodology for finger mark research. *Science & Justice*, *52*(3), 145-160.

2. Bailey, M. J., Bright, N. J., Croxton, R. S., Francese, S., Ferguson, L. S., Hinder, S., Jickells, S., Jones, B.J., Jones, B.N., Kazarian, S.G. & Ojeda, J. J. (2012). Chemical characterization of latent fingerprints by matrix-assisted laser desorption ionization, time-of-flight secondary ion mass spectrometry, mega electron volt secondary mass spectrometry, gas chromatography/mass spectrometry, X-ray photoelectron spectroscopy, and attenuated total reflection Fourier transform infrared spectroscopic imaging: an intercomparison. *Analytical chemistry*, *84*(20), 8514-8523.

3. *Critical Surface Tension and Contact Angle with Water for Various Polymers*. (2018, March 30). Retrieved from https://www.accudynetest.com/polytable_03.html?sortby=contact_angle

4. Liston, E. M., Martinu, L., & Wertheimer, M. R. (1993). Plasma surface modification of polymers for improved adhesion: a critical review. *Journal of adhesion science and technology*, *7*(10), 1091-1127.

5. Isabell, T. C., Fischione, P. E., O'Keefe, C., Guruz, M. U., & Dravid, V. P. (1999). Plasma cleaning and its applications for electron microscopy. *Microscopy and Microanalysis*, *5*(2), 126-135.

6. Jokinen, V., Suvanto, P., & Franssila, S. (2012). Oxygen and nitrogen plasma hydrophilization and hydrophobic recovery of polymers. *Biomicrofluidics*, *6*(1), 016501.

7. Binnig, G., Quate, C. F., & Gerber, C. (1986). Atomic force microscope. *Physical review letters*, *56*(9), 930.

8. Green, C. P., Lioe, H., Cleveland, J. P., Proksch, R., Mulvaney, P., & Sader, J. E. (2004). Normal and torsional spring constants of atomic force microscope cantilevers. *Review of Scientific Instruments*, *75*(6), 1988-1996.

9. Eaton, P., & West, P. (2010). *Atomic force microscopy*. Oxford University Press, pp. 15-16.

10. Haugstad, G. (2012). *Atomic force microscopy: understanding basic modes and advanced applications*. John Wiley & Sons pp. 91-136.

11. Paine, M., Bandey, H. L., Bleay, S. M., & Willson, H. (2011). The effect of relative humidity on the effectiveness of the cyanoacrylate fuming process for fingermark development and on the microstructure of the developed marks. *Forensic science international*, *212*(1-3), 130-142.

12. Lee, H. C., Ramotowski, R., & Gaensslen, R. E. (Eds.). (2001). Methods of Latent Fingerprint Development. *Advances in Fingerprint Technology Second Edition*. CRC press.

13. Tasumi, M. (Ed.). (2014). Introduction to Infrared Spectroscopy. *Introduction to experimental infrared spectroscopy: Fundamentals and practical methods*, *pp. 8-10*. John Wiley & Sons.

14. Knight, R. D. (2013). Wave Optics, Interferometers. *Physics for Scientists and Engineers: A Strategic Approach with Modern Physics, Third Edition, pp. 722*. Pearson Education Limited.

15. Thorne, A. P. (1988). Interferometers, Michelson interferometers and Fourier transform spectroscopy. *Spectrophysics, Second Edition, pp. 185-190*. Chapman and Hall.

16. Barth, A. (2007). Infrared spectroscopy of proteins. *Biochimica et Biophysica Acta (BBA)-Bioenergetics*, *1767*(9), 1073-1101.

17. Jordan, D. W., & Smith, P. (1997). Mathematical techniques: An introduction for the engineering, physical, and mathematical sciences. *Second Edition.* Oxford University Press.

18. Blitz, J. P., & Klarup, D. G. (2002). Signal-to-noise ratio, signal processing, and spectral information in the instrumental analysis laboratory. *Journal of Chemical Education*, *79*(11), 1358.

19. Poole, A. B., & Sims, I. (Eds.). (2016). *Concrete Petrography: A Handbook of Investigative Techniques, pp. 34-37*. CRC Press.

20. Hsu, C. P. S., & Settle, F.A. (Ed.). (1997). Infrared spectroscopy. *Handbook of Instrumental Techniques for Analytical Chemistry, pp. 251 - 257*. Prentice Hall PTR.

21. Iwata, T., Paddock, M. L., Okamura, M. Y., & Kandori, H. (2009). Identification of FTIR bands due to internal water molecules around the quinone binding sites in the reaction center from Rhodobacter sphaeroides. *Biochemistry*, *48*(6), 1220-1229.

22. Schloss, J. M. (2011). *Infrared Spectroscopy of Trapped Gases in Metal-Organic Frameworks* (Honors Thesis, Oberlin College).

23. Griffiths, P. R., & De Haseth, J. A. (2007). Attenuated Total Reflection. *Fourier Transform Infrared Spectrometry*, *Second Edition, pp. 323-325*. John Wiley & Sons.

24. Milosevic, M. (2013). On the nature of the evanescent wave. *Applied spectroscopy*, *67*(2), 126-131.

25. Vickerman, J. C., & Briggs, D. (Eds.). (2001). *ToF-SIMS: surface analysis by mass spectrometry*. IM Publications and SurfaceSpectra Limited.

26. Linford, M. R. (2014). An Introduction to Time-of-Flight Secondary Ion Mass Spectrometry (ToF-SIMS). *Vacuum Technology & Coating*, 30-35.

27. Senoner, M., & Unger, W. E. (2012). SIMS imaging of the nanoworld: applications in science and technology. *Journal of Analytical Atomic Spectrometry*, *27*(7), 1050-1068.

28. Shard, A. G., Green, F. M., Brewer, P. J., Seah, M. P., & Gilmore, I. S. (2008). Quantitative molecular depth profiling of organic delta-layers by C60 ion sputtering and SIMS. *The Journal of Physical Chemistry B*, *112*(9), 2596-2605.

29. Postawa, Z., Czerwinski, B., Szewczyk, M., Smiley, E. J., Winograd, N., & Garrison, B. J. (2004). Microscopic insights into the sputtering of Ag {111} induced by C60 and Ga bombardment. *The Journal of Physical Chemistry B*, *108*(23), 7831-7838.

30. Schwieters, J., Cramer, H. G., Heller, T., Jürgens, U., Niehuis, E., Zehnpfenning, J., & Benninghoven, A. (1991). High mass resolution surface imaging with a time-of-flight secondary ion mass spectroscopy scanning microprobe. *Journal of Vacuum Science & Technology A: Vacuum, Surfaces, and Films*, *9*(6), 2864-2871.

31. Hagenhoff, B. (2000). High resolution surface analysis by TOF-SIMS. *Microchimica Acta*, *132*(2-4), 259-271.

32. Cotter, R. J. (1994). Time-of-flight mass spectrometry: Basic principles and current state. In *Time-of-Flight Mass Spectrometry* (p. 16).

33. Green, F. M., Gilmore, I. S., & Seah, M. P. (2006). TOF-SIMS: Accurate mass scale calibration. *Journal of the American Society for Mass Spectrometry*, *17*(4), 514-523.

34. Radionova, A., Filippov, I., & Derrick, P. J. (2016). In pursuit of resolution in time-of-flight mass spectrometry: A historical perspective. *Mass spectrometry reviews*, *35*(6), 738-757.

35. Vanbellingen, Q. P., Elie, N., Eller, M. J., Della-Negra, S., Touboul, D., & Brunelle, A. (2015). Time-of-flight secondary ion mass spectrometry imaging of biological samples with delayed extraction for high mass and high spatial resolutions. *Rapid Communications in Mass Spectrometry*, *29*(13), 1187-1195.

36. Sodhi, R. N. S. (2004). Time-of-flight secondary ion mass spectrometry (TOF-SIMS):—versatility in chemical and imaging surface analysis. *Analyst*, *129*(6), 483-487.

CHAPTER 4

Latent Fingermarks on Surfaces of Different Wetting Properties

4.1 Introduction

In this chapter, the influence of the surface wetting properties on the deposited latent fingermark during the application of latent fingermark development technique is discussed. The study is demonstrated on polymer substrates, chosen in view of their widespread use in common everyday life objects (cling film, plastic bags, polyethylene cups) of forensic relevance, onto which is developed through cyanoacrylate fuming [1,2]. Cyanoacrylate fuming was selected based on it being a widely used forensic tool for the development of latent marks on non-porous surfaces by police, forensic labs, but more significantly this technique can be easily carried out in the lab by using simple set up as described in detail in Chapter 3, section 3.9.

The polymerisation of cyanoacrylate onto a fingermark causes physical and chemical changes in fingermark appearance and chemical structure. The physical changes experienced by fingermark deposited on surfaces with different water contact angle during the cyanoacrylate fuming process was analysed using camera observation. The chemical changes that occur within fingermark residue during the fuming process were obtained using Fourier Transform Infrared (FTIR) spectroscopy with Attenuated Total Reflection (ATR) technique.

4.2 Experimental

4.2.1 Polymer Solution Preparation

The glass microscope slides had been spin coated with 2 wt. % solutions of polymers, including polystyrene (M_w = 350K Da, Sigma Aldrich), poly (t-butyl methacrylate) (M_w = 977K Da, Polymer Source), poly (vinyl acetate) (M_w = 500K Da, Sigma Aldrich), and poly (methyl methacrylate) (M_w = 350K Da, Sigma Aldrich). All the polymers were dissolved in toluene, spin coated (spin speed 2500 rpm) and then annealed at ~ 120°C for 45 minutes to remove residual solvent. In order to prepare the polydimethylsiloxane (Sylgard TM 184 Silicone Elastomer Kit, Dowsil) polymer, the elastomer and curing agent were mixed in the10:1 ratio. It was also spin coated at 2500 rpm before annealed for ~ 24 hours at a temperature of ~ 120°C.

Zinc Selenide (ZnSe) crystal (Specac) had been spin coated with the same polymers but of 1 wt. % solution, and the polydimethylsiloxane (PDMS) was dissolved to 10 parts of toluene to make it less viscous. Lower weight percentage polymer solutions and further diluted PDMS was used for the FTIR technique in order to produce a thinner uniform polymer layer as the evanescent wave penetrates only up to a specific number of microns into the sample. Since the typical refractive index of ZnSe crystal is 2.40 and typical values for polymers used in this study range from 1.40 – 1.55, the penetration depth of the evanescent wave at any wavelength, λ can be determined.

The wavelength range of infrared source used in this study is of 3.33 μm to 10 μm was determined through the wavenumber in the FTIR spectra obtained, using the formula: $\lambda = \frac{1}{k}$ where k is the wavenumber. Note that at (λ) of 3.33 μm, the wavenumber, k is 3000 cm^{-1} and at (λ) of 10 μm, the wavenumber, k is 1000 cm^{-1} is the range of spectra used to determine the change in chemical structure of fingermarks during cyanoacrylate polymerisation. Using Equation 3.3 in Chapter 3, section 3.12, an example of the calculation carried out to determine the penetration depth, d_p is shown below. Substituting the values for a wavelength of infrared source, the angle of infrared incidence and the refractive index of both ZnSe and polymer substrate into Equation 3.3 gives

$$d_p = \frac{10\ \mu m}{2\pi(2.40)\sqrt{(sin^2 45° - \left(\frac{1.40}{2.40}\right)^2)}} = 1.66\ \mu m \qquad (4.1)$$

the penetration depth of the evanescent wave in the sample film consisting of a layer of polymer film and fingermark residue. It should also be noted that at the wavelength, λ = 3.33 μm the penetration depth, d_p is found to be 0.353 μm using the same value of the refractive index in Equation 4.1. Hence, thinner polymer film allows further penetration of evanescent wave into the fingermark residue for the range of wavenumbers that are used to work in this study.

An additional polymer surface that was used apart the polymers mentioned earlier in the study of latent marks is 'cling film'. It was chosen although it is known to be a problematic surface was because it has importance in forensics due to its numerous illicit uses including drug wraps as well as used for wrapping explosives [3]. The 'cling film' is manufactured from either polyvinylidene chloride (PVC) or more commonly polyethylene (PE) polymers.

Cling film (Safe Wrap) used in this study is of PE-base surface, was confirmed from the composition of the cling film by means of FTIR measurements. Since the surface of cling film was used fresh from the roll and was checked to be free of fingermarks, this surface did not require an additional cleaning process and it was used as it is. The cling film was secured to the microscopic glass sides by using double-sided tape at the edges to make sure it was tightly attached.

Additionally, cling film was studied using camera observations only for two reasons, mainly due to the thickness of the cling film that is of ~ 0.021mm (~ 21μm) which is too thick for the evanescent wave to be able to pass through into the fingermark residue and secondly the cling film could not be attached on Zinc Selenide (ZnSe) crystal without ruining the ZnSe crystal.

The list of polymers used along with their corresponding measured water contact angle are tabulated in Table 4.1 below. It is important to note that the polymers are sometimes referred to as hydrophilic or hydrophobic polymer surfaces/substrates in this thesis. The term hydrophilic and hydrophobic refers to the surface with water contact angle less and greater than 90° respectively. The reason for the water droplet to spread more on hydrophilic surface is because this surface has a high surface energy

that creates a strong attractive force to pull the water droplet down, causing it to spread out. Meanwhile, the hydrophobic surfaces have low surface energy meaning the water can keep its droplet shape better as there is not enough force from the surface to pull the water droplet down.

Polymer	**Measured Water Contact Angle (Degrees)**	**Literature Water Contact Angle (Degrees) [4]**	**Refractive Index, n [6]**
Polystyrene treated with oxygen plasma (PS Plasma)	15.0° ± 6.6°	5° - 50° [5]	1.49
Polyvinyl Acetate (PVA)	60.2° ± 1.3°	60.6°	1.47
Polyethylene / Cling Film (PE)	65.9° ± 4.8°	96°	1.51 – 1.55
Poly (methyl methacrylate) (PMMA)	74.2° ± 2.3°	70.9°	1.47
Polystyrene (PS)	86.0° ± 2.4°	87.4°	1.49
Polydimethylsiloxane (PDMS)	101.3° ± 3.5°	107.2°	1.40 [7]
Poly (t-butyl methacrylate) (PtBMA)	102.8° ± 1.6°	108.1°	1.46

Table 4. 1: Table above lists the types of polymers used in this study with the measured water contact angle and their respective literature water contact angle. The refractive index, of each polymer has been included to study its influence in the penetration depth of evanescent wave during FTIR measurement. Water contact angle measurement has been explained in detail in Chapter 3, section 3.7.

4.2.2 Fourier Transform Infrared Spectroscopy

FTIR spectroscopy measurements were collected using a Varian FTS40 Pro spectrometer equipped with Resolutions Pro 4.0 software. Each averaged spectrum was collected using a spectral resolution of 4 cm^{-1} while the time between the collections of the averaged spectra is 15 seconds. Spectral subtraction was performed on the infrared spectra obtained for eccrine fingermark deposits. A spectrum of water vapour (see Figure 4.1 (b)) was used to subtract the high content of water vapour absorbance in the eccrine fingermark deposits due to the 60% level humidity from the NaCl salt solution that was kept in the fuming chamber to ensure optimum level for the cyanoacrylate fuming process.

The spectral subtraction was not needed for sebaceous fingermark deposits because of the much stronger intensity of the peaks (see Figure 4.2) compared with the water vapour, and therefore was not affected due to the high level of humidity in the FTIR fuming chamber. The intensity of a peak in an absorbance spectrum corresponds to the amount of material being deposited. The reason for the much weaker intensity of the peaks for eccrine mark is presumably due to the eccrine mark residue composition that is made up of mainly dilute aqueous solution. This aqueous solution contains less than 1% of dissolved solids in which the concentration of the composition can vary due to many factors such as sweating rate, the temperature of the skin, age, seasonal changes and consumption of salt by an individual [8].

The baseline of the spectra tilted for both type of fingermark deposition over the course of the experiments (typically ~ 7 hours) due to variations in the intensity of the infrared (IR) light source used in the spectrometer. This tilting was corrected by subtracting a linear baseline which was calculated using the flat regions of the spectra in the ranges of 1900 – 2250 cm^{-1} and 2260 – 2800 cm^{-1} for sebaceous rich marks while 900 – 1000 cm^{-1} and 2000 – 2100 cm^{-1} for eccrine marks. Both the baseline and water vapour corrections were performed similarly on all the collected IR spectra, which were then analysed in the same manner throughout this study.

An example of water vapour subtraction and baseline correction for eccrine mark spectra are shown in Figure 4.1.

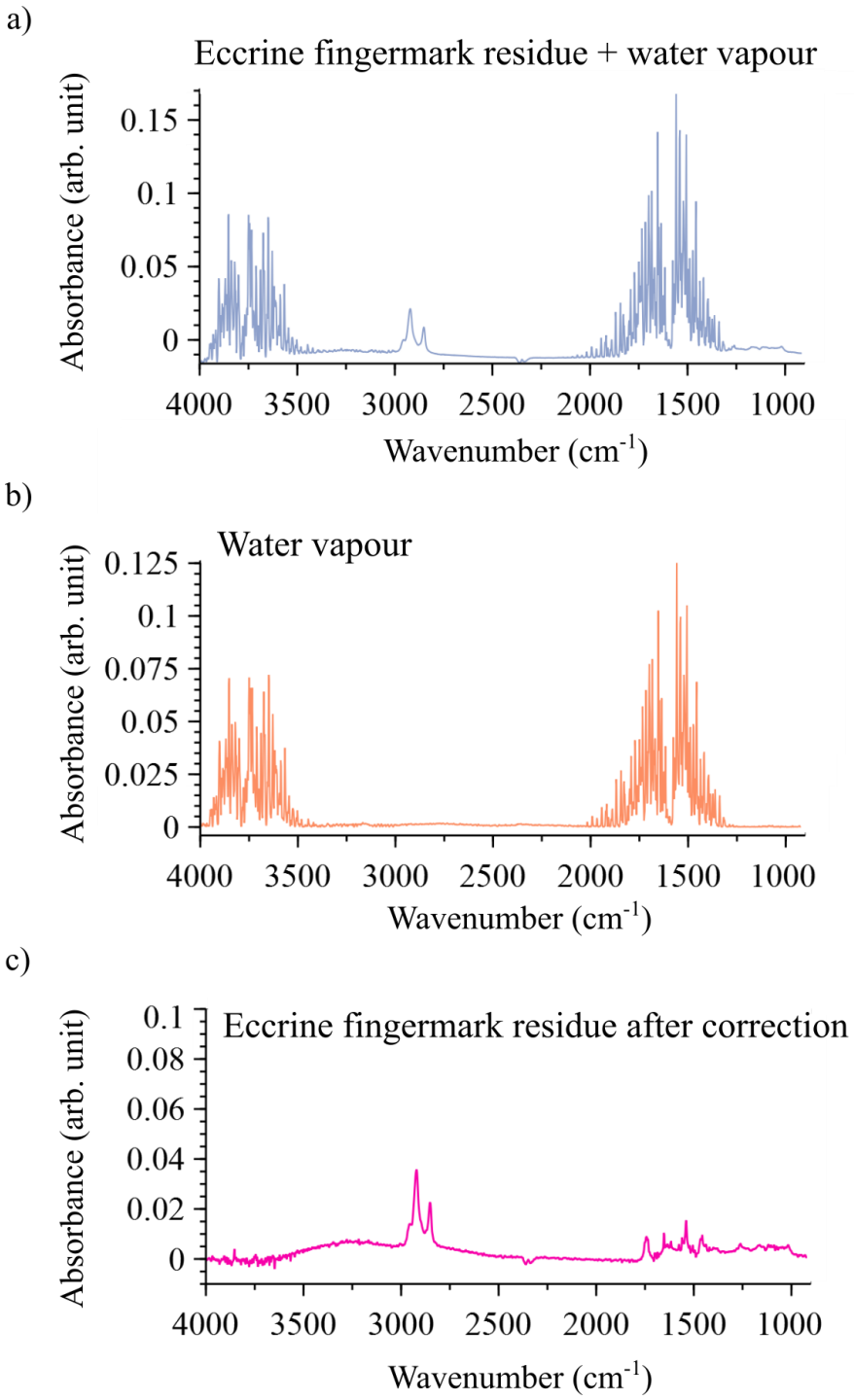

Figure 4. 1: Figure depicts a) the raw spectra of eccrine mark residue deposited on oxygen plasma treated polystyrene (PS Plasma), with high water vapour content within the regions of 2000 – 1300 cm^{-1} and 4000 – 3400 cm^{-1}, b) Water vapour spectra obtained on PS plasma surface represents the water vapour present in the same region as found in a), c) Represents spectra of eccrine mark residue after the baseline correction and water vapour minimisation using Matlab code.

Figure 4.2 shows an example of how the spectral baseline correction was performed to set the baseline at 0 and correct the tilted IR spectra of sebaceous fingermark residue after cyanoacrylate fuming using the Matlab program.

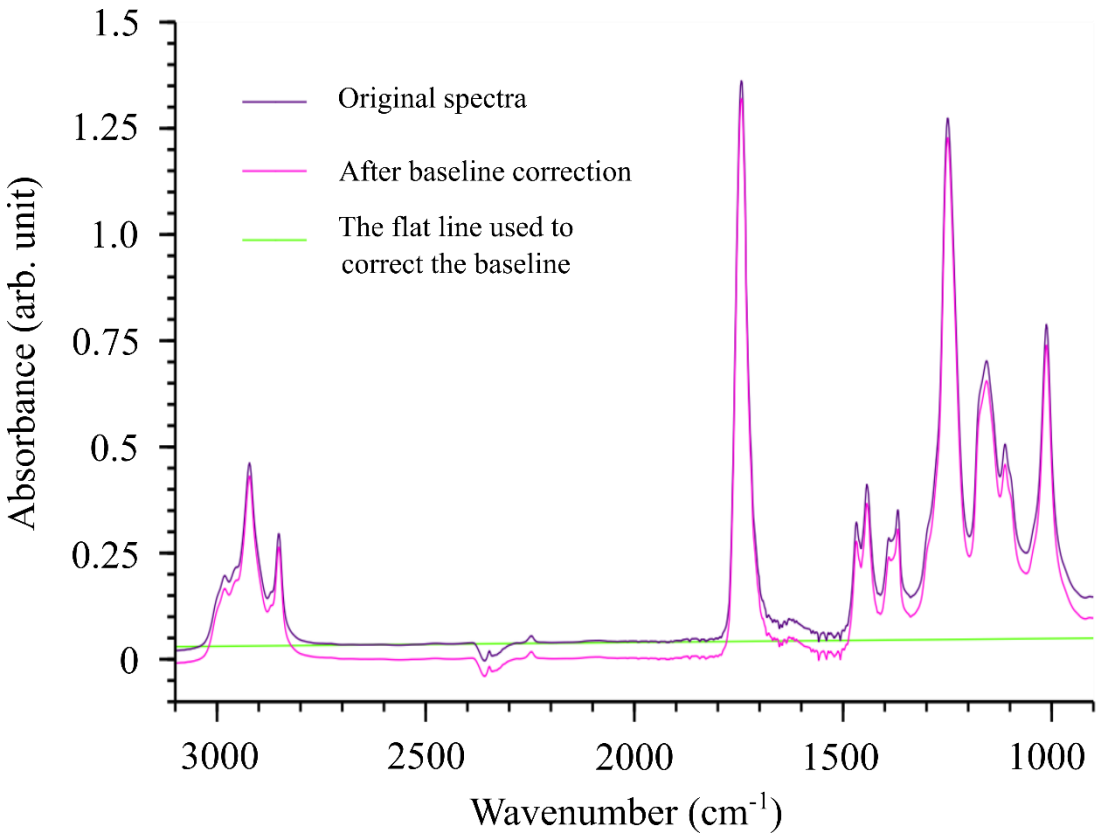

Figure 4. 2: An example of IR spectrum of sebaceous fingermark deposited and then fumed on PtBMA polymer with the baseline corrected to be flat using the software written in Matlab.

Prior to experiments, once ZnSe crystal was spin-coated with the polymer solution and then annealed for t = 45 minutes, it was left to cool down for about 10 minutes before fitting it in the Attenuated Total Reflection (ATR) cell. A background spectrum of the ZnSe crystal with the coated polymer was collected before depositing fingermark on the polymer surface. Then, five drops of superglue (RS Components, ethyl-2- cyanoacrylate) were dropped on the heater prior to closing the environmental chamber using a glass lid. The FTIR cell cover was closed and the kinetics scan was initiated immediately for spectra collection. Spectra were collected with a time resolution of 300 seconds (5 minutes) by averaging 265 scans. All the spectra were

then ratioed to the spectrum obtained from both the ZnSe crystal and the polymer substrate.

Data collection of cyanoacrylate polymerisation on bare polymer substrate without fingermark deposition was also carried out by setting up the FTIR cell exactly as shown in Figure 3.18 in Chapter 3, sub-section 3.12.7. The spectra of cyanoacrylate polymerisation on the bare polymer substrates were extracted in a similar way as for with fingermark deposition using the same number of scans and spectral resolution.

4.2.3 Camera Measurements

For the camera measurements, once the cyanoacrylate fuming setup is prepared as shown in Chapter 3, section 3.11, the deposition of a fingermark on a polymer substrate coated on glass microscope slide was carried out. Then the cyanoacrylate fuming process was started by dropping five drops of superglue on the heater. Immediately afterwards, images of the latent fingermark developed via cyanoacrylate fuming were captured using a Manta G – 125 (Allied Vision technologies) camera. The camera was controlled using a written python script to take several images within a set time frame and stored them in a directory set by the user.

In this study, images were taken every minute up to 333 minutes. This was performed to examine the differences in physical change/fingermark development (i.e. brightness due to the white deposition of the superglue polymerisation on the fingermark residue) that occurred on fingermark residue deposited on substrates with varying water contact angle from the captured images. Capturing the image of fingermark during enhancement has great importance; it is these images that allow to measure the differences that arise during the fuming process for the same type of fingermark residue on different surfaces by measuring the change in brightness of an image with respect to fuming time.

4.2.4 Thickness of Polymer Films

Since the intensity of electric field of the evanescent wave decays exponentially as a function of distance, the IR spectra that are obtained using this technique are extremely sensitive to material that is close to the interface. Hence, it is important to know the thickness of polymer films that were spin coated on ZnSe crystal. The thickness of the polymer film was measured using the tapping mode as described in Chapter 3, section 3.8. The polymers were spin coated and annealed in the same way as was mentioned for the fingermark deposition experiment. After the annealing process, the polymer coated ZnSe crystal was left to cool down before a scratch was made on the deposited polymer film using a scalpel.

Figure 4.3 a) displays an example of the image obtained using AFM, measuring the area of a scratch. Analysis of height fields from Figure 4.3 a) was done using Gwyddion Version 2.51 a modular program. Using this program, the thickness of each of the polymer film used in this study was obtained as shown in Figure 4.3 b). The list of the polymers along with their respective thickness on ZnSe crystal is tabulated in Table 4.2.

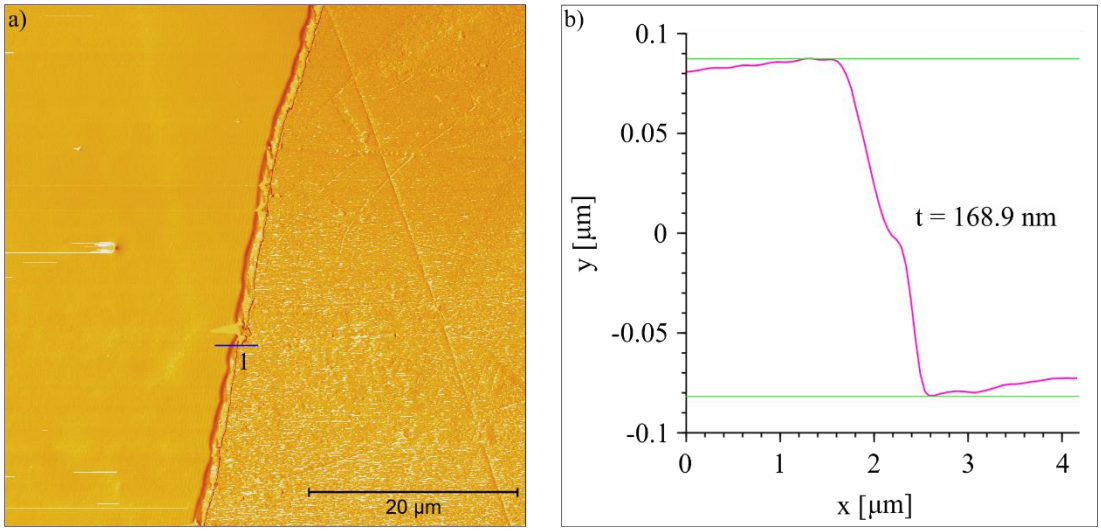

Figure 4. 3: (a) AFM image taken of a scratch made on polyvinyl acetate (PVA) polymer that was spin coated onto ZnSe crystal. The blue line represented with number 1 is the region used to measure the thickness of the polymer. (b) Using Gwyddion software, the measured thickness was obtained using two horizontal lines as shown, giving a total thickness of 0.169 µm.

Polymer	Measured Thickness of Polymer Film (μm)
Polystyrene treated with oxygen plasma (PS Plasma)	0.065 ± 0.004
Polyvinyl Acetate (PVA)	0.182 ± 0.021
Polyethylene / Cling Film (PE)	21.111 ± 2.437
Poly (methyl methacrylate) (PMMA)	0.172 ± 0.035
Polystyrene (PS)	0.135 ± 0.018
Polydimethylsiloxane (PDMS)	0.240 ± 0.040
Poly (t-butyl methacrylate) (PtBMA)	0.223 ± 0.027

Table 4. 2: Table represents the measured thickness of the polymer film used in this study. The thickness of all the polymer films are thinner than the evanescent penetration depth, d_p except for cling film as mentioned earlier is too thick to be studied using FTIR-ATR technique.

4.2.5 Optical Microscopy

Optical microscopy is used to view samples on a larger scale than possible with the naked eye. In this study, an Olympus BX51 optical microscope was used to obtain a detailed view of fingermark deposition on substrates of different wetting properties. The microscope uses transmitted visible light to illuminate the fingermark with an eyepiece of 50 times magnification to view the sample. The microscope was connected to a computer and was operated using Image-Pro Plus, Copyright 1993-2004 Media Cybernetics.Inc.

4.3 FTIR Measurements of Cyanoacrylate Polymerisation on Latent Fingermarks

This section demonstrates the extraction of information from the FTIR spectra to analyse the chemical changes in the fingermark functional groups during cyanoacrylate polymerisation for the two types of sweat, sebaceous and eccrine.

4.3.1 Sebaceous Deposits

Figure 4.4 shows an example of a typical FTIR spectrum of the sebaceous rich fingermark residue that was obtained using the attenuated total reflectance technique. The spectra was divided into two most informative regions in the ranges of 1000 – 1850 cm^{-1} (zone 1) and 2700 – 3100 cm^{-1} (zone 2) for analysis purposes.

Sebaceous materials are indicated by C-H, $C-H_2$, and $C-H_3$ bands with high absorbance at the wavenumber of 2953, 2922, 2853, 1464, and 1368 cm^{-1}. These bands correspond to the presence of fatty acids and wax esters. Besides that, C=O stretches were also observed at 1744 and 1653 cm^{-1}, C-O-C stretches at 1146 cm^{-1}, and O-C-C stretches at 1117 and 1016 cm^{-1}. These peaks represent saturated esters and thus leads to the verification of the presence of lipid compounds.

A few functional groups of lipid such as O-C-C stretch, C-C-O stretch, C-N stretch and CH_3 asymmetric bend were not observed due to the complex nature of fingermark constituents and variations among individuals. The main functional groups identified in all fresh sebaceous fingermark have been numbered with their corresponding vibration in Figure 4.4. The peak assignment and the most likely origin of its secretion are tabulated in Table 4.3.

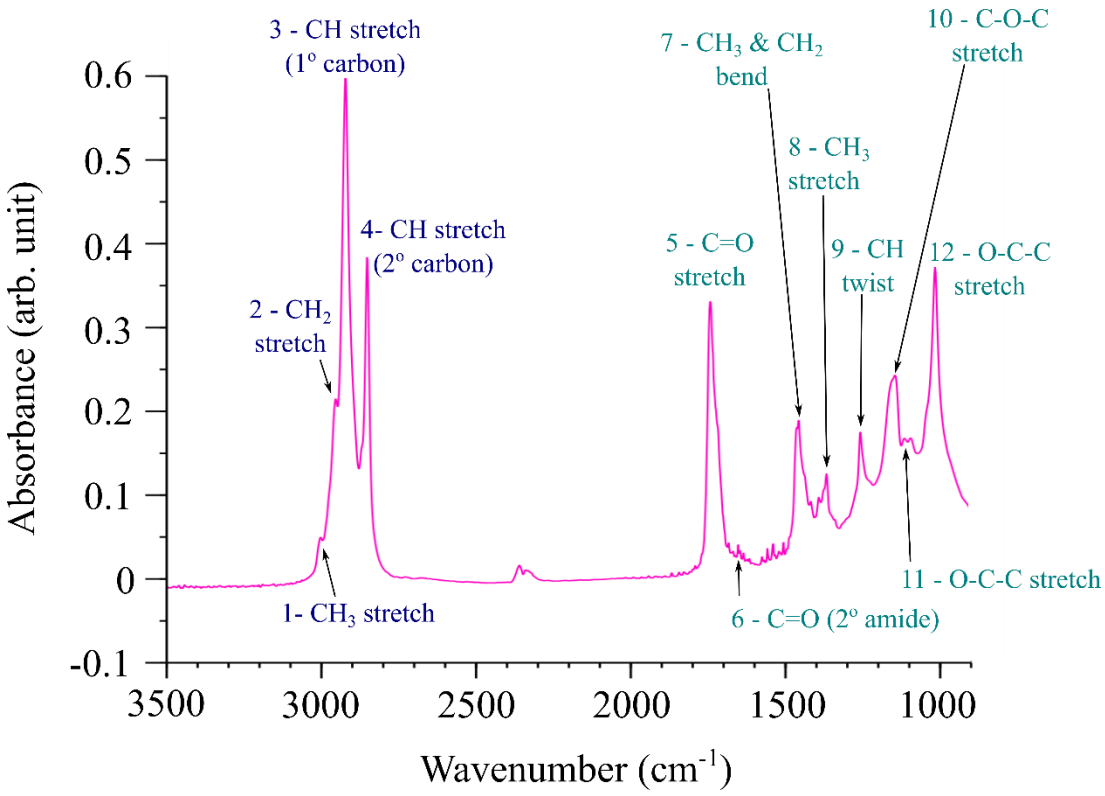

Figure 4. 4: Figure displays an example of FTIR spectrum of sebaceous fingermark deposited on PtBMA surface with their corresponding vibrational bands. Two different colours were used to number the peaks along with their vibrational bands to display the two most informative regions of FTIR spectra in this present study. The peak assignment corresponding to both eccrine and sebaceous compounds identified in the FTIR spectra are tabulated in Table 4.3 with their respective number along with the most likely origin of its secretion.

Peaks	Wavenumber (cm^{-1})	Vibration	Lipid/Protein Assignment	Secretion
	3281	N–H stretch (2° amide)	Protein	Eccrine [9,10,11]
	3150 - 3600	Large water peak		[9]
1	**3003**	Asymmetric =C-H_3 stretch	Fatty acids, lipids	Sebaceous [12]
2	**2953**	C–H_2 stretch	Wax esters or fatty acids	Sebaceous [9]
3	**2922**	C–H stretch (1° carbon)	Lipid	Sebaceous [9,11,13]
4	**2853**	C–H stretch (2° carbon)	Lipid	Sebaceous [9,11,13]
5	**1744**	C=O stretch (saturated ester)	Phospholipid	Sebaceous [9,10,11]
6	**1653**	C=O (2° amide)	Protein	Eccrine [9,10,11]
	1537	Major: N–H in-plane bend (2° amide) Minor: C–N stretch	Protein Protein	Eccrine [9]
7	**1464**	CH_3 asymmetric bend CH_2 symmetric bend	Lipid Lipid	Sebaceous [9,10,11]

	1411	CH_3 asymmetric bend	Lipid	Sebaceous [9]
	1379	CH_3 symmetric bend	Lipid	Sebaceous [9,10,11]
8	**1368**	CH_3 symmetric stretch	Phospholipid	Sebaceous [14]
9	**1258**	C-H twisting	Lipid	Sebaceous [12]
	1250 - 1253	C-O stretch	Amino acid side chain	Eccrine [15]
	1246	C-C-O stretch (asymmetric bend)	Esters	Sebaceous [9]
	1233 / (1200-1250)	C–N stretch (2° amide)	Protein	Eccrine [9,10,11,12]
	1160	C–C–O stretch (saturated ester)	Lipid	Sebaceous [10,11]
10	**1146**	C-O-C stretch	Glycogen	Sebaceous [12]
11	**1117**	O–C–C stretch (saturated ester)	Lipid	Sebaceous [9]
	1096	C-N stretch	Lipid	Sebaceous [14]
	1090 - 1096	C-N stretch, C-H bend	Amino acid	Eccrine [15]
	1051	O–C–C stretch (saturated ester)	Lipid	Sebaceous [9]

12	**1016**	O–C–C stretch (saturated ester)	Glycogen	Sebaceous [13]
	1012 - 1018	C-C stretch, C-H bend	Amino acid	Eccrine [15]

Table 4. 3: Functional groups corresponding to eccrine and sebaceous compounds found in fresh latent fingermark residue with their corresponding IR spectroscopy signals. The observable peaks that were identified from Figure 4.4 are numbered accordingly in the table.

The infrared spectra in Figure 4.4 depicts the fingermark residue to be a complex composition that is made up of amino acids, fatty acids, lipids, urea, proteins, glycerides mixed together with inorganic constituents such as chlorides, phosphates, sulphates and ammonia [16]. The cyanoacrylate polymerisation occurs anionically, thus constituents like chloride, moisture, carboxylic acids and amines can act as nucleophilic initiators to trigger the cyanoacrylate polymerisation mechanism [17].

Considering the importance of understanding the reaction that occurs between the latent mark residue and superglue, a FTIR spectrum (see Figure 4.5) of the superglue fumes attached to the bare surface of ZnSe crystal spin coated with PVA (without any fingermark deposition) was collected. Additionally, Figure 4.5 displays spectra of freshly deposited fingermark residue and spectra of the same mark after being exposed to the cyanoacrylate vapour. The peaks in fingermark residue spectra were numbered exactly as in Figure 4.4 for easier comparison with the changes observed in the peaks after the cyanoacrylate fuming process.

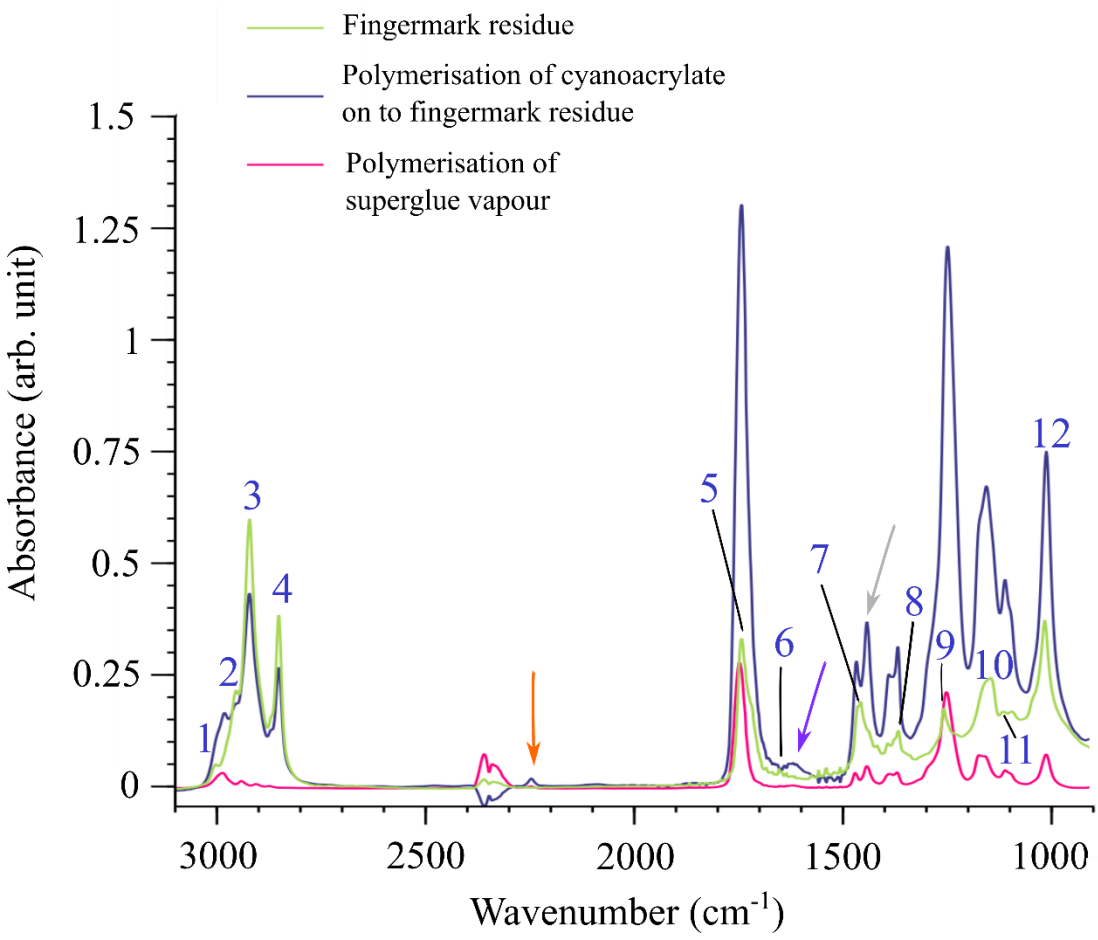

Figure 4. 5: Figure displays the FTIR spectrum of freshly deposited sebaceous fingermark residue on PtBMA surface (0 minute) in green. The fingermark residue was then exposed to the cyanoacrylate fumes, represented in blue was taken at the 120th minute of the fuming process. The red spectra correspond to the polymerisation of cyanoacrylate vapour at the 120th minute on bare PVA polymer that was spin coated onto the ZnSe crystal. The same vibrational bands indicated in Figure 4.3 were shown again to observe the changes in the spectra during the cyanoacrylate fuming process. Additional arrows with colours of orange, purple and grey each represents formation of new peak after the cyanoacrylate fuming process.

All the vibrational peak absorbance values within the wavenumber range of 1000 – 1800 cm^{-1} increased after the fuming process with formation of new peaks. Two new peaks emerged at wavenumber 1443 cm^{-1} (pointed with grey arrow) next to peak numbered 7 with a much higher absorbance and the other at 1618 cm^{-1} (pointed with purple arrow) were observed at the time of fuming. The formation of these new peaks

i.e. new absorbance peaks or shoulders were produced as a result of changes that occurred due to the cyanoacrylate polymerisation process on to the fingermark residue compound [18].

Peaks numbered 8, 9, and 11 showed a significant amount of increase as these peaks became more distinct after the exposure of cyanoacrylate vapour. A new small peak emerged at wavenumber 2237 cm^{-1} (pointed with an orange arrow) after the fuming process started in between the two zones is attributed to C≡N stretching vibration found in the ethyl-2-cyanoacrylate chemical structure was also observed by both Tahtouh *et al.* and Edwards *et al*. [19,20].

On the other hand, the absorbance value of all vibrational peaks that lie within the wavenumber range of 2700–3100cm^{-1} decreased upon fuming process. Change in peak height in the infrared spectra could be due to either change occurred in the amount of material present or change in the bond's orientation. In this case it suggests that reduction in peak intensities had occurred due to the changes in the bond's orientation as the cyanoacrylate vapour polymerises on to the fingermark residue, since reduction of material is not possible with the increasing amount of cyanoacrylate polymerisation as a function of the fuming time [21]. It is important to note that the shoulder observed at wavenumber 3003 cm^{-1} in the fingermark residue had increased, but this shoulder got shifted to a higher frequency after cyanoacrylate fuming started indicates the reduced strength in the hydrogen bond.

The chemical changes occurred in the spectra at the different times of cyanoacrylate fuming process can be seen clearly from Figure 4.6. The peaks corresponding to C-H twisting and C=O stretch vibration shows the most prominent changes occurred due to the polymerisation of cyanoacrylate on the sebaceous fingermark residue. This is evident from Figure 4.6 as these peaks absorption had increased over a factor of 4 in comparison to other vibration peaks intensity during the fuming process. To elucidate the change that occurred in vibrational peak intensity during the fuming process by means of the surface wetting properties the fingermark residue was deposited on, the C=O stretch vibration peak at wavenumber 1744 cm^{-1} was chosen for further analysis.

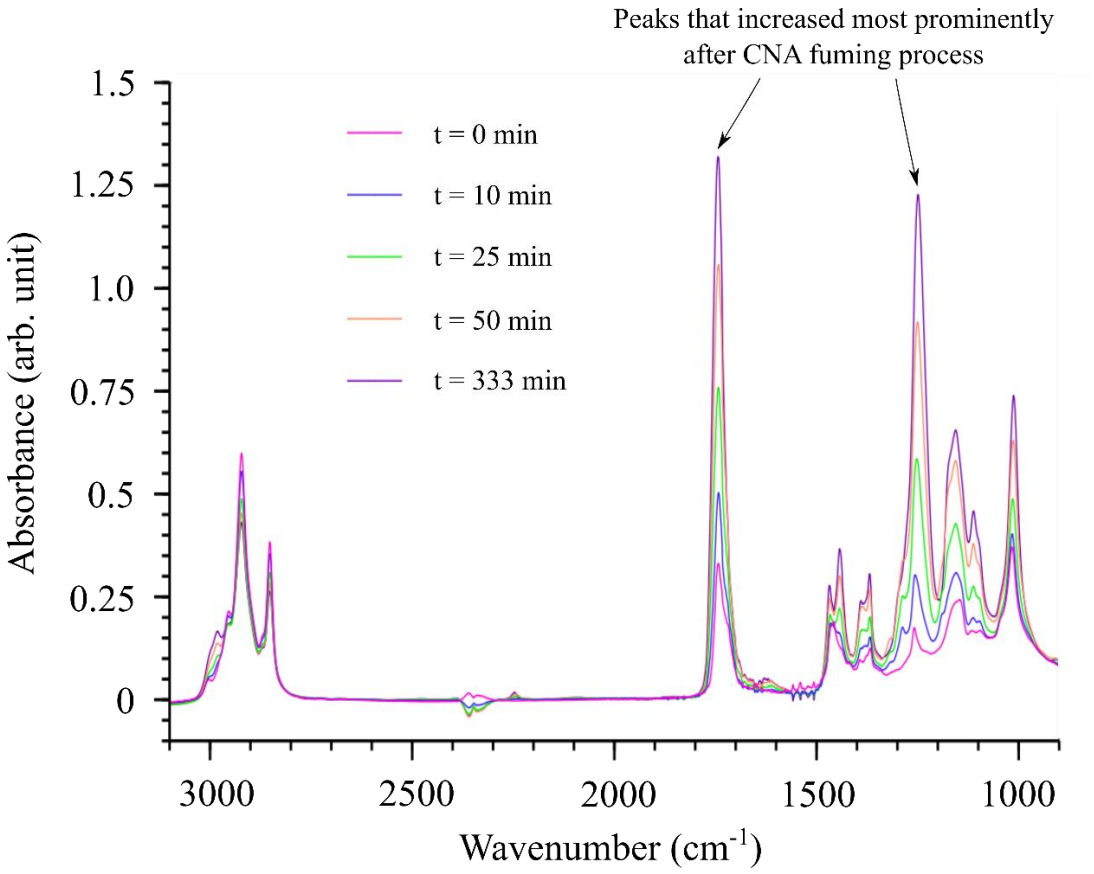

Figure 4. 6: Figure shows a FTIR spectrum of cyanoacrylate polymerisation on sebaceous fingermark deposited on PtBMA polymer surface. The IR spectra were taken at 5 different times from the start of fuming process (0 minute), 10 minutes, 25 minutes, 50 minutes and the end of fuming process (333 minutes).

The changes occurred in the peak height due to cyanoacrylate fuming was analysed using the Matlab program that allows the user to choose a peak from the infrared spectra. The written program then extracts the peak height (absorbance value) for the chosen peak. In this study, the value of the peak height at wavenumber 1744 cm^{-1} was extracted from all the spectra obtained, was stored in an array that were then used to produce a graph of peak height (absorbance) as a function of fuming time (see Figure 4.7). The plot will be referred to as kinetics plot hereafter, allows to determine the deposition rate of cyanoacrylate polymerisation onto sebaceous fingermark residue from the steepness of the slope. The steep kinetics curve of both polymer surfaces with water contact angle of 15.0° and 60.2° in Figure 4.7 indicates a rapid rate of cyanoacrylate polymerisation on the sebaceous fingermark residue deposited on these hydrophilic surfaces has led to a maximum increase in the absorbance for the peak at

1744 cm^{-1} of the C=O stretch functional group. Meanwhile, the slowest rate of cyanoacrylate polymerisation was on the fingermark residue that was deposited on the polymer surface of water contact angle 101.3° as it demonstrates a moderate slope with smaller kinetic curve, which also exhibits the least change in absorbance value. Data points produced in any given plots throughout this chapter are the averaged values from five fingermarks. The uncertainty for the data points were calculated by using the standard error of the mean values.

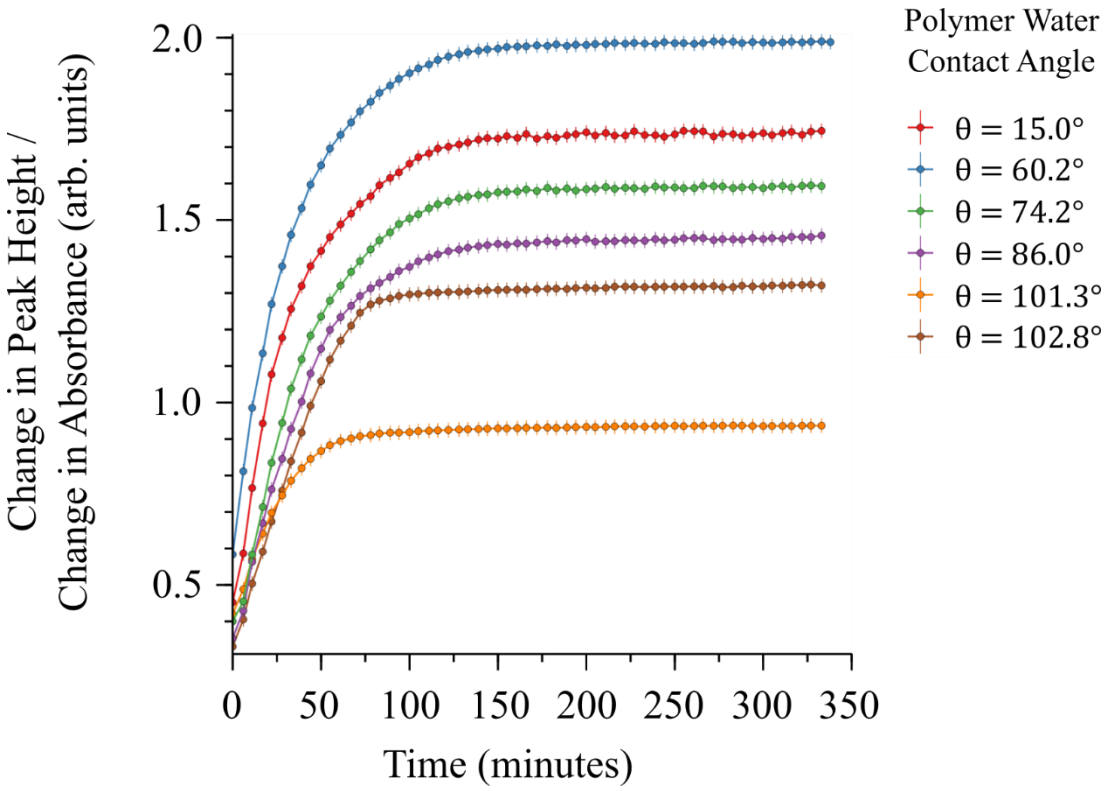

Figure 4. 7: Figure depicts the kinetics of the peak due to C=O stretch at 1744 cm^{-1} during the cyanoacrylate fuming process on sebaceous rich fingermark residue deposited on polymer surfaces of water contact angle varying from 15° to 102.8°.

Besides the steepness of the slope, the kinetics plot provided three important pieces of information on cyanoacrylate polymerisation on fingermark residue when deposited on polymer substrates of varying water contact angle when examined in detail (see Figure 4.8). This information includes the time taken for the cyanoacrylate to fully polymerise into fingermark residue, was extracted from the kinetics plot at the point when it starts to saturate (i.e. flatten out), is known as saturation time.

Acquiring the maximum value of absorbance (the absorbance value obtained when the kinetic plot saturates) from the kinetics plot indicates cyanoacrylate polymerisation depends on the underlying substrate's wetting properties.

Finally, the kinetics plot allows to quantify the amount of cyanoacrylate deposited onto the fingermark residue by subtracting the final absorbance value (maximum height of the peak after cyanoacrylate polymerisation) with the initial absorbance value (corresponds to the initial fingermark material) which also referred to as the change in absorbance. Figure 4.8 shows in detail how these information were extracted from the kinetics plot obtained in Figure 4.7.

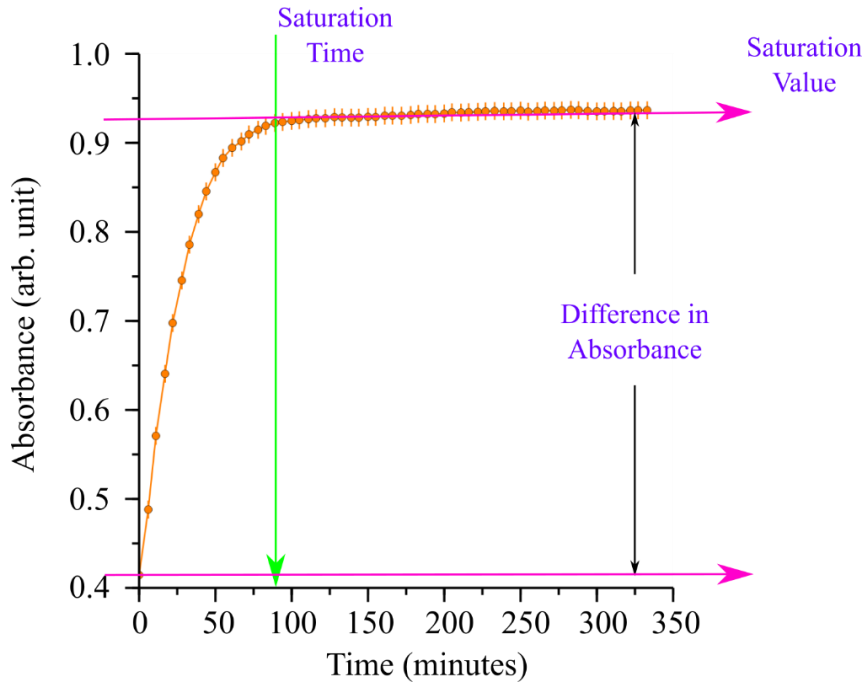

Figure 4. 8: Figure shows how the saturation value, saturation time and difference in absorbance values were obtained from the kinetics plot shown in Figure 4.7. The kinetic plot corresponds to cyanoacrylate polymerisation onto sebaceous fingermark residue deposited onto the polymer surface of water contact angle, 101.3°. The saturation value from the kinetics plot is 0.937 ± 0.065, the saturation time is 91 ± 4.7 minutes and the amount of cyanoacrylate polymerised is 0.523 ± 0.039.

The trend of saturation value, saturation time, and change in absorbance are discussed in detail in section 4.5.1 along with the camera measurements for a direct correlation between both the techniques.

4.3.2 Eccrine Deposits

Eccrine mark residue was generated using the methods mentioned in Chapter 3, section 3.6.1. The main vibrational bands identified in eccrine fingermark residue via FTIR spectra are included in Table 4.3. For eccrine mark study, the FTIR spectra were collected every 60 seconds up to 385 minutes. A large peak corresponding to water could be observed from Figure 4.9 at the time t = 0 minutes at wavenumber 3600 – 3150 cm^{-1}, with the C-H, C-H_2 and C-H_3 peaks in the region of 3100 – 2700 cm^{-1} correspond to the sebaceous residue component.

The reason for the sebaceous peaks could be observed in a predominantly eccrine mark is because of the stratum corneum. Stratum corneum refers to the outermost layer of the epidermis that is composed of dead, keratin-filled cells consisting of cholesterol, free fatty acids, wax esters, phospholipids and squalene. However, these peaks showed weaker absorbance of IR in comparison to the sebaceous mark residue which contained all the lipid constituents mentioned above in much abundance since the fingertips were rubbed around the chin and nose region prior to fingermark deposition [8].

Figure 4.9 presents the FTIR spectra at different times of cyanoacrylate fuming onto eccrine fingermark. The FTIR spectra at the time t = 0 minutes corresponds to eccrine fingermark residue at the time of deposition, depicts much smaller peaks (i.e. lower absorbance value) indicating of approximately 191% percentage difference between the amount of eccrine material deposited in comparison to the sebaceous fingermark residue.

Figure 4.9 displays similar trends as was observed for sebaceous residue fumed on PtBMA surface shown in Figure 4.5, where the region in zone 1800 – 1000 cm^{-1} increased while the region in zone 3100 – 2700 cm^{-1} decreased with increasing fuming time. Similarly, the shoulder observed at 3003 cm^{-1} increased, as well as shifting to a higher frequency after cyanoacrylate fuming process started. This observation

displays the consistency of cyanoacrylate polymerisation between the two types of fingermark residue. The broad water peak reduced by 33% within the first 10 minutes, proves that water is rapidly lost from the mark residue by evaporation [8]. As the region of 3100 – 2700 cm^{-1} was mainly due to the presence of dead skin cells, further analysis was carried out in the region of 1800 – 1000 cm^{-1} as the peaks in this region mostly corresponded to eccrine constituents such as amino acids, ammonia and urea [8].

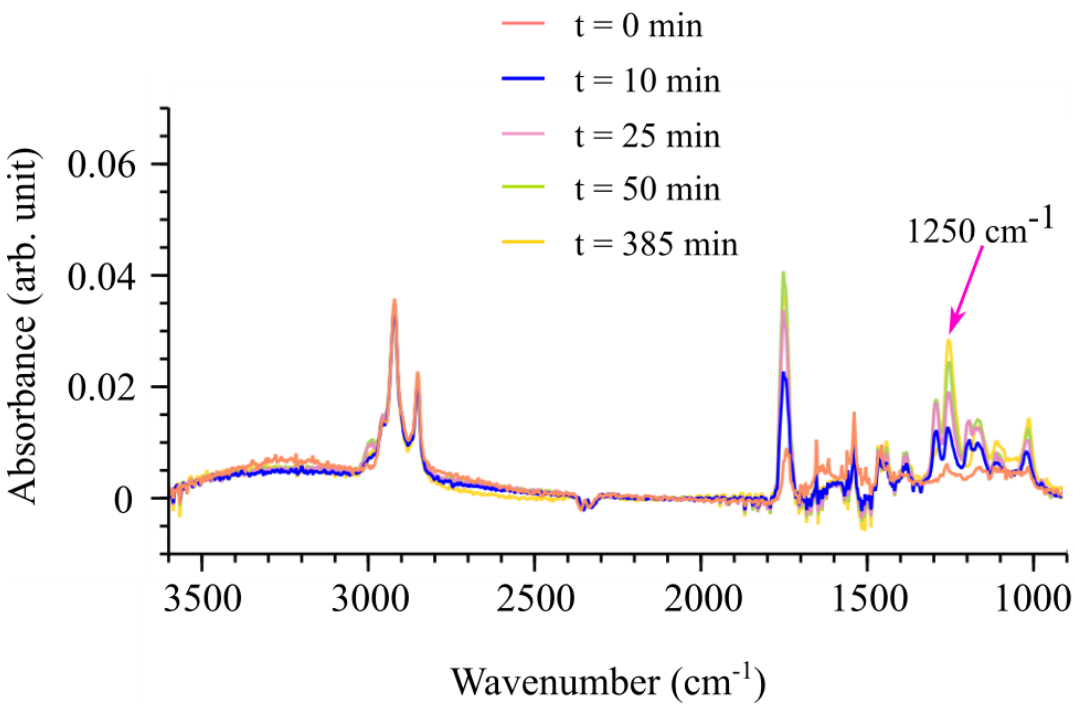

Figure 4. 9: Figure portrays FTIR spectra of eccrine mark residue collected at different times of fuming process on oxygen plasma treated polystyrene (PS Plasma) surface. The increase in the peak height for peaks within the range of 1800 – 1000 cm^{-1} is due to the fuming process can be observed clearly. In the study of eccrine mark, peak at wavenumber 1250 cm^{-1} marked with a pink arrow was chosen for further analysis (1250cm^{-1} – 1256cm^{-1}) (see Table 4.3).

For eccrine fingermark studies, C-O stretch vibration peak at wavenumber 1250 cm^{-1} was chosen for further analysis to distinguish the differences in cyanoacrylate polymerisation on eccrine residue when deposited on polymer substrates of varying water contact angle. The written Matlab program prompts the user to choose a peak.

Once the user has chosen the peak, the program extracts the peak height (absorbance value) of the chosen peak by storing the values in an array that was then used to produce a graph similar to Figure 4.8 by plotting peak height (absorbance) as a function of cyanoacrylate fuming time.

Kinetic plot for the peak at wavenumber 1250 cm^{-1} is presented in Figure 4.10. The FTIR data for eccrine mark deposits were then analysed in a similar way as how the data for sebaceous deposits were analysed.

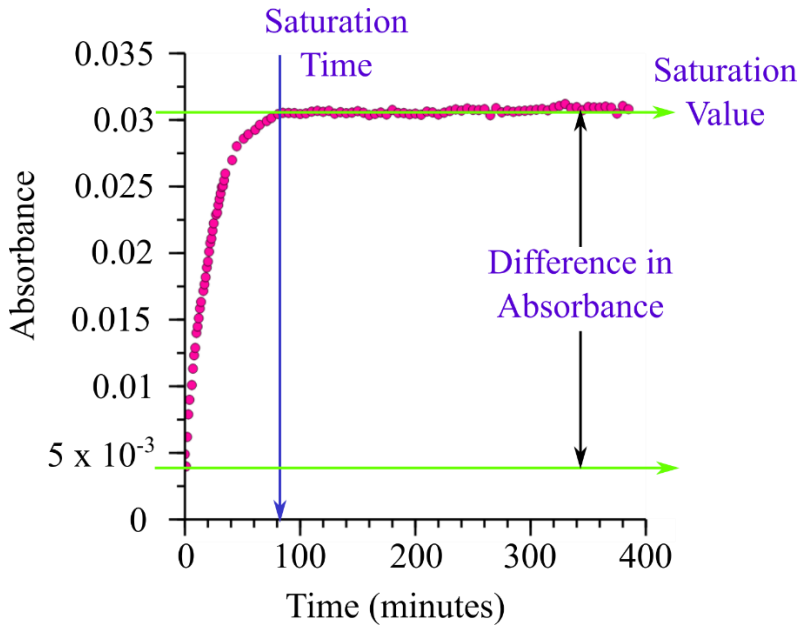

Figure 4. 10: Figure shows the kinetic plot corresponding to the peak of C-O stretch functional group at wavenumber of 1250 cm^{-1} during the cyanoacrylate fuming process on predominantly eccrine fingermark residue deposited onto polymer surface of water contact angle, 15.0°. The saturation value obtained from the kinetics plot is 0.0312 ± 0.0022, the saturation time is 80 ± 5.5 minutes and the amount of cyanoacrylate polymerised is 0.0263 ± 0.0016.

The trend of saturation value, saturation time, and change in absorbance are discussed in detail in section 4.5.2 along with the camera measurements for a direct correlation between both the techniques.

4.4 Camera Measurements of Cyanoacrylate Polymerisation on Latent Fingermarks

This section elaborates the analysis of the images obtained from developed fingermarks to understand the role of cyanoacrylate polymerisation in the physical changes for the two types of sweat, sebaceous and eccrine.

4.4.1 Sebaceous Deposits

White polymer residue was accumulated on the ridges of the fingermark when fingermark deposits were exposed to the cyanoacrylate fume, hence making it visible to the naked eye. This is possible due to the scattering of light from the white polymer growth of cyanoacrylate fume with the fingermark components. Therefore, the camera measurements were carried out to investigate the changes which occurred in the intensity of the freshly deposited sebaceous fingermark during the fuming process.

A python script was written to control the camera, to take a number of images within a set of time frame and store them in a directory set by the user. In this study, images were taken every minute up to 333 minutes, to study the time when the fuming process starts to saturate i.e. no more changes observed in terms of the brightness / intensity in the developed fingermark image. Figure 4.11 shows the image that was taken at the beginning and at the end of the fuming process to show the development of the fingermarks.

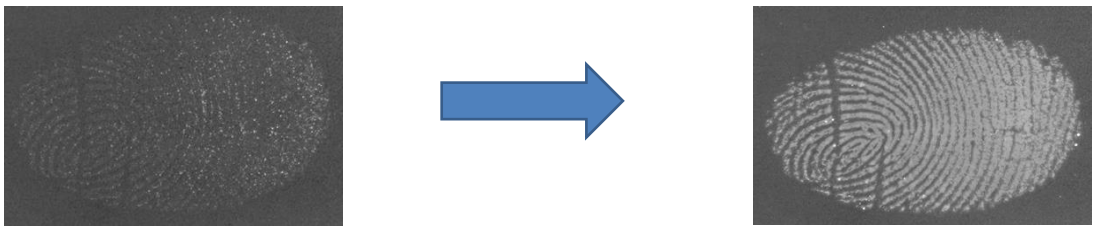

Figure 4. 11: An example of fresh sebaceous fingermark deposited at the time t = 0 minutes and fumed on PtBMA surface after 333 minutes.

All the images were analysed in the same exact way to quantify the differences in cyanoacrylate polymerisation on fingermark deposited on polymer substrates of varying water contact angle. The sequence of analysing the developed fingermark images using a written Matlab code is described step by step in detail below:

1. In the series of images captured during the fuming process, the final image was selected to extract just the fingermark region as the exact area where a fingermark was deposited can be observed clearly from the well-developed fingermark (see Figure 4.13 a)).
2. A mask was applied on the last image (image taken at time t = 333 minutes) to define the region of interest (i.e. fingermark region). The binary mask made up of values 0 and 1 designates the pixels within the fingermark region to a value of 1 and all the pixels outside this region to 0, generating an output as shown in Figure 4.12 below.

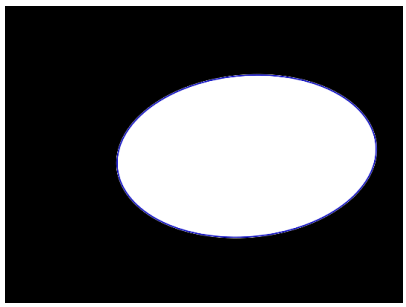

Figure 4. 12: Figure displays the image in Figure 4.13 a) converted to a binary image with values 0 and 1 after the application of mask.

3. The image was then thresholded since the application of mask had assigned all the pixels in the fingermark region to the value of 1 (including the furrows of fingermark). The function of the threshold is to turn the pixel intensity value below the standard value inputted by the user to 0. In this study the threshold condition was set to the pixel intensity to be greater than 0.4, which means that any pixel with intensity less than 0.4 was set to 0 while the pixel intensity with intensity greater than 0.4 was set to 1. This turns the image in Figure 4.12 to look as the image displayed in Figure 4.13 b) where all the regions

(including the furrows of fingermarks) except the fingermark ridges were set to 0 (i.e. appears black).

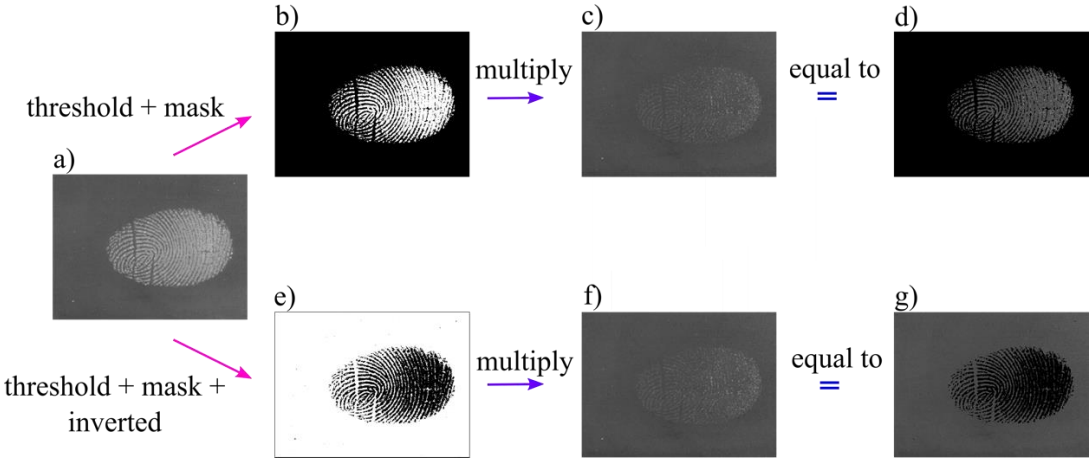

Figure 4. 13: A schematic diagram describing the analysing process of fumed images of both the fingermark and bare polymer surface (i.e. without fingermark). Fingermark region was analysed by selecting the final image from the series of images captured during the fuming process represented in a) which, was then masked and thresholded resulting in an output image as shown in b). The image in b) was then multiplied with all the other images in the sequence where d) shows an example of the resulting image of c) taken at the time t = 0 minute after multiplied with b). This was done similarly for bare polymer surface except that the image in a) was also inverted apart from being masked and thresholded.

It should be noted that the image obtained from the camera is of 8-bit (meaning each pixel can have intensity value in the range between 0 and 255 where minimum value 0 corresponds to black and the maximum value 255 corresponds to white, while the intensity values in between these two numbers corresponds to different shades of grey). However, when the image is masked and thresholded the pixel intensity is now in terms of 0 to 1, for example if the pixel intensity in the original image was equal to 150, the pixel intensity in the binary image now will be equal to 0.5859.

4. The binary image was used as a mask by multiplying it with all the other images in the sequence. For an example, the original image was taken at the time, t = 0 minutes shown in Figure 4.13 c) was multiplied with the mask in Figure 4.13 b) gives out Figure 4.13 d) as the resulting image. Figure 4.13 d)

displays white for the pixel values that are greater than 0.4 in Figure 4.13 c) while the rest of the fingermark region appears to be black.

5. The sum of the intensity of all pixels from Figure 4.13 d) (for each of the fumed fingermark images in the sequence) was divided by area of the fingermark region to give the average intensity of pixels in fingermark region, was then stored in an array. An example of obtaining the average intensity of pixels in the fingermark region is shown with the aid of a diagram in Figure 4.14.

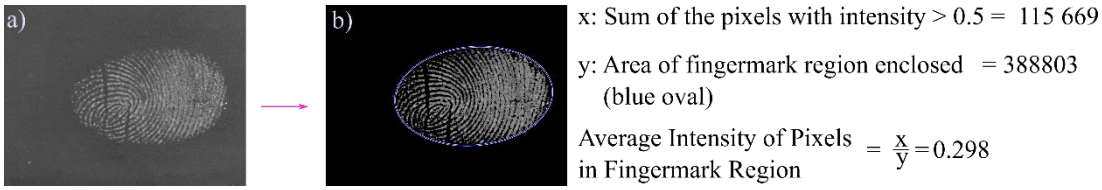

Figure 4. 14: Figure a) displays the sebaceous fingermark developed during cyanoacrylate fuming time at the time t = 20 minutes. Figure b) is the resultant image of a) after multiplied with the mask in Figure 4.13 b). When all the pixels with intensity value greater than 0.4 is added for the image in b) it gives a value of 115 669. The area of the fingermark region in this case is equal to 388803, was acquired by taking the area of the mask shown in Figure 4.12 (the white region enclosed by an ellipse). Hence, to determine the average intensity of the pixels within the fingermark region, the sum of pixels with intensity greater than 0.4 was divided by the area enclosed by the fingermark resulted in a value of 0.298.

It is important to note that the finger contact area varied in the study despite, care being taken to make sure the fingermark deposition was as consistent as possible by using the same finger with a constant force of 2N (measured by placing all the glass microscope slide coated with polymer solution on a zeroed weighing scale during each fingermark deposition). The contact area of the finger will affect the value obtained for the sum of the pixel intensity as larger contact area would have more pixels with intensity greater than 0.4 leading to a higher value for the sum of the pixel intensity in comparison to the smaller contact area. Hence, by dividing sum of the pixel intensity with the area enclosed by fingermark, expressed as the average intensity of pixels

allowed for a direct comparison of fingermark development on the polymer surfaces of different wetting properties.

6. By plotting the average intensity of pixels in fingermark region as a function of fuming time generates a kinetic plot as shown in Figure 4.15.

The amount of cyanoacrylate attached to the bare polymer surface due to cyanoacrylate fuming was analysed in a very similar way except that the image in Figure 4.13 a) was also inverted in addition to the application of mask and threshold. Image (a) was inverted to make the fingermark ridges black and everything else to be white as shown in Figure 4.13 e). In this case, image (e) was used as a mask to multiply with all the other images in the sequence. For an example, fingermark image at the time t = 0 minute displayed in Figure 4.13 f) was multiplied with (e) producing Figure 4.13 g) as the resulting image of the multiplication between images (e) and (f).

As mentioned in step 6, plotting the average intensity of pixels in the fingermark region as a function of fuming time gives a kinetic plot that is similar to the one obtained in FTIR measurements is shown in Figure 4.15. The kinetic plot was then analysed in the same manner by acquiring three important pieces of information such as saturation time, saturation value and difference in brightness. Saturation time and saturation value represent the time and value when the cyanoacrylate polymerisation starts to saturate (i.e. when no further changes observed in the brightness of the developed fingermark, the flat region in the kinetic plot). The difference in brightness was obtained simply by subtracting the initial average intensity of all pixels in the fingermark region from the maximum average intensity of all pixels attained from the fuming process. The change in the average intensity of all pixels determines the amount of cyanoacrylate polymerised on to the fingermark residue.

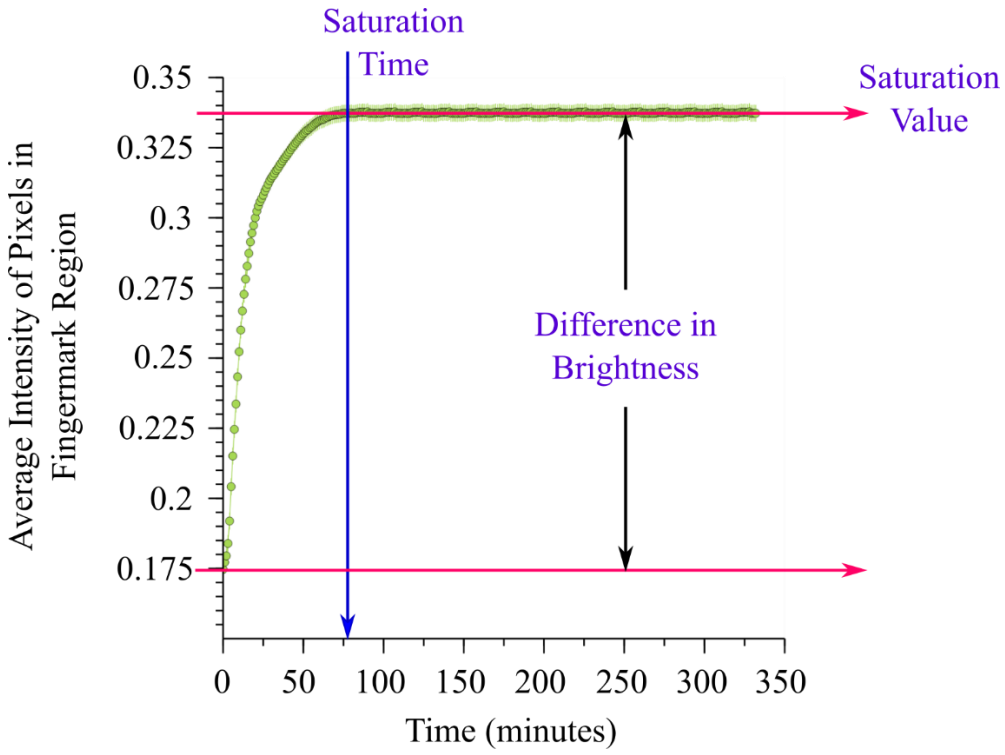

Figure 4. 15: Figure portrays the average intensity of all pixels in the fingermark region as a function of cyanoacrylate fuming time. The kinetics graph corresponds to cyanoacrylate polymerisation of sebaceous fingermark residue on the polymer surface of water contact angle, 102.8°. The saturation value from the kinetics plot is 0.337 ± 0.035, the saturation time is 78 ± 5.7 minutes and the difference that occurred in the brightness (intensity) of the fingermark is 0.162 ± 0.054.

4.4.2 Eccrine Deposits

Camera analysis for eccrine mark deposits was done similarly as described in Figure 4.13. In this study, images were collected up to the 385th minute to be analysed and the threshold value was set to 0.3 rather than 0.4 as the intensity of the developed eccrine mark deposits were of approximately 46% lower than the intensity of the developed sebaceous mark deposits. An example of kinetics plot for eccrine mark developed with cyanoacrylate fuming is displayed in Figure 4.16 along with the fingermark images taken at different times during the fuming process.

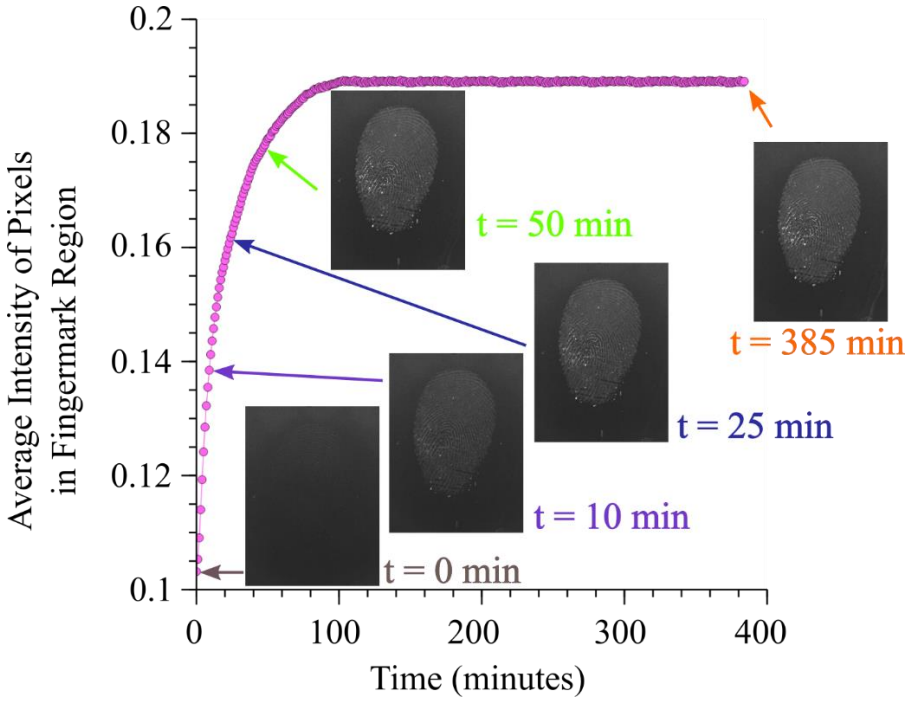

Figure 4. 16: Figure represents the average intensity of all pixels in the fingermark region as a function of cyanoacrylate fuming time for eccrine mark deposited on polymer surface of water contact angle 15°. Inset images of the eccrine mark developed at different times of fuming process were included to show the increase in the average intensity of pixels in the fingermark region due to cyanoacrylate polymerisation. The saturation value from the kinetics plot is 0.1875 ± 0.0293, the saturation time is 87 ± 3.7 minutes and the difference that occurred in the brightness (intensity) of the fingermark is 0.0675 ± 0.0043 was obtained in a similar way as described in Figure 4.15.

4.5 Discussion of Latent Fingermarks based on FTIR and Camera Measurements

4.5.1 Sebaceous Marks

Examples of sebaceous fingermark deposited on polymers of varying water contact angle are shown in Figure 4.17. The microscopic observation indicated that there is a mediating factor between the nature of the substrate and the distribution of material within the relatively thin film of fingermark deposit.

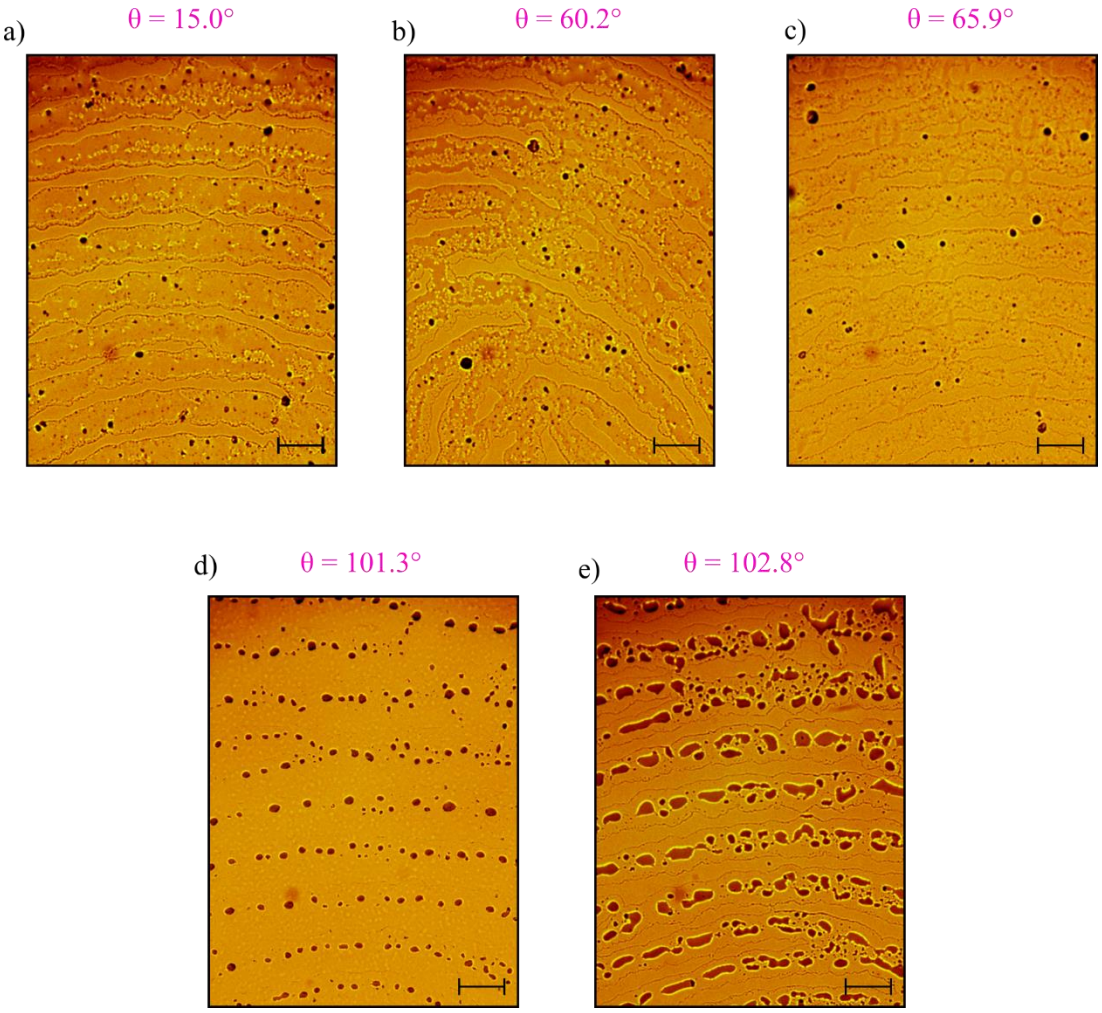

Figure 4. 17: Figure shows freshly deposited sebaceous fingermark on polymer substrates of water contact angle a) 15.0°, b) 60.2°, c) 65.9°, d) 101.3°, and e) 102.8°. The images were obtained from Olympus BX51 optical microscope using an eyepiece of 50 times magnification. The fingermarks deposited on surfaces with different wetting properties display different characteristics, where the thin monolayer fingermark residue on hydrophilic substrates depicted a continuous film while the same type of fingermark deposited on hydrophobic substrates showed large irregularly shaped islands of material. All the images are of the same scale bar, 0.2 mm.

When sebaceous fingermarks were deposited on hydrophilic polymer substrates, they form a continuous pool of material while the same type of deposit on hydrophobic polymer substrates favoured to take up large irregularly shaped islands of material. This observation accounts for the adsorption of the sebaceous material on to the polymer substrates during contact of the finger. Considering the relatively low surface

energies of the sebaceous constituents composed of organic materials (containing dissolved polar and non-polar compounds), it is expected for the sebaceous deposits to spread freely on polymer substrates of low water contact angle, as this would lead to a large decrease in the surface free energy of the system [22].

Polar constituents present in free fatty acids and sterols are commonly found components in sebaceous fingermark residue. These constituents are known to adsorb on hydrophilic surfaces and spread freely on the substrate to form a close-packed monolayer, as observed in Figure 4.17 (a, b and c). The contrary happens when a predominantly sebum loaded finger touches a hydrophobic surface where no absorption of polar constituents occur which leads to the sebaceous material taking the form of blobs rather than being spread on the surface (Figure 4.17 d and e).

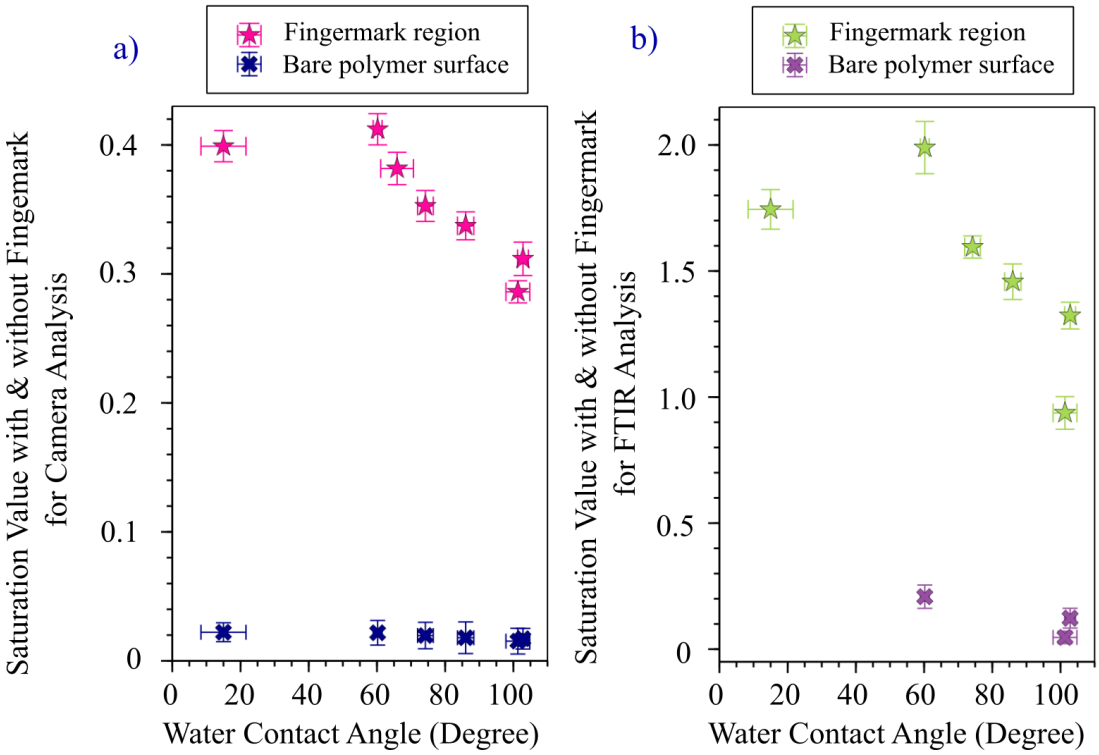

Figure 4. 18*:* (a) Displays the saturation value of the cyanoacrylate polymerisation onto sebaceous fingermark residue and bare polymer surface for camera analysis while (b) displaying the saturation value of absorbance at the peak 1744 cm^{-1} during the fuming process of both the sebaceous fingermark and without fingermark deposition for FTIR analysis. It could be seen clearly that both the method results were consistent with each other given that the saturation value with fingermark displaying a higher value in comparison to the saturation value of the bare polymer surface.

The results for saturation of cyanoacrylate polymerisation on both the sebaceous fingermark and bare polymer substrates of varying water contact angle via FTIR and camera are displayed in Figure 4.18.

It could be observed from Figure 4.18, the saturation value of the cyanoacrylate polymerisation on fingermark residue decreased as the water contact angle of the polymer surface increased. This could be explained by the increase in spreading of the sebaceous components on polymer substrates of lower water contact angle allowed more area for cyanoacrylate to polymerise on. Hence, this gave out more scattering of light leading to higher saturation value for marks developed on hydrophilic substrates.

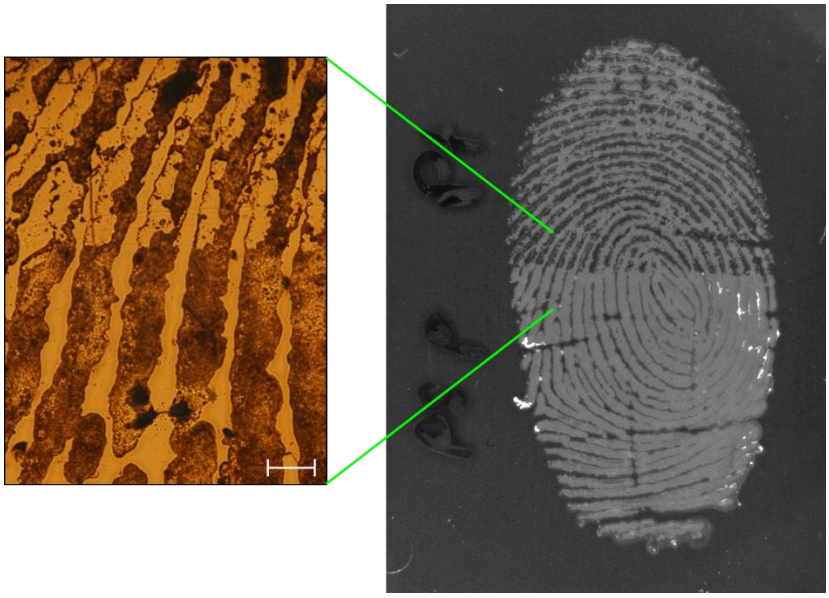

Figure 4. 19: Figure on the right shows the sebaceous fingermark deposited on top- PtBMA (θ = 102.8°) and bottom- PS Plasma (θ = 15°) developed with cyanoacrylate fuming taken at time t = 333 minutes. The left image was obtained for the region in between the PS plasma and PtBMA to illustrate the differences in cyanoacrylate polymerisation caused by the distribution of the sebaceous material on the two types of surfaces. The scale bar of the microscope image corresponds to 0.2 mm.

In order to confirm the above observation is not influenced by the nature of fingermark being complex and variation in the fingermark composition, half of a glass microscope slide was spin-coated with hydrophilic polymer and the other half with hydrophobic

polymer, and this surface was then deposited with a predominantly sebaceous fingermark; the fingermark was developed using cyanoacrylate fuming technique under the same conditions and process as mentioned earlier for camera measurements is shown in Figure 4.19. It is evident that the spreading of sebaceous residue occurs on low water contact angle polymer substrates from Figure 4.19.

As mentioned earlier, the FTIR-ATR technique is very sensitive to the material that is close to the interface hence, the penetration of infrared beam is influenced by the distribution of sebaceous residue. The well spread thin film of fingermark on hydrophilic substrates allows for full coverage of cyanoacrylate polymerisation when exposed to the cyanoacrylate fumes which enables the infrared beam to penetrate further into the developed fingermark residue resulting in higher absorbance value. Conversely, the cyanoacrylate polymerisation would only occur in the region of large irregularly shaped islands of fingermark material on hydrophobic surfaces leading to a much lower saturation value. The lateral view of the distribution of sebaceous fingermark residue in the ridge deposited on hydrophilic and hydrophobic substrate is illustrated in the Figure 4.20.

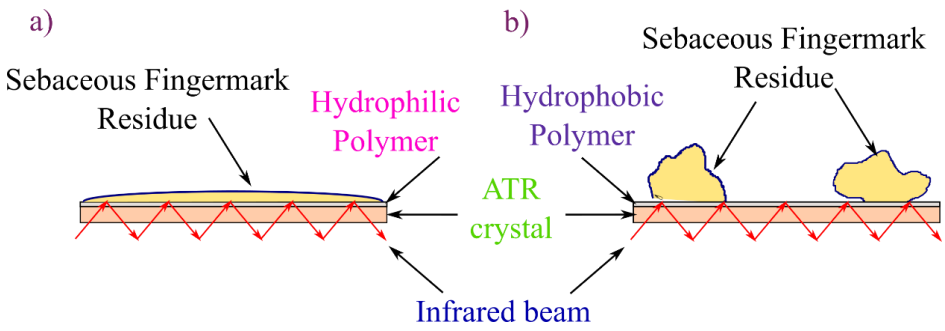

Figure 4. 20: A schematic diagram showing the lateral view of fingermark deposits in fingermark ridge on (a) hydrophilic and (b) hydrophobic polymer spin-coated on ATR crystal.

During the cyanoacrylate fuming process, cyanoacrylate fume attaches or adsorbs on any surface left inside the fuming cells which include the polymer surface region without fingermark deposition. Figure 4.18 shows very low saturation value for cyanoacrylate polymerisation on bare polymer substrates, is as expected and evident from Figure 4.19. The fingermark takes up far more cyanoacrylate than the substrate

(as is the case for all the substrates) which indicates that polymerisation of superglue on polymer substrates is unlikely to occur. Thus, polymerisation of cyanoacrylate is most likely to occur either on a continuous film or on large irregular shaped of fingermark. This is because of the sufficient initiators being present in the fingermark residue which allows the adsorbed cyanoacrylate to polymerise further and accumulate on the ridges of the fingermark whereas nothing happens to the cyanoacrylate fume attached to the bare polymer surface resulting in lower saturation value.

The amount of cyanoacrylate polymerised on sebaceous fingermark shows a similar trend as observed for saturation value, where the amount of cyanoacrylate polymerised on the sebaceous deposit decreased with the increase of substrate's water contact angle. Figure 4.19 clearly depicts and supports the above statement as the coverage area of cyanoacrylate polymerisation varies with respect to the nature of the substrate.

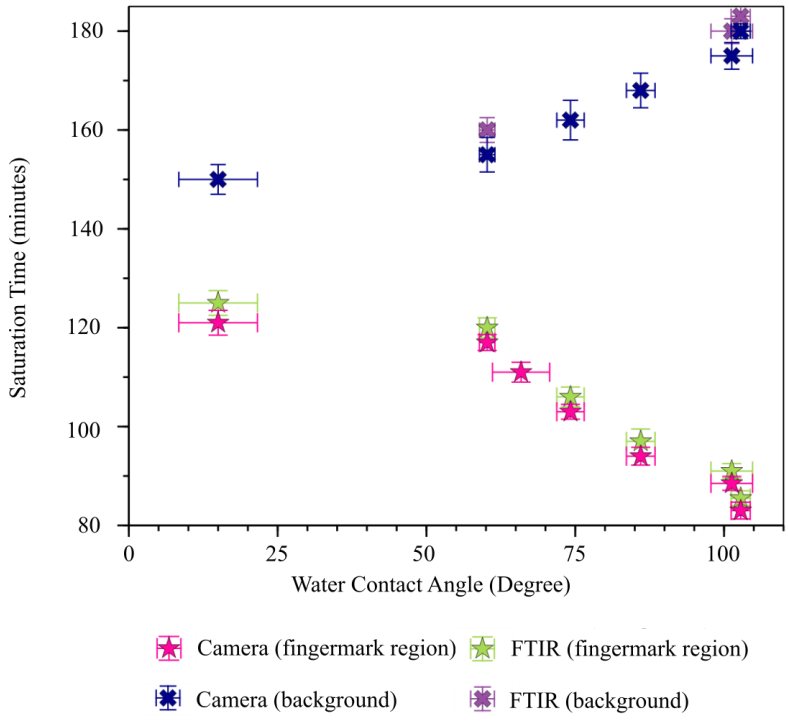

Figure 4. 21: Figure represents data points of the time taken for the cyanoacrylate polymerisation to saturate on sebaceous fingermark deposited on polymer substrates of varying water contact angle for both the techniques, camera and FTIR. The figure also includes the data points of the saturation time for the cyanoacrylate to polymerise on the bare polymer substrates for both the techniques.

Saturation time shows a trend of decreasing as the water contact angle of the substrate increases. This is mainly due to the lesser area of fingermark material required to be covered by cyanoacrylate polymerisation on the higher water contact angle substrates leading to low saturation time. In contrast, cyanoacrylate polymerisation would take a longer time to fully polymerise on to the well spread fingermark material on a hydrophilic substrate.

As discussed earlier, adsorption of cyanoacrylate on a bare polymer substrate is unlikely to occur (which is evident from Figure 4.19), which resulted in a much longer time for the cyanoacrylate vapour to adhere on any given polymer surface compared to the polymerisation of cyanoacrylate on to the fingermark residue. It is expected for the cyanoacrylate polymerisation to saturate faster on fingermark residue, which is the reason for observing a clear visible mark. If it was to be the other way round, we would see the inverse fingermark being developed on the polymer surface fully covered with cyanoacrylate. It is also evident from Figure 4.21 that the time taken for the cyanoacrylate vapour to adhere on the bare polymer substrate increases as the substrates water contact angle increase. This is attributed to the differences in the surface energy and interfacial tension properties of both the hydrophilic and hydrophobic substrates. The hydrophilic substrates (lower water contact angle) with high adhesive force displayed greater affinity towards the cyanoacrylate polymer in comparison to the hydrophobic surface (higher contact angle) [23].

4.5.2 Eccrine marks

Both the FTIR and camera data for eccrine mark residue were analysed in a similar way as for sebaceous deposits. It is important to note that the vibrational peak absorbance values within the wavenumber range of 1000 – 1800 cm^{-1} of eccrine residue is to be of approximately 40 times less in comparison to the sebaceous residue, is evident from the infrared spectra shown in Figures 4.6 and 4.9 respectively.

An example image of fresh eccrine sweat deposited on a hydrophilic and hydrophobic substrate indicating the formation of droplets on the hydrophilic substrate is displayed in Figure 4.22. Observing in detail, visible traces of dead skin cells on both the polymer substrates in Figure 4.22 can be seen clearly. Thus, the presence of sebaceous

components observed in the IR spectra on eccrine fingermark is due to the shedding of dead skin cells during deposition.

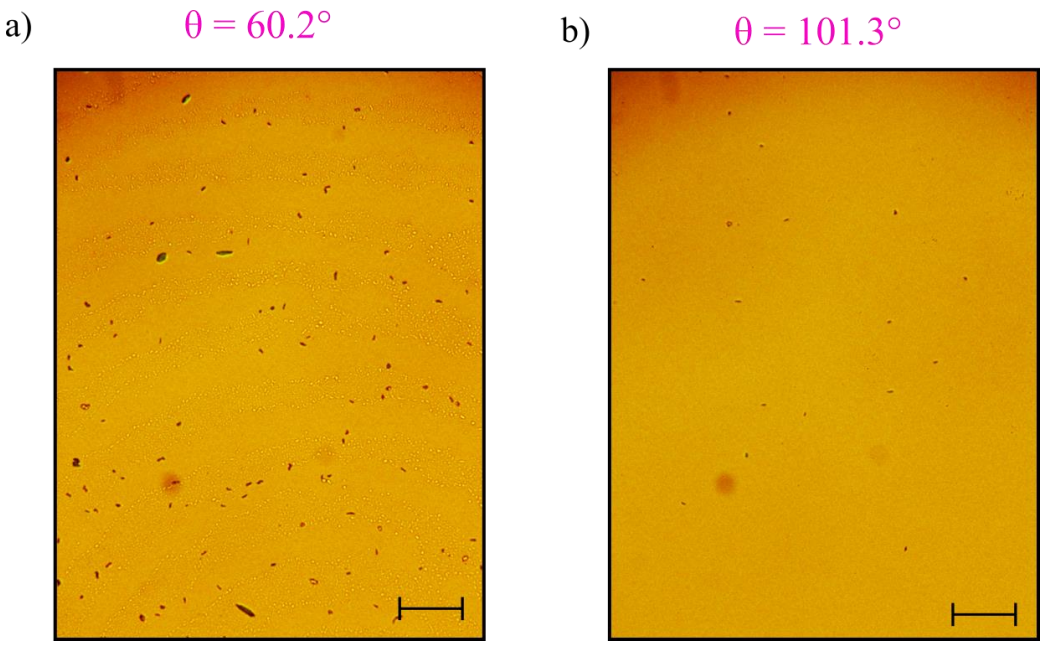

Figure 4. 22: Figure shows freshly deposited eccrine fingermark on polymer substrates of water contact angle a) 60.2° and b) 102.8°. The images were obtained from Olympus BX51 optical microscope using an eyepiece of 50 times magnification. The fingermark deposited on these two substrates displays different characteristic, where the fingermark residue on hydrophilic substrate depicted high mobility droplets while the same type of fingermark deposited on hydrophobic substrate showed no visible fingermark ridges. All the images are of the same scale bar, 0.2 mm.

It is also apparent from Figure 4.22 that the amount of sweat transferred during fingermark deposition on the surfaces was influenced by the substrates water contact angle, as there were clear droplets of eccrine sweat on the hydrophilic substrate indicating the presence of fingermark while no evidence of fingermarks was observed on the hydrophobic substrate.

The saturation value of the cyanoacrylate polymerisation on substrates of different wetting properties for the two techniques, FTIR and camera are displayed in Figure 4.23. The decreasing saturation value with increasing substrate water contact angle in Figure 4.23 is due to the influence of substrate upon fingermark deposition which is

evident from the observation of Figure 4.22. When a sweat-rich fingermark is lifted from a surface it causes the meniscus of the sandwiched eccrine film to recede thus leaving along each ridge deposit to take the form of droplets that can be noticed in Figure 4.22 (a), in which case these droplets in the fresh mark are highly mobile [8].

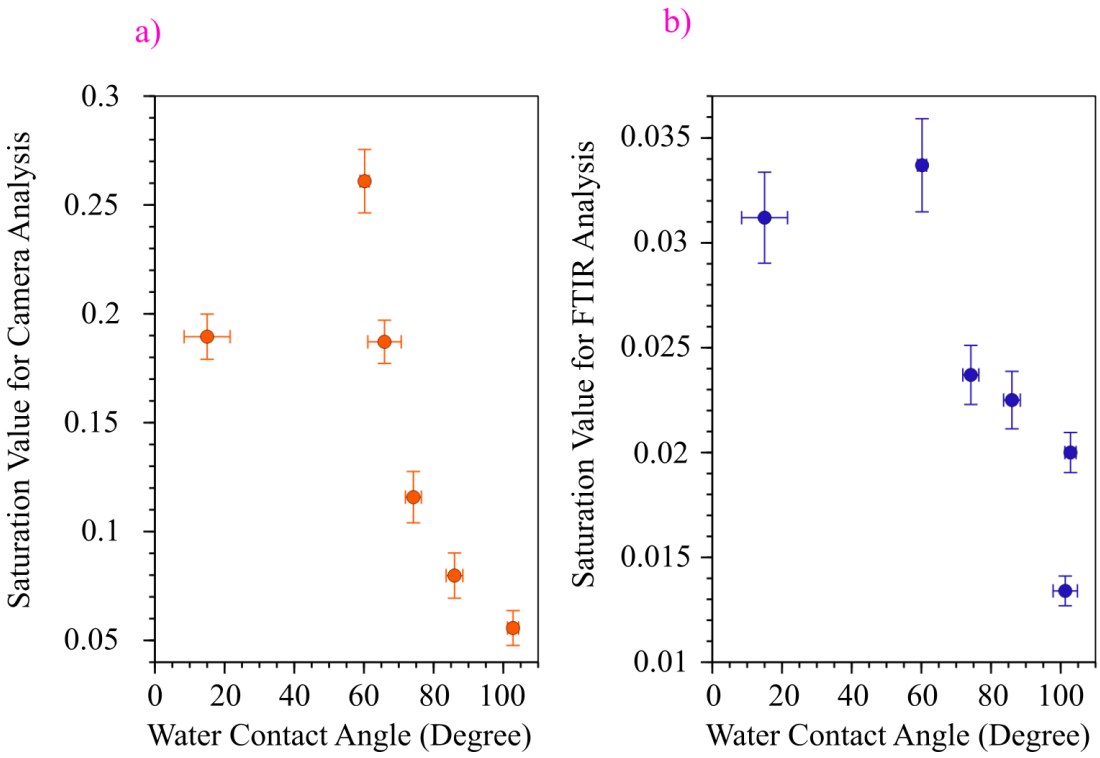

Figure 4. 23: Figure represents data points of a) the saturation value of the cyanoacrylate polymerisation on eccrine residue deposited onto polymers of different wetting properties in camera studies and b) displaying the saturation value of absorbance at the peak 1250 cm^{-1} during the fuming process in FTIR studies. Results from both the techniques were consistent with each other as seen.

Therefore, as a result the droplets on the lower water contact angle polymer surfaces would be able to move easily and thereby, leading to larger amount of cyanoacrylate polymerisation, resulting in a higher saturation value while for higher water contact angle polymer surfaces, the droplets tend to have a higher surface tension causing the droplets to have less mobility and hence reducing the diffusion rates of cyanoacrylate polymerisation generating lower saturation value.

To confirm this, one half of a microscope glass slide was spin coated with a hydrophilic polymer whereby the other half was spin coated with a hydrophobic

polymer, was deposited with the same finger loaded with eccrine sweat which was then developed via cyanoacrylate fuming is displayed in Figure 4.24. From Figure 4.24 it is evident that the mobility of the droplets is highly influenced by the surface property of the respective polymer substrates.

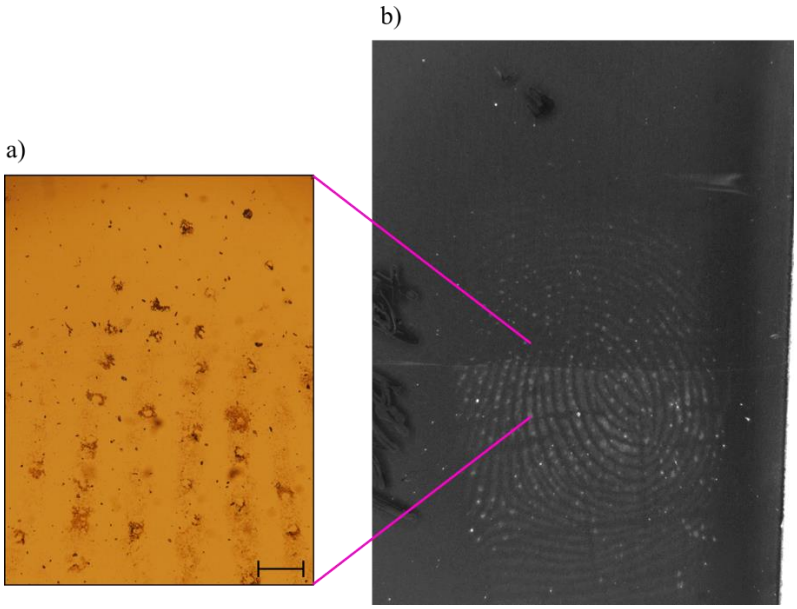

Figure 4. 24: Figure in the right shows the eccrine fingermark deposited on top- PtBMA (θ = 102.8°) and bottom- PVA (θ = 60.2°) developed with cyanoacrylate fuming taken at the time t = 333 minutes. The left image was obtained in the region between the PVA and PtBMA to illustrate the differences in cyanoacrylate polymerisation caused by the droplet's mobility in eccrine material on these two types of surfaces. The scale bar of the microscope image corresponds to 0.2 mm.

In Figure 4.24, despite of the same eccrine fingermark, a distinct difference was observed in the developed fingermark which was deposited on both the hydrophilic and hydrophobic surface. It can be clearly inferred that the amount of cyanoacrylate polymerised on the eccrine marks tends to decrease as the water contact angle of the respective substrate increases. The eccrine marks predominantly composed of the dilute aqueous solution (i.e. liquid) would have more difficulty adhering onto the hydrophobic polymer surfaces. As a consequence, a much lesser cyanoacrylate polymerisation occurred within the mark residue deposited on these low energy surfaces.

Both Figures 4.18 (sebaceous mark) and 4.23 (eccrine mark) displayed the same pattern where the saturation value increased and attained peak value at θ = 60.2° before it diminished for both the techniques, camera and FTIR. This results suggest that the surface wettability optimum value for fingermark deposition and development is at θ = 60.2°.

Figure 4.25 shows the image of the fumed eccrine fingermarks on polymer substrates of different wetting properties. It can be clearly seen that there is a decrease in the amount of cyanoacrylate polymerised onto fingermark residue over hydrophobic polymer substrates at the fuming time t = 20 minutes.

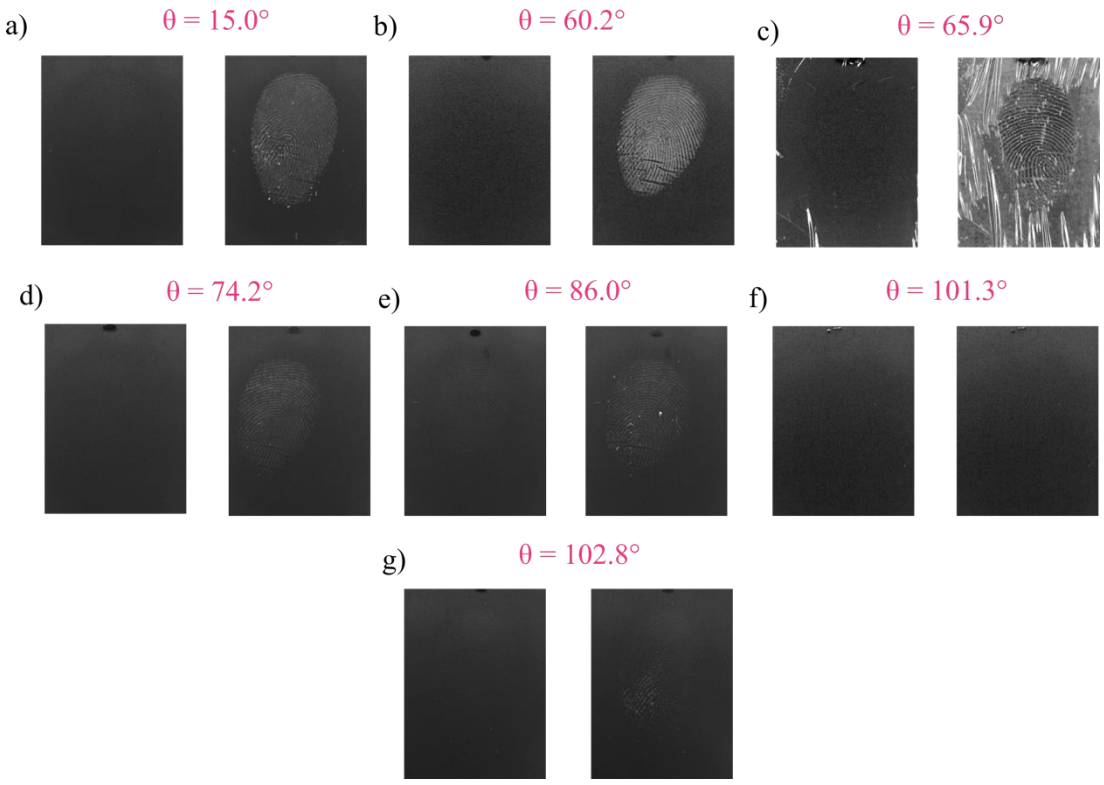

Figure 4. 25: Figure above represents left - the freshly deposited eccrine mark residue (i.e. prior to fuming process) and right - the corresponding mark fumed at the time t = 20 minutes on polymer surfaces of water contact angle a) 15.0°, b) 60.2°, c) 65.9°, d) 74.2°, e) 86.0°, f) 101.3° and g) 102.8° used in this study. Despite the eccrine mark deposited on the surface of water contact angle 101.3° did not show any response during cyanoacrylate fuming, it was included to show that it is one of the surfaces for which is hard for an eccrine mark to be retrieved.

However, it must be noted that the mark fumed on cling film (Figure 4.25 c) produced a very interesting image as this image exhibits the development of fingermark furrows instead of fingermark ridges, which is known to be a 'reverse' development. The 'reverse' developed mark could be produced by any enhancement processes since this is affected by the condition of the surface.

It is explained by Bleay *et al*. [24] that this type of development occurs presumably due to the surface being coated with a thin layer of contaminant or coatings (such as plasticisers) [25] that is removed upon contact of the finger on the surface. If the contaminant itself is enhanced by the process, then a 'reverse developed' mark can occur, as shown in Figure 4.25 c) for θ = 65.9°. Since the cling film is used as it is, it is most likely due to the coating present on the cling film resulted in the 'reverse development'.

The saturation time of the cyanoacrylate polymerisation on substrates of different wetting properties for the two techniques are plotted in the same plot for a direct comparison of trends on each substrate (see Figure 4.26).

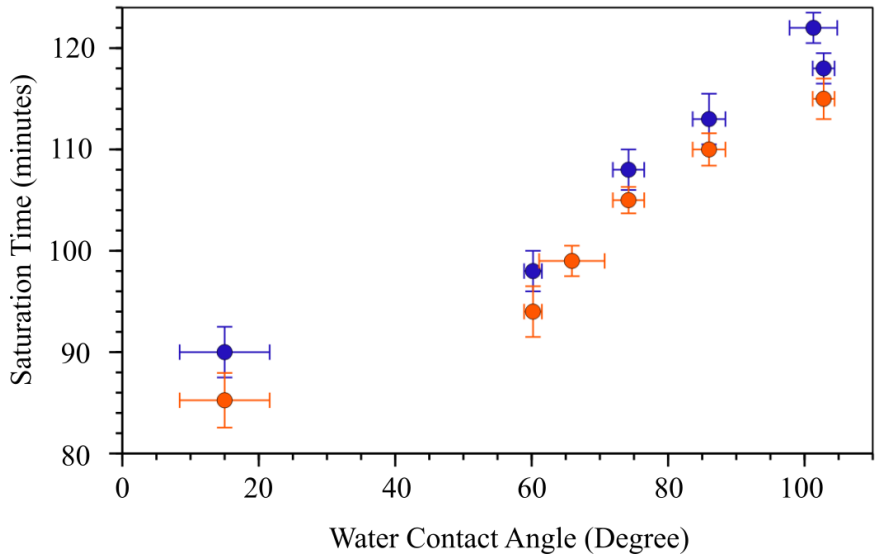

Figure 4. 26: Figure represents data points of saturation time for cyanoacrylate polymerisation onto eccrine residue deposited onto polymers of different wetting properties for the two different techniques used, camera studies (orange circle) and FTIR studies (blue circle). Saturation time is the time when the eccrine mark does not undergo further changes either in brightness intensity or absorbance value.

The time for the cyanoacrylate polymerisation to saturate seems to increase with the increasing water contact angle of the underlying substrate. This implies that the high rate of cyanoacrylate polymerisation (implying more adsorption of cyanoacrylate vapour) on fingermarks deposited on hydrophilic substrates led to a much earlier time of saturation. This agrees to the observation of the developed eccrine mark at the time t = 20 minutes in Figure 4.25.

4.6 Conclusion

In conclusion, this study demonstrated the observation of both physical and chemical changes occurred within sebaceous and eccrine fingermark residue that were deposited on polymer surfaces with water contact angle varying from 15° to 102.8° when developed with cyanoacrylate fuming method. These experiments showed that the amount of cyanoacrylate deposited on the fingermark residue decreased with the increasing water contact angle of the polymer surfaces for the both types of mark, sebaceous and eccrine. The distribution of the sweat material varied significantly during the deposition on both the hydrophobic and hydrophilic substrate. On hydrophilic substrates, a continuous film of sebaceous residue and high mobility of eccrine fingermark droplets were observed during deposition, displayed higher amount of cyanoacrylate polymerisation due to the presence of well spread fingermark residue over the substrate. In contrast, in the case of hydrophobic substrates, the presence of large irregular shaped islands of sebaceous sweat and less mobility of eccrine fingermark droplets during deposition led to insufficient fingermark residue over the substrate and resulted in lower amount of cyanoacrylate polymerisation.

However, the time taken for cyanoacrylate polymerisation to saturate showed a clear distinction between the two types of sweat. The saturation time for sebaceous marks showed a trend to decrease as the water contact angle of the underlying substrate increases while saturation time for eccrine marks displayed the saturation time to increase with the water contact angle of the underlying substrate. The well spread sebaceous sweat on hydrophilic substrate took a longer time to saturate since there is more area to cover compared to the pool of sweat on hydrophobic substrate. On the other hand, cyanoacrylate polymerisation is much slower on the hydrophobic surfaces for eccrine marks since the eccrine droplets on these surfaces have less mobility hence, the diffusion rates of cyanoacrylate within the eccrine deposits are much slower on these surfaces.

References

1. Namazi, H. (2017). Polymers in our daily life. *BioImpacts: BI*, *7*(2), 73.
2. Bobev, K. (1995). Fingerprints and factors affecting their condition. *Journal of Forensic Identification*, *45*(2), 176-183.
3. Charlton, D. T., Bleay, S. M., & Sears, V. G. (2013). Evaluation of the multimetal deposition process for fingermark enhancement in simulated operational environments. *Analytical Methods*, *5*(20), 5411-5417.
4. *Critical Surface Tension and Contact Angle with Water for Various Polymers*. (2018, March 30). Retrieved from https://www.accudynetest.com/polytable_03.html?sortby=contact_angle
5. Jokinen, V., Suvanto, P., & Franssila, S. (2012). Oxygen and nitrogen plasma hydrophilization and hydrophobic recovery of polymers. *Biomicrofluidics*, *6*(1), 016501.
6. Brandrup, J., Immergut, E. H., & Grulke, E. A. (1999). *Polymer handbook, Fourth Edition, vol. II, pp. VI 578 – VI 581*. John Wiley & Sons.
7. Whitesides, G. M., & Tang, S. K. (2006, September). Fluidic optics. In *Optofluidics* (Vol. 6329, p. 63290A). International Society for Optics and Photonics.

8. Scruton, B., Robins, B. W., & Blott, B. H. (1975). The deposition of fingerprint films. *Journal of Physics D: Applied Physics*, *8*(6), 714.

9. Girod, A., Xiao, L., Reedy, B., Roux, C., & Weyermann, C. (2015). Fingermark initial composition and aging using Fourier transform infrared microscopy (μ-FTIR). *Forensic Science International*, *254*, 185-196.

10. Williams, D. K., Schwartz, R. L., & Bartick, E. G. (2004). Analysis of latent fingerprint deposits by infrared microspectroscopy. Applied Spectroscopy, 58(3), 313-316.

11. Fritz, P., van Bronswjik, W., Lepkova, K., Lewis, S. W., Lim, K. F., Martin, D. E., & Puskar, L. (2013). Infrared microscopy studies of the chemical composition of latent fingermark residues. *Microchemical Journal*, *111*, 40-46.

12. Dukor, R. K. (2002). Vibrational spectroscopy in the detection of cancer. Handbook of Vibrational Spectroscopy, Volume 1, pp. 3335 - 3337. John Wiley & Sons.

13. Crane, N. J., Bartick, E. G., Perlman, R. S., & Huffman, S. (2007). Infrared spectroscopic imaging for noninvasive detection of latent fingerprints. Journal of Forensic Sciences, 52(1), 48-53.

14. Movasaghi, Z., Rehman, S., & Rehman, I. U. (2007). Raman spectroscopy of biological tissues. *Applied Spectroscopy Reviews*, *42*(5), 493-541.

15. Barth, A. (2000). The infrared absorption of amino acid side chains. *Progress in biophysics and molecular biology*, *74*(3-5), 141-173.

16. Knowles, A. M. (1978). Aspects of physicochemical methods for the detection of latent fingerprints. *Journal of Physics E: Scientific Instruments*, *11*(8), 713.

17. Day, J. S., Edwards, H. G., Dobrowski, S. A., & Voice, A. M. (2004). The detection of drugs of abuse in fingerprints using Raman spectroscopy II: cyanoacrylate-fumed fingerprints. *Spectrochimica Acta Part A: Molecular and Biomolecular Spectroscopy*, *60*(8-9), 1725-1730.

18. Campbell, P. G., & Wright, J. R. (1964). Infrared spectra of asphalts: some aspects of the changes caused by photooxidation. *Journal of Research of the*

National Bureau of Standards s-C. Engineering and Instrumentation, Vol. 68C, No. 2.

19. Tahtouh, M., Kalman, J. R., Roux, C., Lennard, C., & Reedy, B. J. (2005). The detection and enhancement of latent fingermarks using infrared chemical imaging. *Journal of Forensic Science*, *50*(1), JFS2004213-9.

20. Edwards, H. G., & Day, J. S. (2004). Fourier transform Raman spectroscopic studies of the curing of cyanoacrylate glue. *Journal of Raman Spectroscopy*, *35*(7), 555-560.

21. Li, P., & Ng, L. M. (1995). Surface chemistry of alkyl and perfluoro ethers: a FTIR study of adsorption and thermal desorption of (C2H5) 2O and (C2F5) 2O on SiO2. *Surface science*, *342*(1-3), 359-369.

22. Zisman, W. A. (1964). Relation of the equilibrium contact angle to liquid and solid constitution. In: Fowkes, F. M., (Ed.). *Contact Angle, Wettability and Adhesion, pp.11-12*. American Chemical Society.

23. *Contact Angle and Surface Tension – A Fascinating Liaiason.* (2018, December 15). Retrieved from https://www.cscscientific.com/csc-cientific-blog/how-does-contact-angle-relate-to-surface-tension

24. Bleay, S. M., Croxton, R. S., & De Puit, M. (2018). *Fingerprint Development Techniques: Theory and Application, pp. 480-482*. John Wiley & Sons.

25. Moret, Sebastien, Xanthe Spindler, Chris Lennard, and Claude Roux. "Microscopic examination of fingermark residues: Opportunities for fundamental studies." *Forensic science international* 255 (2015): 28-37.

CHAPTER 5

Aging of Latent Fingermarks on Surfaces of Different Wetting Properties

5.1 Introduction

The previous chapter demonstrated the impact of substrate's wetting phenomena on fresh latent fingermark development using cyanoacrylate fuming method via FTIR and camera measurements. This chapter focuses on influence of wetting properties of the underlying substrates on aging of latent fingermarks and how this affects cyanoacrylate polymerisation onto the fingermark residue. The effect of surface wetting properties and influence of environmental conditions on the aging process of latent fingermark as well as during the development of the aged mark was investigated.

The physical changes in fingermark appearance with respect to the wetting properties of polymer substrates since deposition time were observed using optical microscopy, while the chemical changes within the fingermark composition were analysed using the FTIR spectra. Both the outcomes were then compared to determine the change observed in the latent fingermark chemical composition and were correlated to the images obtained from optical microscopy for the polymers used in this study.

5.2 Experimental

5.2.1 Sample Preparation

The polymer substrates of varying water contact angle were spin coated onto glass microscope slides and zinc selenide (ZnSe) crystal, for analysis using the camera and FTIR measurements respectively.

Samples for aging latent fingermark residue for camera measurement were obtained from the index and middle fingers for both sebaceous and eccrine deposition. Following the deposition, the samples were stored in an open container located on a working bench in the laboratory at room temperature of 20.4 – 26.5 ± 0.5°C and relative humidity of 38.8 – 44.9 ± 1 % until the subsequent development was carried out over the time period of 1 – 7 days. It must be noted that the fingermark samples were exposed to airflow due to the air conditioning system and light from the fluorescent tube light in the laboratory when stored in an open container.

For FTIR measurement, spectra were collected immediately upon fingermark deposition to determine the initial composition of fingermark residue on different polymer surfaces. Upon the completion of spectra collection immediately after deposition, the removable plastic window located on FTIR cell lid (see Figure 3.18 in Chapter 3, sub-section 3.12.7) was left open in the laboratory at room temperature of 20.4 – 26.5 ± 0.5°C and relative humidity of 38.8 – 44.9 ± 1 % till the subsequent development was carried out over a time period of 1 – 7 days. The FTIR cell lid was left open to ensure the fingermark deposited on the polymer coated ZnSe crystal was exposed to ambient conditions (airflow and light) in a similar way as the fingermark samples were stored for camera measurements.

The conditions of airflow and light were not controlled in order to resemble realistic conditions encountered in an operational laboratory [1] as the fingermarks left behind by a criminal in a crime scene can be exposed to airflow and light prior to the investigation by law enforcement agencies. However, all the fingermark samples were stored in the same place on the working bench throughout the fingermark aging study. Control marks were aged in a microscope slide box at a room temperature of 22 ± 2°C and relative humidity of 40 ± 1 %, shielded the marks from both light and air flow for comparison with the fingermarks exposed to the environmental conditions.

5.2.2 Fourier Transform Infrared Spectroscopy

Spectra of fingermark residue were collected on days 1, 3, 5 and 7 respectively prior to the fuming process in order to observe the chemical changes that occurred within the fingermark residue as it aged on underlying substrate of different wetting properties. Once the fingermarks had aged for the required period, five drops of superglue (RS Components, ethyl-2-cyanoacrylate) were dropped on the heater prior to closing the environmental chamber using a glass lid.

The FTIR cell cover was also closed with the removable plastic window attached since it was left open during the aging process intentionally to expose the fingermark to the air flow and light. The kinetics scan was initiated immediately for spectra collection with time resolution of 60 seconds. In each case 60 spectral scans were averaged per spectrum. All spectra were then ratioed to the spectrum obtained from both the ZnSe crystal and the polymer substrate. Each averaged spectrum was collected using a spectral resolution of 4 cm^{-1}.

Small variations in the intensity of the IR light source used in the spectrometer resulted in a tilting of the spectral baseline. This was corrected by subtracting a linear baseline as discussed in detail in Chapter 4, section 4.2.2. Although no spectral subtraction was performed on the infrared spectra obtained for sebaceous fingermark deposits, a spectrum of water vapour was used to subtract the high content of water vapour absorbance in the eccrine fingermark deposits as described in section 4.2.2. This was due to the differences in the amount between sebaceous material and eccrine material that was deposited. Example images of how the baseline correction and water vapour correction was done are shown in depth in Figures 4.1 and 4.2 in Chapter 4, section 4.2.2.

This non-destructive technique is very valuable for fingermark aging studies as this technique is extremely sensitive to material that is close to the interface and it allows the same fingermark to be quantified in its initial state and over time, being advantageous in determining any changes that occur within the fingermark residue during the time frame of fingermark aging as well as during cyanoacrylate fuming process.

5.2.3 Camera Measurements

Images of aged latent fingermarks developed on polymer surfaces with different wetting properties via CNA fuming for the two different types of deposition, sebaceous and eccrine were acquired as mentioned in section 4.2.3. In this study, measuring the change in brightness of an image with respect to fuming time allowed the differences that arise during the fuming process for the same type of fingermark residue on different surfaces to be determined.

5.3 Results & Discussion

After deposition, fingermark composition changes with time due to mechanisms such as loss of moisture and other volatile compounds, chemical reactions and oxidation [2,3]. The rate at which this occurs can vary significantly due to influence by several factors, including surface type and environment conditions such as, level of exposure to light, ambient temperature, humidity and air flow across the surface [4].

The aging trends observed from IR spectra and images from the optical microscope for aged latent fingermark deposits on different wetting properties are discussed. Effect of substrate wetting properties in development of aged latent fingermark using cyanoacrylate fuming are also discussed using the camera and FTIR measurements.

5.3.1 Aging of Sebaceous Marks

The main functional groups from fresh latent fingermarks were identified for the aged fingermark and were numbered with their corresponding vibration in Figures 5.1 and 5.2. The spectra of aged fingermarks containing mainly lipid compounds (i.e. sebaceous secretions predominantly) showed a decrease in the intensity of all vibrational bands over time since fingermark deposition. The chemical functional groups of unsaturated compounds related to lipid molecular structure such as palmitic acid and stearic acid at wavenumbers 3003 cm^{-1}, 2953 cm^{-1}, 2922 cm^{-1}, 2853 cm^{-1} and 1744 cm^{-1} found in sebaceous compounds displayed a decrease in concentration due to the chemical degradation as a function of time [3].

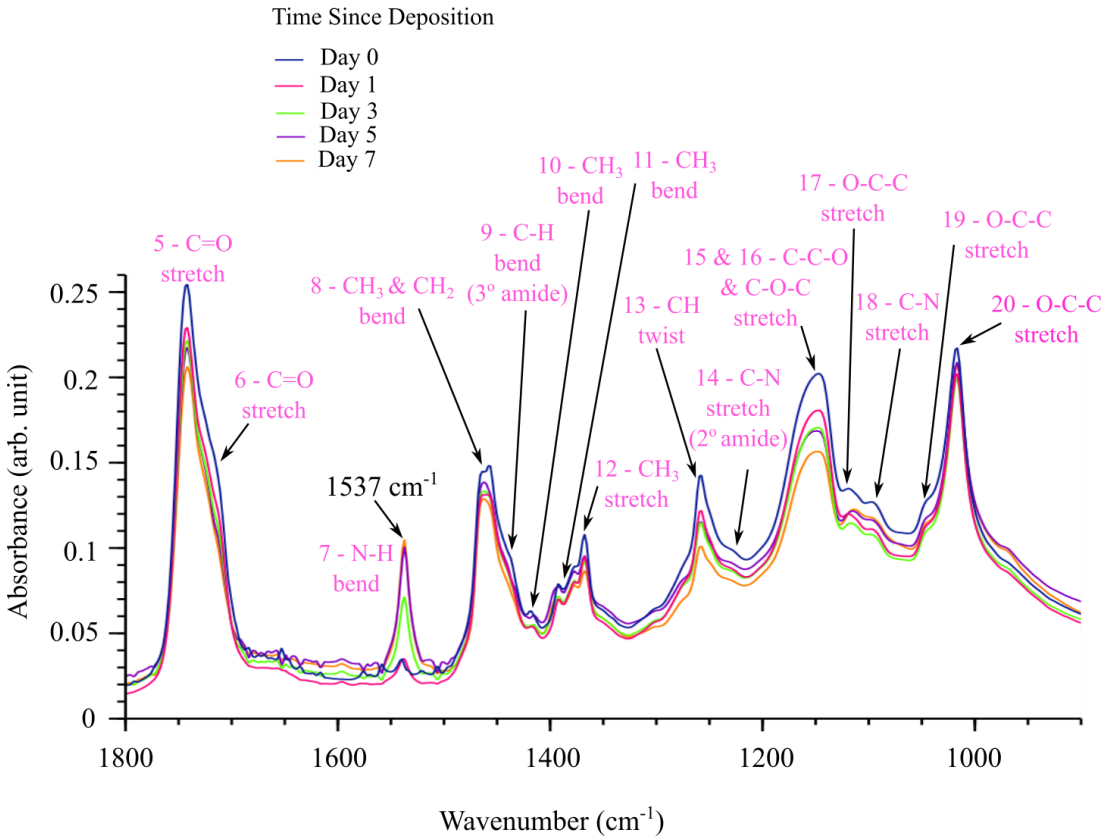

Figure 5. 1: Figure displays an example of FTIR spectrum (zone 1800 – 1000 cm^{-1}) of predominantly sebaceous fingermark residue deposited on surface of water contact angle 102.8° that was taken at the time interval of t = 0 day, 1 day, 3 days, 5 days, and 7 days. The increase of N-H in-plane vibrational band corresponding to secondary amide (peak numbered 7) with time of fingermark residue age is shown with an arrow.

However, N-H in-plane bend vibration corresponding to secondary amide assignment (e.g. proteins) at 1537 cm^{-1} increased with the time since deposition. The relative protein contribution in the amide I band increased as other species degrade faster was also observed by Andersson *et al*. upon fingermark aging, suggesting the reason to be either due to oxidation of protein aromatic amino acid side chains or protein conformational changes or both [5]. The increase could be also due to the redistribution of material within the fingermark residue.

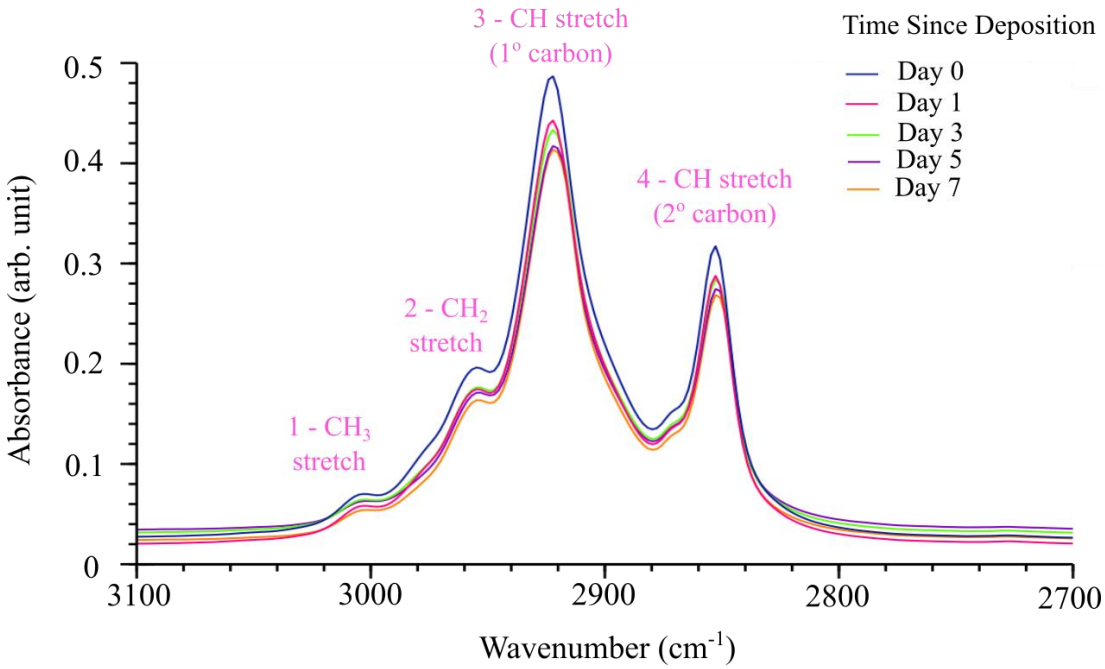

Figure 5. 2: Figure represents the FTIR spectrum of predominantly sebaceous fingermark residue deposited on the surface of water contact angle 102.8° that was taken at the time interval of t = 0 day, 1 day, 3 days, 5 days, and 7 days in zone 2700 – 3600 cm^{-1}. It was observed that the C-H, C-H_2 and C-H_3 bands attributed to lipids, wax esters, and fatty acids decayed with the increasing time since fingermark deposition.

It is important to note that the changes observed in the shape of the spectra displayed in both Figure 5.1 and 5.2 are real and reproducible since repeat measurements for the same type of fingermark on the same polymer substrate produced same features in the spectra. However, despite all consideration were taken into account to deposit same amount of sebaceous deposits between the depositions on all the polymer substrates, some variations in absorbance occurred since the amount of sweat or sebum produced varies in accordance to the changes in weather, physical activities, eating habit, and emotion [6].

The peak assignment along with the changes occurred in the peaks were tabulated in Table 5.1.

Peaks	Wavenumber (cm^{-1})	Vibration	Lipid/Protein Assignment, Secretion	Comment
	3281	N–H stretch (2° amide)	Protein, Eccrine	Not visible
	3150 - 3600	Large water peak		
1	**3003**	Asymmetric =C-H_3 stretch	Fatty acids, lipids, sebaceous	Decline
2	**2953**	C–H_2 stretch	Wax esters or fatty acids, sebaceous	Decline
3	**2922**	C–H stretch (1° carbon)	Lipid, sebaceous	Decline
4	**2853**	C–H stretch (2° carbon)	Lipid, sebaceous	Decline
5	**1744**	C=O stretch (saturated ester)	Phospholipid, sebaceous	Decline
6	**1711**	C=O stretch (saturated ester)	Hydroxylated fatty acids [7], sebaceous	Decline, in days
	1653	C=O (2° amide)	Protein, eccrine	Not visible
7	**1537**	Major: N–H in-plane bend (2° amide) Minor: C–N stretch	Protein, eccrine Protein, eccrine	Increase, visible at longer times
8	**1464**	CH_3 asymmetric bend CH_2 symmetric bend	Lipid, sebaceous Lipid, sebaceous	Decline
9	**1439**	C-H bend (3° amide) [7]	Protein, eccrine	Decline
10	**1411**	CH_3 asymmetric bend	Lipid, sebaceous	Decline
11	**1379**	CH_3 symmetric bend	Lipid, sebaceous	Decline

12	**1368**	CH_3 symmetric stretch	Phospholipid, sebaceous	Decline
13	**1258**	C-H twisting	Lipid, sebaceous	Decline
	1250 - 1253	C-O stretch	Amino acid side chain, eccrine	Not visible
	1246	C-C-O stretch (asymmetric bend)	Esters, sebaceous	Not visible
14	**1233 / (1200-1250)**	C–N stretch (2° amide)	Protein, eccrine	Decline
15	**1160**	C–C–O stretch (saturated ester)	Lipid, sebaceous	Decline
16	**1146**	C-O-C stretch	Glycogen, sebaceous	Decline
17	**1117**	O–C–C stretch (saturated ester)	Lipid, sebaceous	Decline
18	**1096**	C-N stretch	Lipid, sebaceous	Decline
	1090 - 1096	C-N stretch, C-H bend	Amino acid, eccrine	Not visible
19	**1051**	O–C–C stretch (saturated ester)	Lipid, sebaceous	Decline
20	**1016**	O–C–C stretch (saturated ester)	Glycogen, sebaceous	Decline
	1012 - 1018	C-C stretch, C-H bend	Amino acid, eccrine	Not visible

Table 5. 1: Functional groups corresponding to the eccrine and sebaceous compounds found in aged latent fingermark residue with their corresponding peak signals with respect to the aging time. The observable peaks that were identified in Figures 5.1 and 5.2 from the table are numbered accordingly.

To examine the differences in aging process of fingermark residue deposited onto hydrophilic polymer substrates, an example of IR spectra of sebaceous fingermark aged on polymer substrate of water contact angle 60.2° is shown in Figure 5.3.

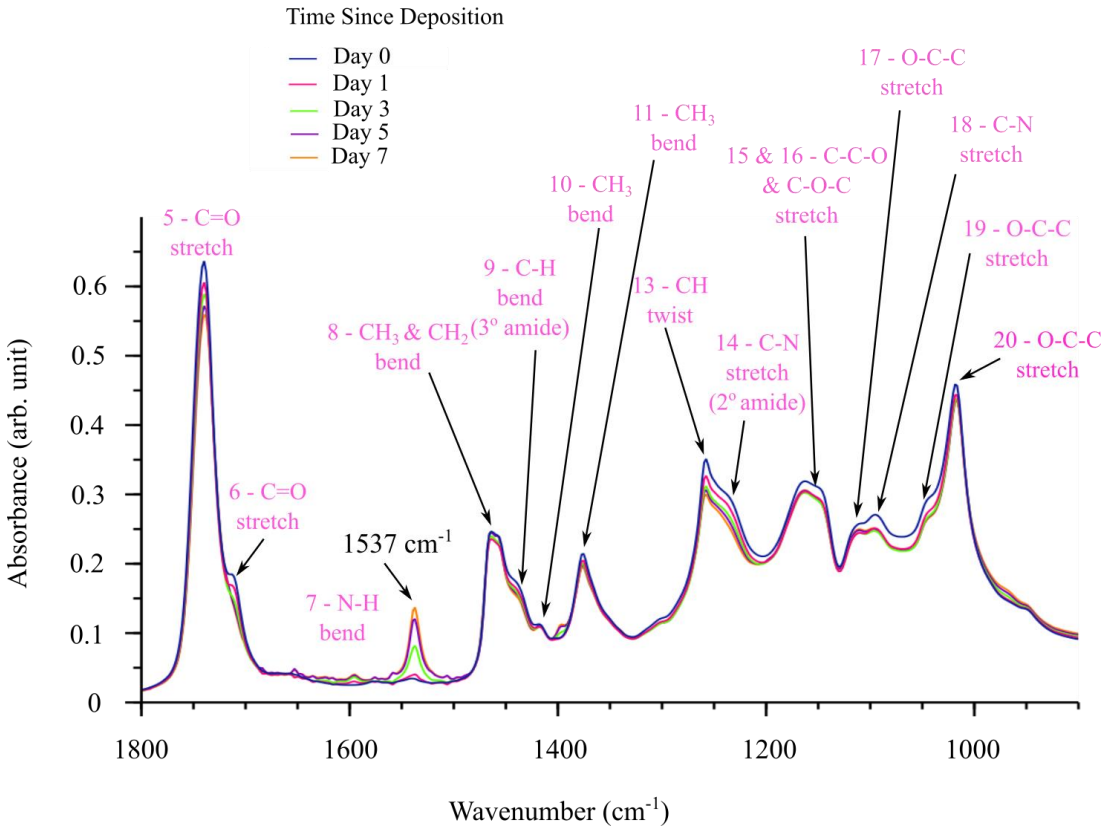

Figure 5. 3: Figure displays an example of FTIR spectrum (zone 1800 – 1000 cm^{-1}) of predominantly sebaceous fingermark residue deposited on the hydrophilic surface of water contact angle 60.2° that was taken at the time interval of t = 0 day, 1 day, 3 days, 5 days, and 7 days.

The most common differences between the spectra of sebaceous fingermarks on polymer of different wetting properties are the shape of spectra in the wavenumber region of 1800 cm^{-1} – 1000 cm^{-1}. The band vibrations at 1711 cm^{-1} (peak numbered 6) and at 1233 cm^{-1} (peak numbered 14) appear as a shoulder rather than a peak on hydrophobic polymer surface whereas in the case of hydrophilic polymer surface they appear as a peak. This observation is attributed to the differences in chemical interaction between neighbouring molecules in fingermark constituents as distribution of the constituents in fingermark varies hugely depending on the wetting properties of the surfaces the fingermark was deposited on [8].

It must be noted that on both types of substrate a broadened peak due to overlap of two peaks can be observed. Peak numbered 15 of C-C-O stretch vibration at 1160 cm^{-1} has been broadened due to overlap with peak numbered 16 of C-O-C stretch band

centred near 1146 cm^{-1}. The widths of these two bands are larger than the distance by which they are separated and therefore they overlap forming a complex band with two maxima.

However, the bands within wavenumber region of 3100 cm^{-1} – 2700 cm^{-1} remained same in terms of the shape of spectra for sebaceous fingermark on both the hydrophobic and hydrophilic polymer surfaces.

To further investigate the influence of substrate on the distribution of the secreted sebaceous material / how the deposits behaved (i.e. physical changes) during the fingermark aging process on the same polymer substrate, images of the same areas were taken using optical microscope (see Figure 5.4). Observation of fingermarks deposited on the various wetting properties, non-porous polymer substrates in Figure 5.4 showed that the substrate type has a non-negligible influence on the morphology of the marks and the distribution of sebaceous components within ridges.

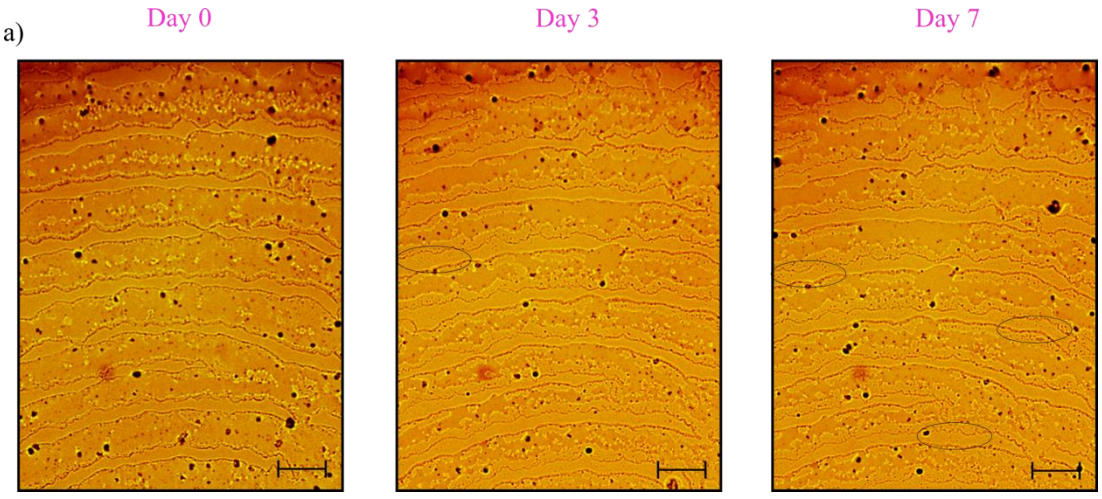

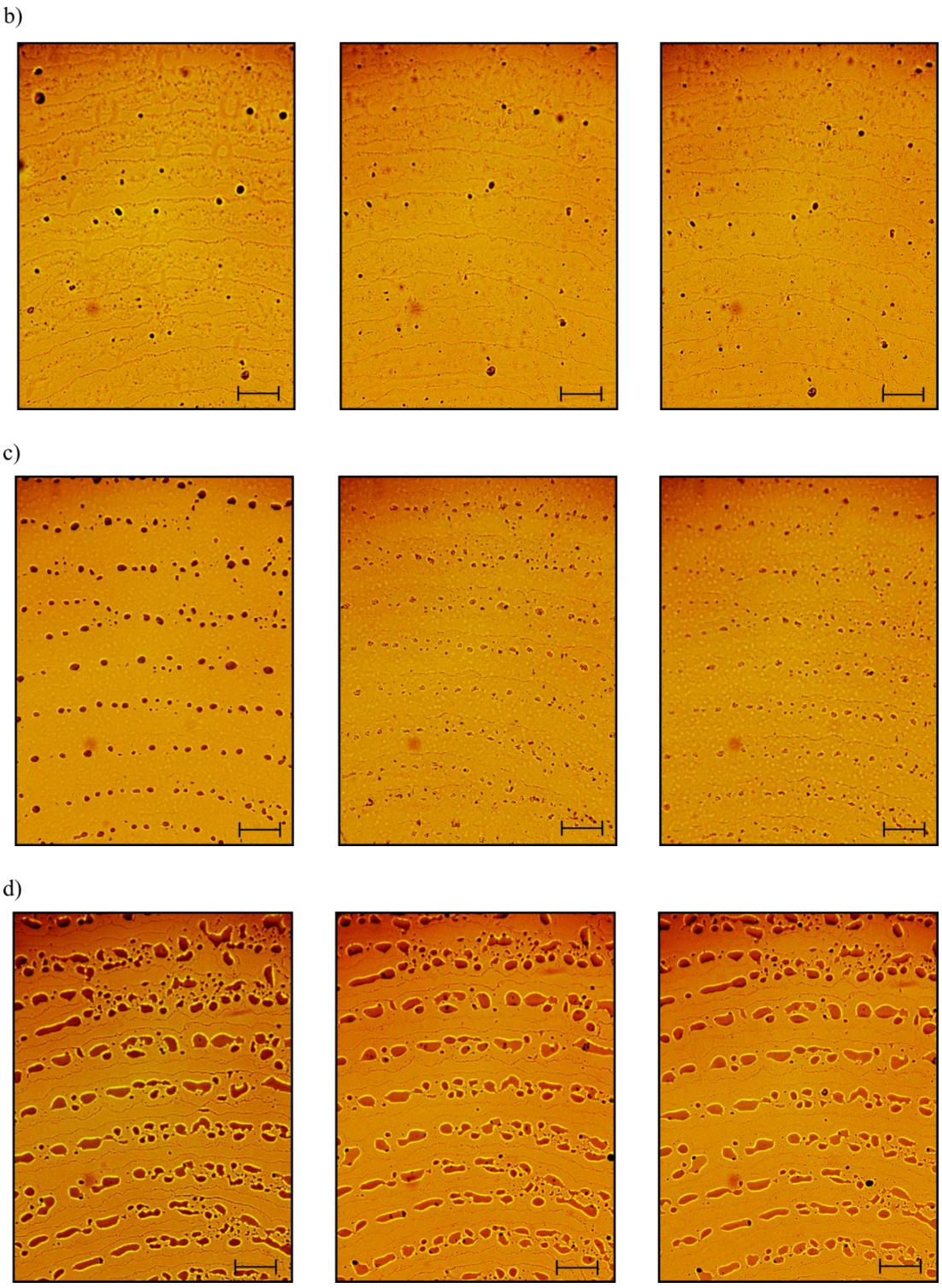

Figure 5. 4: All images are displayed in the order of left: freshly deposited sebaceous fingermark, middle: the same fresh fingermark after aged for 3 days and right: the fresh fingermark after aged for 7 days since deposition on polymer substrate of water contact angle, θ a) 60.2°, b) 65.9°, c) 101.3° and d) 102.8°. The images were obtained from Olympus BX51 optical microscope using an eyepiece of 50 times magnification. All the images are of the same scale bar, 0.2 mm.

On polymer substrate of water contact angle, 60.2° (Figure 5.4 a) the ridge outlines were clearly defined, and the droplet size was heterogeneous with some heavier droplets appearing brighter could be observed. The comparison with the same type of marks (sebaceous) deposited on cling film ($\theta = 65.9°$) showed significant differences (Figure 5.4 b). The sebaceous secretions were more spread across the ridge surface and a very fine well-defined outline could be systematically observed, and no droplets were present.

Conversely, the sebaceous fingermark on PDMS substrate ($\theta = 101.3°$) displayed a significantly different morphology (Figure 5.4 c) where the major part of the secretions was concentrated towards the middle of the ridges. Interestingly, the ridge outline was not well defined on the freshly deposited mark on this surface. Similar results were observed on polymer substrate of water contact angle, 102.8° (Figure 5.4 d) but the secretions were of larger irregular shaped island of material and the ridge outline was still well defined.

Very impressive results were obtained for the fingermarks aged on polymer substrates of different wetting properties. The most interesting and surprising change in the marks deposited on polymer substrate of water contact angle, 60.2° did not occur within the ridges, but in furrows. The furrows were visible as a clean substrate immediately after deposition (see Figure 5.4 a), but droplets started to appear within the furrows and remained visible after 7 days (these are marked on the image with black circles). Similar phenomenon was observed by Moret *et al.* indicated this observation is presumably due to a redeposition of the more volatile sebaceous compounds [9].

The marks were clearly visible post-deposition on the cling film (Figure 5.5 b) but by day 3, marks showed signs of fading and only tiny droplets of substances retained their original positions on marks aged 7 days. This observation cannot solely be attributed to the environmental factors since all samples were collected and stored together. This observed phenomenon suggests that the fingermark secretions seem to dissolve into contaminants or coatings present on the cling film surface such as plasticisers as the cling film was used as it is without any cleaning process.

For marks on polymer substrate of water contact angle 101.3°, the droplets of secretions showed signs of shrinkage but only to a limited extent. However, the ridge

outline appeared on the mark aged 3 days and remained on the surface until the mark aged up to 7 days. This observation suggests that as the secretions tend to dry, it comes closer to the surface allowing the appearance of the ridge to be observed.

No drastic changes were observed in the thin monolayer fingermark on the polymer substrate of water contact angle, 102.8° after 7 days since the large irregularly shaped islands of sebaceous material retained their shape and size over the period of 7 days. However, it must be noted that the fingermark ridge outline seems to fade away on the fingermark aged 7 days.

These observations indicate that the wetting property of the substrate has an influence on the distribution of the secreted material and therefore plays an important role in the morphology of the fingermark deposit as it aged. This would then have an effect during the development of the aged fingermark with cyanoacrylate fuming.

The aging process of sebaceous fingermarks on substrates of different wetting properties showed variation in the spectra that were obtained as the fingermark residue aged (see Figure 5.5). This emphasises that upon deposition of fingermark residue on the polymer surfaces, interactions occur between the polymer and the fingermark residue molecules across the contact area in which the intermolecular forces (attraction or repulsion) that develop between the fingermark residue and the polymer surfaces would be different [10]. These interactions induce the distribution of fingermark residue at the interface to be equilibrated differently which also affect the aging process of the fingermark residue on polymer surfaces of different wetting properties.

Data points produced in any given plots throughout this chapter are the averaged values from three fingermarks. The uncertainty for the data points were calculated by using the standard error of the mean values.

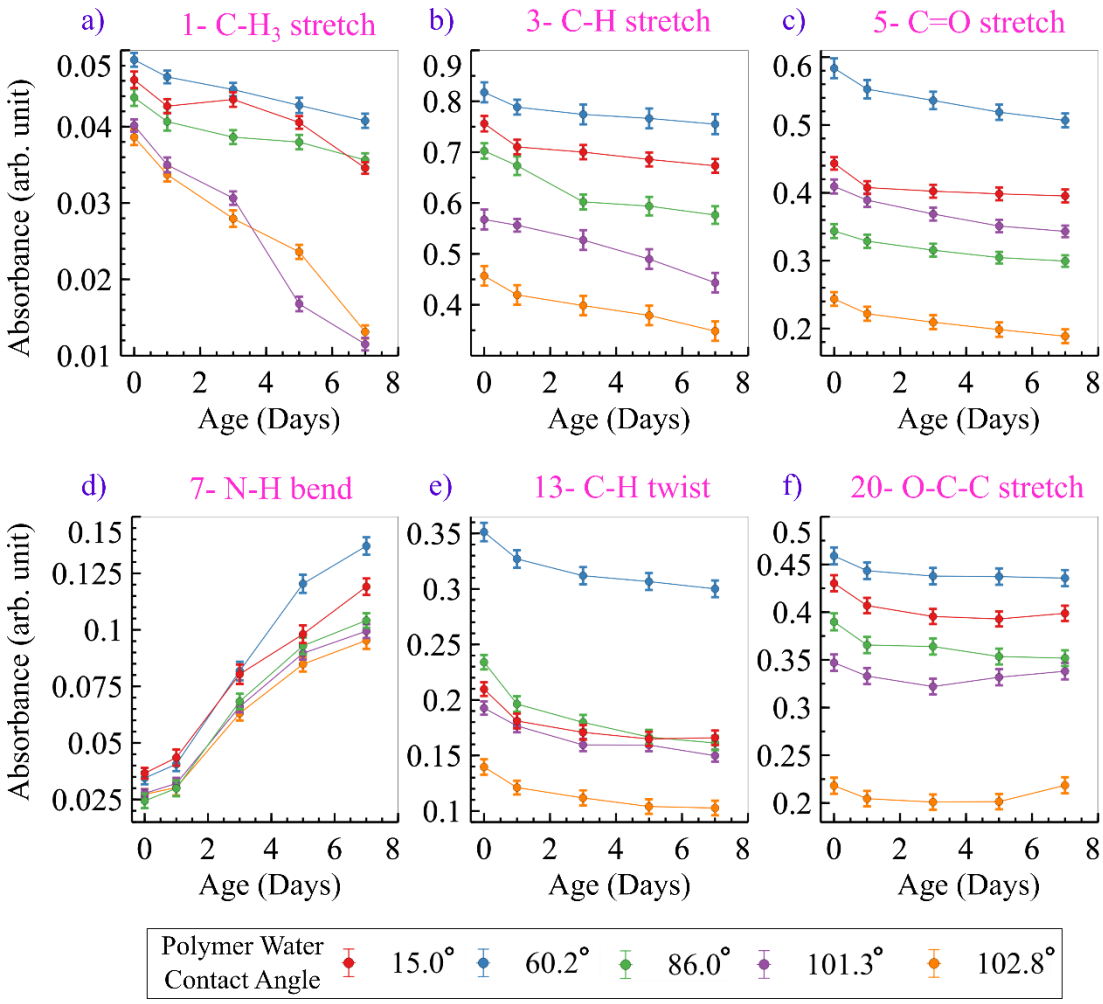

Figure 5. 5: Absorbance value as a function of time after fingermark deposition with peak assignments for functional groups that displayed the most prominent changes due to the aging process of fingermark residue. Error bars were calculated using the standard error of the mean of absorbance value obtained from different spectra on the same substrates.

It is evident from Figure 5.5 that the initial amount of fingermark residue deposited on polymer substrate differs significantly with respect to the polymer water contact angle. It is important to note that although it was mentioned earlier, the absorbance value depends on the thickness of the polymer film and sebaceous layer which are related to the penetration depth of evanescent wave, the variation in the initial amount observed in Figure 5.5 is not governed by the thickness of the polymer film. The thickness of the polymer film along with the amount of IR absorbed is discussed in detail below.

For the same type of fingermark residue (sebaceous), the absorbance value of the fingermark constituents on these substrates decreased in the order of 60.2° > 15.0° > 86.0° > 101.3° > 102.8°. Meanwhile, the thickness of polymer films for 60.2°, 15.0°, 86.0°, 101.3° and 102.8° were measured (using the AFM, see section 4.2.4) to be 0.182, 0.065, 0.135, 0.240 and 0.223 μm respectively. Hence, comparing these values with the amount of fingermark residue deposited, it is clear that the absorbance value did not need to be corrected due to the varying thickness of polymer films. This reveals that the wettability of the substrate governs the amount of residue that is deposited on when a sebaceous loaded fingertip touches the surface.

Spectra of fingermark residue fumed on a hydrophobic surface of water contact angle 102.8° at different aging times is shown in Figure 5.6 to obtain information about the cyanoacrylate fuming process on aged fingermark residue. According to Figure 5.6, the extent of CNA polymerisation decreases as the aging time increases.

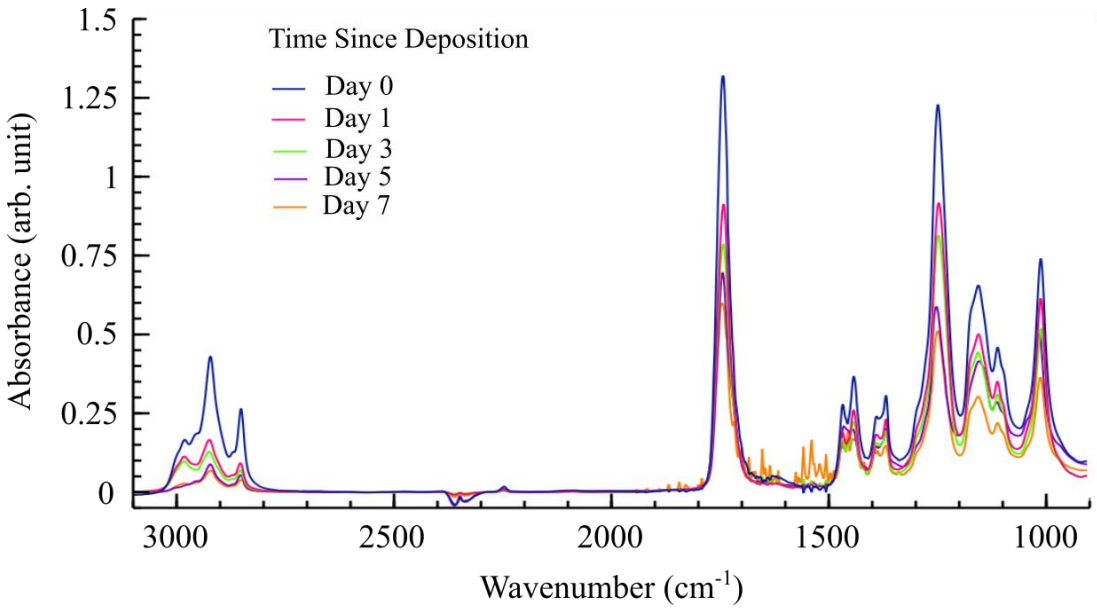

Figure 5. 6: Examples of the aged fingermark spectra with time frame from 0 to 7 days that contained predominantly sebaceous material, deposited on PtBMA surface (θ = 102.8°) fumed for 333 minutes in FTIR chamber.

After 7 days, the amount of cyanoacrylate that had polymerised on the fingermark residue dropped by a factor of 2. It must be noted that the primary components of the

fingermark residue that are responsible for the initiation of the cyanoacrylate polymerisation such as moisture, carboxylic acids and amines are volatile and readily lost [4] resulted in the amount of cyanoacrylate polymerised on the aged fingermark residue dropped rapidly with the time since deposition, despite the other lipid compounds remain anchored to the substrate during the aging process, which could be observed in Figure 5.4.

During the fuming process, the amount of the poly (ethyl cyanoacrylate) that polymerises within the mark was monitored as a function of fuming time by obtaining FTIR spectra for every 5 minutes to produce a kinetic graph. The kinetic graph represents the total amount (absorbance value) of cyanoacrylate polymerised on the mark as a function of time up to 333 minutes for the peak at wavenumber 1744 cm^{-1} corresponding to C=O stretch, is shown in Figure 5.7. Photographs of the fingermarks aged for a period of time t = 0 day, 1 day, 3 days, 5 days and 7 days were taken with a camera during the exposure of cyanoacrylate vapour. The resulting images of fingermarks at time t = 20 minutes of cyanoacrylate fuming are shown as insets in Figure 5.7 to correlate the result obtained via the two different techniques.

The fresh mark (aged 0 days) had good ridge definition and contrast with the substrate. However, after just 1 day of aging, periodic breaks in the ridgelines becomes evident and after an entire week of aging in laboratory in presence of light and airflow, the ridge definition was very poor as the points of development became increasingly sporadic along with cyanoacrylate polymerisation occurring within fingermark valleys. From Figure 5.7, it is clear that as the mark ages it loses the capability of initiating polymerisation of cyanoacrylate fumes as the growth of cyanoacrylate decreases by a percentage difference of ~ 70 % than that of the fresh marks.

These results show that chemical interaction between CNA and the sebaceous fingermark residue diminishes with the age of fingermark. Consequently, the camera measurements on the development of fingermark displayed a decrease in sensitivity on the quality of fingermark as the age of marks increases as seen in Figure 5.7.
This conclusively shows that FTIR measurements of cyanoacrylate polymerisation for aged marks is consistent with the images obtained for the similar aged marks on the same substrate.

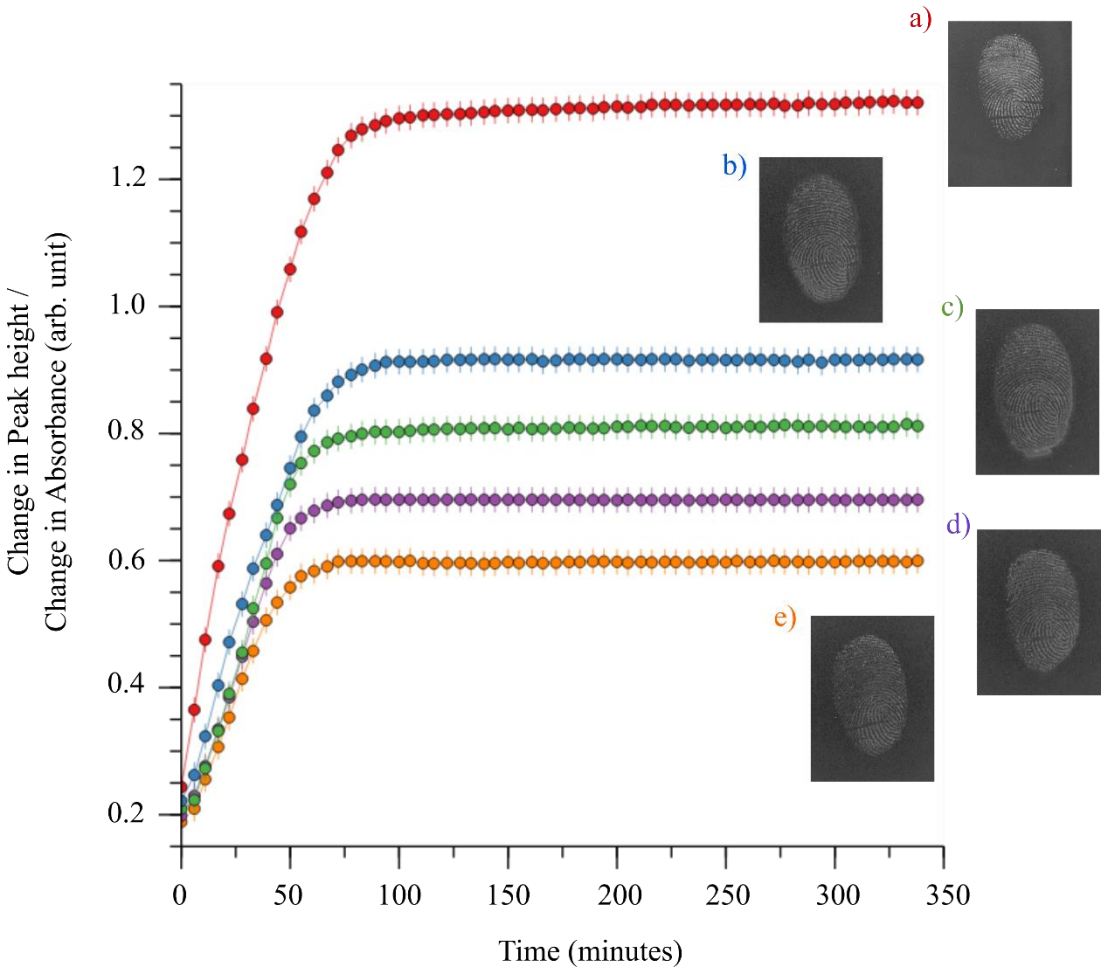

Figure 5. 7: The graph represents the growth of cyanoacrylate polymer onto sebaceous based aged marks at various period on PtBMA (θ = 102.8°) polymer substrate as a function of time exposed to the cyanoacrylate (monomer) vapour obtained from FTIR spectra. The red dotted line presents kinetic plot for mark aged 0 days, blue dotted line for mark aged 1 day, green dotted line for mark aged 3 days, purple dotted line for mark aged 5 days and orange dotted line for marks aged 7 days. Meanwhile, the photographs next to each graph were obtained for the similar type of mark developed on PtBMA substrate by cyanoacrylate fuming method at time t = 20 minutes for marks that have been aged for (a) 0 days, (b) 1 day, (c) 3 days, (d) 5 days, and (e) 7 days using a camera.

A quantitative measure on the influence of the substrate wetting properties in sebaceous rich mark aging process for an entire week is shown in Figure 5.8, where the growth of cyanoacrylate polymer onto the fingermark surface is plotted as a

function of fuming time for the different substrates. The fingermark residue aged on a hydrophilic substrate showed higher magnitude of cyanoacrylate polymerisation onto the marks than that of the marks aged on hydrophobic substrates. Additionally, the images of the developed marks at fuming time t = 20 minutes are included (see Figure 5.8), to compare the quality of the fumed marks aged for one week on substrates with varying water contact angle of 15.0° up to 102.8°.

Despite the much lower (~ 1.6 times) cyanoacrylate polymerisation occurred on the aged marks deposited on the hydrophobic surface (θ = 101.3°) in comparison to the mark aged and fumed on a hydrophilic surface (θ = 60.2°), fumed fingermark images in Figure 5.8 demonstrate clear visible marks to the naked eye at time t = 20 minutes of the fuming process for the sebaceous rich deposits on all the polymer surfaces except for the mark developed on PtBMA surface, where the ridge definition is not clear.

Figure 5.7 shows that development quality of sebaceous marks dropped due to the approximately 2 times lesser growth of cyanoacrylate being observed on the aged marks in comparison to the freshly deposited sebaceous mark. Additionally, the mark on PtBMA substrate is proven to display the poorest development quality when compared to other substrates indicating the nature of substrate play an important role on the mark deposited and the way they age resulting in different outcomes after the development process.

As displayed in Figure 5.5, the initial amount of fingermark deposited on each polymer substrate was different and this added to the aging of fingermark residue for a week, led to different values to begin with is the reason for the initial value not starting at the same value in Figure 5.8. The different distribution of sebaceous fingermark on polymers of varying water contact angle led to different amounts of cyanoacrylate polymerisation onto the residue although the initial amount of fingermark at day 7 did not differ significantly from each other for substrates of water contact angle 15.0°, 86.0° and 101.3° respectively.

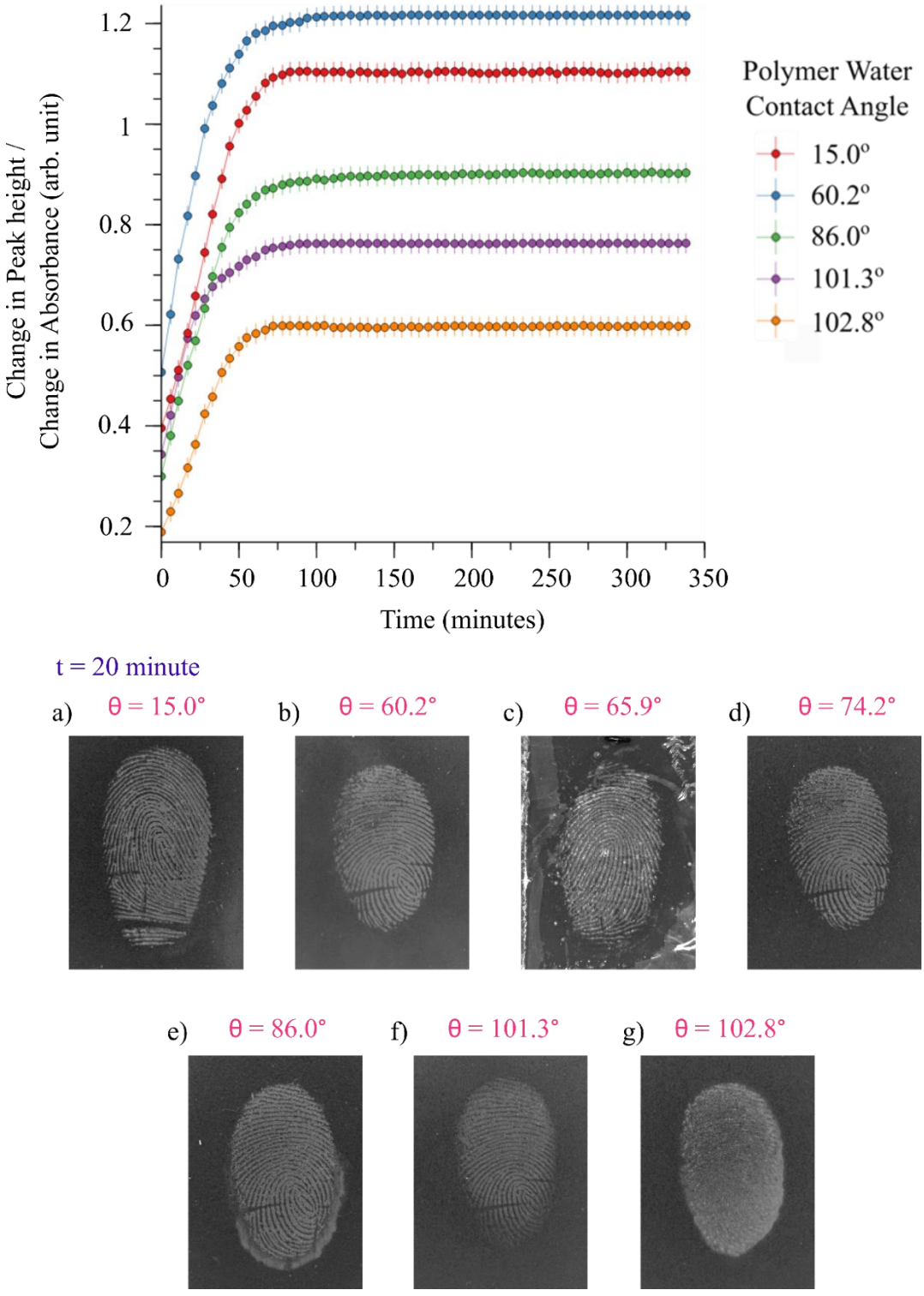

Figure 5. 8: A direct correlation of polymer substrates containing sebaceous marks that have been aged for one week in an open container on a working bench in laboratory developed with cyanoacrylate fuming method up to 333 minutes : top – FTIR kinetics plot of peak 1744 cm^{-1} and bottom - sebaceous marks developed on polymer substrates with water contact angle of a) 15.0°, b) 60.2°, c) 65.9°, d) 74.2°, e) 86.0°, f) 101.3° and f) 102.8° obtained from camera.

The kinetics plot obtained from FTIR and camera measurements were analysed in the same way as in Chapter 4 to determine the saturation time, saturation value and the amount of cyanoacrylate polymerised onto the sebaceous mark that aged on polymer substrate of different water contact angle for 0 day, 1 day, 3 days, 5 days and 7 days as shown in Figure 5.9 below. Similarly, peak at wavenumber 1744cm^{-1} corresponding to C=O stretch was chosen for the analysis and to compare with the results obtained from the development of freshly deposited mark in Chapter 4.

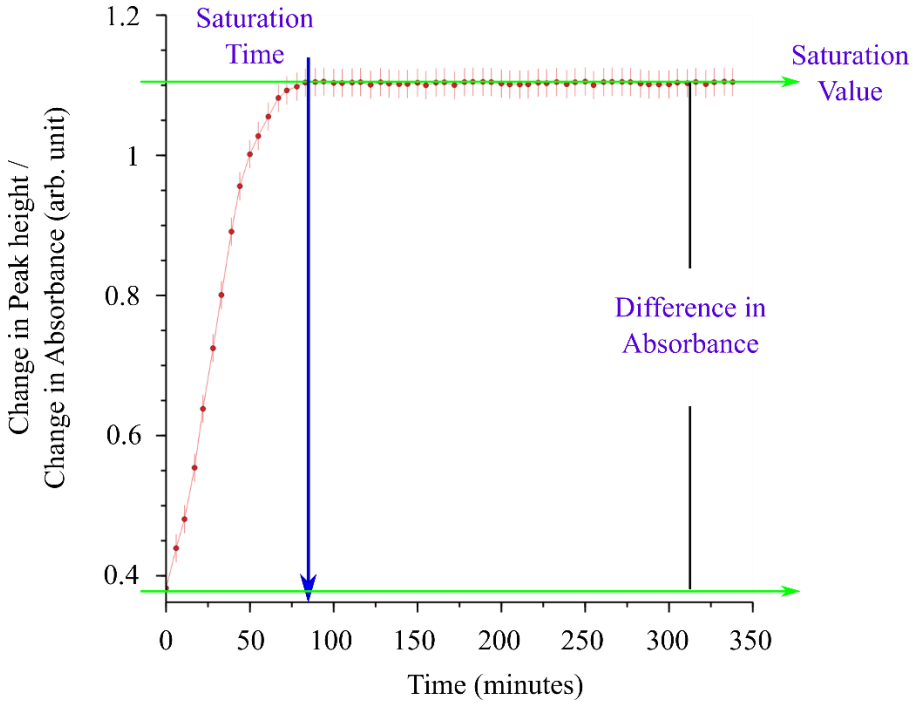

Figure 5. 9: Figure shows how the saturation value, saturation time and difference in absorbance values were obtained from the kinetics plot shown in Figure 5.8. This kinetic plot corresponds to cyanoacrylate polymerisation onto one week aged sebaceous fingermark residue deposited onto the polymer surface of water contact angle, 15.0°. The saturation value from the kinetics plot is 1.105 ± 0.065, saturation time is 80 ± 4.7 minutes and the amount of cyanoacrylate polymerised is 0.732 ± 0.038.

The time taken for the aged mark to attain saturation for both the FTIR measurements and camera kinetics that were extracted from each kinetic curve, is shown in Figure 5.10. Saturation time for all the polymer substrates used in this study displayed the

same trend where the time taken for cyanoacrylate polymerisation to reach saturation point decreased with the age of fingermark.

The reason for cyanoacrylate polymerisation saturating much faster on the aged marks in comparison to the fresh marks is that the termination of cyanoacrylate polymerisation occurs faster on the aged marks due to the decrease in the number of initiators that remain on the mark surface as an effect of the aging process.

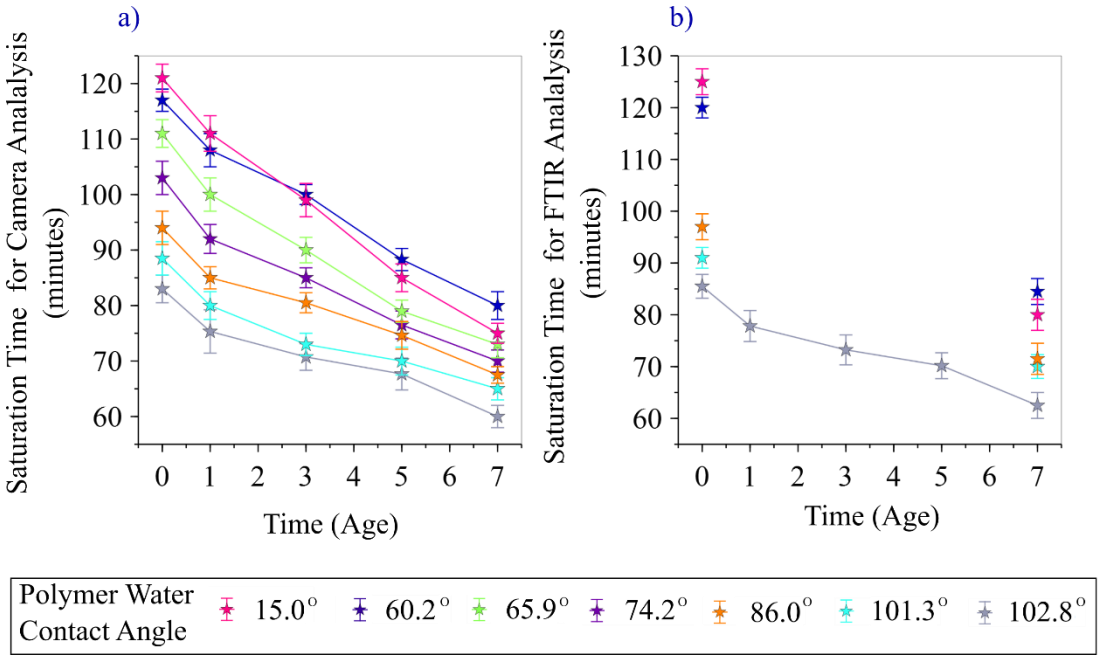

Figure 5. 10: Figure represents data points of saturation time for sebaceous based latent fingermark residue aged from 0 up to 7 days developed on polymer substrates with varying water contact angle for the two different techniques used, a) camera and b) FTIR measurements.

It should be noted that the missing data points in intermediate times for FTIR measurements was due to the FTIR equipment failure. However, the analysis remains unbiased as the saturation time for aged sebaceous mark on the polymer surface of water contact angle 102.8° acquired from both the camera and FTIR techniques are consistent with each other. Hence, the trend for the saturation time for other polymers should be similar to as what is seen in graph a) Figure 5.10. Also, the saturation time for the one week aged and fumed sebacous deposits falls within the same range for

both the camera and FTIR analysis ensuring both techniques are in agreement with each other.

The time taken for cyanoacrylate to saturate on aged marks deposited on hydrophilic substrate is longer compared to the aged mark deposited on hydrophobic polymer substrates. This relates back to the sebaceous secretions taking up large irregular shaped island of material on hydrophobic substrate in contrast to the same type secretion being more spread across the ridges on hydrophilic substrate after deposition and remained in the same way even after aged for one week led to longer time for the cyanoacrylate to polymerise on hydrophilic substrate as it requires more coverage area in comparison to the mark on hydrophobic substrate. This is backed up from the observation from Figure 5.4 displaying the distribution of sebaceous residue in freshly deposited mark and the same mark aged for a week on polymer substrates of different water contact angle.

As the sebaceous marks aged, the saturation value decreased for any given substrates implying that reduction within the aged fingermark residue chemical composition (evident from Figure 5.5 where the intensity of all vibrational bands decreased with fingermark age) led to a much lesser cyanoacrylate polymerisation. However, Figure 5.11 is a good illustration of the fact that as the water contact angle of the polymer substrate increases, the saturation value decreases.

This suggests that despite the majority of the substances such as fatty acids, glycerol, and phospholipids undergoing declination during aging, these compounds are still in a greater amount in marks deposited on substrates with lower water contact angle as seen in Figure 5.5 which attributes to the higher saturation value. This observation is supported by Lewis *et al.* describing the ability to develop good quality of sebaceous marks that are older than two days is attributed to the presence of fatty acids, mono and diacyl glycerols within the sebaceous material of the mark [11].

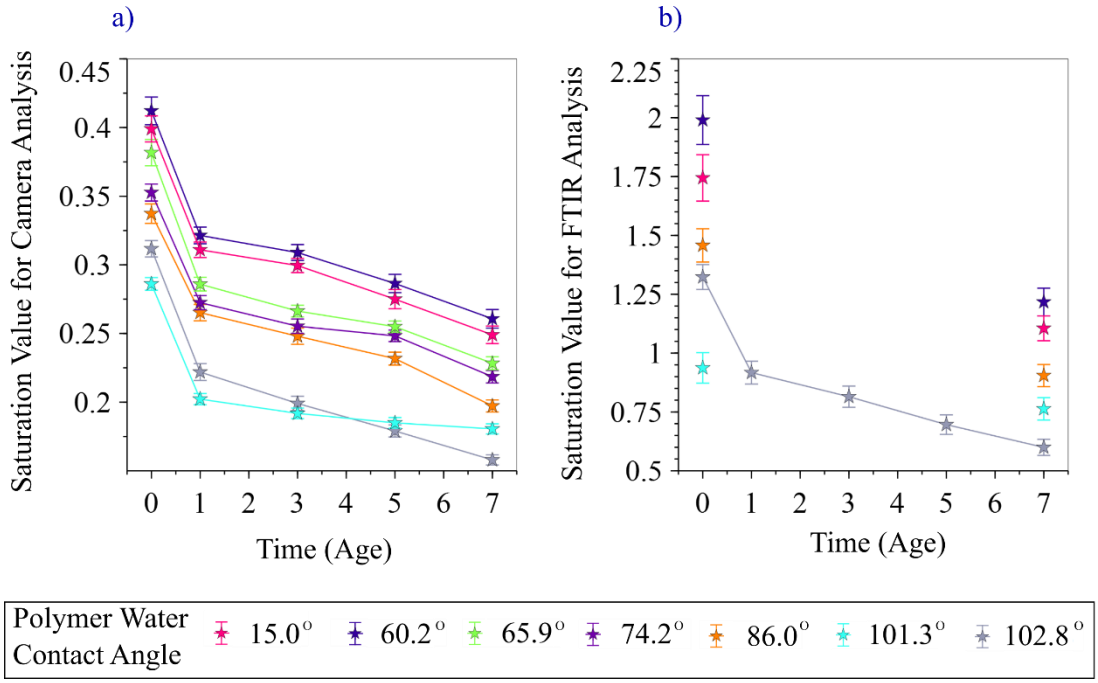

Figure 5. 11: a) A comparison of the saturation values of the sebaceous fingermark residue fumed from camera analysis for all the marks aged for 0, 1, 3, 5, and 7 days on substrates of varying water contact angle while (b) displaying the saturation value of absorbance at peak 1744 cm^{-1} during the fuming process for the sebaceous fingermark deposits aged 0 and 7 days on all polymer substrates except for polymer of water contact angle 102.8°, sebaceous marks were aged for 0, 1, 3, 5, and 7 days before being fumed for FTIR analysis. It could be observed that both the method results are consistent with each other given that the saturation value decreases with respect to two factors, firstly with the increase in marks age while secondly with the ascending of substrates water contact angle.

Similar to the saturation value, the total amount of cyanoacrylate deposited onto the marks displayed two most distinct trends which are:

1. when the marks were exposed to cyanoacrylate fumes, it showed a clear decrease in the cyanoacrylate deposition with the age of the marks regardless of the substrate the mark was deposited onto.
2. the amount cyanoacrylate polymerised was of higher order for marks deposited on the hydrophilic polymer.

This demonstrates that the effectiveness of the cyanoacrylate fuming development method decreases as the marks age which is further affected by the substrates wetting properties especially on the polymer of water contact angle 102.8° due to the distribution of material on the polymer substrates.

In spite of a very short period of aging, the results displayed a notable difference in both the saturation value and the amount of cyanoacrylate polymerised on the aged sebaceous fingermark residue deposited on substrates with different water contact angle which played an important role in the deposition of fingermark (distribution of fingermark residue), that then influenced the aging process hence, affecting the cyanoacrylate polymerisation.

To investigate the environmental effect (air flow and light) other than the substrates wetting properties in the aging of sebaceous fingermark and thus the development; control marks were aged for a week in microscope slide box that shielded the marks from both light and air flow were then fumed in the same exact way as the marks stored outside. The developed sebaceous marks stored inside were then compared with the developed mark stored outside is displayed in Figure 5.12.

Figure 5.12 shows the sebaceous fingermark images aged for 1 week in an open container and inside a closed container on polymers of water contact angle a) 15°, b) 60.2°, c) 101.3° and d) 102.8° which were then fumed. There is not much correlation between how the fingermarks fumed due to the storage conditions for the fingermarks deposited on the hydrophilic substrates. However, the fingermarks deposited on the two hydrophobic polymer substrates showed a better quality of fingermark development when stored inside a container. This, therefore, indicates strongly that the wetting properties of substrate play an important role in fingermark deposition, aging process and fingermark development which also can be affected by the environmental effect more than the other.

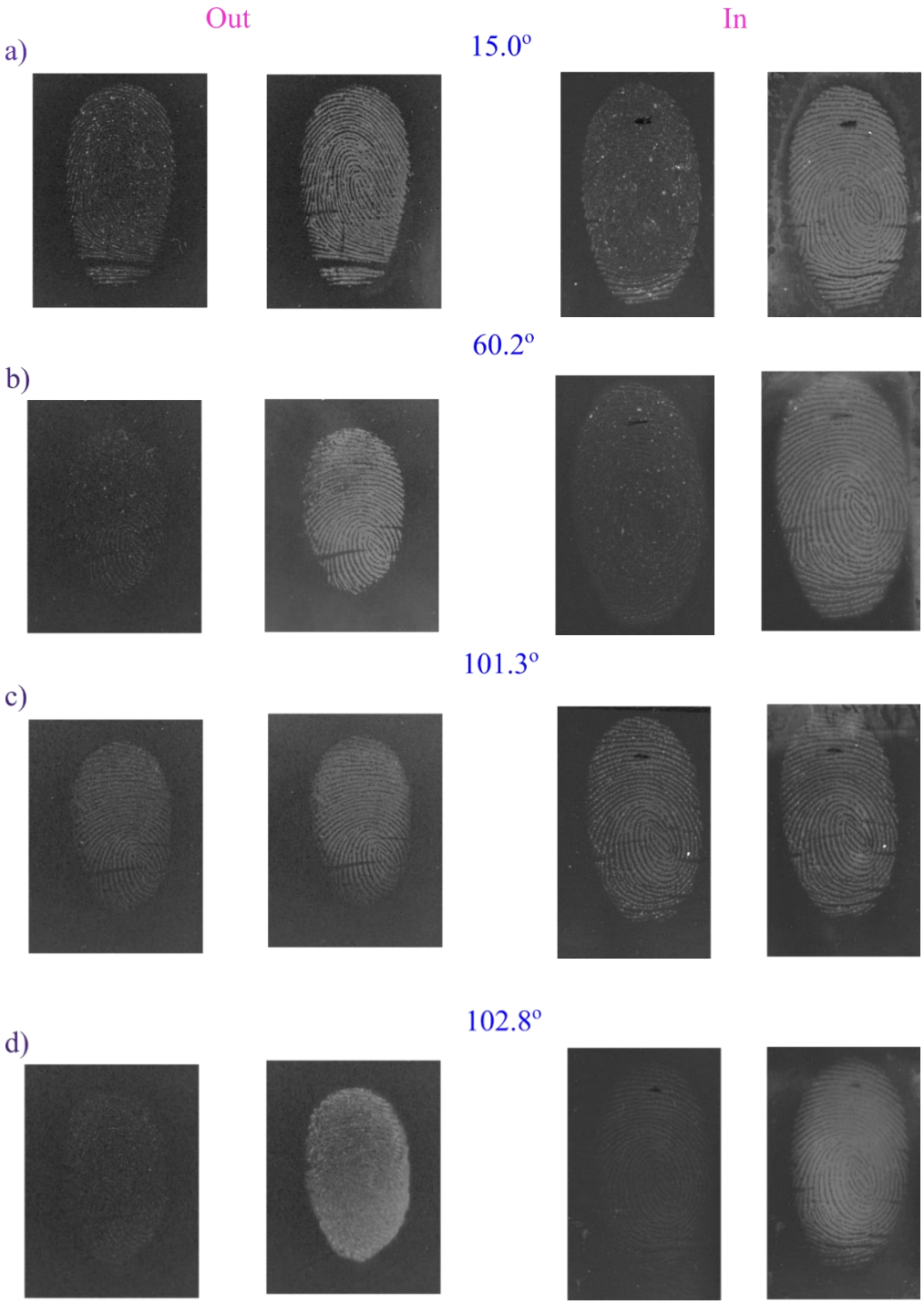

Figure 5. 12: Figure shows sebaceous fingermark deposited on polymer substrates of water contact angle a) 15.0°, b) 60.2°, c) 101.3° and d) 102.8° that were aged for one week in two different environmental conditions, left: fingermarks were left to age in an open container left on working bench exposed to light and air flow and right: fingermarks were left to age in a closed microscope glass slide box without any exposure to the environmental conditions which were then fumed with cyanoacrylate.

5.3.2 Aging of Eccrine Marks

Eccrine secretion for the aged marks were observed through the most prominent C-O stretch at 1250 cm^{-1} in Figure 5.13 which represents amino acids, displayed a significant decrease in the intensity with the increase in aging time [12] despite the percentage difference of 191 in absorbance of eccrine deposits in comparison to sebaceous deposits due to the lower eccrine sweat concentration.

It is important to note that the broad water peak in the wavenumber region of 3150 – 3600 cm^{-1}, shows a dramatic decrease within 24 hours of deposition which then gradually decreased revealing no broad peak in the FTIR spectrum for eccrine mark aged one week. The fingermarks were stored as mentioned earlier in sub-section 5.2.1 and the NaCl solution along with water beaker in the fuming cell did not show any kind of rehydration in the fingermarks as the broad water peak was not observed again in any of the spectra during the fuming process.

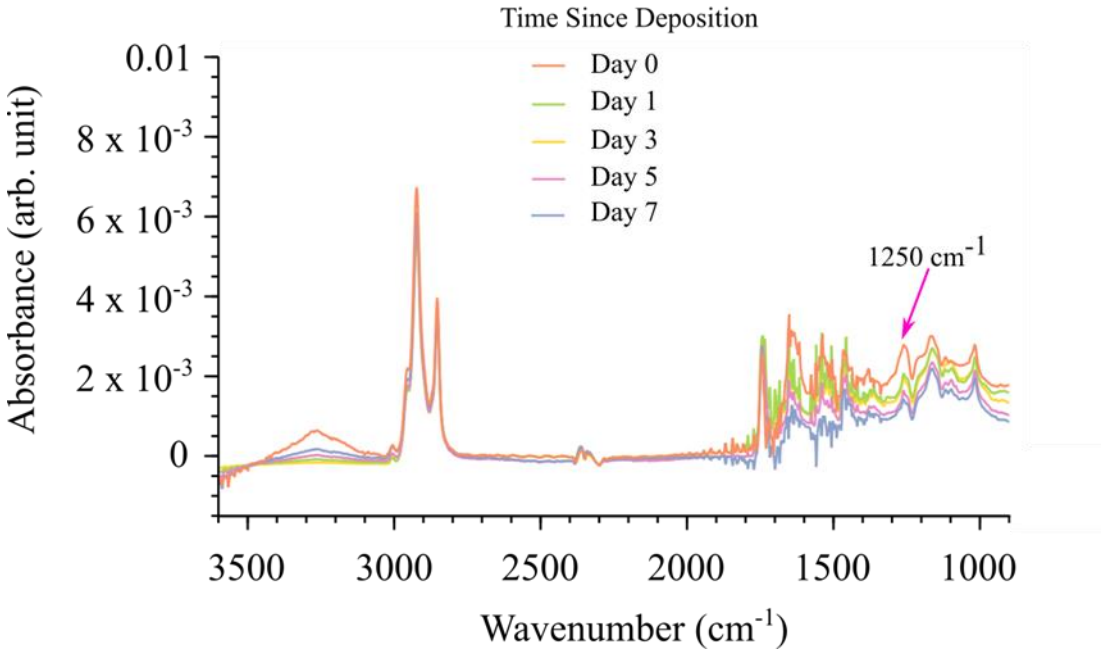

Figure 5. 13: Examples of typical FTIR spectrum of primarily eccrine fingermark residue deposited on PVA surface (water contact angle of 60.2°) that was collected at the time interval of : 0 day, 1 day, 3 days, 5 days, and 7 days since deposition.

Example of images obtained from the optical microscope to view the physical changes that occurred within fingermark due to the aging process is shown in Figure 5.14.

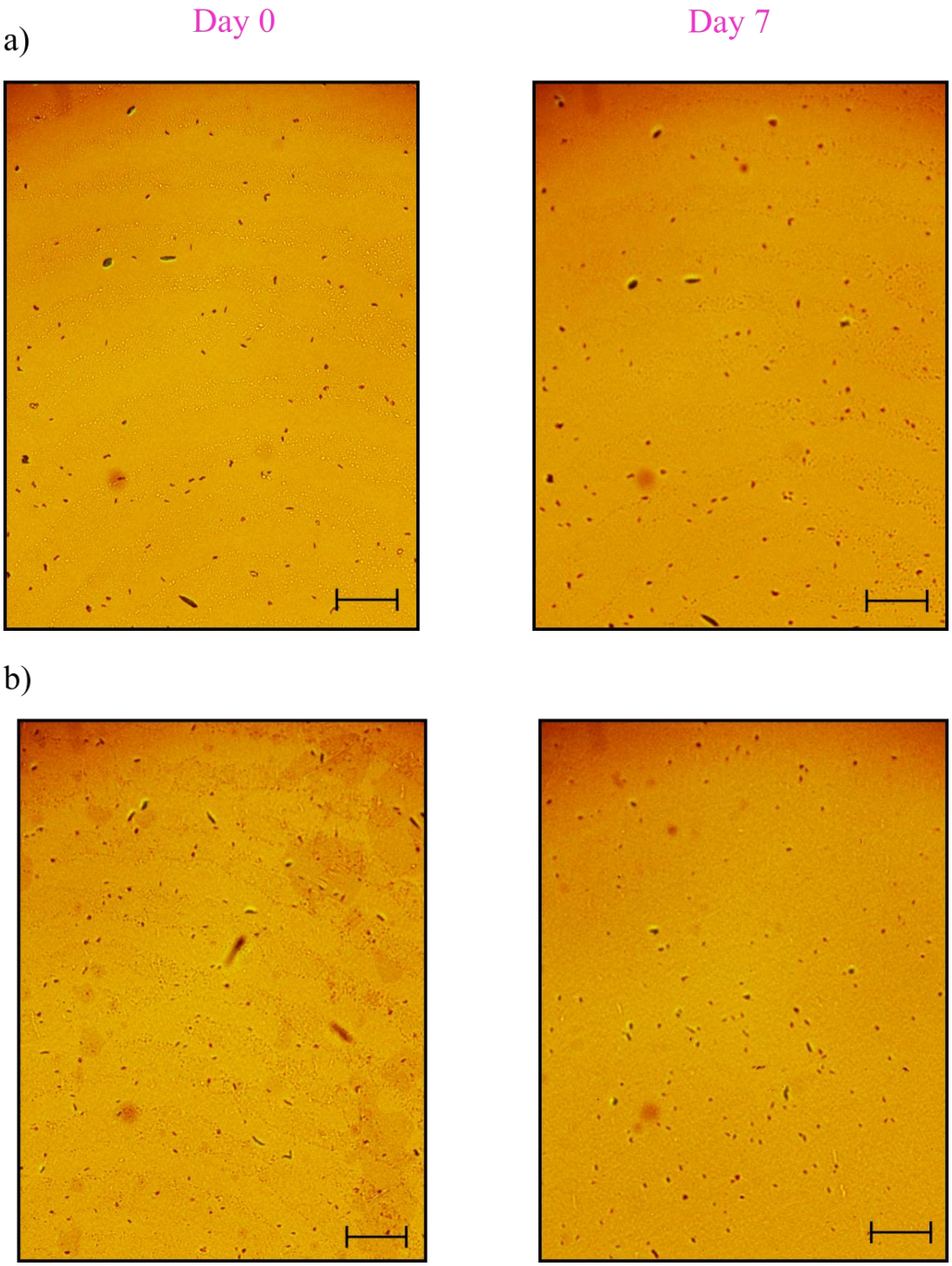

c)

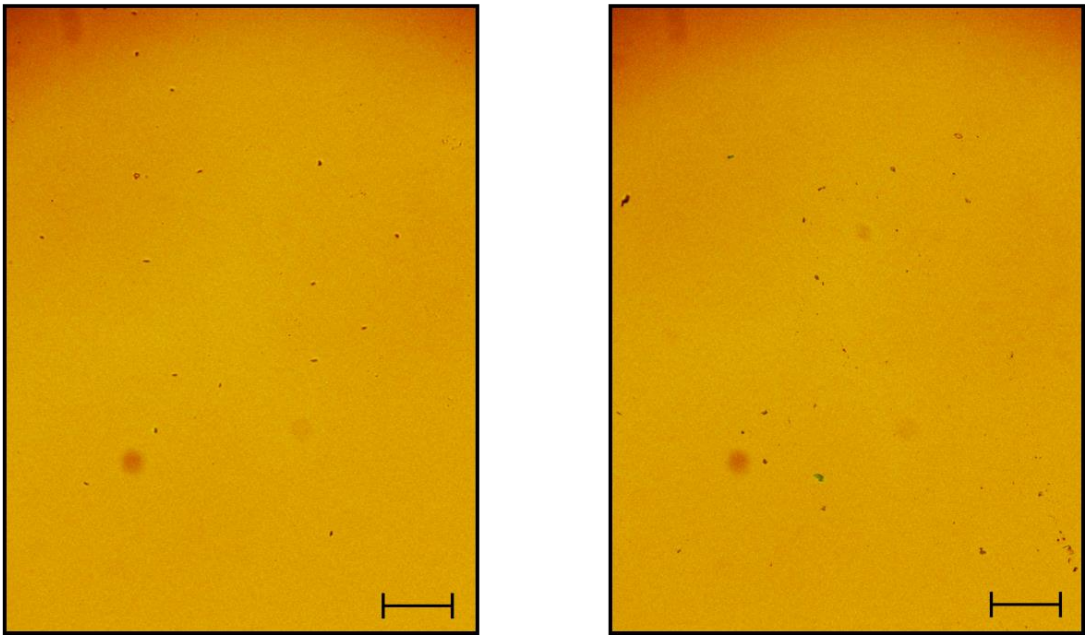

Figure 5. 14: All images are displayed in the order of left: freshly deposited eccrine fingermark, and right: the fresh fingermark after aged for 7 days since deposition on polymer substrate of water contact angle, θ a) 60.2°, b) 65.9° and c) 101.3°. The images were obtained from Olympus BX51 optical microscope using an eyepiece of 50 times magnification. All the images are of the same scale bar, 0.2 mm.

Eccrine marks due to a lower amount of secretions as observed in the IR spectra in Figure 5.13 resulted in weaker contrast (see appendices for a clearer view, page number : pp. 235 - 237) but still sufficient to visualise some ridge outlines deposited on the polymer of water contact angle, 60.2° (Figure 5.14 a). Freshly deposited eccrine mark displayed droplet size and shape, inner ridge structure, and material distribution with adequate detail. These details were mostly faded away on the fingermark after aged for 7 days; when left in an open container on a working bench in laboratory, exposed to light and air flow.

The comparison with the same type of marks (eccrine) deposited on cling film ($\theta = 65.9°$) showed significant differences (Figure 5.14 b). The fingermark ridge outline was visible but was not well defined as observed on the polymer in Figure 5.14 a. However, after aging for one week the mark disappeared almost completely, but the skin cells, embedded in the secretions right after deposition remained and was visible.

Very interesting result was obtained (Figure 5.14 c) for marks on PDMS ($\theta = 101.3°$), as no evidence of fingermark deposition was present even for the freshly deposited eccrine mark, hence the aging of fingermark on this surface could not be observed. The only evidence for fingermark was deposited on this surface was the observation of the dead skin cells that were deposited along with the eccrine rich sweat.

This reveals that the wettability of the substrate governs the amount of residue that is left on when eccrine sweat loaded fingertips touch the surface. Figure 5.15 displays the amount left initially and the aging of eccrine deposits are affected by the underlying substrate given that at day 7 of aging process the intensity of peak 1250 cm^{-1} was significantly much higher on the two lowest water contact angle substrates leaving the hydrophobic surface with a lot lesser concentration of amino acid.

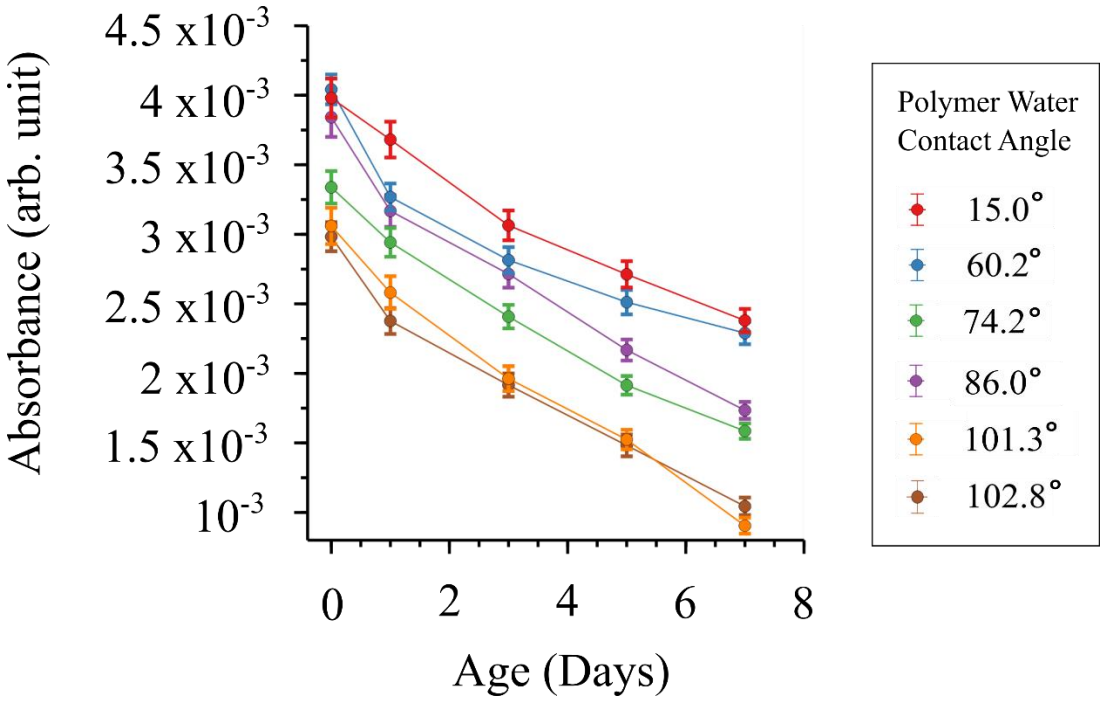

Figure 5. 15: Absorbance value as a function of time after deposition for peak at the wavenumber of 1250 cm^{-1} displayed the most prominent changes due to the aging process of fingermark residue in comparison to other eccrine components. Error bars were calculated using the standard error of the mean of absorbance value obtained from different spectra on the same substrates.

In addition to the aging factor of eccrine compounds in fingermark residue such as the underlying substrate, the mark deposited onto, exposing the marks to light while being stored for the aging process caused the eccrine compounds (N-H, C-N) to degrade faster which led to a larger decrease in the absorbance value [13].

The aging kinetics indicating different aging patterns for the eccrine compound on different substrate, led to further exploration of cyanoacrylate polymerisation between fingermark aging and influence of the substrates. An example of FTIR spectrum of aged eccrine mark residue of 0, 1, 3, 5, and 7 days on hydrophilic surface (θ = 60.2°) at time t = 385 minutes of cyanoacrylate fuming is displayed in Figure 5.16 while the corresponding developed images of fingermark obtained from camera on the same substrate is shown in Figure 5.17.

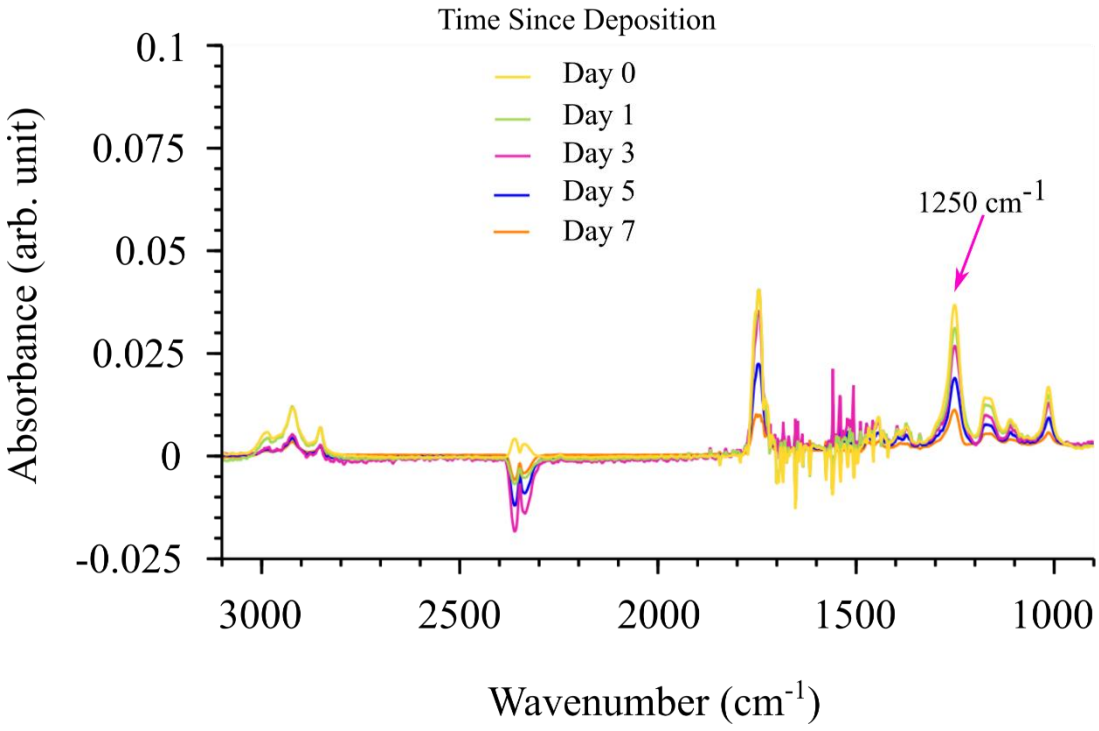

Figure 5. 16: Image displays the FTIR spectrum for aged eccrine marks of day 0, 1, 3, 5, and 7 at the time t = 385 minutes of cyanoacrylate fuming process on hydrophilic polymer surface of water contact angle 60.2°.

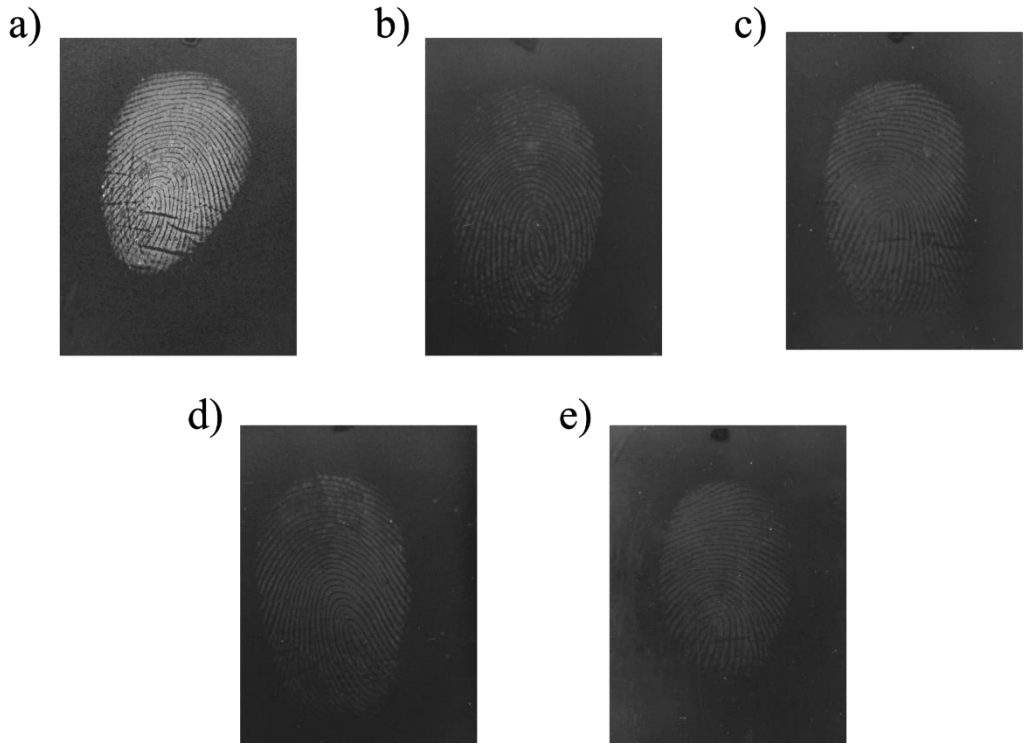

Figure 5. 17: The images were captured by camera at time t = 385 minutes during the cyanoacrylate fuming process on the same substrate of water contact angle, 60.2° for eccrine marks aged at a) 0 day, b) 1 day, c) 3 days, d) 5 days, and e) 7 days respectively.

The FTIR spectra and images of the developed fingermark allowed for a direct correlation between the results obtained via the two different techniques (FTIR and camera), whereby the reduction in peak height (chemical changes) observed in the FTIR spectrum for older eccrine marks (Figure 5.16) resulted in the declining quality of the developed fingermark image (physical change) as could be observed in the images (Figure 5.17).

The spectra of eccrine mark fumed on PVA substrate (θ = 60.2°) in Figure 5.16 displayed a decrease in the amount of cyanoacrylate polymerisation by a factor of 3 on the mark aged 7 days when compared to the fresh mark. Figure 5.17 a) illustrates the grainy, white polymer formation producing a well-developed fingermark structure of a fresh clean mark. However, after just one day of aging, the characteristics of one

day old developed mark, Figure 5.17 b) is remarkably different than the fresh mark. The development of mark structure was greatly diminished, and the grainy, white ridge detail was absent. This is because of the nature of eccrine fingermark composition that is low in concentration declines further during the aging phase, which diminishes the interaction between the cyanoacrylate and the mark. This led to lesser amount of cyanoacrylate being polymerised on the mark resulting in poor quality of fingermark development for the aged marks.

This result shows that the cyanoacrylate polymerisation on aged clean marks tend to diminish quickly just within a span of one week that is consistent with the declination in the quality of the developed images that could be observed from the developed mark in Figure 5.17 as the amount of visible cyanoacrylate polymer was reduced to only faint traces. During the fuming process, the amount of the poly (ethyl cyanoacrylate) that polymerises within the mark was monitored as a function of fuming time by taking photographs of the developing fingermarks (increase in brightness of fingermark depending on the amount of cyanoacrylate polymerises) with a camera during the total exposure time of cyanoacrylate vapour.

This was then used to produce a kinetic graph of the total amount (average intensity of all pixels in fingermark region) of cyanoacrylate polymerised on the mark as a function of time up to 385 minutes for camera technique, is shown in Figure 5.18 for development of eccrine marks on all the polymer substrates. The average intensity of pixels was obtained from the fingermark region in the very similar way as discussed in Chapter 4, sub-section 4.4.2 using a mask and threshold function in Matlab written programme whereby the intensity range of the image now is of 0 to 1. The kinetics graph was compared directly with the photographs of the aged marks that were developed by cyanoacrylate fuming taken at time t = 385 minutes in Figure 5.18.

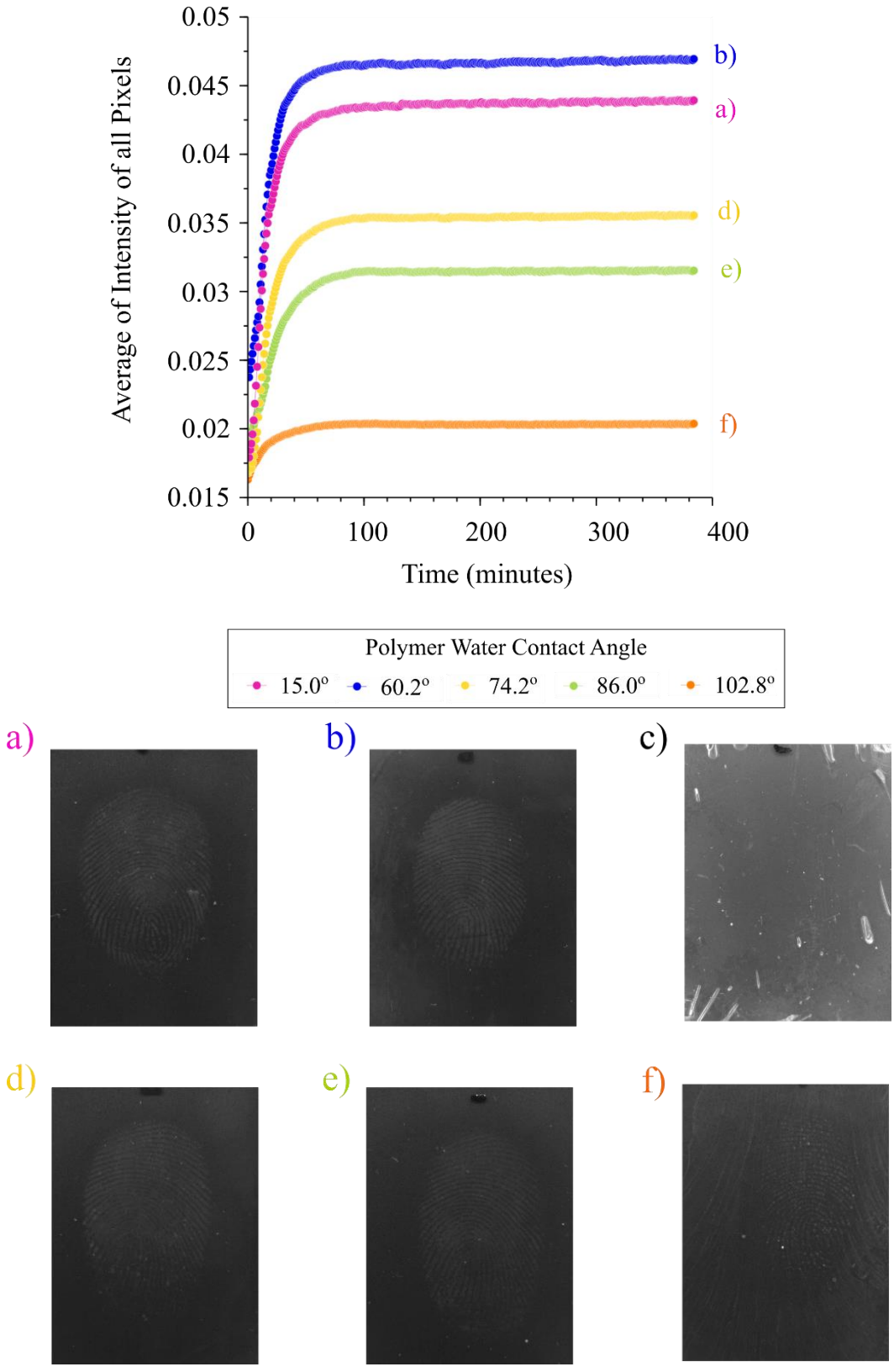

Figure 5. 18: The graph represents the growth of cyanoacrylate polymer onto eccrine based, one week aged marks on polymer substrate of varying water contact angle as a function of time exposed to the cyanoacrylate (monomer) vapour obtained from Matlab analysis by measuring the brightness of mark. Meanwhile, the photographs

represent the kinetic graph obtained using a camera for the similar type of mark, aged one week developed with cyanoacrylate fuming method on polymer substrates of water contact angle a) 15.0°, b) 60.2°, c) 65.9°, d) 74.2°, e) 86.0° and f) 102.8° at the time t = 385 minutes. Except for the photograph c) the kinetic graph was not plotted as no fingermark were developed on the one week aged mark and was included to show the variations in the eccrine fingermark development on substrates of varying wetting properties.

Even though a week aged developed marks are all very faint from the photographs in Figure 5.19, it is still observable that the quality of the developed marks decreases with the increase in substrates water contact angle. However, in the case of cling film substrate (Figure 5.18, c), there is no noticeable of fingermark traces of development despite being exposed to cyanoacrylate vapour for 385 minutes. This is explained by the disappearance of fingermark residue after aged for one week in an open container as observed in the images obtained from an optical microscope in Figure 5.14 b).

So, this implies that the very minimal residue in fresh eccrine marks degrades drastically upon aging process when left on the cling film surface resulting in no development of fingermark at all. Therefore, it is more evident now why cling film is categorised as one of the problematic surface to develop a fingermark when encountered in operational work since cling films are widely used as cheap drugs wrap [14]. If the mark left on this substrate is predominantly eccrine sweat and it has aged beyond 24 hours and exposed to the environmental conditions, then there is unlikely any chances left to acquire the mark from this surface using the cyanoacrylate fuming technique.

The saturation time for the cyanoacrylate polymerisation on one week aged eccrine marks deposited on the polymer substrates of varying water contact angle is displayed in Figure 5.19.

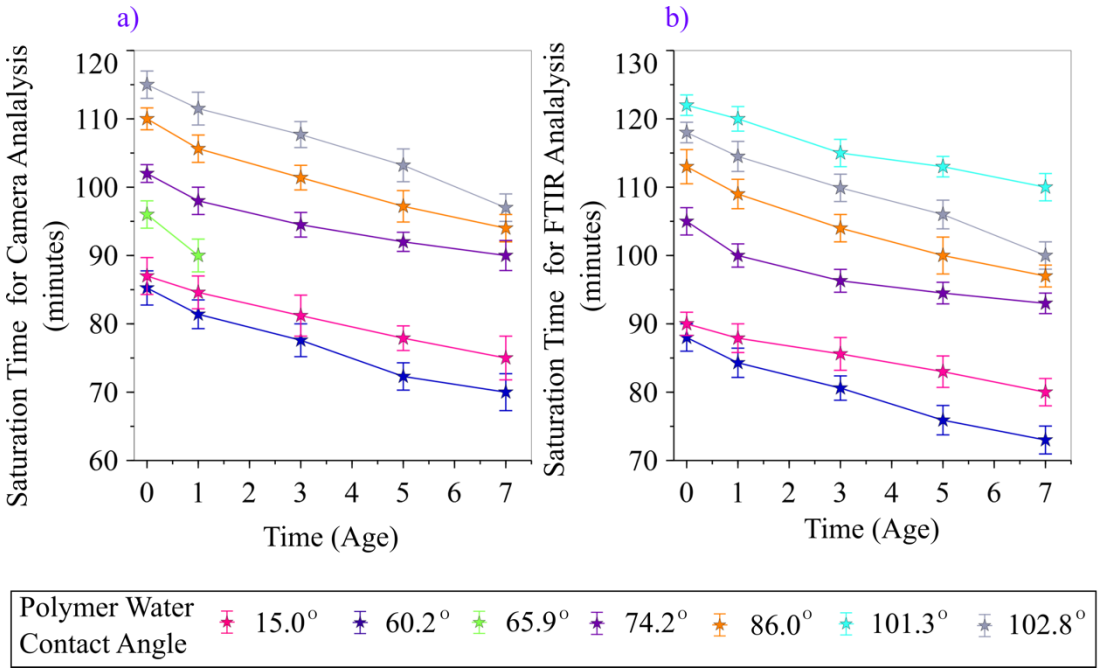

Figure 5. 19: Figure represents data points of saturation time for eccrine deposits aged 0, 1, 3, 5, and 7 days developed on seven polymer substrates of different water contact angle for the two different techniques used, a) camera and b) FTIR analysis. Both techniques displayed a similar pattern for saturation time indicating consistency in the results obtained.

The time taken for both the camera and FTIR techniques used, it is apparent from Figure 5.19 that cyanoacrylate fuming process to attain saturation tends to decrease as the eccrine mark age increases on any given substrate. This suggests that the cyanoacrylate polymerisation terminates faster on eccrine marks that are aged longer due to the nominal amount of residue that is still being present on the surface after undergoing degradation and evolution due to the aging process.

However, the saturation time increases with respect to water contact angle of the polymer surfaces as seen in Figure 5.19, is due to the higher amount of eccrine residue that is retained on the hydrophilic surface in comparison to the hydrophobic surface, leading to higher rate of cyanoacrylate polymer growth resulting in production of a better quality fingermark in lesser amount of time.

It is deduced from Figure 5.17, that the amount of cyanoacrylate deposited on an eccrine mark decreases with the marks aging time as the intensity of the developed marks decreases as the age of mark increases. This is due to the reduced ability of the

aged eccrine fingermark residue to initiate and polymerise the cyanoacrylate vapour during the fuming process leading to the lesser amount of cyanoacrylate polymerisation on the aged mark.

These results conclusively show that wetting properties of the underlying substrate on which the eccrine mark deposited onto plays a significant role in the loss of mark quality for older marks when developed by cyanoacrylate fuming. The amount of cyanoacrylate deposited onto the fingermark ridges on hydrophobic surface decreased dramatically as a function of aging for the eccrine marks as shown in Figure 5.18. This agrees with the observation of eccrine mark from the optical microscope in Figure 5.14 whereby, the freshly deposited mark on the hydrophobic was not visible, while a faded fingermark was still observable on the hydrophilic substrate even after aged for a period of 7 days and exposed to the environmental conditions (light and airflow).

The amount of cyanoacrylate polymerises onto the marks is found to be consistently decreasing with the increasing water contact angle of the underlying substrate. This can be observed clearly in Figure 5.18, through the photographs of the developed eccrine marks on these two substrates where the development of one week aged mark on the substrate of $\theta = 60.2°$ has developed much better than the mark developed on the substrate of $\theta = 102.8°$. It is also evident from Figure 5.17 that when the aged marks were exposed to cyanoacrylate vapour, it showed a clear decrease in the cyanoacrylate polymerisation with the increase in the age of marks which is true for the aged marks on all of the polymer substrate. This shows that there is a dependency in the amount of cyanoacrylate polymerised with the water contact angle of the polymer surface on which the eccrine fingermark is deposited, aged, and fumed.

The saturation value of the cyanoacrylate polymerisation on one week aged eccrine marks deposited on the polymer substrates of varying water contact angle are displayed in Figure 5.20.

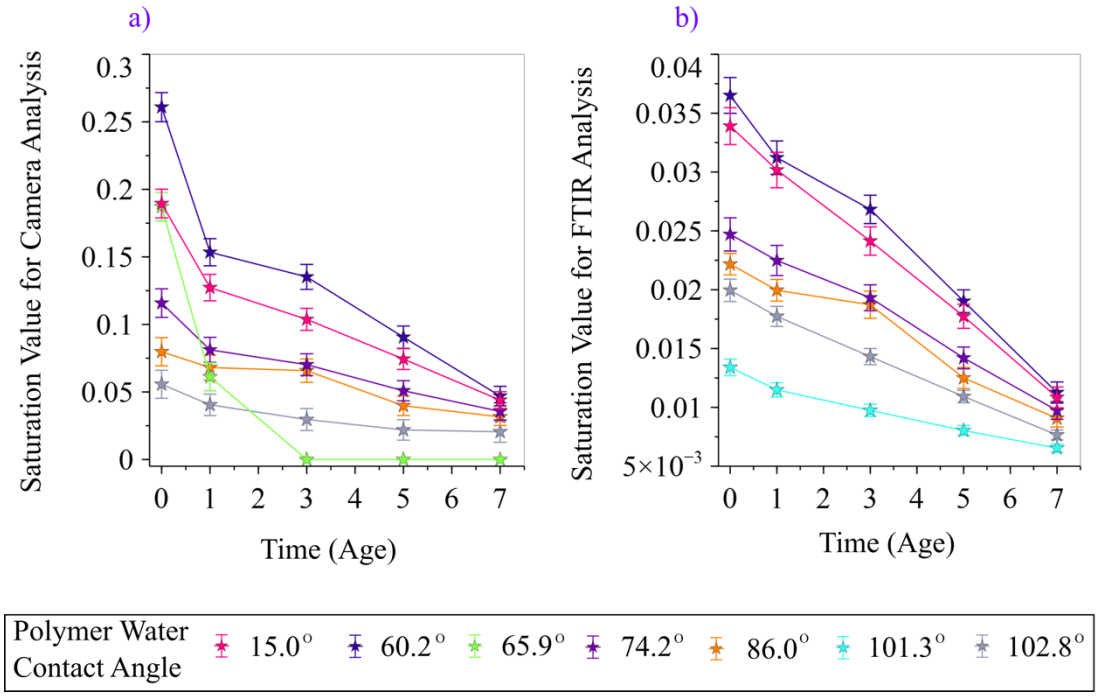

Figure 5. 20: Figure a) displays the saturation value of the eccrine fingermark residue fumed from camera analysis for the marks aged for 0, 1, 3, 5, and 7 days while (b) displaying the saturation value of absorbance value at the peak of wavenumber 1250 cm^{-1} during the fuming process for the eccrine deposits aged for 0, 1, 3, 5, and 7 days for FTIR analysis.

The saturation value plot in Figure 5.20 for the two different techniques (FTIR and camera) demonstrate two definite trends which are:

1. the saturation value of the developed eccrine mark reduces as the marks are aged longer regardless of the underlying substrates is correlated with the amount of cyanoacrylate polymerised on the aged eccrine mark.
2. the saturation value of fingermark residue deposited, aged and fumed on hydrophilic substrate displayed a much higher value in comparison to the saturation value of eccrine mark deposited, aged and fumed on the hydrophobic polymer surfaces. This is due to the underlying substrate wetting properties influencing the deposition of eccrine mark. Eccrine marks deposited on hydrophilic substrate displayed adequate detail of inner ridge structure and material distribution whereas the observation of fingermark ridge outline is less defined on hydrophobic polymer substrate. However, no evidence of fingermark deposition was observed on polymer substrate of water contact

angle 65.9°. This, therefore, affected the aging process of the fingermark on substrates of different wetting properties which in turn influenced the cyanoacrylate polymerisation.

Figure 5.20 displays the results obtained for cyanoacrylate polymerisation via scattering of light method (camera analysis) had a good agreement with results acquired through scattering of molecules method (FTIR analysis).

The results presented for aged eccrine marks showed a poor development using cyanoacrylate fuming is not unusual as study done on eccrine mark reported that it can go undetected as soon as the marks age over a few hours [9,15]. This added to the eccrine mark being exposed to the environmental conditions such as humidity, light, air flow, surface matrix, etc. causes the eccrine marks to quickly become undetectable with conventional technique [15]. The reason for this occurrence is mainly due to the nature of eccrine sweat of being a dilute aqueous solution with more than 98% water and containing less than 1% of dissolved solids of which inorganic salts constitute about one half with the remaining made up of free amino acids, free organic acids and urea [15,16].

To determine the effect of the environmental condition (air flow and light) other than the substrates wetting properties on the eccrine fingermark aging phase and the subsequential development of the aged mark; control marks were aged for a week in microscope slide box that shielded the marks from both light and air flow which were then fumed in the same exact way as the marks stored outside. The comparison between the developed eccrine marks stored inside and developed eccrine marks stored outside can be observed from Figure 5.21.

Figure 5.21 shows the developed eccrine fingermark images with cyanoacrylate fuming after aged for one week in an open container and inside a closed container on polymers of water contact angle a) 15.0°, b) 60.2°, c) 65.9° and d) 102.8°. From Figure 5.21 the correlation between how the fingermarks fumed due to the storage conditions can be observed as the eccrine fingermarks deposited on all the polymer substrates showed a better quality of fingermark development when stored in a closed box.

In

Out

a)

15.0°

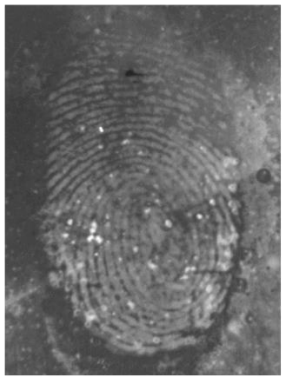

b)

60.2°

c)

65.9°

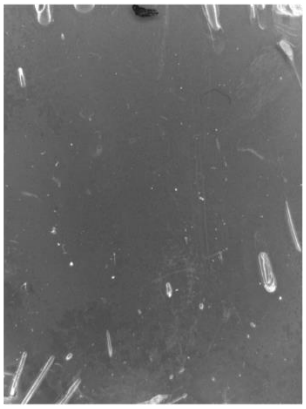

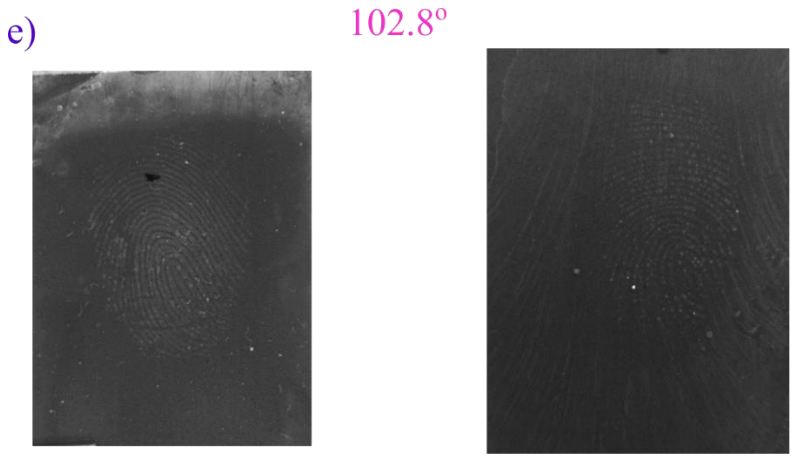

Figure 5. 21: Figure shows eccrine fingermark developed using cyanoacrylate polymerisation technique on polymer substrates of water contact angle a) 15.0°, b) 60.2°, c) 65.9° and d) 102.8° after being aged for one week in two different environmental conditions, left: fingermarks were left to age in a closed microscope glass slide box without any exposure to the environmental conditions and right: fingermarks were left to age in an open container left on working bench exposed to light and air flow.

In the case of no fingermark development on cling film ($\theta = 65.9°$) when the eccrine mark was aged for one week and stored outside, showed fingermark development after aged for the same one week when stored inside a microscope slide box indicating the storage conditions affect the fingermark aging and hence the development of the aged mark with conventional techniques. However, it is important to note that the eccrine fingermark deposited on the more hydrophilic substrate and stored inside showed a better quality of fingermark development in comparison to the same type of mark (eccrine) and storage condition on hydrophobic surfaces.

From Figure 5.21 it can be concluded that when eccrine marks are exposed to environmental conditions during the aging process, it accelerates (light can cause the degradation of the organic components in the eccrine sweat while air flow can cause the eccrine sweat to dry at faster rate) the aging process of the eccrine mark to an extent of not observing any fingermark developed after cyanoacrylate fuming on certain substrates within a week of aging.

It is important to note that a similar trend (better quality of fingermark development on hydrophilic substrate) for the eccrine fingermark development were observed for both types of storage conditions and this therefore indicates strongly that the wetting properties of substrate plays an important role in fingermark deposition, aging process and thus the fingermark development; which also can be affected by the environmental effect more than the other.

Both types of marks (sebaceous and eccrine) displayed a similar trend for saturation time and saturation value where the time taken decreases along with the amount of cyanoacrylate polymerised as the age of mark increases. The development quality of aged fingermark for both the sebaceous and eccrine decreased with time for the underlying substrate of higher water contact angle (hydrophobic) indicating that regardless the type of sweat, the wetting properties of underlying substrate plays an important role on fingermark deposition, aging process and consequently influences the development of the aged marks.

5.4 Conclusion

To conclude, this chapter presents both the physical and chemical changes that occurred within the sebaceous and eccrine marks deposited on different polymer substrates of varying water contact angle due to the aging process (time frame of 0-7 days) and their effect on CNA polymerisation was observed and analysed. Results indicated that for both types of mark, the substrate has an influence on the distribution of the secreted material and played an important role in the morphology of the deposit. The physical changes undergone by sebaceous and eccrine marks observed through optical microscopy revealed that few deposits aged slowly while some disappeared within a week of deposition, depending on the type of mark and wetting property of the deposited surface.

In both sebaceous and eccrine marks, the amount of cyanoacrylate deposited on the fingermark residue decreased with the increase of aging time and water contact angle of the polymer substrates. Irrespective of the fingermark, hydrophobic substrate exhibited a decrease in the amount of cyanoacrylate polymerised on the aged mark and a concurrent decrease in the developed mark quality was observed in the photographs obtained during the fuming process. This is due to the degradation of the initiators when left outside and being exposed to light and air flow. However, distinct differences in the chemical behaviour and aging effects of both the mark type have been noted, as the sebaceous mark aging results were not as dramatic as the results obtained in the eccrine mark aging study. This was mainly due to the more volatile eccrine fingermark composition that degraded faster when exposed to environmental conditions.

The development of sebaceous marks was of better quality on the hydrophobic surfaces when the marks were aged inside a microscopic slide box for one week prior to development. On the contrary, development of eccrine marks displayed better contrast irrespective of the polymer substrates when the eccrine marks were aged for a week without being exposed to the environmental conditions. It is evident that wetting property of the substrate plays a significant role in fingermark deposition, development and aging process; which also can be affected by the environmental effect more than the other.

References

1. Sears, V. G., Bleay, S. M., Bandey, H. L., & Bowman, V. J. (2012). A methodology for finger mark research. *Science & Justice*, *52*(3), 145-160.
2. Girod, A., Ramotowski, R., & Weyermann, C. (2012). Composition of fingermark residue: a qualitative and quantitative review. *Forensic Science International*, *223*(1-3), 10-24.
3. Cadd, S., Islam, M., Manson, P., & Bleay, S. (2015). Fingerprint composition and aging: a literature review. *Science & Justice*, *55*(4), 219-238.
4. Bleay, S. M., Croxton, R. S., & De Puit, M. (2018). *Fingerprint Development Techniques: Theory and Application, pp. 69-95,43*. John Wiley & Sons.
5. Andersson, P. O., Lejon, C., Mikaelsson, T., & Landström, L. (2017). Towards Fingermark Dating: A Raman Spectroscopy Proof-of-Concept Study. *ChemistryOpen*, *6*(6), 706-709.
6. Popov, K. T., Sears, V. G., & Jones, B. J. (2017). Migration of latent fingermarks on non-porous surfaces: Observation technique and nanoscale variations. *Forensic science international*, *275*, 44-56.
7. Mazurek, S., Mucciolo, A., Humbel, B. M., & Nawrath, C. (2013). Transmission F ourier transform infrared microspectroscopy allows

simultaneous assessment of cutin and cell-wall polysaccharides of A rabidopsis petals. *The Plant Journal*, *74*(5), 880-891.

8. Smith, B. C. (1998). *Infrared spectral interpretation: a systematic approach*, *pp. 19-21*. CRC press.

9. Moret, S., Spindler, X., Lennard, C., & Roux, C. (2015). Microscopic examination of fingermark residues: Opportunities for fundamental studies. *Forensic science international*, *255*, 28-37.

10. Rios, P. F., Dodiuk, H., Kenig, S., McCarthy, S., & Dotan, A. (2007). The effect of polymer surface on the wetting and adhesion of liquid systems. *Journal of adhesion science and technology*, *21*(3-4), 227-241.

11. Lewis, L. A., Smithwick, R. W., Devault, G. L., Bolinger, B., & Lewis, S. A. (2001). Processes involved in the development of latent fingerprints using the cyanoacrylate fuming method. *Journal of Forensic Science*, *46*(2), 241-246.

12. Yamashita, B., & French, M. (2011). Chapter 7: Latent print development. *The Fingerprint Sourcebook, US Dept. of Justice, Office of Justice Programs, National Institute of Justice, Washington, DC*, pp. 7-15.

13. Girod, A., Xiao, L., Reedy, B., Roux, C., & Weyermann, C. (2015). Fingermark initial composition and aging using Fourier transform infrared microscopy (μ-FTIR). *Forensic Science International*, *254*, 185-196.

14. Charlton, D. T., Bleay, S. M., & Sears, V. G. (2013). Evaluation of the multimetal deposition process for fingermark enhancement in simulated operational environments. *Analytical Methods*, *5*(20), 5411-5417.

15. Connatser, R. M., DePaoli, G., Gardner, C., & Lewis, L. (2012). *Latent Print Detection by Macroraman Imaging*. BiblioGov.

16. Scruton, B., Robins, B. W., & Blott, B. H. (1975). The deposition of fingerprint films. *Journal of Physics D: Applied Physics*, *8*(6), 714.

CHAPTER 6

Fingermarks on Metal Substrates

6.1 Introduction

Violent crimes involving knives were on the rise, at the time of writing and were at their highest levels since 2011 [1]. Stainless steel knife blades and firearms are therefore promising sources for providing fingermark evidence and that could help solve these cases and link persons of interest to the crime scene. To keep pace with the escalating crime rates, it is crucial to attain approaches for a prompt and reliable identification of forensic evidence. The standard procedure that has been employed as an endeavour to retrieve latent fingermark from these type of surfaces has been based on conventional enhancement techniques such as cyanoacrylate fuming [2]. However, a lack of observed contrast during latent fingermark development on metal substrates, has led to routine use of additional contrast enhancement techniques such as fluorescent dyes (e.g. basic yellow 40 (BY40)) [3], vacuum metal deposition [4], powder dusting [5] (non-magnetic and magnetic powders), gun blue [3,6], acidified hydrogen peroxide [7,8], crystal violet [9], and sudan black [10] to provide a better visualisation of latent fingermarks. Unfortunately, a significant number of them have minimal success in enhancing latent fingermarks on metal surfaces [11], meaning that new, more sensitive fingermark detection and enhancement techniques are required.

There are various factors that influence the nature of a deposited fingermark composition such as the environmental conditions that the metal surfaces were presented to at the crime scene, the age of the fingermark that has been deposited, the

nature of the interactions between the fingermark residue and the metal surfaces, and also the way each developing reagent reacts with the surface [12]. Thus, metals and alloys fall into one vital category of substrates that are proved to be challenging when it comes to latent fingermark recovery.

As a result of suboptimal performance by the conventional enhancement techniques, a substantial amount of research has been carried out to develop new applications with existing technologies. For instance, negative images of the fingermark residue were generated via processes that involves the deposition of electrochromic polymers onto metal surfaces to coat regions of metal surfaces between fingermark ridges [13-15]. Xu *et al.* [16] have also proposed an electrochemiluminescence (ECL) technique for the visual enhancement of sebaceous latent fingermarks that was shown to give adequate visual contrast. In addition to this, separate studies using scanning electrochemical microscopy (SECM) [17], scanning Kelvin microprobe [18,19] and electrostatic deposition [20,21] techniques have also proven capable of visualising identifiable latent fingermarks on metal surfaces.

Time-of-flight secondary ion mass spectrometry (ToF-SIMS) is a technique that allows for both rapid and high spatial resolution chemical imaging. This technique has been used by Hinder and Watts to obtain high quality images of fingermarks on organic substrates such as silicon wafers, carrier-bags, cling film, poly (vinylidene difluoride) PVdF coating and polyester coatings [22]. Szynkowska *et al.* have also shown that ToF-SIMS can be used to produce images of complete fingermarks on inorganic surfaces such as metals and glass. However, the clarity of the images produced in the study by Szynkowska and team mates were of poor quality [23]. On the other hand, Bailey *et al.* managed to acquire better quality images of fingermarks deposited on hand grenades made of galvanised steel substrate, 24 hours and 48 hours after deposition of the marks [9].

This chapter describes an experimental study to compare the use of a conventional technique, cyanoacrylate fuming and staining with chemical images that can be procured using the ToF-SIMS technique. ToF-SIMS is shown to be able to visualise fingermarks on metal surfaces for periods of up to 26 days after deposition.

6.2 Experimental

6.2.1 Pilot Study

The pilot study was performed with one male donor (Donor A) and female donor (Donor B), who each deposited a depletion series of six, primarily eccrine latent fingermarks on aluminium, brass and stainless steel disks, every day for a period of 14 days. Fingermarks were deposited following the simple hand cleansing procedure and after wearing gloves for a period of 30 minutes as mentioned in chapter 3, section 3.2. The sweat that accumulated on the fingertips during this time was used to represent the natural eccrine compounds that are found in a fingermark.

Fingermarks were deposited using the right index finger which was pressed down onto the surface of metal disks and then lifted off. The maximum force applied during deposition was maintained at a constant 2 N for 2 s in all experiments and was measured by placing the disks on a weighing scale (Model CS 5000E, Ohaus Corporation) during the deposition process. In each case the same finger was used to deposit six sequential marks on to different disks of the same type of metal. This was done in order to form a depletion series to determine how repeated contact influenced the quantity of fingermark secretions that were deposited on each of the metal substrates was studied.

After the deposition of each depletion series the samples were stored in a closed microscope slide box in room at a temperature of 22 ± 2°C and 40 ± 1 % relative humidity ready until required. After 14 days of storage, all the samples aged for 1, 2, 3, 4, 7, 8, 9, 10, 11 and 14 days were taken out to be treated simultaneously to ensure that the effects of aging of the fingermarks on each substrates could be determined. The resulting fingermarks were developed using techniques that are performed by East Midlands Special Operations Unit- Forensic Sciences (EMSOU-FS) and other police forensics laboratories across the UK when attempting to develop fingermarks on non-porous substrates such as metal surfaces that were obtained from a crime scene.

The techniques were applied in the order of: cyanoacrylate (superglue) fuming, accompanied by staining consequentially with the dyes, Basic Yellow 40 (BY40), Crystal Violet (CV) and lastly Sudan Black (SB). In each case, cyanoacrylate fuming was performed at the EMSOU-FS forensics lab using a superglue fuming cabinet

(MVC5000 Mason Vactron, Foster and Freeman) as described in detail in chapter 3, section 3.9. The samples then were applied with the staining dyes as the order mentioned earlier and were photographed between each staining procedure. The details of how each techniques were performed is explained meticulously in chapter 3, section 3.10.

6.2.2 Main Study

The main study involved all the six different donors (see Table 6.1) depositing a depletion series of six, predominantly eccrine latent fingermarks on stainless steel disks. The disks were stored exactly the same way as mentioned in the pilot study following the fingermark deposition of each donor. The fingermarks acquired from each one of the six donors was imaged using a ToF-SIMS IV instrument (ION-TOF GmbH., Münster, Germany), after a total of thirteen days kept in storage. In all cases, the second deposition in the depletion series was used for imaging (instead of the first) in order to get rid of the effects of any possible transients that could be present in the first deposition such as potential excess of fingermark secretions or initial errors in deposition by the donors.

Donor	Gender	Ethnicity	Age
A	Male	White British	20
B	Female	Asian (Indian)	27
C	Male	Asian (Indian)	28
D	Male	White British	43
E	Male	White British	44
F	Female	White British	49

Table 6. 1: Information of the six donors that participated in fingermark deposition experiments for this study.

For both the positive and negative sample imaging by ToF-SIMS, a 25kV Bi_3^+ primary ion beam delivering a pulsed target current of about 1.0A was rastered at an incidence angle of 45° to the surface normal of the stainless steel disks. The secondary ions were extracted using an accelerating potential of 2kV in the mass spectrometer while the pressure in the imaging chamber was maintained between 1×10^{-7} and 1×10^{-8} mbar. All the samples were placed into the ToF-SIMS chamber at the same time. The samples were imaged at a temperature of 23 °C and each took approximately 15 min to image over an area of 5 mm × 5 mm. A spatial resolution of 0.02 mm/pixel and an average of 20 scans were used to obtain each chemical image. The steel sample imaged for Donor A on day thirteen was also reimaged on day twenty-six. This second image of the sample was taken over a larger area (18 mm × 18 mm, spatial resolution of 0.01 mm/pixel, imaging time 150 min) of the surface and was acquired using the same imaging parameters described above. Data acquisition and analysis were performed using SurfaceLab 6 software (IONTOF GmbH).

The other five stainless steel samples in the depletion series were kept as control samples to determine whether there was any loss of material in the fingermark residue after imaging with ToF-SIMS (either as a result of the high vacuum conditions in the imaging chamber or as a result of ablation of the fingermark residue by the primary ion beam). On day twenty-eight, all thirty six samples (including the six samples that went through ToF-SIMS analysis) were fumed together using cyanoacrylate, before being stained with the fluorescent dyes BY40, CV, and SB using identical procedures to those that were used in the pilot study.

6.3 Results & Discussion

Examples of fingermark in a depletion series developed with cyanoacrylate fuming followed by staining of the cyanoacrylate deposits with the dyes BY40, CV and SB in the pilot study are shown in Figures 6.1, 6.2 and 6.3 respectively. Examples of images are shown for fingermarks that were developed on each of the metal disks after a period of one day following deposition. Each of the samples was inspected immediately after cyanoacrylate fuming and no evidence of fingermarks could be detected. In this sense, each sample could be rated with a score of 1 according to the scheme proposed in Table 6.2. This inability to detect fingermarks on metal surfaces

using cyanoacrylate fuming alone is common and promotes the need for further staining of the cyanoacrylate deposits with dyes that can improve the optical contrast of any latent fingermark that is present.

Score	Definition
1	No visible ridges or contacted area – Nothing of interest
2	Weak development; evidence of contacted area but no visible ridge details present
3	Partial development; up to 1/3 of ridges present including clear evidence of ridge flow and pattern (first level detail) and partial evidence of individual ridge minutiae - bifurcations and ridge endings (second level detail). Significant distortion evident.
4	Strong development; between 1/3 and 2/3 of ridges present including clear evidence of ridge flow and pattern (first level detail), individual ridge minutiae - bifurcations and ridge endings (second level detail) and partial evidence of pore position and shape (third level detail). Minor distortion evident
5	Very strong development; >2/3 of ridges present including clear evidence of ridge flow and pattern (first level detail), individual ridge minutiae - bifurcations and ridge endings (second level detail) and pore position and shape (third level detail). Very minor or no obvious distortion evident.

Table 6. 2: Scoring scheme used for evaluating the quality of fingermarks developed using cyanoacrylate fuming followed by BY40, Crystal Violet and Sudan Black dyes for each of the three metal surfaces studied (Aluminium, Brass and Stainless Steel) as adapted from Sears et al. [24]. The definitions of first, second and third level of details on the fingermark have been adapted from Jain et al. [25].

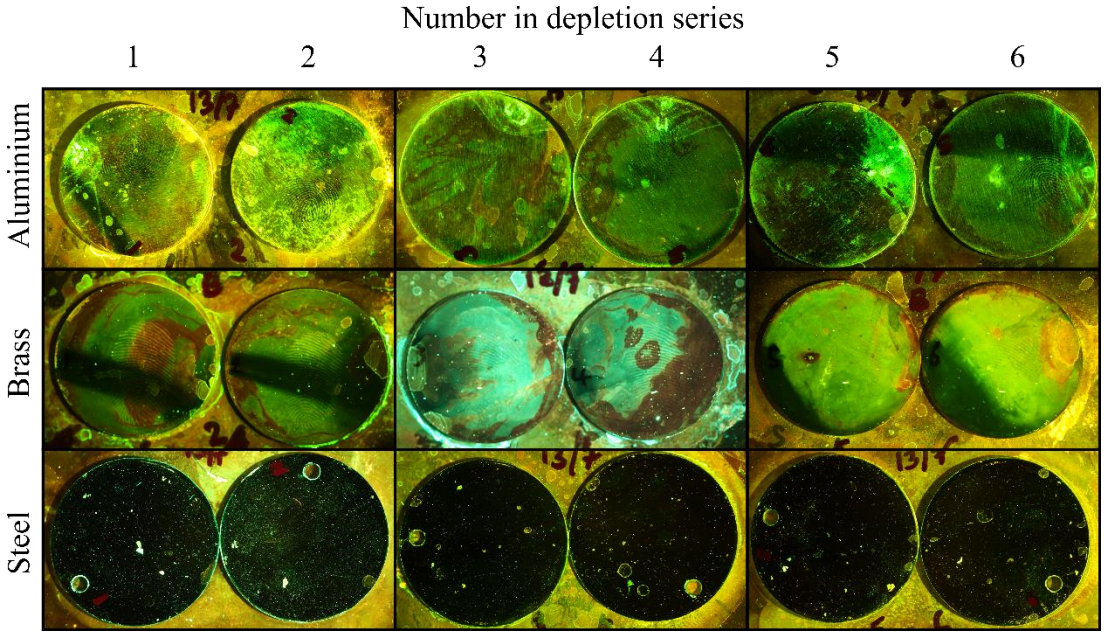

Figure 6. 1: Example images of fingermarks that were stained using BY40 in the order of 1 to 6, from left to right (in the depletion series) after development with cyanoacrylate fuming. The fingermarks on each metal substrates were deposited by the same donor, Donor B. The fingermarks were aged one day prior to the development. The images were obtained under constant illumination and imaging conditions using a Nikon D7200 digital camera with a yellow filter (75 mm × 75 mm No.12, Kodak Wratten gelatin filter, excitation wavelength: 510–530 nm) under blue light illumination with CrimeLite® 2 light source emitting wavelengths in the range 420–470 nm (Foster and Freeman).

Figure 6.1 proves that the marks that were not evident after cyanoacrylate fuming can be significantly increased by fluorescent dye staining followed by fluorescence examination. The success of the BY40 dye staining the polycyanoacrylate (referred to the polymerisation of a cyanoacrylate monomer) could be due to the fact that the dye form Van der Waals bonds with the polycyanoacrylate fibres. It is suggested that weak binding occurs between the dye cations and the anions associated with the CN^- groups in the polymer fibres [26]. From Figure 6.1, it could be observed that the appearance of latent fingermark development on each metal surfaces were very different despite being enhanced in the same way. If the development of fingermarks were to be rated from the best to worst in comparison to the substrate it was deposited onto, it will be aluminium, brass and steel. From Figure 6.1 it can be concluded that underlying metal

substrates influence the cyanoacrylate polymerisation, as fingermarks deposited on aluminium are strongly developed while fingermarks on brass are partially developed, no visible ridges or contacted area can be observed on stainless steel metal.

The metal substrates were then stained with CV, the next procedure performed by all police forensics laboratories across the UK to enhance the visualisation of fingermark on the metal substrates. Figure 6.2 displays photographed images of the same exact metal substrates in Figure 6.1, after stained with CV dye.

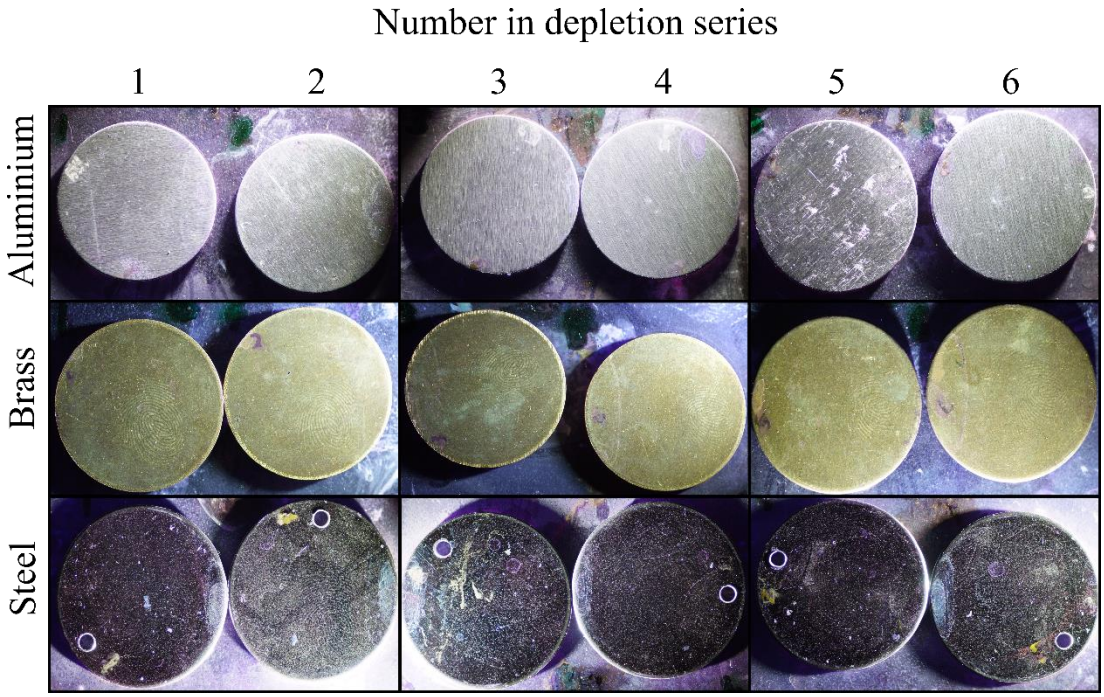

Figure 6. 2: Example images of fingermarks that were stained using CV in the order of 1 to 6, from left to right (in the depletion series) after fluorescence staining, BY40. The images were obtained under constant illumination and imaging conditions using a Nikon D7200 digital camera under white light illumination (Crimelite® 2, Foster and Freeman, wavelength range 400–700 nm) without any filters.

The role of CV dye is selectively to stain the fingermarks by promoting the transfer of the dye into the lipids in the fingermark residue [27]. CV dye can also strongly stain any skin cells shed from the fingertip because CV dye is positively charged and is attracted to epithelial cells that have a net negative charge [27]. Since the fingermark

deposited is predominantly eccrine, it was not expected to obtain a better development image of fingermark after the application of CV stain.

However, from Figure 6.2 it is noticed that the development of fingermarks on only brass substrates showed a clear pattern of fingermark with very weak development on aluminium substrate to no visible of any fingermark on steel substrate. In the preliminary study, fingermarks were deposited at different time frame of the day (i.e. morning: 9.00 a.m. - 10.30 a.m., afternoon: 12.00 p.m. – 1.30 p.m. and evening: 3.00 p.m. – 4.30 p.m.) on the three metal substrates. The fingermarks aged for one day were deposited in depletion series of six on metal substrates in the order of brass, aluminium and steel. This suggests that fingermark deposition on brass substrate in the beginning of the day could have shed more skin cells from the fingertip and reduced towards the end of fingermark deposition process. Hence, the CV stain did improve the appearance of the latent fingermark on brass in comparison to development with BY40 fluorescence staining, but CV did not help in improving optical contrast of fingermark on neither aluminium nor stainless steel.

Finally, the metal substrates were stained with SB dye as per protocol followed by all police forensics laboratories across the UK when non-porous metal objects are found in a crime scene. Figure 6.3 displays photographs of the metal substrates that were obtained after the staining process.

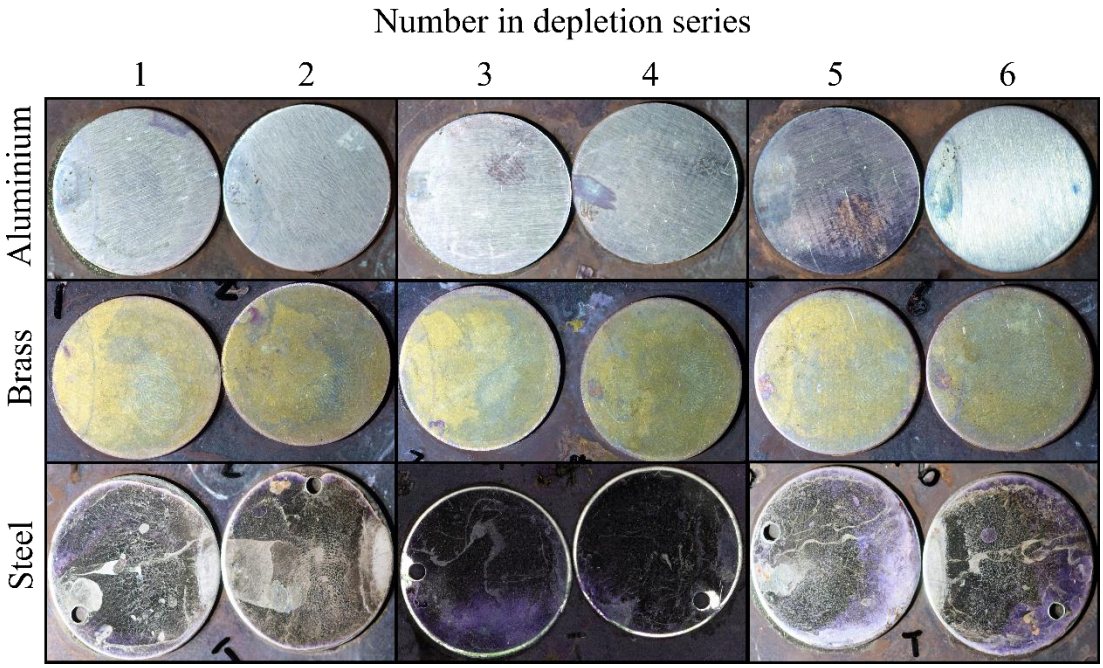

Figure 6. 3: Example images of fingermarks that were stained using SB in the order of 1 to 6, from left to right (in the depletion series) after staining with CV dye. The images were obtained using a Nikon D7200 digital camera under white light illumination (Crimelite® 2, Foster and Freeman, wavelength range 400–700 nm) without any filters.

The role of SB is to act as the dye that further enhances the fingermark after CV application by staining lipid materials including triglycerides and fatty acids that may be present in fingermark residue [27]. In addition to the primary staining action of SB by dissolving into lipids, it can also stain materials ionically [27]. This could be observed directly from Figure 6.3, where the metal surfaces are in a deep blue-black colour but due to oxidation process can turn into brown in colour over time. Similar to CV dye, SB dye is expected not to increase quality of the predominantly eccrine fingermark development on any metal substrates.

Figure 6.3 demonstrates satisfying fingermark development on all the depletion series of the brass substrates, with a score of 2 for fingermark development on four out of the six aluminium substrates and with no development of fingermark on stainless steel by using the SB dye. This suggests that in this pilot study, SB dye had only further enhanced the contrast obtained after CV staining.

In order to be consistent for data analysing purpose, the photographed images of the fingermarks that were developed with each of the staining sequential dyes were then analysed and graded according to the scheme presented in Table 6.2.

All the grading of the images was performed by the same individual in the same sitting and this person has previous experience of fingermark identification. In this way, the use of a single person in a single session allowed us to maintain consistency in the grading across all the samples studied. Grading of the fingermarks was performed using the images rather than using the live samples. This was done in an attempt to follow (as closely as possible) the procedures that are used by fingermark examiners when examining evidence. Fingermarks are rarely analysed at the scene of a crime, or at the point of collection from an object. In fact, digital images often need to be captured under optimal illumination conditions to ensure that a digital record is captured for evidential purposes. It is these images that are analysed to try to identify key features on a fingermark and to link it to a person of interest.

In the pilot study it was observed that the marks developed at each stage in the depletion series were to be very similar in appearance on each of the metal substrates examined for each of the staining techniques implemented. Thus, the comparability of the marks acquired from each deposition in a given depletion series in the pilot aging study allowed for better statistics to be obtained for the score or quality of the fingermarks.

In each case, digital images of samples that were stained with each of the dyes were collected, compiled and graded/scored according to the scheme presented in Table 6.2. Plots of the mean scores of six images obtained from the depletion series performed on each metal surface are given in Figure 6.4 as a function of the number of days following deposition for both the donors, Donor A and Donor B. In each case, the error bars were obtained from the standard error of the scores given to each mark in the depletion series.

From Figure 6.4, it is evident that BY40 staining initially produced identifiable marks with mean scores between 3 and 4 on both aluminium and brass but the quality of the marks developed steadily deteriorates with aging time. This suggests that as the eccrine fingermarks age, less cyanoacrylate polymerisation on fingermark residue occurs leading to deterioration in fingermark quality.

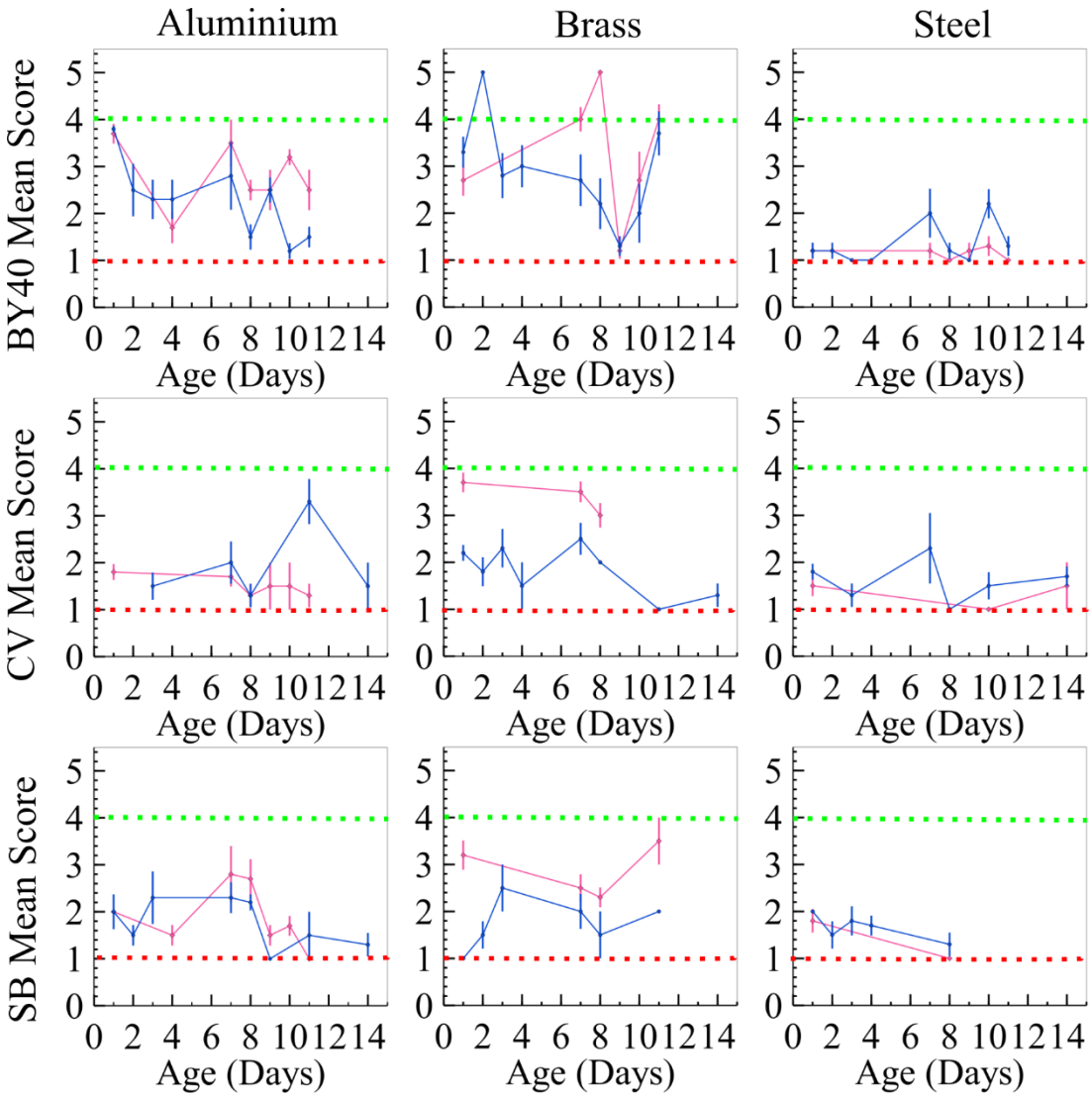

Figure 6. 4: Mean scores for two different donors (Donors A and B) as a function of time after deposition for the three different staining techniques. The blue line corresponds to the mean score for the fingermarks deposited by Donor A while the pink line represents mean score of fingermarks deposited by Donor B. Error bars were calculated using the standard error of the mean of scores obtained from fingermarks in the same depletion series. The horizontal red dotted line denotes the score when a fingermark is considered to be unidentifiable (score ≤ 1, see table 6.2) while the green dotted horizontal line represents the threshold score above which a fingermark is considered to be sufficient for identification purposes (score ≥ 4).

Further staining with both CV and SB showed significantly lower quality of marks developed in comparison to development using BY40 dye in the case of brass and aluminium which is as expected due to the fact that they do not stain for the eccrine

components that are targeted in the present study. In the case of the steel surfaces, very few fingermarks were able to be recovered using any of the staining protocols even after just one day following deposition (mean score 1–2). No visible ridges were observed on these surfaces. In fact, steel consistently displayed significantly poorer quality fingermarks compared to the other two metal surfaces over the duration of 14 days experiment.

Figure 6.5 shows examples of images for fingermarks that were developed on each of the metal disks after periods of three and eight days respectively following deposition, in order to have a better view of the fingermark development that declined as a function of aging time. These fingermarks were developed using cyanoacrylate fuming followed by staining of the cyanoacrylate deposits with the dyes BY40, CV, and SB. As mentioned earlier, no evidence of fingermarks could be detected when each of the samples were inspected immediately after cyanoacrylate fuming.

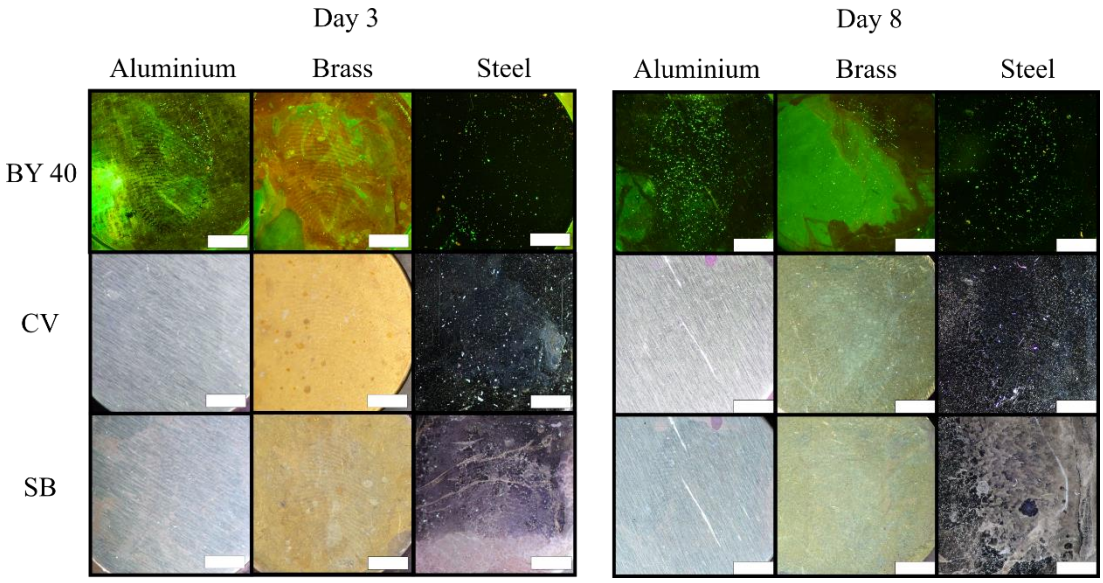

Figure 6. 5: Optical micrographs of representative examples of fingermarks that were developed using BY40, CV and SB on each of the three different metals. The left-hand panel shows fingermarks that were deposited by Donor A and then developed three days after deposition. The right-hand panel shows fingermarks from the same donor that were developed eight days after deposition. The white scale bar corresponds to 5 mm in all cases.

There was, however, clear evidence of fingermarks following BY40 staining of the cyanoacrylate on both aluminium and brass surfaces after three days. However, the quality of the marks appear deteriorated within eight days of aging on both of these surfaces. In the case of marks aged three days on the stainless steel surfaces, were found to be unrecognisable when developed using BY40. BY40 fluorescence has previously been shown to be effective for enhancing the contrast and details of eccrine fingermarks on non-porous surfaces following cyanoacrylate fuming [28,29]. However, these initial experiments demonstrate that this staining technique gives unreliable results when developing predominantly eccrine fingermarks on metal surfaces such as those studied here.

The second row of images in Figure 6.5 shows that CV staining of the cyanoacrylate deposits was capable of developing fingermark ridges after three days of exposure to ambient conditions on the brass substrates. However, this was not the case for aluminium and steel as these substrates varied between having no visible ridges and giving weak development; resulting in mean scores of 1.5 ± 0.29 and 1.3 ± 0.25 respectively.

The third row of images show that enhancement was also possible with SB on all the three metal substrates after 3 days since fingermark deposition. The marks observed on brass were generally found to be of a higher quality than those found on aluminium substrates, which were in turn better than steel substrates. Although there was some residual evidence of fingermarks on brass and aluminium after three days, little to no evidence of fingermarks was observed on all three of the metals studied after eight days.

It was observed that marks were generally less prevalent when developed with SB and CV than with BY40. This is to be expected because these dyes are used to detect sebaceous deposits and the fingermarks used here contained predominantly eccrine material. Crystal violet (CV) binds to lipids (fats) and to dead skin cells in the fingermark residue while sudan black (SB) preferentially dissolves into lipids that are present in larger quantities in sebaceous secretions and further enhances any contrast obtained by prior CV staining [29].

It should be stressed here that these two dyes (CV and SB) were used in order to reproduce standard operating protocols in UK forensic labs and the fact that they do

not stain for the eccrine components that are targeted in the present study perhaps makes their use unreasonable for the present work. However, the occasional observation of fingermarks following the use of these two stains does not rule out their use entirely. The fact that some features were observed suggest that the dyes are capable of detecting skin cells or residual sebaceous deposits on the surface of the metal substrates which may not have necessarily been observed using cyanoacrylate fuming alone.

From both the Figures 6.4 and 6.5 it could be concluded that steel reproducibly failed to provide identifiable fingermarks for all the staining techniques in the pilot study for both the donors. This is clearly a cause for concern for forensic practitioners trying to visualise fingermarks on knife blades and firearms. Therefore, this metal substrate was chosen as the focus for more detailed studies using ToF-SIMS.

ToF-SIMS instrumentation was used in the main study because it has the capability to obtain high spatial resolution images of the chemical properties of the sample via the acquisition of highly localised mass spectra of material deposited on a surface. Acquiring mass spectra at each position on the sample surface enables the construction of images of the distribution of particular chemical species on a substrate. In particular, these images are constructed by plotting the number of counts obtained for secondary ions with a given mass-to-charge (*m/z*) ratio as a function of position on the surface. As different materials emit different types and quantities of secondary ions when bombarded with the primary ion beam, the spatial variation in the type and quantity of emitted secondary ions can be used to build up highly specific chemical maps of any deposited material. The variations in the chemical properties of the substrate and any thin layer of fingermark residue deposited on it can therefore, be detected with a high sensitivity (femtomolar) and high spatial resolution ~0.002 μm [30,31].

The eccrine fingermarks that were deposited onto the steel substrate by each of the six donors were analysed directly in both positive and negative ionisation modes, using the method described in Chapter 3, section 3.13. ToF-SIMS was used to identify the constituents of fingermark which can be detected and to determine if fingermark imaging was feasible. The positive ion mode spectra were calibrated using the signal peaks of H^+ and CH_3^+, while the negative ion mode spectra were calibrated using signal peaks of H^- and OH^-.

Both the positive and negative ion mass spectra acquired in the regions where fingermarks had been deposited by each of the six donors identified a number of different positive and negative secondary ionic species that correspond to the constituents that make up fingermark residue. Figures 6.6 and 6.7 represent an example of the positive and negative ToF-SIMS mass spectra of predominantly eccrine fingermark deposited by Donor B.

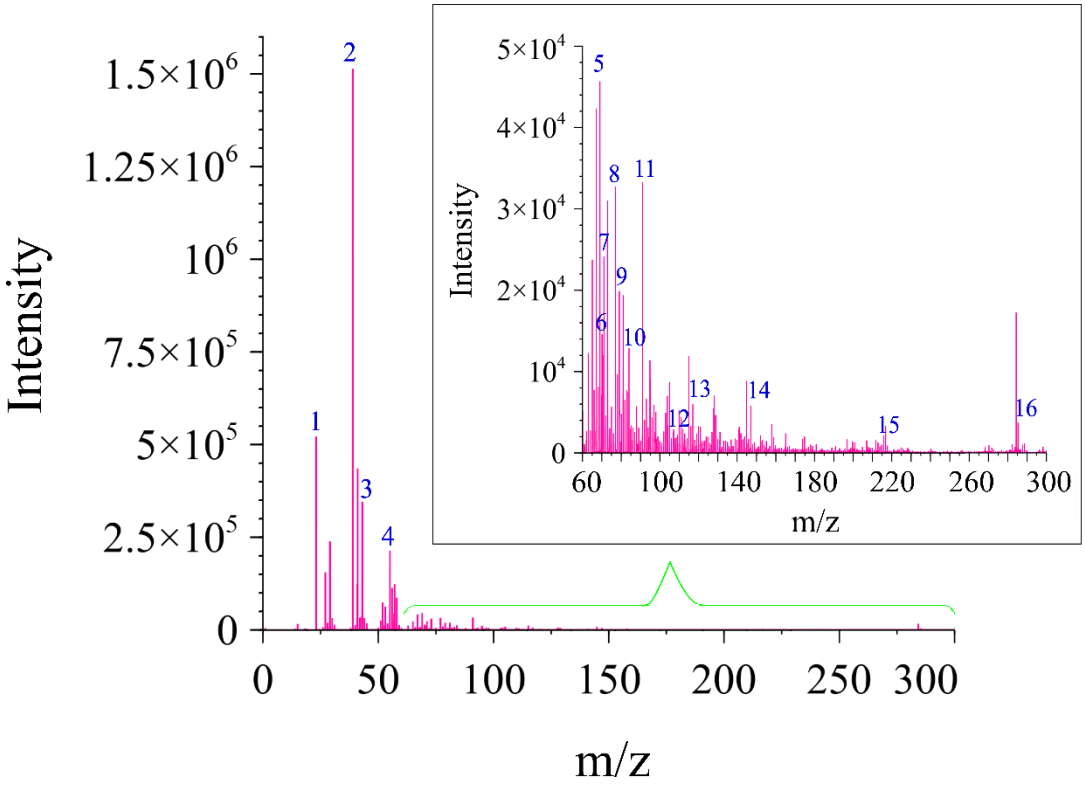

Figure 6. 6: A representative mass spectrum of the chemical composition of Donor B fingermark, collected in positive ion mode. Peak assignments of the identified components are highlighted and tabulated in Table 6.3.

A number of eccrine components along with a few sebaceous components have been identified in the ToF-SIMS spectra. Of the components that were identified in the positive spectrum (Figure 6.6) of the fingermark aged for thirteen days, amino acids were the most prevalent, with eleven out of sixteen amino acids being identified and tabulated in Table 6.3 [32]. Meanwhile, strong signals were obtained from the

inorganic ions, sodium (Na^+), potassium (K^+), and iron (Fe^{2+}) that are among the most common ions found in fingermark residue. Also present in the positive ion scans was a very low signal of fatty acids. Identification of these compounds were based on literature comparisons.

Peak	Monoisotopic Mass	Assignment	Chemical Formula
1	22.99	Sodium	Na^+
2	38.96	Potassium	K^+
3	43.05	Isoleucine, Leucine	$C_3H_7^+$
4	55.05	Iron	Fe^{2+}
5	69.07	Threonine	$C_4H_5O^+$
6	70.06	Proline, Asparagine	$C_4H_8N^+$, $C_3H_4NO^+$
7	71.09	Serine	$C_3H_3O_2^+$
8	73.04	Arginine	$C_2H_7N_3^+$
9	81.07	Histidine	$C_4H_5N_2^+$
10	84.08	Lysine, Glutamine, Glutamic Acid	$C_5H_{10}N^+$, $C_4H_6NO^+$
11	91.05	Phenylalanine, Tyrosine, Alanine	$C_7H_7^+$
12	107.05	Tyrosine	$C_7H_7O^+$
13	117.06	Methionine	$C_5H_9SO^+$
14	147.06	Tyrosine, Glutamic acid	$C_9H_7O_2^+$
15	215.77	Tridecanoic acid	$C_{13}H_{26}O_2^+$
16	285.32	Stearic acid	$C_{18}H_{36}O_2^+$

Table 6. 3: Lists of positive chemical ions identified in a fingermark residue with high intensity count [33-36].

In the negative ion spectrum, displayed in Figure 6.7, fewer components of interest have been identified compared to the positive ion spectrum. As with the positive ion spectrum, the negative ion exhibit peptide backbone and a number of amino acid

present in the eccrine secretions. Free fatty acid along with different types of phospholipids anions were also present with a much stronger signal in the negative ion mode than in the positive ion mode. Phosphatidylethanolamine (PE) is one of the main classes of glycerophospholipids (including phosphatidylcholine (PC), phosphatidylinositol (PI) and phosphatidylserine (PS)) that are made of a glycerol backbone esterified with two fatty acids and a polar headgroup that defines the class they belong to. Glycerophospholipids belong as one of the two main groups of phospholipids with sphingolipids as the other [37]. Presence of the PE head group ions in fingermark residue is most likely due to the contents of this component in common human food consumption such as soy and egg yolk [38].

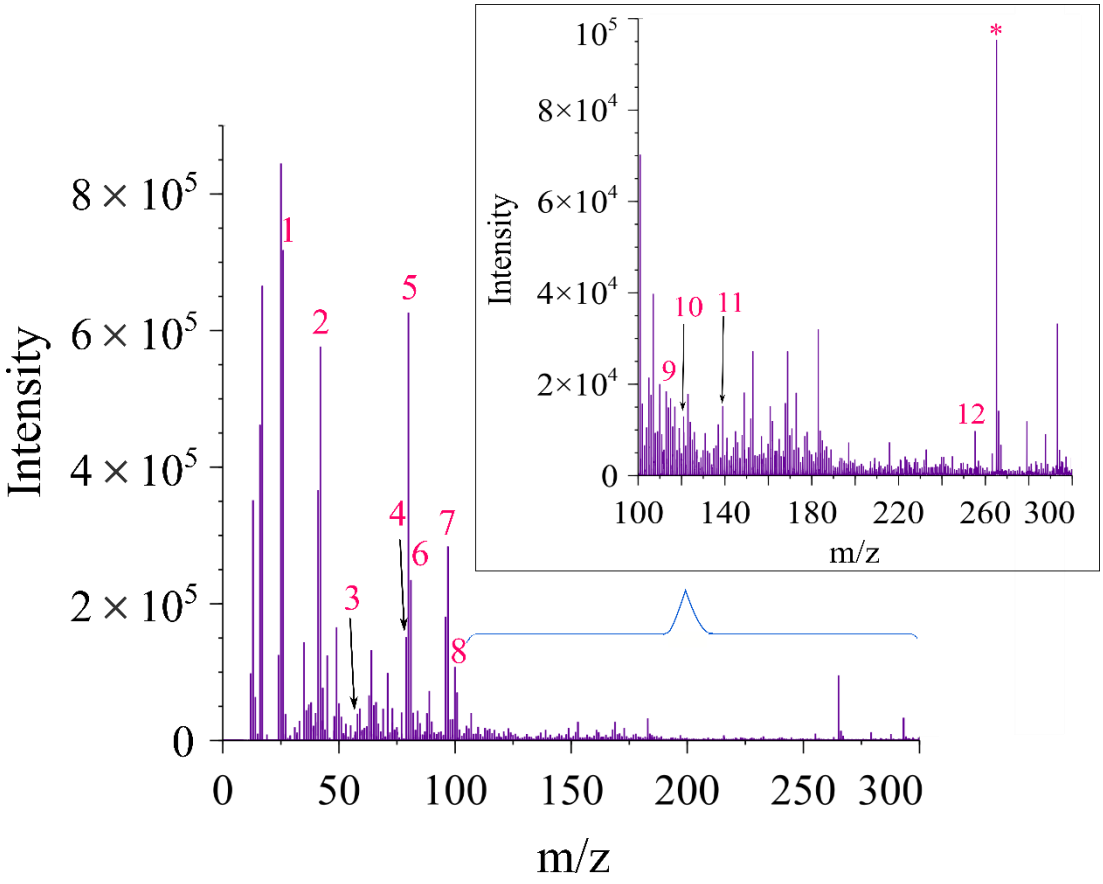

Figure 6. 7: A representative mass spectrum of the chemical composition of Donor B fingermark, collected in negative ion mode. The peak marked with * of mass 265.15 is an exogenous compound that was found in all the six fingermarks that were analysed. This ion is likely to originate from the soap used during the hand washing procedure in these experiments. Peak assignments of the identified components are highlighted and tabulated below.

Additionally, an exogenous compound in the negative spectrum, marked by an asterisk of mass 265.15 was found in all the six fingermarks that were analysed. This ion was observed by Poleunis et al. [39] and is commonly found in the residue from household washing treatments and personal care products, which contain sulphur surfactants such as dodecyl benzene sulphonic acid [40]. Thus, this ion is likely to originate from the hand washing procedure used in these experiments.

Peak	Monoisotopic Mass	Assignment	Chemical Formula
1	26.01	Peptide backbone	CN^-
2	42.00	Peptide backbone	CNO^-
3	58.01	Glycine	$C_2H_4NO^-$
4	78.96	Phosphate (Phospholipids)	PO_3^-
5	79.96	Sulphite	SO_3^-
6	95.95	Sulphate	SO_4^-
7	96.96	Dihydrogen Phosphate (Phospholipids)	$H_2PO_4^-$
8	99.93	Valine	$C_5H_{10}NO^-$
9	113.93	Leucine	$C_6H_{12}NO^-$
10	121.94	Phosphatidylethanolamine	$C_2H_5NO_3P^-$
11	139.95	Phosphatidylethanolamine	$C_2H_7NO_4P^-$
12	255.23	Palmitic Acid	$C_{16}H_{31}O_2^-$

Table 6. 4: Lists of negative chemical ions identified in a fingermark residue with high intensity count [41-45].

In addition to the peak assignments shown in Table 6.3 and Table 6.4, a number of additional positive and negative ions were identified. These include positive secondary ion fragments of lipids [44] which correspond to free fatty acids such as dodecanoic acid, tetradecanoic acid, palmitic acid, and cholesterols with mass (m/z 201, 229, 257, 369 and 387). However, the signal intensities were much weaker in comparison to the strong signals obtained from both the inorganic Na^+ and K^+ ions present in the eccrine fingermark residues (Figure 6.8). The negative ion spectra of the fingermark also

contained evidence of additional secondary ions that are consistent with the presence of lipids in the form of glycerolipid such as the glycerol fragments observed at m/z 91.02 ($C_3H_7O_3^-$) and m/z 57.04 ($C_3H_5O^-$) [43].

The qualitative variability of fingermark residue between donors (inter-variability) was minimal for the six donors whose fingermarks were analysed in this study, since there were no noticeable differences in the mass spectra between the six donors. However, it must be noted that although all the chemical ions identified both in Figure 6.6 and 6.7 were detected in each fingermark, the intensity of amino acids, fatty acids and lipids varied between the six donors.

Images of the spatial distribution of both the positive and negative ions for fingermarks on steel substrate were obtained with high contrast are shown in Figures 6.8 and 6.9 respectively.

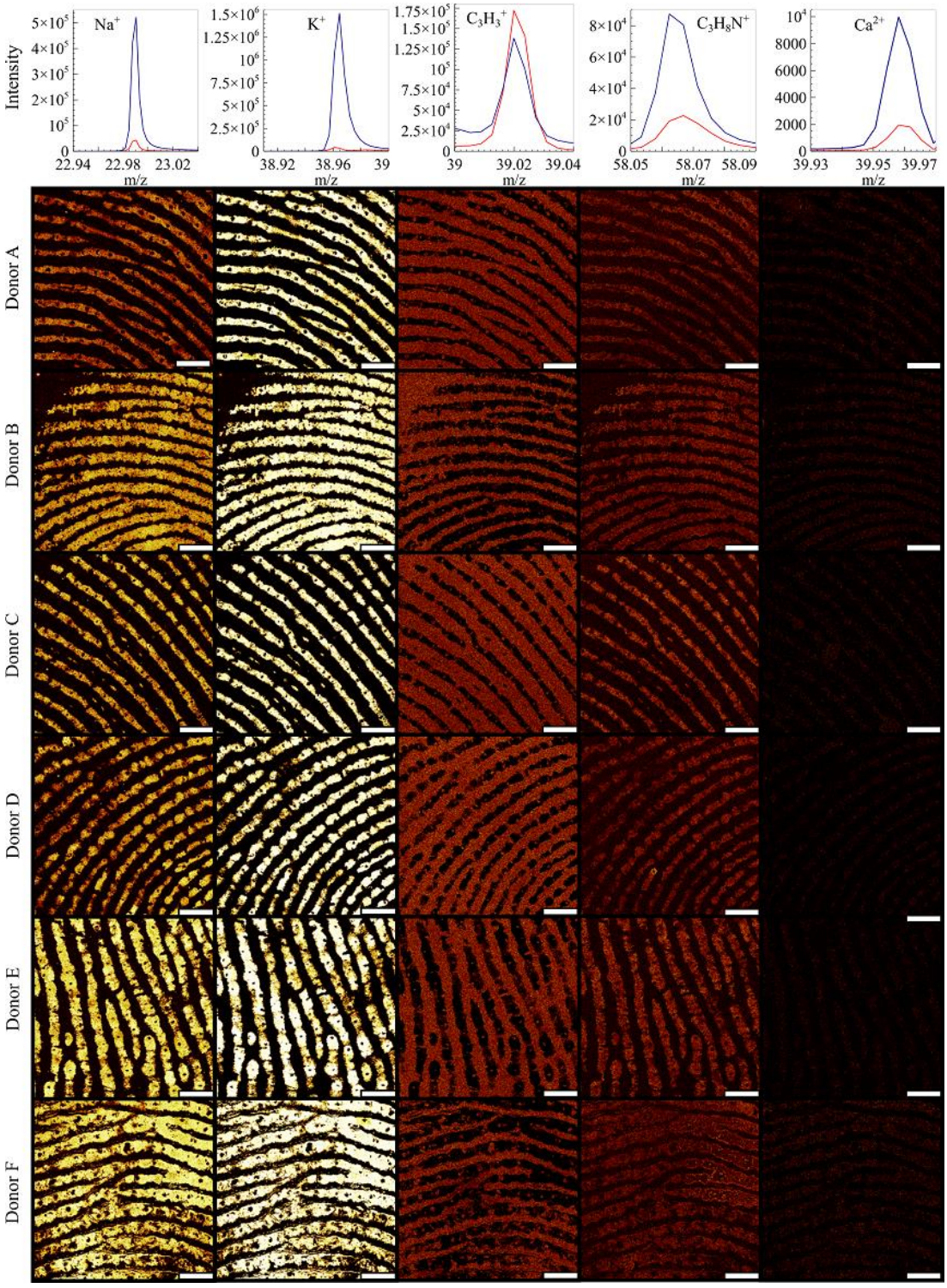

Figure 6. 8: ToF-SIMS fingermark images on stainless steel surfaces after 13 days of deposition. The top row represents the typical ToF-SIMS spectra corresponding to Donor B for the positive secondary ions that were emitted from the surface of the samples. In each case, the ionic species responsible for the peak is labelled. The blue line represents a typical spectrum taken from a region on the fingermark and the red line represents the spectrum collected from the substrate. The images below each

spectrum display show spatial variations in the number of counts or signal intensity measured at each position on the sample surface. Data are shown for each of the six donors. Each image took approximately 15 minutes to acquire. Scale bar: 1 mm.

The chemical fingermark images exhibit excellent ridge detail including first and second level detail (see table 6.2 for definitions) and additionally revealed third level detail clearly in the form of the position and localisation of individual pores as well as the unique individual ridge profiles or ridge edges. This was observed for all the donors irrespective of gender, age, and ethnicity with a clear contrast between the fingermark and the substrate on steel samples equivalent to those which showed no evidence of fingermarks when stained and imaged using the conventional techniques. Despite the fact that these fingermarks were imaged thirteen days after deposition, they still reveal high level details with individual epidermal ridge patterns and sweat pores in which the quality of the ridges exhibited in the ToF-SIMS images matches to a score of 5 which is an exceptional quality, according to the scoring system described in Table 6.2.

The greatest contrast in the images for positive ions came from abundant endogenous inorganic components of eccrine origin fingermark residue which are the Na^+ and K^+ ions. Besides that, calcium (Ca^{2+}) ions were also identified in the fingermark regions, albeit at a lower intensity that is likely due to degradation of the ion since deposition [32]. An additional organic ion $C_3H_8N^+$ was present in the fingermark regions as shown in Figure 6.8. This ion is presumably as a result of the dimethyl (methylene) ammonium ion – a fragment from precursor amino acids such as serine or the betaines (choline or glycine betaine) [46].

ToF-SIMS instruments operate in pulse counting mode. As there is a detector "dead time" following each detected ion at any given mass, the instrument can only detect one ion each time the source is fired. Since, the $C_3H_3^+$ ion falls within the dead time window generated by the K^+ ion, any $C_3H_3^+$ that is generated by the same primary ion pulse as K^+ ion will not be detected [47]. So, in regions of the image where the K^+ signal is close to saturating the detector, the $C_3H_3^+$ signal disappears. The dark region in the $C_3H_3^+$ image corresponding to the most intense K^+ regions because $C_3H_3^+$ falls within the dead time window for K^+. Hence, this is the reason for the chemical image

of $C_3H_3^+$ ion was detected at higher concentrations on the steel substrate than that in the fingermark regions.

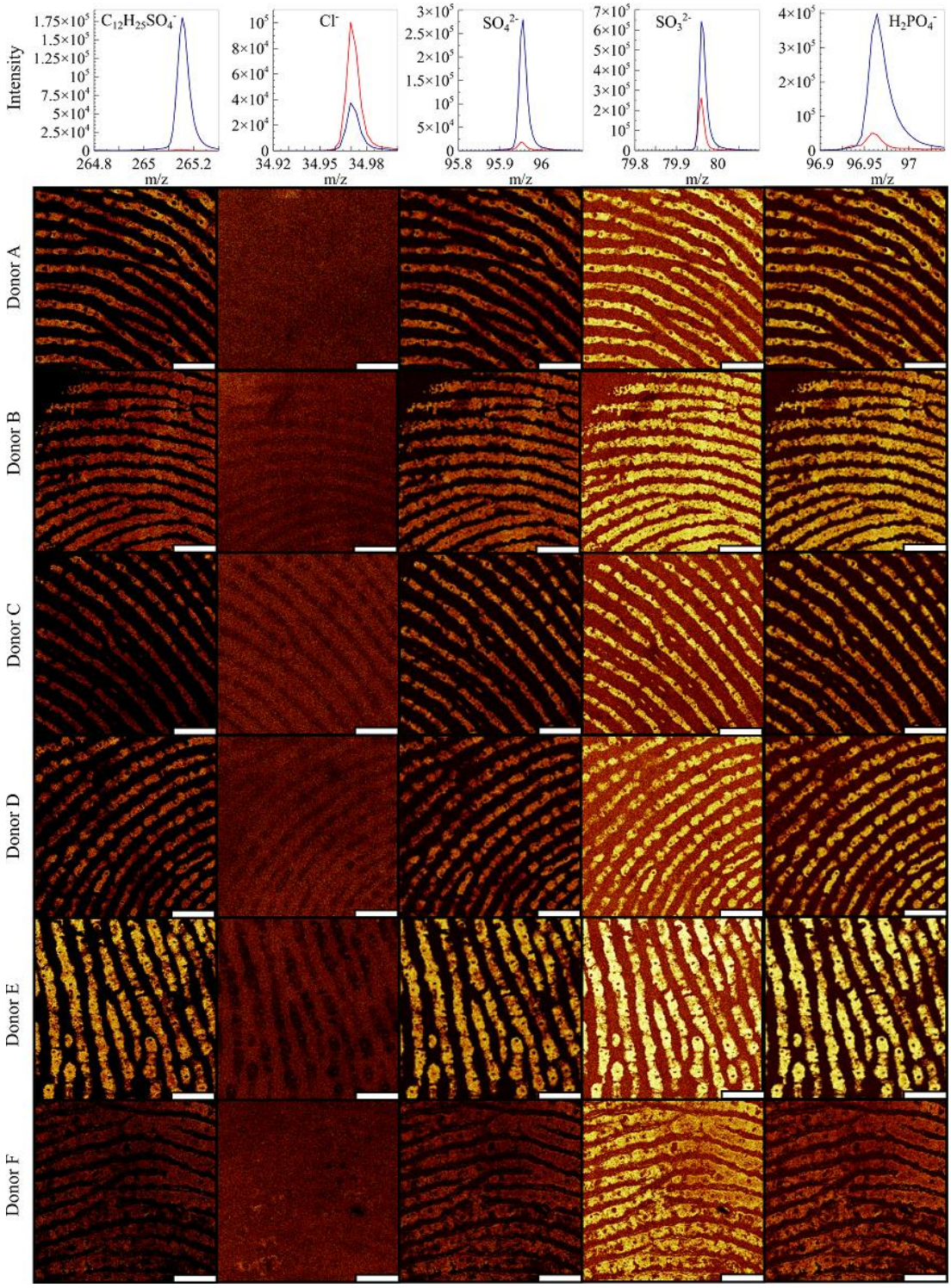

Figure 6. 9: ToF-SIMS fingermark images on stainless steel surfaces after 13 days of deposition. The top row represents the typical ToF-SIMS spectra corresponding to

Donor B for the negative secondary ions that were emitted from the surface of the samples. In each case, the ionic species responsible for the peak is labelled. The blue line represents a typical spectrum taken from a region on the fingermark and the red line represents the spectrum collected from the substrate. The images below each spectrum display show spatial variations in the number of counts or signal intensity measured at each position on the sample surface. Data are shown for each of the six donors. Each image took approximately 15 minutes to acquire. Scale bar: 1 mm.

In the negative ionic species that are shown in Figure 6.9, the Cl^- ion was the least prevalent. The presence of this ion could be expected since this is one of the most common negative ion that is found in fingermark residue. However, the images in Figure 6.9 of all the six donors exhibit that the substrate regions in between the fingermark contain more of the Cl^- ion than in the fingermark regions. This negative contrast implies that the chloride ions were present on the surface and were removed by the contacting finger upon deposition. The excess chloride ions on the steel surface could be originating from the washing procedure which was used to clean the metal surfaces, that is the residual salt traces dissolved in the water.

The greatest positive contrast among the negative ions for all the donors studied was from sulphite ions (SO_3^{2-}). The reasons for the presence of sulphite ions are not entirely clear, but it is suggested that these ions are found in fingermark residue from all six donors are most probably through their food consumption since sulphites are one of the most widely used food preservatives in the UK [47].

The next negative ion which gave a clear contrast for all the six donors was dihydrogen phosphate ($H_2PO_4^-$) ion. The presence of this ion is most likely due to the presence of trace amounts of phospholipid in the fingermarks residue [43]. Sulphate (SO_4^{2-}) ions were also detected in the fingermark residue obtained from all donors. These metabolites can be found in food such as bread, nuts, alcohol (fermented beverages), dried fruits, and vegetables in high concentrations [48].

As mentioned earlier, an exogenous compound of high molecular weight ion ($C_{12}H_{25}SO_4^-$) was also observed within fingermark region with a strong signal, producing a clear image of fingermark pattern for all donors.

Figure 6. 10: a) Chemical image of an entire fingermark on stainless steel surface from Donor A using ToF-SIMS. The image represents the spatial distribution of the K^+ ion after 26 days of deposition. This fingermark is the same as that shown in Figure 6.8, which was reimaged after a further 13 days of aging. The scale bar corresponds to 3 mm. The same sample shown in a) was treated with b) BY40, c) CV, and d) SB dyes was captured using conventional photographic techniques. All the three optical micrographs have the equivalent scale bar of 5 mm and portray the same region of the fingermark deposition as shown in a).

Figure 6.10 shows a large area (18 mm x 18mm) scan of the K^+ ion distribution in a fingermark that was deposited on stainless steel by Donor A that was reimaged using ToF-SIMS after a period of twenty-six days following deposition. Remarkably, this image exhibits a similar level of detail to the images shown in Figures 6.8 and 6.9 even though conventional techniques (BY40, CV, and SB) showed no evidence of useable marks after this period of time. The insets shown in Figure 6.10 are photographs of the same sample that was removed from the ToF-SIMS chamber,

fumed using CNA and stained using the three dyes, BY40, CV, and SB according to the protocol described previously. These images show the same region of the sample that was imaged using ToF-SIMS and display no evidence of the fingermark shown in the main panel.

One potential criticism of this approach is that exposure to the high vacuum conditions in the ToF-SIMS chamber could have removed much of the material in the fingermark and thus rendered the stains useless once the sample had been imaged using ToF-SIMS. However, samples which had been aged for the same time but without being placed in the ToF-SIMS chamber were also stained using the same dyes and showed no evidence of fingermarks when photographed. In fact, the digital photograph images of the stained samples that were not exposed to high vacuum conditions were very similar to those shown in Figure 6.10 b, c and d.

It is clear from the data shown in Figure 6.10 that ToF-SIMS can be used to visualise an entire fingermark with an exceptional level of detail (first, second, and third level detail being evident) on a steel surface despite it being aged for twenty-six days. Whereas, when the same steel sample was treated with BY40, CV, and SB the procedure described in Table 6.2 consistently gave a score of one as no fingermark evidence could be observed on the steel surfaces. Residual traces of components such as potassium (K^+) and sodium (Na+) ions as well as a number of less abundant ions remain on the surface even after exposure to the high vacuum imaging conditions used in ToF-SIMS. Notably, the sample imaged in Figure 6.10 was also one of the samples that was imaged after thirteen days (see Figure 6.8, Figure 6.9). This demonstrates that the ToF-SIMS imaging technique is non-destructive and can be repeatedly used to image fingermarks without compromising their quality. The application of ToF-SIMS therefore has the potential for applications in the detection of latent fingermarks and could be used to more reliably link persons of interest to the scene of a crime.

This study clearly demonstrates that fingermarks that have been deposited on metal (stainless steel) surfaces can be visualised with an exceptional level of detail using ToF-SIMS. The resulting images are significantly better than those obtained using conventional development techniques on the same/similar samples (which show no visible marks). However, further studies on ‘real-world’ samples are required to demonstrate the applicability of ToF-SIMS to a broader range of fingermarks and

samples surfaces. The fingermarks used in this study were produced to contain consistent levels of eccrine and sebaceous secretions. However, real-world samples are likely to contain variable amounts of these deposits. Such variability could influence the level of detail recovered using ToF SIMS as well as potentially altering the degradation times associated with fingermarks that are present on the samples.

The steel surfaces that were used in this work also had a flat surface topology and a relatively small size (30 mm diameter). Real forensic samples are likely to have greater roughness and/or to have curved surfaces. Moreover, such samples are likely to be quite large and one potential limitation of the work performed here is that the maximum sample size that can be imaged using the ToF-SIMS instrument is 9 cm × 9 cm. While this is acceptable for many objects, it may not be large enough for a gun or a knife and some cutting of the samples may be required.

Figure 6.11 displays stainless steel samples of the entire depletion series deposited by Donor A that was fumed with CNA and stained with dyes in order to be able to compare the image obtained from the ToF-SIMS imaging.

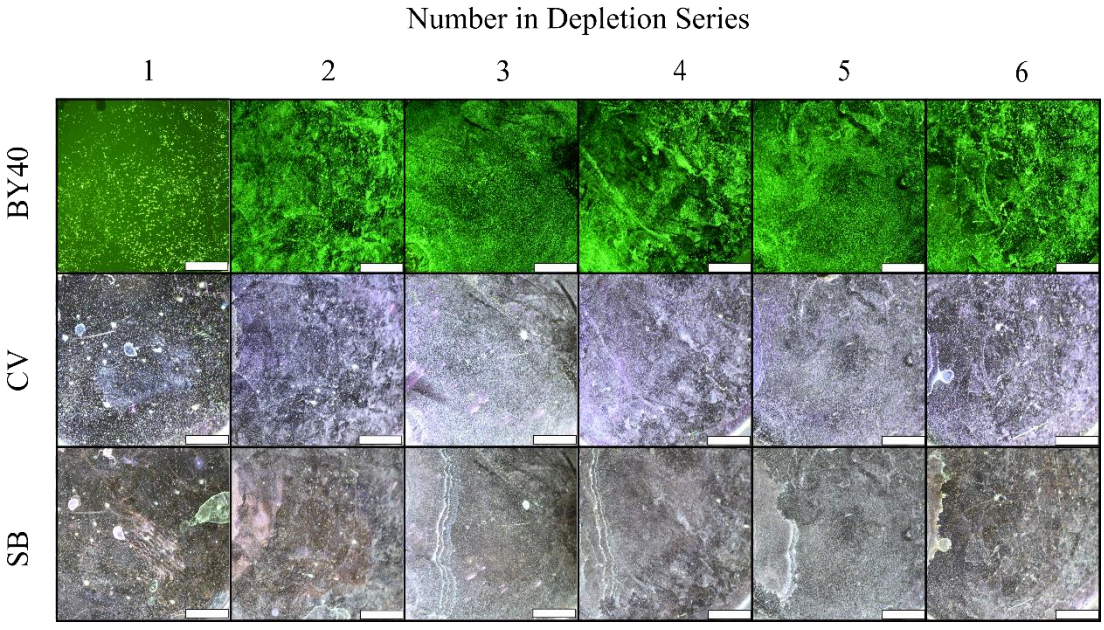

Figure 6. 11: Each row represents optical micrographs of stainless steel samples in the depletion series from Donor A, including number 2 in the series which was imaged twice in ToF-SIMS which were stained with BY40, CV and SB respectively. The white scale bar corresponds to 5 mm in all cases.

Considering ToF-SIMS produced exceptionally excellent quality of fingermark image, but when the same stainless steel sample was treated with BY40, CV, and SB it persistently produced a score of one as no traces of fingermark could be observed on this metal surfaces. The images in Figure 6.11 agree with the constantly poor scores of fingermark development on stainless steel samples in pilot study. This suggests the efficacy of cyanoacrylate polymerisation can vary depending in their interaction with the fingermark residue and its substrate leading to no development on stainless steel substrates [50].

It could be then expected for no further contrast enhancement of fingermark appearance with the use of BY40 fluorescence dye, given that the role of the dye is only to enhance the cyanoacrylate that polymerised on the fingermark residue. The marks were less prevalent when developed with CV and SB since the role of CV and SB dyes are to bind with any lipids or fatty acids that are present in fingermark residue, while the fingermarks used in this study contained predominantly eccrine material. Likewise, similar outcome was observed when the depletion series of fingermarks that were deposited by the other five donors were fumed with CNA and further stained with the three dyes. There was no sign or indication of fingermark present in most cases for all the donors resulting in a score of 1.

Quantitative approach was made by plotting mean scores for all the six different donors for the three different staining techniques, are represented in Figure 6.11. This is to compare with the results obtained from Figure 6.4 and be certain that the outcome for employing the conventional technique results in indistinguishable end result for all donors regardless of gender, age, and ethnicity on stainless steel surface.

Figure 6.12 shows that unidentifiable fingermarks were observed for all the staining techniques for all the donors. However, a weak development disclosed for only Donor B after SB dye was applied. The reason for the weak development of fingermark after application of SB dye is most likely due to the minimal occurrence of lipids in eccrine sweat, with the C_{18} free fatty acids as shown in both the Figures 6.6 and 6.7 of Donor B [51]. Free fatty acids are found in eccrine sweat as they are produced on the skin surface and not by the sebaceous glands [12]. Hence, when SB dye came into contact with the lipids present on the stainless steel it dissolved into it producing contrast between fingermark deposition and the stainless steel surface.

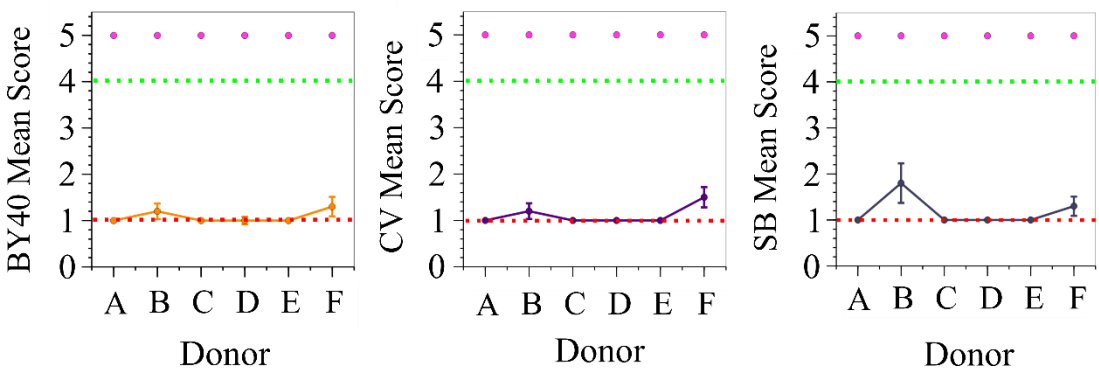

Figure 6. 12: Mean scores of the six donors for the three different staining techniques with error bars that were calculated using the standard error of the mean of scores obtained from fingermarks in the depletion series. The horizontal red dotted line denotes the score when a fingermark is considered to be unidentifiable (score ≤ 1, see table 6.2) while the green dotted horizontal line represents the threshold score above which a fingermark is considered to be sufficient for identification purposes (score ≥ 4). The chemical images of fingermarks obtained from ToF-SIMS for all 6 donors are of an exceptional quality and hence the images are scored as 5 according to the scoring scheme in Table 6.2, is plotted in each staining dye graphs with pink circles.

ToF-SIMS also has the potential to be used to image fingermarks following the use of other imaging techniques. However, the efficacy of the technique under these circumstances is likely to depend upon the nature of the previous imaging technique that was used (destructive or non-destructive) and on the chemical properties of any contrast agents that may have been used to enhance the fingermark. If a contrast agent was used to try to enhance a mark and subsequently covered it up, then the initial ToF SIMS signal would be dominated by the secondary ions that are emitted from the contrast agent rather than the fingermark.

However, repeated rastering of the primary ion beam could be used to etch away any coating layers to reveal the fingermark as has been done previously for polymer layers [52]. Previous work by Sisco and co-workers [44] has also shown that mass spectroscopy techniques are relatively insensitive to the prior use of contrast agents such as black fingerprint power, magnetic powders and some fluorescent dyes.

6.4 Conclusion

ToF-SIMS has demonstrated the capability to obtain exceptional quality fingermarks where conventional development techniques produce no evidence of marks. The application of this technique to steel surfaces, in particular, has shown that it is capable of identifying pore level detail on all ridge patterns by imaging the spatial distribution of inorganic ions such as sodium and potassium on metal surfaces. Moreover, samples that have been aged under ambient conditions for up to twenty-six days display the same exceptional quality of detail and can be repeatedly imaged with no obvious evidence of deterioration in the quality of the fingermarks produced. ToF-SIMS imaging therefore has the potential and could be a valuable tool in helping to visualise fingermarks on objects such as stainless steel knife blades and firearms.

References

1. Flatley, J. Statistical bulletin: Crime in England and Wales: year ending June 2017, Office for National Statistics [GB]: https://www.ons.gov.uk/peoplepopulationandcommunity/crimeandjustice/bulletins/crimeinenglandandwales/june2017

2. Girelli, C. M., Lobo, B. J., Cunha, A. G., Freitas, J. C., & Emmerich, F. G. (2015). Comparison of practical techniques to develop latent fingermarks on fired and unfired cartridge cases. *Forensic science international*, *250*, 17-26.

3. Dominick, A. J., & Laing, K. (2011). A comparison of six fingerprint enhancement techniques for the recovery of latent fingerprints from unfired cartridge cases. *Journal of Forensic Identification*, *61*(2), 155.

4. Ramos, A. S., & Vieira, M. T. (2012). An efficient strategy to detect latent fingermarks on metallic surfaces. *Forensic Science International*, *217*(1-3), 196-203.

5. Freeman, H. N. (1999). Magnetic fingerprint powder on firearms and metal cartridges. *Journal of Forensic Identification*, *49*(5), 479.

6. Dove, A. (2017). Fingerprint Development on Cartridge Cases Through the Electrodeposition of Gun Blue. *Journal of Forensic Identification*, *67*(3), 391.

7. Edmiston, K. E., & Johnson, J. (2009). Determining an optimal sequence for chemical development of latent prints on cartridge casings and shotgun shells. *Journal of Forensic Sciences*, *54*(6), 1327-1331.

8. Cantu, A. A., Leben, D. A., Ramotowski, R., Kopera, J., & Simms, J. R. (1998). Use of acidified hydrogen peroxide to remove excess gun blue from gun blue-treated cartridge cases and to develop latent prints on untreated cartridge cases. *Journal of Forensic Science*, *43*(2), 294-298.

9. Bailey, M. J., Ismail, M., Bleay, S., Bright, N., Elad, M. L., Cohen, Y., Geller, B., Everson, D., Costa, C., Webb, R.P., & Watts, J. F. (2013). Enhanced imaging of developed fingerprints using mass spectrometry imaging. *Analyst*, *138*(21), 6246-6250.

10. Tilstone, W. J., Savage, K. A., & Clark, L. A. (2006). *Forensic science: An encyclopedia of history, methods, and techniques, pp. 151*. ABC-CLIO.

11. Wightman, G., Emery, F., Austin, C., Andersson, I., Harcus, L., Arju, G., & Steven, C. (2015). The interaction of fingermark deposits on metal surfaces and potential ways for visualisation. *Forensic Science International*, *249*, 241-254.

12. Frick, A.A, Fritz, P. & Lewis, S.W. (2016). Chemistry of Print Residue. In: Houck, M., (Ed.). *Forensic Fingerprints, pp.31-32*. Academic Press.

13. Bersellini, C., Garofano, L., Giannetto, M., Lusardi, F., & Mori, G. (2001). Development of latent fingerprints on metallic surfaces using electropolymerization processes. *Journal of Forensic Science*, *46*(4), 871-877.

14. Beresford, A. L., & Hillman, A. R. (2009). Electrochromic enhancement of latent fingerprints on stainless steel surfaces. *Analytical Chemistry*, *82*(2), 483-486.

15. Brown, R. M., & Hillman, A. R. (2012). Electrochromic enhancement of latent fingerprints by poly (3, 4-ethylenedioxythiophene). *Physical Chemistry Chemical Physics*, *14*(24), 8653-8661.

16. Xu, L., Li, Y., He, Y., & Su, B. (2013). Non-destructive enhancement of latent fingerprints on stainless steel surfaces by electrochemiluminescence. *Analyst*, *138*(8), 2357-2362.

17. Qin, G., Zhang, M., Zhang, T., Zhang, Y., McIntosh, M., Li, X., & Zhang, X. (2012). Label-Free Electrochemical Imaging of Latent Fingerprints on Metal Surfaces. *Electroanalysis*, *24*(5), 1027-1032.

18. Williams, G., McMurray, H. N., & Worsley, D. A. (2001). Latent fingerprint detection using a scanning Kelvin microprobe. *Journal of Forensic Science*, *46*(5), 1085-1092.

19. Williams, G., & McMurray, H. N. (2007). Latent fingermark visualisation using a scanning Kelvin probe. *Forensic Science International*, *167*(2-3), 102-109.

20. Bond, J. W., & Heidel, C. (2009). Visualization of latent fingerprint corrosion on a discharged brass shell casing. *Journal of Forensic Sciences*, *54*(4), 892-894.

21. Bond, J. W. (2008). Visualization of latent fingerprint corrosion of metallic surfaces. *Journal of Forensic Sciences*, *53*(4), 812-822.

22. Hinder, S. J., & Watts, J. F. (2010). SIMS fingerprint analysis on organic substrates. *Surface and Interface Analysis*, *42*(6-7), 826-829.

23. Szynkowska, M. I., Czerski, K., Grams, J., Paryjczak, T., & Parczewski, A. (2007). Preliminary studies using imaging mass spectrometry TOF-SIMS in detection and analysis of fingerprints. *The Imaging Science Journal*, *55*(3), 180-187.

24. Sears, V. G., Bleay, S. M., Bandey, H. L., & Bowman, V. J. (2012). A methodology for finger mark research. *Science and Justice*, *52*(3), 145-160.

25. Jain, A. K., Chen, Y., & Demirkus, M. (2007). Pores and ridges: High-resolution fingerprint matching using level 3 features. *IEEE Transactions on Pattern Analysis and Machine Intelligence*, *29*(1), 15-27.

26. Bleay, S. M., Croxton, R. S., & De Puit, M. (2018). 7. Vapour phase techniques. Fingerprint Development Techniques: Theory and Application. John Wiley & Sons, pp. 169-171.

27. Bleay, S. M., Croxton, R. S., & De Puit, M. (2018). 11. Lipid reagents. Fingerprint Development Techniques: Theory and Application. John Wiley & Sons, pp. 285-295.

28. Yamashita, B., & French, M. (2011). Latent print development. In: McRoberts, A., (Ed.). *The Fingerprint Sourcebook, pp. 7-31*. National Institute of Justice.

29. Bleay, S. M., Sears, V. G., Bandey, H. L., Gibson, A. P., Bowman, V. J., Downham, R., Fitzgerald, L., Ciuksza, T., Ramadani, J. & Selway, C. (2012). Finger mark development techniques within scope of ISO 17025. *Fingerprint Source Book, Home Office Centre for Applied Science and Technology (CAST)*, 233-289.

30. Michel, R., & Castner, D. G. (2006). Advances in time-of-flight secondary ion mass spectrometry analysis of protein films. *Surface and Interface Analysis*, *38*(11), 1386-1392.

31. Muramoto, S., Graham, D. J., Wagner, M. S., Lee, T. G., Moon, D. W., & Castner, D. G. (2011). ToF-SIMS analysis of adsorbed proteins: principal component analysis of the primary ion species effect on the protein fragmentation patterns. *The Journal of Physical Chemistry C*, *115*(49), 24247-24255.

32. Girod, A., Ramotowski, R., & Weyermann, C. (2012). Composition of fingermark residue: a qualitative and quantitative review. *Forensic Science International*, *223*(1-3), 10-24.

33. Bailey, M. J., Bright, N. J., Croxton, R. S., Francese, S., Ferguson, L. S., Hinder, S., Jickells, S., Jones, B.J., Jones, B.N., Kazarian, S.G. & Ojeda, J. J.

(2012). Chemical characterization of latent fingerprints by matrix-assisted laser desorption ionization, time-of-flight secondary ion mass spectrometry, mega electron volt secondary mass spectrometry, gas chromatography/mass spectrometry, X-ray photoelectron spectroscopy, and attenuated total reflection Fourier transform infrared spectroscopic imaging: an intercomparison. *Analytical Chemistry*, *84*(20), 8514-8523.

34. Ryadnov, M., & Hudecz, F. (Eds.). (2016). *Amino Acids, Peptides and Proteins* (Vol. 41), *pp. 241*. Royal Society of Chemistry.

35. Welch, N. G., Madiona, R. M., Scoble, J. A., Muir, B. W., & Pigram, P. J. (2016). ToF-SIMS and principal component analysis investigation of denatured, surface-adsorbed antibodies. *Langmuir*, *32*(42), 10824-10834. "Supporting Infromation. Table S1. A compiled list of known ToF-SIMS mass fragments of amino acids."

36. Tyler, B. J., Bruening, C., Rangaranjan, S., & Arlinghaus, H. F. (2011). TOF-SIMS imaging of adsorbed proteins on topographically complex surfaces with Bi3+ primary ions. *Biointerphases*, *6*(3), 135-141.

37. Zhou, L., Le Grandois, J., Marchioni, E., Zhao, M., Ennahar, S., & Bindler, F. (2010). Improvement of total lipid and glycerophospholipid recoveries from various food matrices using pressurized liquid extraction. *Journal of agricultural and food chemistry*, *58*(18), 9912-9917.

38. Poleunis, C., Everaert, E. P., Delcorte, A., & Bertrand, P. (2006). Characterisation of human hair surfaces by means of static ToF-SIMS: A comparison between Ga+ and C60+ primary ions. *Applied surface science*, *252*(19), 6761-6764.

39. Committee for Veterinary Medicinal Products, Linear Alkyl Benzene Sulfonic Acids, summary report (1), European Medicines Agency, EMEA/MRL/755/00-FINAL July 2000.

40. Wagner, M. S., & Castner, D. G. (2001). Characterization of adsorbed protein films by time-of-flight secondary ion mass spectrometry with principal component analysis. *Langmuir*, *17*(15), 4649-4660.

41. Wagner, M. S., & Castner, D. G. (2001). Characterization of adsorbed protein films by time-of-flight secondary ion mass spectrometry with principal component analysis. *Langmuir*, *17*(15), 4649-4660.

42. Mantus, D. S., Ratner, B. D., Carlson, B. A., & Moulder, J. F. (1993). Static secondary ion mass spectrometry of adsorbed proteins. *Analytical chemistry*, *65*(10), 1431-1438.

43. Heim, C., Sjövall, P., Lausmaa, J., Leefmann, T., & Thiel, V. (2009). Spectral characterisation of eight glycerolipids and their detection in natural samples using time-of-flight secondary ion mass spectrometry. *Rapid Communications in Mass Spectrometry*, *23*(17), 2741-2753.

44. Sisco, E., Demoranville, L. T., & Gillen, G. (2013). Evaluation of C60 secondary ion mass spectrometry for the chemical analysis and imaging of fingerprints. *Forensic science international*, *231*(1-3), 263-269.

45. Amaya, K. R., Sweedler, J. V., & Clayton, D. F. (2011). Small molecule analysis and imaging of fatty acids in the zebra finch song system using time-of-flight-secondary ion mass spectrometry. *Journal of neurochemistry*, *118*(4), 499-511.

46. Preedy, V. R. (Ed.). (2015). *Betaine: Chemistry, Analysis, Function and Effects*, *pp. 188*. Royal Society of Chemistry.

47. Vickerman, J. C., & Briggs, D. (Eds.). (2013). 18. ToF-SIMS image analysis. *ToF-SIMS: materials analysis by mass spectrometry*. IM Publications, pp. 488.

48. Tytgat, G., Bartelsman, J. F. W. M., & van Deventer, S. J. H. (Eds.). (1995). *Inflammatory Bowel Diseases.* Falk Symposium 85. Springer Science & Business Media.

49. Florin, T., Neale, G., Gibson, G. R., Christl, S. U., & Cummings, J. H. (1991). Metabolism of dietary sulphate: absorption and excretion in humans. *Gut*, *32*(7), 766-773.

50. Casault, P., Gilbert, N., & Daoust, B. (2017). Comparison of various alkyl cyanoacrylates for fingerprint development. *Canadian Society of Forensic Science Journal*, *50*(1), 1-22.

51. Harker, M., Coulson, H., Fairweather, I., Taylor, D., & Daykin, C. A. (2006). Study of metabolite composition of eccrine sweat from healthy male and female human subjects by 1H NMR spectroscopy. *Metabolomics*, *2*(3), 105-112.

52. Bailey, J., Havelund, R., Shard, A. G., Gilmore, I. S., Alexander, M. R., Sharp, J. S., & Scurr, D. J. (2015). 3d tof-sims imaging of polymer multilayer films using argon cluster sputter depth profiling. *ACS applied materials & interfaces*, *7*(4), 2654-2659.

CHAPTER 7

Summary and suggestions for future work

7.1 Summary of Findings

The primary emphasis in this thesis has been elucidating some of the key features of fingermark enhancement on substrates with different wetting properties. In chapter 4 the role of wetting properties of the surface and its influence on the two types of deposited latent fingermark (eccrine and sebaceous) using cyanoacrylate fuming was probed. It was found that the wetting properties of the polymer substrate influenced the distribution of both types of sweat (sebaceous and eccrine) material within ridges. The amount of cyanoacrylate deposited on the fingermark residue decreased with the increase in polymer water contact angle of the substrate. This suggested that the higher rate of cyanoacrylate polymerisation onto lower water contact angle of polymer substrate is caused by the well spread of sweat material on this surface as a continuous film allowed more surface area for cyanoacrylate to polymerise on it. In this chapter it was also shown that the cyanoacrylate polymerisation was higher on sebaceous mark in comparison to eccrine mark. This was due to the higher amount of material being present in sebaceous fingermark as observed in the FTIR spectra in comparison to the eccrine material besides the different type of compounds found in both types of the sweat.

Chapter 5 developed the work of chapter 4 by trying to investigate the relationship between fingermark deposition and the substrate wetting properties as a function of time. It was found that the fingermark constituents decreased over the timescale of few days (0 – 7 days) following fingermark deposition. The images from optical microscope strongly hinted the degradation occurred during fingermark aging process was relatively depended on the type of mark (either sebaceous / eccrine) and the wetting properties of the substrate deposited onto. The degradation of marks deposited on hydrophobic substrates was found to occur more rapidly regardless of the storage conditions (left inside a microscopic slide box / left outside on a working bench in laboratory exposed to light and air flow) due to the distribution of fingermark during the deposition. The eccrine marks showed a much poorer fingermark development than sebaceous mark since the amount present in eccrine mark was less to begin with and the eccrine sweat is mainly made up of volatile substances that can degrade faster when exposed to the environmental conditions. However, the amount of cyanoacrylate developed on sebaceous and eccrine marks that were stored inside a box for one week prior to cyanoacrylate fuming showed a much better quality of fingermark in comparison to the same marks that were exposed to the environmental conditions. In this chapter it was also shown that the developed fingermark (for eccrine and sebaceous) on the hydrophilic substrate displayed better quality regardless of the storage conditions. This suggested that the wetting properties does not only affect the fingermark deposition but also influences the marks during the aging process and the fingermark development.

Chapter 6 was motivated as a result of the interest in studying fingermarks on different types of surfaces, in particular metal surfaces to assess the differences in metal compositions which would affect the fingermark deposition and the recovery of fingermark from the surface. Added to it, the suboptimal performance by the conventional enhancement techniques to visualise fingermarks on metal substrates and rise in violent crimes involving stainless steel knife blades and firearms further drove the curiosity to study fingermark on metal substrates. It was found that stainless steel seems to display the poorest quality of fingermark visualisation in comparison to the other two metals (aluminium and brass) after applying a sequence of conventional techniques; cyanoacrylate fuming process followed by staining techniques including Basic Yellow 40, Crystal Violet and Sudan Black in the pilot study. Therefore, the

stainless steel was selected as the focus for further in-depth studies using ToF-SIMS. The chemical images that was procured using the ToF-SIMS technique had shown to be able to visualise fingermarks on stainless steel for periods of up to 26 days after deposition in comparison to the other conventional techniques.

7.2 Future Work

There is more scope to look at how the aging of fingermark over a range of substrates with different surface texture, topography, physio-chemical property, temperature and electrostatic affect the composition of fingermark residue for fingermark dating. Study on ridge spreading kinetics can be used to determine the redistribution of sweat components within the fingermark post-deposition. This has been of particular interest recently due to the concerns over identifying fingermark age which could provide evidence of time the latent fingermark would have been deposited at crime scenes to find the real offender [1].

Studies of fingermark on metal substrates should be explored to a wider range of substrates, which have forensic interest. The next step in utilising the ToF-SIMS technique, as an approved method for fingermark enhancement in criminal cases, would be to undertake pseudo-operational trials [2]. The principle here is to establish whether the results obtained in a laboratory trial are replicable on items and surfaces that may be submitted to a fingermark laboratory.

The work pursued in this thesis provides several interesting avenues of enquiry which has not been possible to pursue due to time constraints.

References

1. Girod, A., Ramotowski, R., Lambrechts, S., Misrielal, P., Aalders, M., & Weyermann, C. (2016). Fingermark age determinations: Legal considerations, review of the literature and practical propositions. *Forensic science international*, *262*, 212-226.
2. Sears, V. G., Bleay, S. M., Bandey, H. L., & Bowman, V. J. (2012). A methodology for finger mark research. *Science & Justice*, *52*(3), 145-160.

Appendices

Enlarged images of eccrine fingermarks aged on polymers substrates of water contact angle of θ a) 60.2°, b) 65.9° and c) 101.3° from optical microscope (Figure 5.14 in Chapter 5, section 5.3.2 : pp.176 - 177).

a)

Day 0

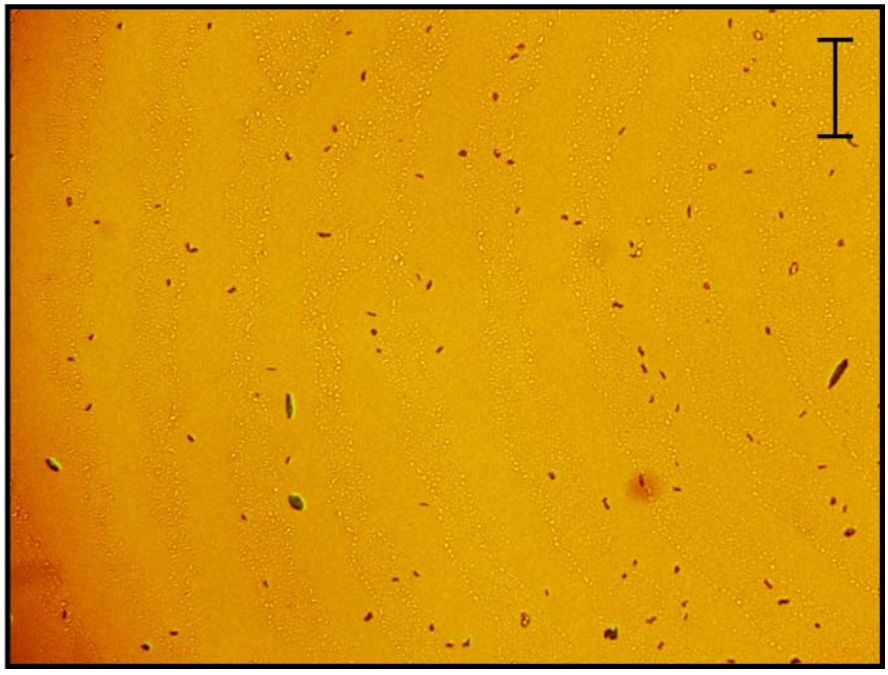

Day 7

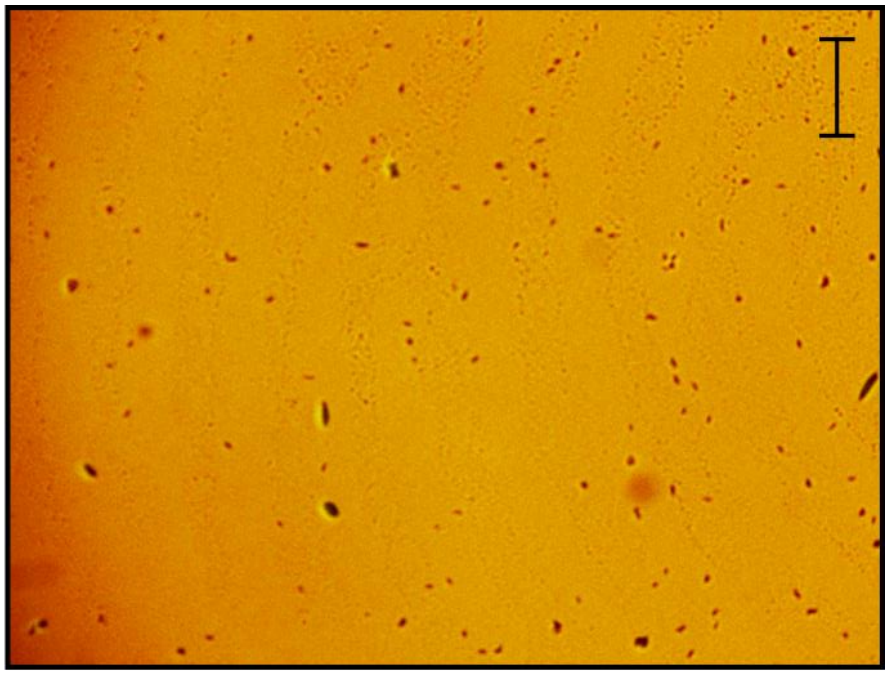

b)

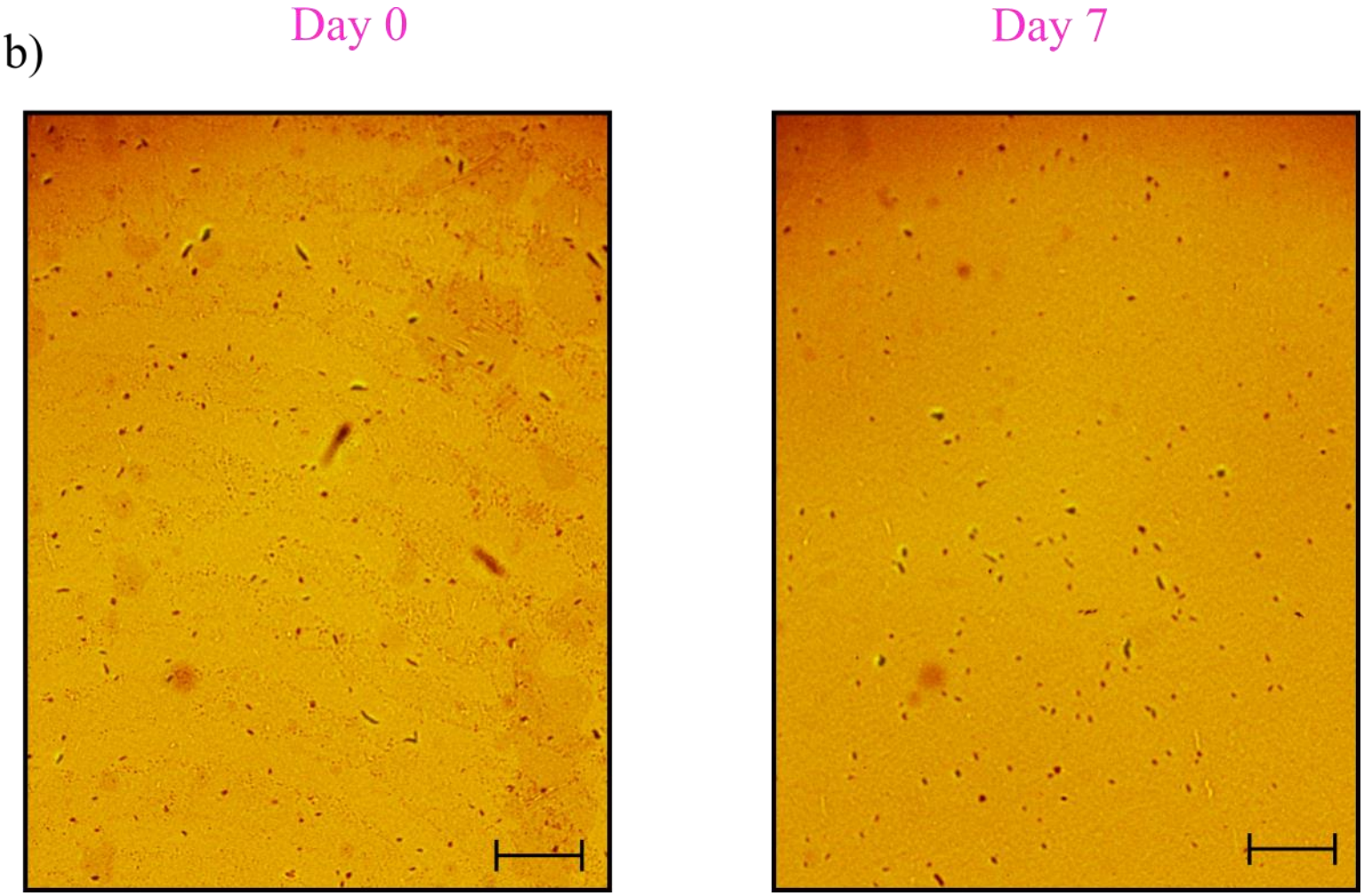

c)
Day 0
Day 7

List of Figures

List of Tables